2016

Synthesis of Amphiphilic Porphyrins and Porphyrin Arrays

Nicholas Roach
University of Wollongong, njilroach@gmail.com

Synthesis of Amphiphilic Porphyrins and Porphyrin Arrays

A Thesis Presented in Partial Fulfilment of the Requirements

for the Degree of Doctor of Philosophy in Chemistry at The University of Wollongong,

Wollongong, Australia

Nicholas John Lambeth Roach

November 2016

Acknowledgements

I want to thank David, Pawel, Chris, Rhys and Dan for their assistance and friendship, and Les Dutton and the group at UPenn for their hospitality and high quality work. I also want to thank my family for their support, and everyone at IPRI and elsewhere who assisted me in completing my studies.

Abstract

The natural photosynthetic systems utilise protein scaffolds to hold their components, which self assemble to form complex structures. Artificial protein maquettes offer the possibility of producing similarly sophisticated molecular assemblies, containing light-harvesting pigments and catalysts for charge separation and energy storage, with a potential application in fuel production using solar energy.

The production of such an assembly requires the binding of light harvesting pigments to the designed binding sites of a protein maquette, but it is not known what functionality on a light harvesting pigment is required for optimal binding. In order to investigate these binding requirements, a variety of single porphyrins with a range of hydrophilic and hydrophobic properties were synthesised, and preliminary investigations into their binding to maquettes were undertaken.

Mixed-aldehyde condensation was used to generate a large variety of porphyrins, which were subsequently metalated with zinc or iron and then converted to their final amphiphilic forms. A porphyrin bearing a ferrocene group and two porphyrins bearing electron-withdrawing pentafluorobenzene groups were also produced in order to explore the modification of the porphyrins' electronic properties. HPLC was used to solve the problem of determining the isomeric purity of *ABAB* and *AABB* porphyrins isolated from mixed-aldehyde condensations.

Porphyrin dyads with a phenylene linkage were produced using similar mixed-aldehyde condensations. Two amphiphilic dyads of this type were produced, bearing carboxylic acid and quaternary ammonium salt hydrophilic substituents. Amphiphilic porphyrin dyads with vinyl linkages were also produced using Wittig and Knoevenagel condensations.

Methods of using bound metal ions to facilitate controlled differential metalation of a phenylene-linked porphyrin dyad were investigated. A method of tagging porphyrins with manganese was developed in order to facilitate the isolation of porphyrin arrays bearing ester groups. This technique allowed the isolation of a porphyrin triad.

A preliminary investigation into the maquette-binding properties of the amphiphilic porphyrins and porphyrin arrays was carried out, and the compounds that bound quickly and strongly were identified. It was found that extremes of hydrophobicity and hydrophilicity were not conducive to maquette binding, and that amphiphilic molecules bound the best. The maquettes were able to accommodate a variety of porphyrins bearing from one to three hydrophilic groups, and porphyrins bearing both carboxylic acids and quaternary ammonium salts were found to be tolerated by the maquette. The best-binding of these porphyrin materials have already formed the foundation of future research into light harvesting porphyrin maquette ensembles.

Table of Contents

List of Figures

List of Abbreviations

ATP	Adenosine triphosphate
CHES	*N*-Cyclohexyl-2-aminoethanesulfonic acid
DBU	1,8-diazabicycloundec-7-ene
DCM	Dichloromethane
DDQ	2,3-Dichloro-5,6-dicyano-1,4-benzoquinone
DMF	Dimethylformamide
DMSO	Dimethylsulfoxide
d	Doublet
E_h	Midpoint potential
HOMO	Highest occupied molecular orbital
HPLC	High pressure liquid chromatography
HRMS	High resolution mass spectrometry
hrs	Hours
LHC	Light harvesting complex
LUMO	Lowest unoccupied molecular orbital
MALDI MS	Matrix-assisted laser desorption/ionization mass spectrometry
min	Minutes
m	Multiplet
NaOAc	Sodium acetate
NMR	Nuclear magnetic resonance
OEC	Oxygen evolving complex
PSII	Photosystem II
QAS	Quaternary ammonium salt

q	Quartet
Rf	Retention factor
s	Singlet
TFA	Trifluoroaceticacid
THF	Tetrahydrofuran
TLC	Thin layer chromatography
TEPP	Tetra-(4-ethylphenyl)porphyrin
TPP	Tetraphenylporphyrin
t	Triplet
UV-vis	Ultraviolet-visible

Chapter 1: Introduction

Billions of years of evolution have endowed nature with phenomenal chemical prowess. Perhaps most impressive is the ability possessed by photosynthetic organisms to synthesise energy-rich structural materials and fuel molecules from water and carbon dioxide using the energy of sunlight. This process is the source of practically all of the energy that animates life on Earth. More than a century of experimentation has revealed much of the complex chemical mechanism of cellular photosynthesis. It relies upon precise control over energy and electron flow through pathways built to molecular-scale precision.[1] If the same degree of control can be achieved in an artificial construct, then the doors will be opened to a new world of technology for solar energy harvesting, materials production and even information processing.

In the oxidative atmosphere of the Earth, it is highly reduced molecules, especially carbon compounds, which may serve as fuels. The polymers which are so widely used in our society are also reduced carbon compounds. Currently our supply of such materials comes from fossil fuels, and it is essential for the welfare of the planet that we become independent of such finite geological deposits.

These doctoral studies form part of a larger effort to prepare a working model of the photosystems of nature. Its goal is to replicate the natural light harvesting antennae and initial electron transfer events which, when combined with the appropriate catalysts currently under development, will provide an adaptable power plant for fuel and materials production. More specifically, this work is aimed at one fundamental component of such a model, the development of an artificial light harvesting reaction centre that could be coupled to catalysts.

1.1 The photosynthetic mechanism

Nature captures solar energy and converts it to chemical energy using photosynthesis. It generates carbon compounds by removing electrons from water and using these electrons to reduce carbon dioxide from the atmosphere. Oxygen is produced in this process and released into the atmosphere, and is utilised to unlock the stored energy of these energy-storage materials, when it is required, *via* oxidation reactions. This system is cyclic and entirely renewable, and has at its disposal the abundant energy source that is sunlight.

There are several forms of photosynthesis found in nature, but they are similar to one another in their general function, and are well represented by the mechanism found inside green plants and cyanobacteria, which will be discussed in the following section.

1.2 Harvesting photons

The natural place to begin an explanation of photosynthesis is at the point of photon absorption. Photons from the sun are collected by arrays of chlorophyll molecules embedded in protein scaffolds, which are themselves embedded in the thykaloid membranes of the chloroplasts of cells.[2]

These protein complexes are called light harvesting complexes 1 and 2 (LHCI and LHCII). LHCII is purely for light collection, and passes the energy it collects on to LHCI (Figure 1). LHCI is part of the complex of photosystem II (PSII), which also contains a reaction centre that drives water oxidation and energy storage (Figure 2). The complex consists of a membrane-spanning scaffold of α helices where chlorophyll molecules are bound, with the reaction centre being located at the centre.[1]

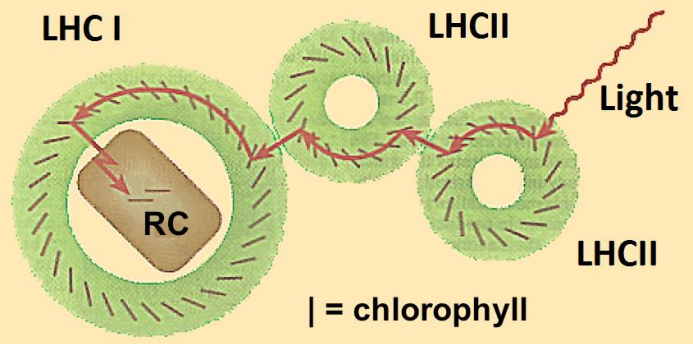

Figure 1: LHCII acts as an auxilliary antenna that collects light and passes it on to LHCI, part of PSII, which contains the reaction centre[3]

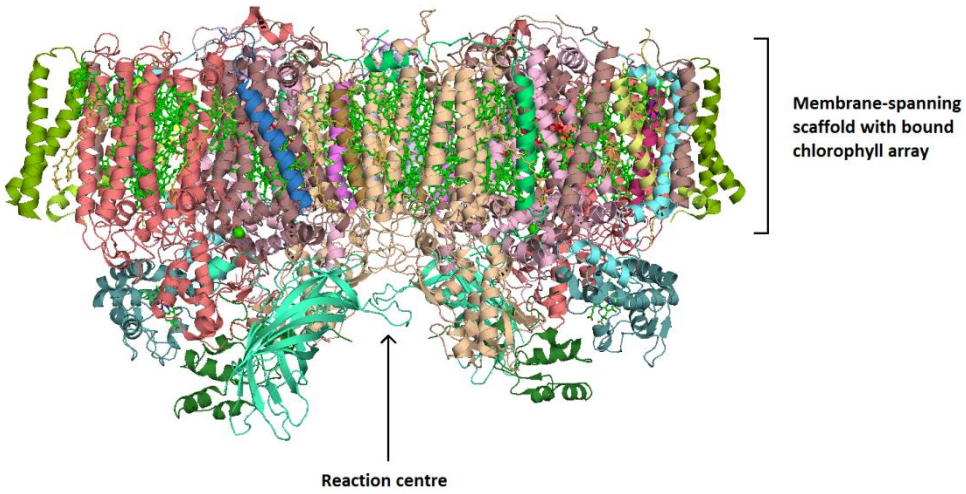

Figure 2: The structure of PSII showing the membrane-spanning α-helices, which bind the array of light-harvesting chlorophyll molecules[4,5]

When a photon is absorbed by the light harvesting array of LHCI or II, it raises a chlorophyll molecule into an excited state by promoting an electron into a higher energy orbital. The excited state represents a unit of energy, and may be referred to as an exciton for convenience. The exciton is then passed between chlorophyll molecules, just as electricity is conducted down a wire, until it reaches the reaction centre of PSII, where it drives electron transfer for energy storage (Figure 3).

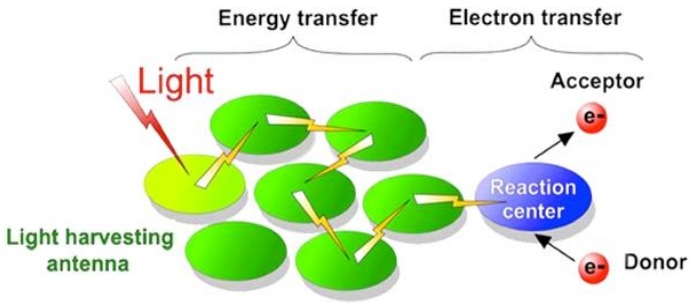

Figure 3: The chlorophyll molecules are arranged so that excitons are conducted to the reaction centre where they are used to drive the removal of electrons from water for use in fuel and materials production[6]

1.2.1 Charge separation and energy storage

When the excitons from the light-harvesting chlorophyll array reach the reaction centre of PSII, they are used to drive charge separation (Figure 4). The reaction centre consists of a "special pair" of chlorophyll molecules (called P680 for their maximum absorption wavelength), which, when excited by photonic energy, pass an electron to a nearby primary acceptor: a non-metalated chlorophyll molecule called "pheophytin" ($PheoD_1$). The electron is then passed to a tightly bound plastoquinone molecule (Q_A), and finally to a second plastoquinone molecule (Q_B), which carries the electron away from the complex.[7] The voltage of the electron while it is carried by reduced Q_B has been determined to be 140 mV *vs* SHE, meaning that is has been raised by 1.37 V since being removed from water.[8] At this voltage it could be used to reduce water to form hydrogen gas, but in the natural system the electron moves on to photosystem I, which uses light in a very similar manner to PSII to further raise the voltage, making it high enough to reduce $NADP^+$ (Figure 5). It is this reduced $NADP^+$ that is used in the reduction of carbon dioxide to produce energy-storage and structural materials *via* the Calvin cycle.

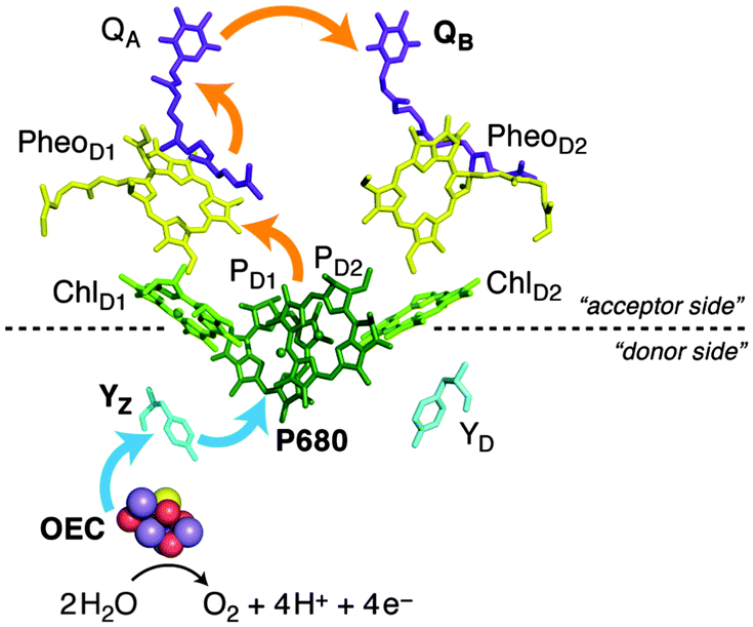

Figure 4: The pathway taken by electrons at the PSII reaction centre. Electrons donated from the special pair (P680) travel first to a pheophytin ($Pheo_{D1}$) and then onto tightly-bound plastoquinone A (Q_A) followed by a second plastoquinone (Q_B) which carries the electron away from the complex. Electrons removed from water, catalysed by the oxygen evolving complex (OEC), move *via* a tyrosine residue (Y_Z) to reduce P680 to its neutral state. Only one branch of the duplicated system is active (fig. reproduced from Retegan *et al.*[9])

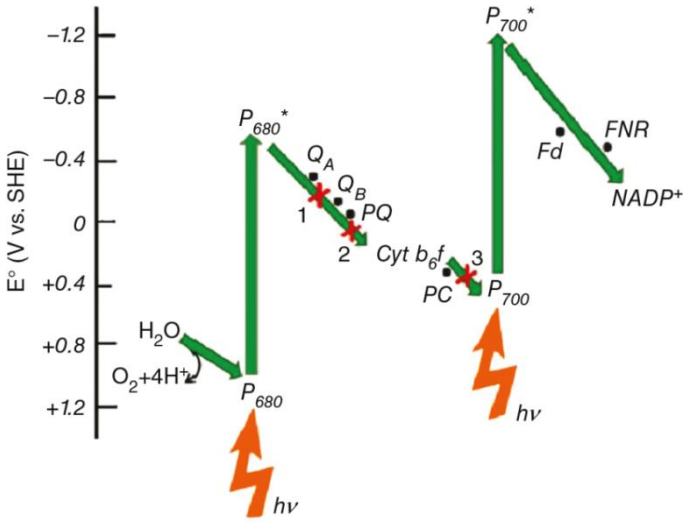

Figure 5: The movement of electrons through the photosystems. Electrons are removed from water and boosted in voltage by photosystem II. They are then carried to photosystem I *via* intermediate electron shuttles, where their voltage is raised further, and eventually used to reduce $NADP^+$ (fig. reproduced from Voloshin *et al.*[10])

Meanwhile, the "hole" left on the special pair is transferred *via* a tyrosine residue to the oxygen evolving complex (OEC) of PSII, which neatly catalyses the four-electron oxidation of water. This reaction is not trivial, and uses a highly effective catalyst in the form of a manganese cluster to accomplish water oxidation with minimal overpotential.[11] A large antenna system is required for light harvesting because on the molecular scale, solar photons are relatively diffuse. If charge separation at the reaction centre were driven by a single pigment, it would occur far too infrequently to keep up with the demand of the OEC, and intermediate states of the catalyst would decay before complete four-electron oxidation of water could be realised.[1]

The process of natural photosynthesis demonstrates the functionality of the combination of a light harvesting array, a reaction centre in which charge separation takes place, and water oxidation and carbon dioxide reduction catalysts. If all of these parts can be brought together in an artificial ensemble, artificial photosynthesis will be realised, and self-assembly of the components in protein scaffolds may offer a way of achieving this.

1.3 Porphyrinoid-protein conjugates

1.3.1 Natural ensembles

The entire molecular machinery of the natural photosystems is housed within highly complex membrane-bound protein scaffolds.[1] The scaffold of PSII holds the array of light-harvesting pigments, the OEC and electron carriers. The crystal structure of PSII illustrates the complexity of the system[2,12] (Figure 2). It consists of a block of membrane-spanning α helices which hold the array of light-harvesting chlorophyll A molecules. In the centre of the complex lies the the OEC, where water oxidation takes place.

PSII is not the only instance of a natural protein ensemble incorporating a porphyrinoid cofactor, and in fact such assembles are common in nature. For example, cytochrome C, a vital electron carrier of the electron transport chain, which generates ATP in mitochondria, consists of a heme B cofactor bound in a protein scaffold. Its function involves the carriage of an electron using the transition of the heme-bound iron ion between the II and III oxidation states.[13] Protein scaffolds have enabled heme B to be adapted to suit a diverse range of other roles, such as catalysts for the oxidation of organic compounds,[14] and oxygen carriers.[15]

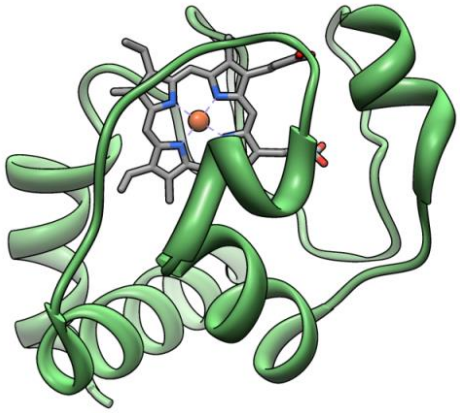

Figure 6: The structure of cytochrome C, showing the α-helices and the bound heme B cofactor[16,17]

Protein scaffolds enable the construction of such complex assemblies by utilising the self-assembly of the cofactors into their binding sites. Clearly the combination of a porphyrin cofactor and a protein scaffold could be a powerful tool for creating functional molecular machines to serve humanity, especially for the much-desired synthesis of fuel and energy-rich materials. However, the protein scaffolds produced by nature are often highly complex and fragile and not amenable to modification for experimentation. *De novo* designed artificial proteins called maquettes have been made as a method of experimenting with such scaffolds.

1.3.2 Protein maquettes

Artificial protein structures called maquettes have been developed in order to research and utilise the advantageous properties of protein scaffolds for the construction of functional molecular devices. They typically consist of four α helices joined by linking regions.[18] The amino acid sequences are chosen to place hydrophobic residues in a line on one side of each α helix, so that hydrophobic packing forces drive the helices to lie alongside one another to form the "block" tertiary structure shown in Figure 7. They have been formed using solid phase peptide synthesis techniques[19] and more recently *via* gene insertion into e-coli bacteria.[20]

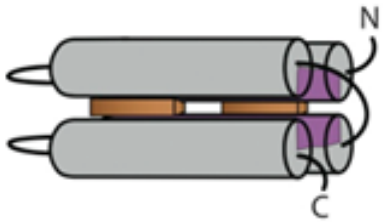

Figure 7: The block structure of the maquettes used in the binding experiments. Bound cofactors appear in brown

A maquette alone has no inherent utility in driving or catalysing chemical reactions; it is merely a scaffold. Maquettes can be endowed with functionality *via* the binding of cofactors, as occurs with many natural proteins. Most porphyrin-maquette ensembles constructed to date have utilised the natural iron porphyrin heme (or a derivative) as the prosthetic group.[19–22] This is because of its ubiquity and adaptability in nature, and the long history of publication regarding its behaviour as an oxygen carrier, electron shuttle and catalyst. In fact, artificial models of electron carriers,[23] oxygen binders[24] and light harvesting proteins have been created using heme.[25,26]

Sharp *et al.* from the group of P. Leslie Dutton produced in 1998 a protein maquette "flavocytochrome" complex containing heme derivatives and flavin molecules[21] (Figure 8). This complex was photochemically active, but was distinctly different from the natural photosynthetic system in that it was the absorbance of a photon by the *flavin* molecule that would trigger an electron transfer event; the porphyrin, metalated with iron, functioned as an electron acceptor.

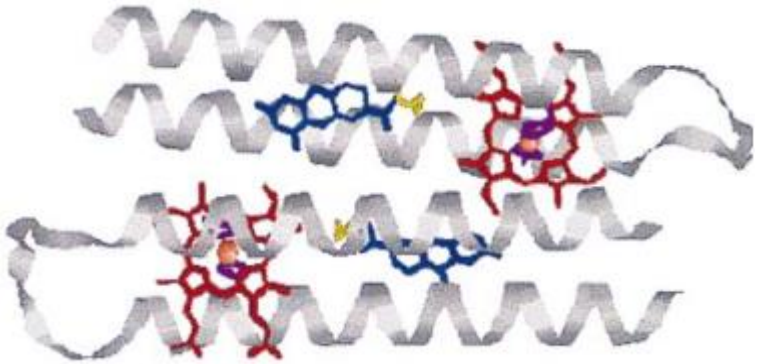

Figure 8: The flavocytochrome maquette of Sharp *et al.* which exhibited electron transfer on photon absorption (fig. reproduced from Sharp *et al.*[21])

More recently, in 2015, the same group published work concerning the creation of a protein maquette in which photoexcitiation of a zinc porphyrin (specifically, a heme molecule in which iron had been replaced with zinc) resulted in an electron transfer to a plastoquinone molecule also bound to the maquette.[27] This is directly analogous to the first electron transfer event in natural photosynthesis in plants in which an electron is transferred from the "special pair" of chlorophyll molecules to a quinone acceptor *via* a pheophytin intermediate.[9]

It is evident from the work described above, that maquette research is at a very exciting stage, and is poised to produce functional ensembles consisting of light harvesting porphyrin arrays to drive electron flow which may be used for chemical energy storage.

Binding of cofactors to maquettes

Heme B is an amphiphilic molecule, as it bears two carboxylic acid groups on one side while the rest of the molecule is hydrophobic (Figure 9). It is proposed that its amphiphilicity is important for binding to proteins; the hydrophilic groups endow it with a degree of water solubility so that it may enter aqueous solution and come in to contact with a protein binding site, while the hydrophobic part of the molecule is naturally pushed into the protein core due to hydrophobic interactions.

Chlorophyll A is much more hydrophobic than heme, bearing no groups that may be easily ionised and a long hydrophobic chain. It may be that hydrophobic partitioning also plays an important role in binding it to the protein scaffolds of the photosystems.

Heme B also possesses an iron atom bound in its centre, which endows it with its useful redox properties and enables it to co-ordinate axially, either to one ligand, forming a pentacoordinate complex, or with one ligand at each face, forming a hexacoordinate complex.[28] Such ligation can be utilised for binding inside a protein scaffold and to tune the porphyrin's redox properties for a specific application.[29] Chlorophyll contains a bound magnesium ion, but this metal is not ligated in the photosynthetic complexes.

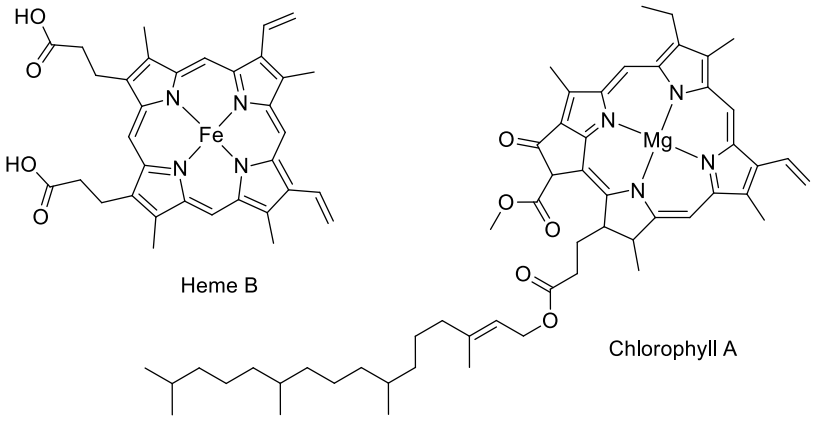

Figure 9: The ubiquitous natural porphyrin, heme B bears hydrophilic and hydrophobic regions while chlorophyll A is more hydrophobic

Although heme effectively performs a variety of roles in nature, and chlorophyll is an effective light-harvester in natural photosystems, they are adapted for the natural systems rather than artificial applications, and to continue maquette research using only these natural compounds would be highly restrictive. Producing entirely novel porphyrins that can be paired with artificial protein maquettes offers the possibility of creating porphyrin-maquette ensembles tailored for a wide range of roles. In order to achieve this, it is necessary to ascertain the properties that a porphyrin must possess in order to bind well to a protein maquette. In order to understand these requirements, it would be advantageous to test the binding properties of a variety of porphyrins with various steric requirements and arrangments of hydrophobic and hydrophilic groups.

Because of the small size of maquettes relative to the natural scaffold of LHCI, it is not possible to construct a large array of light harvesting porphyrins *via* maquette binding; the maquettes currently available bear only two porphyrin binding sites. The construction of a covalently-linked multiporphyrin array around a porphyrin known to bind may offer a solution to this problem (Figure 10), and the synthesis of such arrays is discussed in Section 1.4.4.

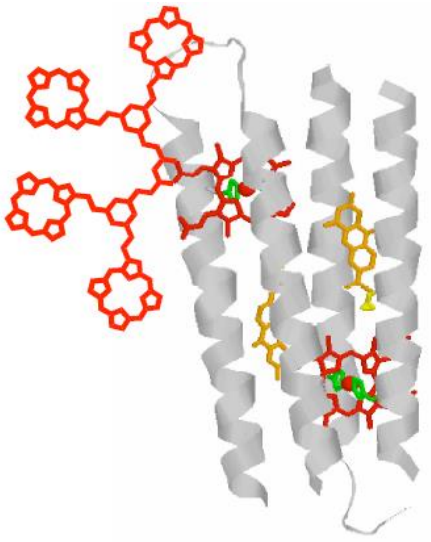

Figure 10: Binding a porphyrin array to a maquette offers a way to increase its light harvesting capability without requiring a large protein scaffold like those used by the natural light harvesting complexes

1.4 The porphyrins

1.4.1 Properties of porphyrins

The porphyrin structure consists of an extended aromatic system of 22 π electrons. There are two types of carbon atom in the molecule with distinctive reactive properties, the β-pyrrolic positions and the *meso* positions (Figure 11).

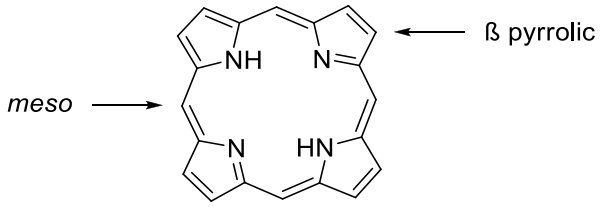

Figure 11: The porphyrin ring structure with the two distinct sites of substitution, the meso and β-pyrrolic postions

The 22 π electrons cannot all participate in the aromatic system at once, and instead the molecule exists as two tautomers, each with an 18 π electron delocalisation pathway and leaving two isolated double bonds (Figure 12).

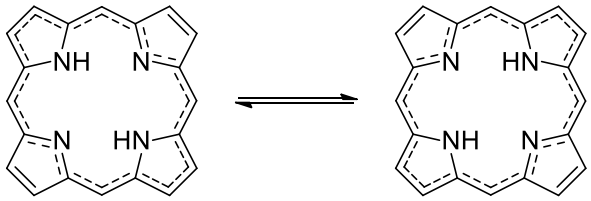

Figure 12: The equilibrium of tautomers of the porphyrin core

The two protons of the core nitrogens can be removed with a strong base to leave a dianion. In this state the porphyrin can act as a tetradentate ligand and bind a variety of

different metal ions (*vide infra*). The core will also accept two extra protons from a relatively weak acid to form a dication.

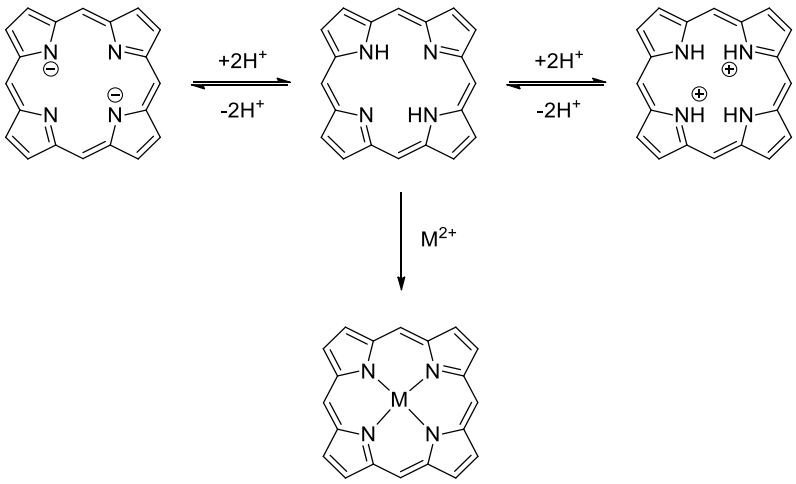

Figure 13: Deprotonation, protonation and metalation of the porphyrin molecule

The extended conjugation gives the structure the property of absorbing visible and UV light, and the spectrum may be modified by substituents on the ring as well as by the binding of metal ions. The spectrum of a typical porphyrin, tetraphenylporphyrin, is shown in Figure 14. The strongest absorption band is at around 420 nm, and this is called the B band or Soret band. There are typically four other less-intense absorption bands between 450 and 700 nm, and these are known as Q bands.

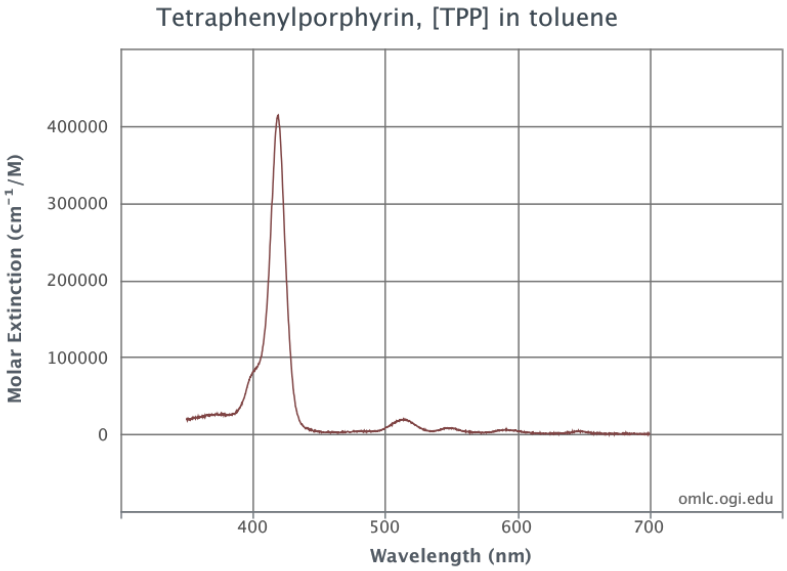

Figure 14: The UV-vis absorption spectrum of tetraphenylporphyrin (TPP) in toluene[30]

It is clear that porphyrins absorb most strongly toward the violet end of the visible spectrum. The utilisation by nature of the partially-reduced porphyrinoid pigments, the chlorins and bacteriochlorins, for light harvesting, can be explained because of their much greater absorption of light at longer wavelengths. However, the porphyrins are by far the simplest to produce synthetically, and have good light absorption and electrochemical properties, and therefore form the foundation of the work described in this thesis.

1.4.2 Laboratory synthesis of porphyrins

Historical syntheses

The earliest porphyrin syntheses were targeted at producing compounds identical or similar to those in nature, often with the aim of merely elucidating the structure of these natural pigments. Hans Fischer accomplished the total synthesis of heme B (Figure 9) in a heroic effort in the days before mass spectrometry and NMR spectroscopy.[22] Throughout the

twentieth century, porphyrin chemistry advanced substantially, and in 1990 Robert B. Woodward published an impressive total synthesis of chlorophyll A (Figure 9).[23] Both Fischer and Woodward were awarded Nobel Prizes for their monumental achievements.

Since then, the direction of porphyrin chemistry has changed significantly. Porphyrins may bear substituents in either the β-pyrrolic positions or *meso* positions (or both). Natural porphyrins are typically functionalised in the β-pyrrolic positions, with the *meso* positions left unsubstituted, and while techniques to produce porphyrins bearing β-pyrrolic substituents were developed earlier, they require many synthetic steps and are consequently low-yielding and time-consuming. The majority of recent porphyrin syntheses therefore produce products with only *meso* substitution, and the most commonly-used method is the condensation of pyrrole with one or more aldehyde reagents.

Porphyrin synthesis via condensation of aldehydes with pyrrole

The most commonly used method of porphyrin formation involves the reaction of the α positions of pyrrole with an aldehyde in a series of acid-catalysed cyclic electrophilic aromatic substitution reactions. Initially the aldehyde and pyrrole condense to form chains which may cyclise to form a porphyrinogen (Figure 15), or continue to grow to form oligomers. The formation of oligomeric side products is the main reason that the yields of these reactions rarely exceed 50%. To form the porphyrin, the porphyrinogen must be oxidised, with six hydrogen radicals being removed. This is most often achieved with atmospheric oxygen or with a quinone oxidant. Historically, the condensation was performed at high temperatures and pressures and over long reaction times, but two main methods have emerged that offer convenient and high yielding syntheses in short reaction times and under gentler conditions.

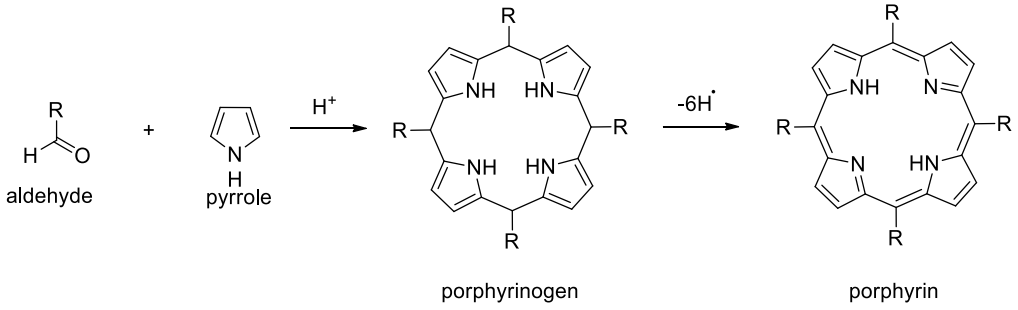

Figure 15: Porphyrin synthesis *via* condensation of an aldehyde with pyrrole, first to form a porphyrinogen, and finally a porphyrin, following oxidation

The method of Adler[31] involves the reaction of pyrrole and an aldehyde in refluxing propanoic acid and offers high yields, but requires that the reagents tolerate the harsh conditions involved.[31] In this type of synthesis, atmospheric oxygen is most often used to oxidise the porphyrinogen. More sensitive reagents may be used in the method of Lindsey,[32] in which the aldehyde and pyrrolic reagents react at room temperature in DCM or chloroform, with a catalytic quantity of acid, and are oxidised to the porphyrin by the addition of a solid oxidant, usually the quinones DDQ or chloranil.[32]

Mixed-aldehyde condensation

When a mixture of two aldehydes is reacted with pyrrole in a porphyrin synthesis reaction, six permutations of product are produced, bearing 0, 1, 2, 3 and 4 of a given functional group, as shown in Figure 16,[33] and in the ratio shown in Table 1 (assuming the aldehydes have similar reactivity). Note that two isomers of the disubstituted porphyrin, bearing two of each functional group, are produced, and these are named according to the cyclic distribution of their functional groups using the shorthand *ABAB* and *AABB*. The benefit of such a synthetic approach is its convenience; although the two products with C_4 symmetry (*AAAA* and *BBBB*)

could be made in a single-aldehyde condensation, the four less-symmetrical of these compounds would otherwise require more complex stepwise syntheses. Thus, by producing all of these compounds in a single reaction, much time and effort is saved. While the literature most often reports only one or two of the product porphyrins being isolated, this technique has been used to make combinatorial libraries of porphyrins for use in photodynamic therapy.[34]

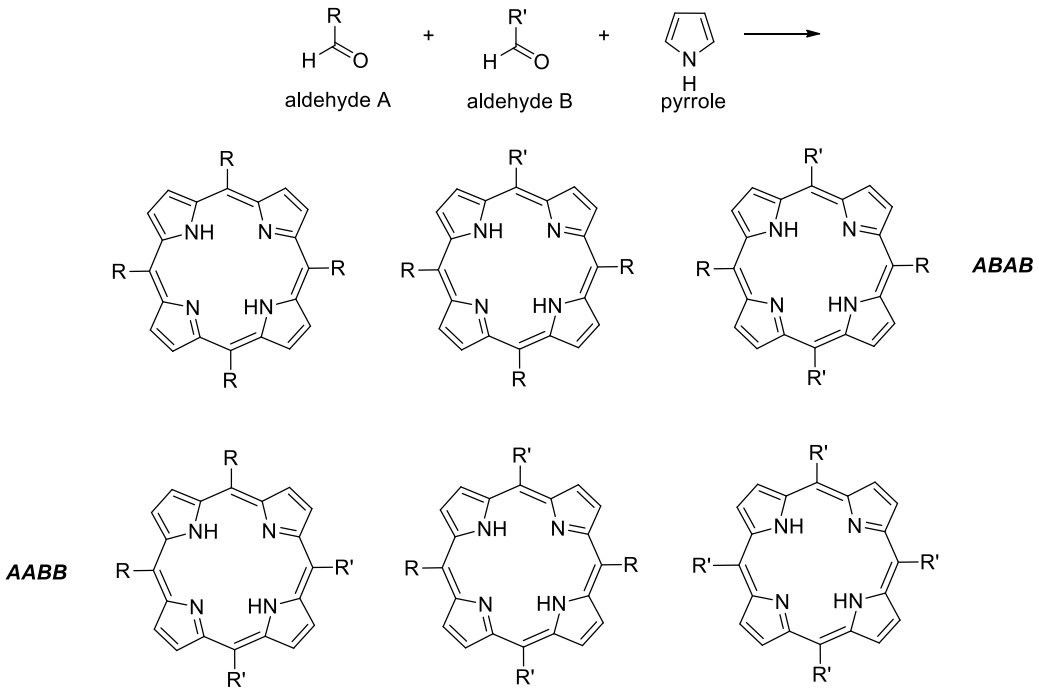

Figure 16: The generation of six porphyrin products from a mixed-aldehyde condensation

Table 1: The statistical ratio of product permutations expected from a condensation of a 1:1 ratio of aldehydes A and B, assuming identical aldehyde reactivity

AAAA	AAAB	ABAB	AABB	ABBB	BBBB
1	4	2	4	4	1

Synthesis via 2+2 condensation

If only the *ABAB* arrangement of *meso* substituents is required, then it may be possible to use a 2+2 synthesis.[35] It involves a two-step process in which firstly a dipyrromethane is formed *via* the condensation of an aldehyde with pyrrole, and secondly this dipyrromethane is condensed with a second aldehyde to form the porphyrin (Figure 17).

A dipyrromethane can be produced by performing the condensation in a large excess of neat pyrrole to prevent the formation of oligomers, with the dipyrromethane being isolated by distilling off the excess pyrrole and then submitting the residue to chromatography.[36] This procedure often results in the polymerisation of much of the pyrrole and of the dipyrromethane product. A newer procedure utilises a biphasic reaction to favour the formation of dipyrromethane and prevent oligomer formation, and thus is much less wasteful than the older method.[37]

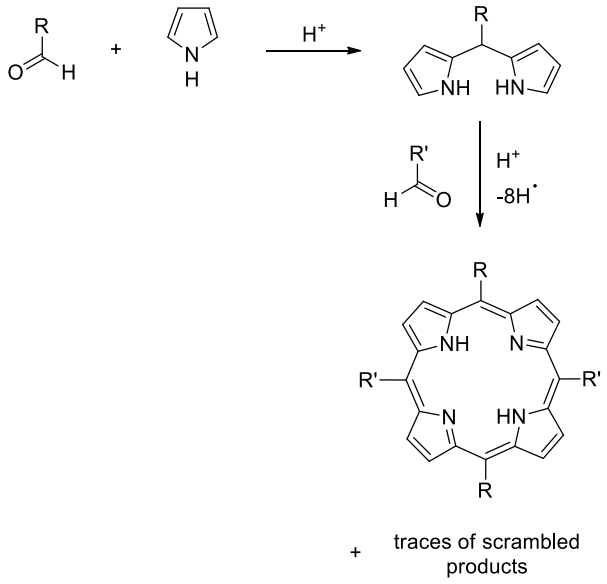

Figure 17: The synthesis of a dipyrromethane *via* the condensation of an aldehyde with pyrrole and its condensation with a second aldehyde to form an *ABAB* porphyrin in a 2+2 synthesis

The condensation of the dipyrromethane with a second aldehyde (Figure 17) produces a product mixture enriched with the *ABAB* porphyrin, but it usually also contains smaller quantities of the other members of the statistical mixture that would be generated from a mixed-aldehyde condensation of the two aldehydes. This is because of an effect called scrambling.[38] This process occurs because the reaction of an aldehyde with pyrrole is reversible; under acidic conditions the pyrromethane oligomers can undergo acidolysis to afford fragments which then may re-form into new oligomers and porphyrinogens. This process of dynamic equilibrium has the effect of scrambling the *meso* substituents to produce a complete six-product statistical mixture, even when a porphyrin is synthesised using a dipyrromethane.

More complex stepwise techniques have been used for porphyrin synthesis, for example the 3+1 synthesis *via* an intermediate tripyrrane.[39] This method can be used to form a desired porphyrin of very low symmetry, but requires many steps and is consequently low yielding, and is only suitable if a single low-symmetry porphyrin is desired. The best way to produce a library of porphyrins is to use mixed-aldehyde condensation forming statistical mixtures, as long as the product mixture is amenable to the isolation of the individual products.

Porphyrin metal complexes

A metal ion may be inserted into the porphyrin core by stirring the porphyrin with a soluble metal salt in one of a variety of solvents. Some metals may be inserted quickly at room temperature *e.g.* zinc,[46] while others require extended heating *e.g.* iron.[47] Some *e.g.* magnesium[48] are weakly bound and may be removed by a trace quantity of acid, while others are far more stable *e.g.* copper.[49] Metal ligation affects the absorption spectrum, the HOMO and LUMO levels of the porphyrin and the excited-state lifetime and fluoroescence yield. Zinc porphyrins have been found to be the most effective in dye sensitised solar cells because of

their good photoinduced electron injection into TiO_2.[40] Various other metal complexes have been found effective in the catalysis of a variety of reactions, for example, CO_2 reduction by iron,[41] cobalt[42] and copper[43] porphyrins, water oxidation by manganese porphyrins,[44] and oxygen[45] and nitrogen[46] reduction by cobalt porphyrins.

If the metal ion is in the (II) oxidation state then the complex is neutral in charge *e.g.* in the cases of zinc and copper. These metals may accept axial ligation from neither, one or both exposed faces, depending on the properties of the metal in question. For example, porphyrin-bound silver will not accept any significant ligation, zinc will typically adopt a singularly-ligated state, while iron will often bind two ligands strongly.[47] Some metals will spontaneously adopt a (III) oxidation state in the presence of atmospheric oxygen, and therefore must be accompanied an anion *e.g.* iron and manganese porphyrins.

1.4.3 Water soluble and amphiphilic porphyrins

Synthetic porphyrin compounds reported in the literature are most often hydrophobic. These compounds are in fact often not very soluble in any solvent due to π stacking interactions, and often bulky *meso* substituents, especially benzene rings, are added in order to suppress this type of aggregation. In order to make these compounds water-soluble, several different hydrophilic groups have been added. Sulfonic acid groups may be added to tetraphenylporphyrin by treating it with sulfuric acid,[48] and this is a common method of water solubilisation (Figure 18). The conditions are harsh however, and not suitable to any porphyrin bearing sensitive functional groups.

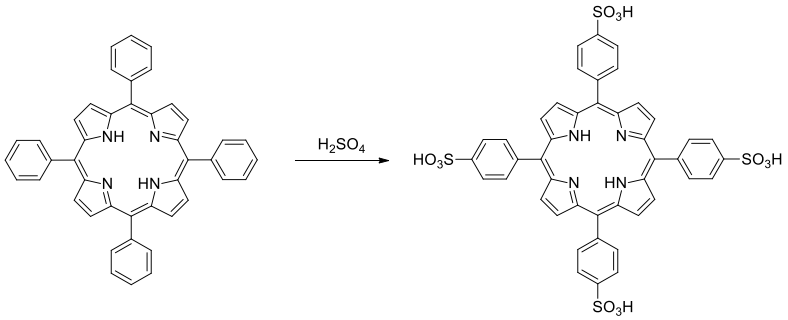

Figure 18: Treatment of tetraphenylporphyrin with sulfuric acid to generate the water soluble tetrasulfonic acid

Another common water solublisation technique is the generation of a tetraquaternary ammonium salt from tetrapyridylporphyrin. This is most often accomplished by treatment of the latter with an alkyl iodide, most often methyl iodide, *e.g.* by Gomes *et al*.[49] (Figure 19).

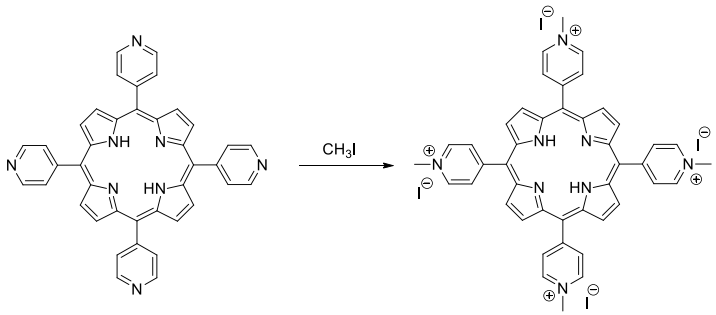

Figure 19: A water soluble tetraquaternary ammonium salt porphyrin may be synthesised by treatment of a tetrapyridyl porphyrin with methyl iodide

Carboxylic acid groups are effective for water solubilisation, and porphyrins may be synthesised with such groups already in place.[50] Often however, the porphyrins are synthesised bearing ester groups, which are then hydrolysed to reveal the carboxylic acid (Figure 20).[51]

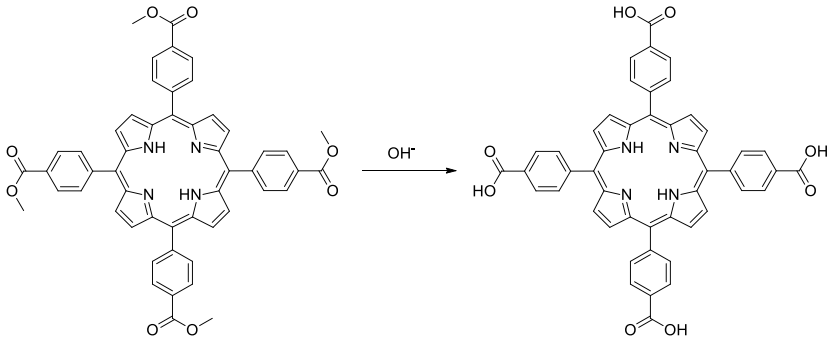

Figure 20: A commonly-used water soluble porphyrin is the tetracarboxylic acid, which is most often generated *via* hydrolysis of the analogous tetraester

The water soluble porphyrins shown above still suffer from solubility problems due to π stacking, and attaching more than four hydrophilic groups to the porphyrin significantly improves solubility. For example, Jee *et al.* produced a porphyrin bearing 16 carboxylic acid groups using the nucleophilic substitution of a bromoporphyrin by diethyl malonate, with subsequent hydrolysis.[52] The hydrophilic groups do not necessarily need to be ionic, and the attachment of poly(ethylene glycol)chains has been used to produce water soluble porphyrins, *e.g.* by Villari *et al.*,[53] and Zhang *et al.* attached cylodextrin molecules using a copper catalysed azide-alkyne cycloaddition[54] (Figure 21).

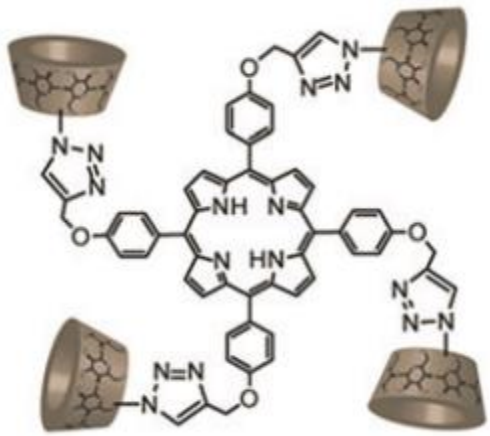

Figure 21: A cyclodextrin-appended water-soluble porphyrin (fig. reproduced from Zhang *et al.*[54])

Amphiphilic porphyrins have been most-often produced for use in photodynamic therapy. This form of medical treatment utilises the singlet oxygen-generating properties of porphyrins under light irradiation to destroy cells. The strategies used to produce porphyrins of this type typically involve the attachment of one or more hydrophilic groups to the otherwise-hydrophobic porphyrin macrocyle. This has been accomplished using mixed-aldehyde condensation (as discussed previously) to produce a statistical mixture of porphyrins with one to four hydrophilic groups (or groups from which a hydrophilic group is then formed or attached). If it is desired to produce a compound that has good water solubility but also has a large hydrophobic part, then it may be necessary to attach a dendritic amphiphilic group. Several examples of this are covered in a review by Pisarek *et al.*,[55] one of which was produced by Choi *et al.* and is shown in Figure 22.[56]

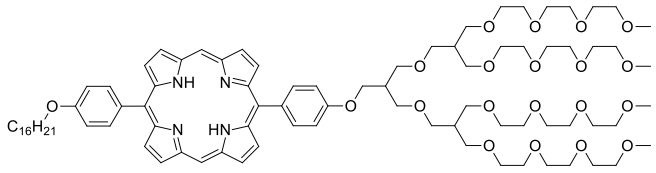

Figure 22: A dendritic amphiphilic porphyrin synthesised by Choi *et al.*[56]

1.4.4 Porphyrin arrays

Inspired by the remarkable light harvesting arrays discovered in plants, a vast number artificial porphyrin-based mimics have been created, and energy transfer within artificial arrays has been observed.[57] Arrays have been constructed using carbon-carbon covalent linkages through the *meso* position, the β-pyrrolic position and combinations of both.[58] Supramolecular assemblies of porphyrins have also been created.[59,60] However, only a small subset of these arrays have been demonstrated to conduct photons or induce electron transfer events following photonic excitation. There is a large amount of literature concerning the

construction of porphyrin arrays, but the general techniques are well represented by a handful of examples, and these are reviewed below.

Covalent linkages

Many different reactions have been used to link porphyrins *via* the *meso* position because of the relative ease of introducing the required reactive functional groups by using appropriate aldehydes during porphyrin synthesis. Norsten and Branda[61] used a nucleophilic substitution reaction to produce a porphyrin pentad with ether linkages (Figure 23). They used the reaction of a deprotonated phenol with a benzylic chloride to form the linkage. The array bore ester groups on the peripheral porphyrins, but these were not hydrolysed to produce a hydrophilic array. No photochemical characterisation was performed on this array.

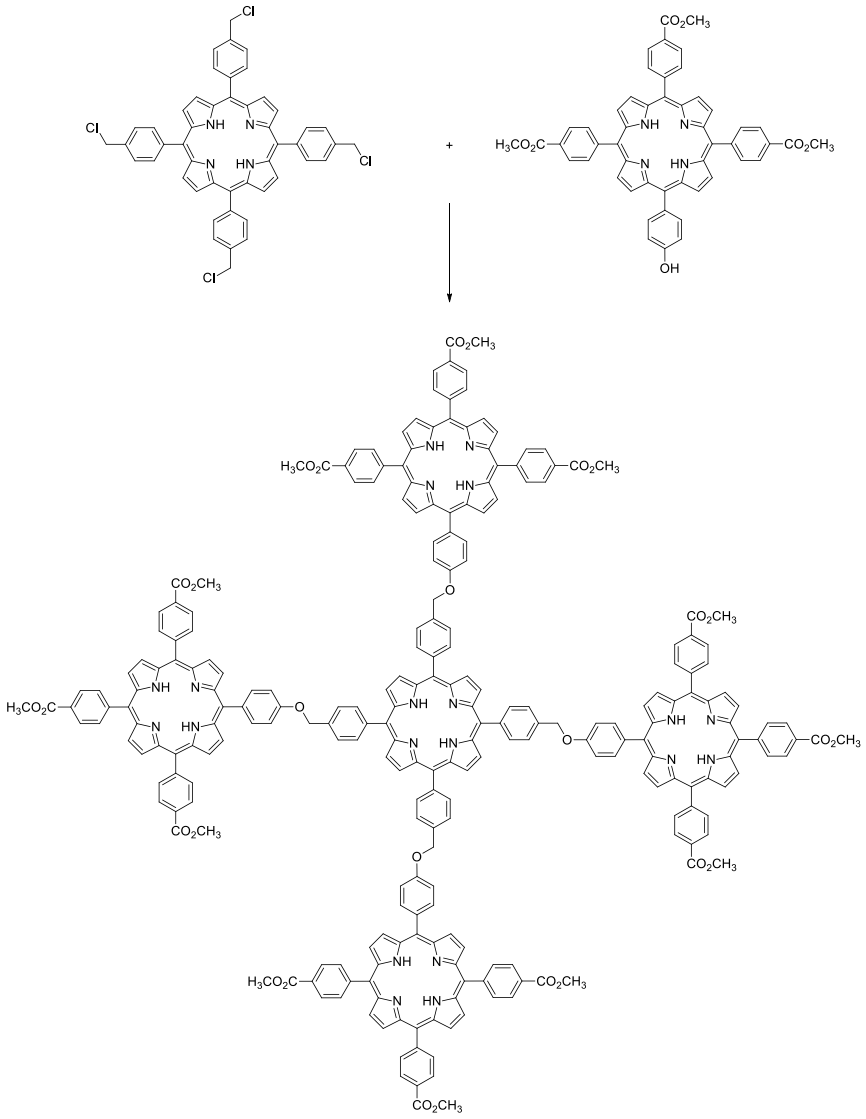

Figure 23: Array formation *via* nucleophilic substitution by Norsten and Branda[61]

Another linker that has been often employed is the amide linkage. Dubowchik and Hamilton[62] were able to produce a cylic tetramer (Figure 24) using the linkage of a porphyrin diamine and a porphyrin dicarboxylic acid, with the carboxylic acid being converted to the acid chloride prior to the reaction. Their tetramer was formed from porphyrins with β-pyrrolic functionalisation, which is perhaps reflective of the fact that the work was published in 1987, before *meso* subsituted porphyrins surpassed such porphyrins in popularity.

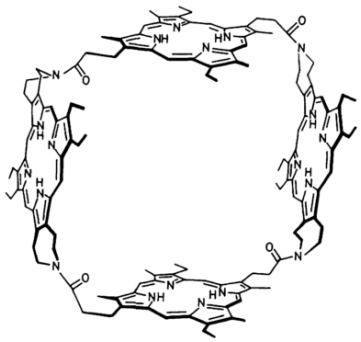

Figure 24: A cyclic porphyrin tetramer formed using amide linkages (fig. reproduced from of Dubowchik and Hamilton[62])

While nucleophilic substitution and amide linkages are relatively easy to form, energy transfer between porphyrin arrays depends on the linker type, with conjugated linkers often being preferable. Metal-catalysed cross-couplings are the most common method for forming such linkers, and a large variety of reaction and linker types may be found in the literature.

Suzuki coupling has been used to form phenylene-linked porphyrin arrays, for example by Yu and Lindsey,[63] and also to form ethene linkages directly joining two porphyrin rings, for example by Locos *et al.* (Figure 25).[64]

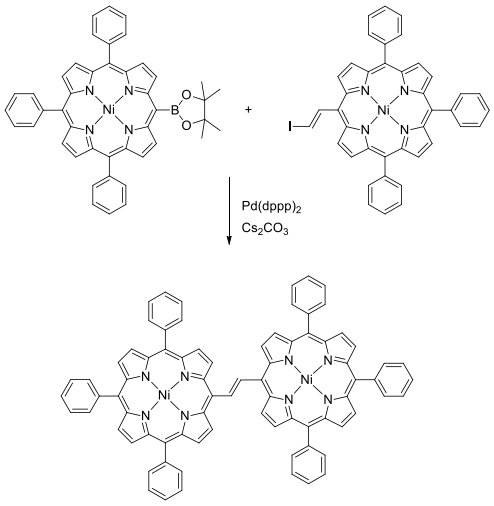

Figure 25: The method used by Locos *et al.* to produce a vinyl-linked dyad *via* Suzuki coupling[64]

Ethynyl linkers formed *via* Songashira coupling have become very popular because of the rigid, linear and conjugated connection between the porphyrins that is produced. Perhaps the most interesting example of a porphyrin array formed in this way is the work of Kuciauskas *et al.*[57] (Figure 26). This array is special because of its demonstrated functionality; photonic excitation of any of the peripheral zinc porphyrins results in energy transfer through the array to the free base porphyrin, which then passes an electron to the fullerene to produce a charge-separated state.

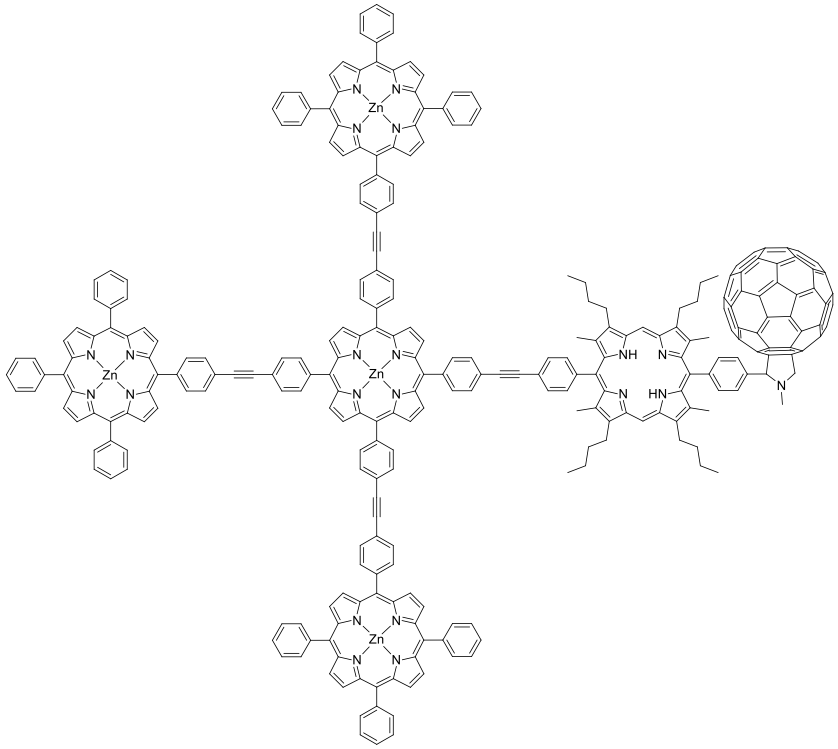

Figure 26: A light harvesting porphyrin array with artificial reaction centre (fig. reproduced from Kuciauskas *et al.*[57])

Porphyrin oligomers linked directly *via* the meso positions were produced by Tsuda and Osuka.[65] The reaction was performed by treating the *meso*-unsubstituted porphyrin reagents with Ag(I). It was also discovered that the β-pyrrolic positions could be linked to form a

porphyrin “tape” by treating the *meso*-linked oligomers with DDQ, with the oxidation reaction being catalysed by scandium(III).

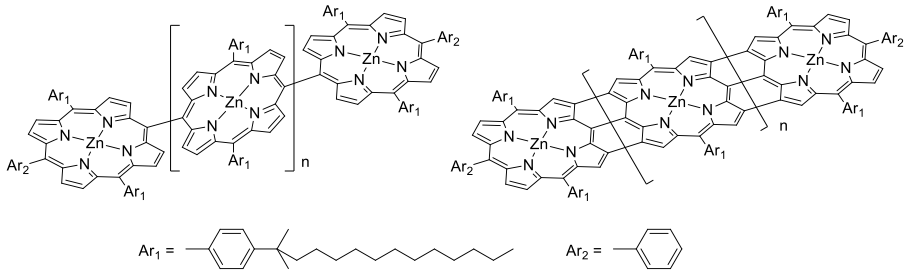

Figure 27: The porphyrin tapes produced by Tsuda and Osuka[65] with both a single direct *meso*-*meso* linkage or a triple linkage consisting of a direct *meso*-*meso* linkage and two direct β-β linkages

Another technique for producing porphyrin arrays is mixed-aldehyde condensation, where one of the aldehydes is already attached to a porphyrin molecule and a new porphyrin is formed around this group. Phenylene-linked arrays have been produced by this method by Wennerstrom,[66] the largest of which was a pentad (Figure 28). The technique can present chromatographic challenges and also makes differential metalation of the porphyrin rings within the array difficult. It does, however, offer the advantage of requiring few chemical steps, proceeding *via* intermediate compounds which are tolerant of oxygen, light and water, and being highly adaptable and robust.

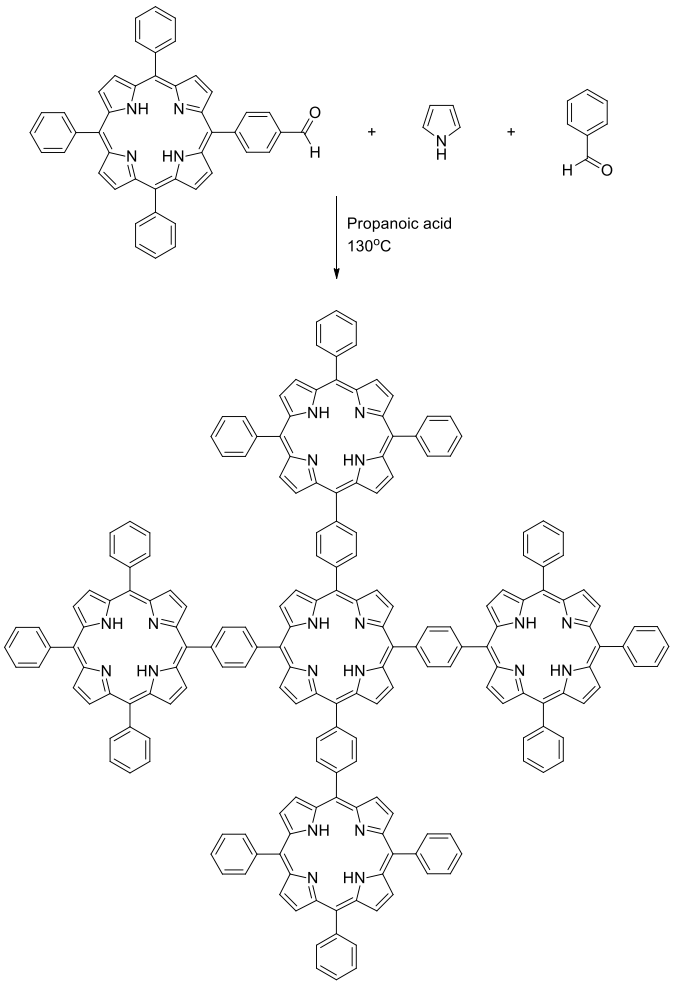

Figure 28: Wennerstrom's synthesis of a porphyrin pentad[66]

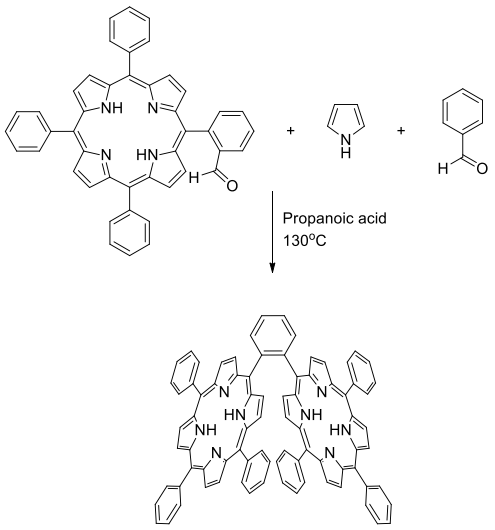

Figure 29: The formation of a "gable type" cofacial porphyrin *via* mixed-aldehyde condensation by Meier *et al.*[67]

A similar method of array synthesis is that used by Meier *et al.,* who produced a "gable type" cofacial porphyrin with an *ortho* phenylene linker (Figure 29).[67] This type of porphyrin arrangement has been found to be effective in the catalysis of the four-electron oxidation of water when metalated with manganese[68] and the reduction of CO_2 when metalated with iron.[41]

Officer *et al.* used porphyrin reagents bearing aldehyde functionality on substituents on the β-pyrrolic position to form a porphyrin pentamer (Figure 30) and a nonamer.[69] The β-pyrrolic substitution was generated *via* Vilsmeier formylation and subsequent conversion to the phosphonium salt which was then reacted with phthaladehyde.

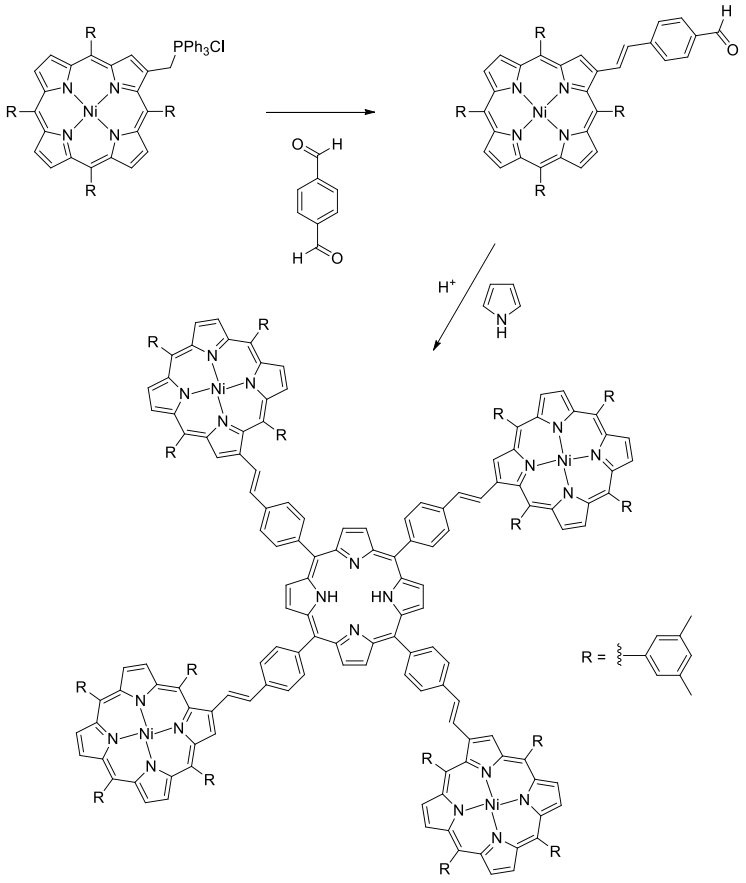

Figure 30: The synthesis of a pentamer by Officer *et al.*[69]

Supramolecular assemblies

There are perhaps more publications concerning supramolecular assemblies of porphyrins than covalently linked arrays. They have most often been produced taking advantage of the two extra co-ordinating sites of a metal ion bound in the porphyrin core.[58] Such complexes have an advantage over covalently-linked arrays in that they self-assemble, and are therefore easier to produce, especially in the case of very large arrays.

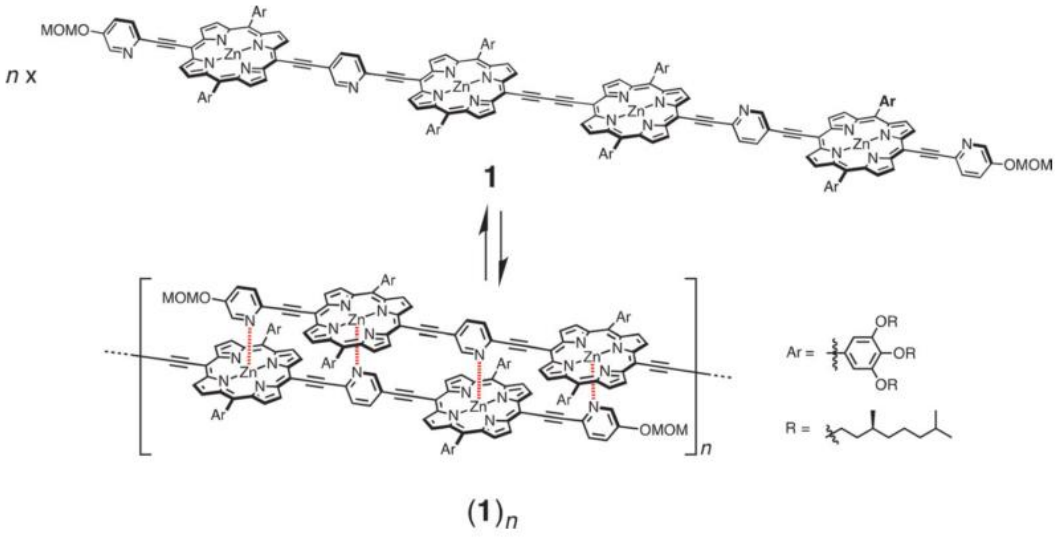

Figure 31: The formation of a supramolecular polymer from a covalently-linked four-porphyrin unit (fig. reproduced from Morisue *et al.*[59])

A functional supramolecular linear array was produced by Furutsu *et al.*[60] (Figure 32). It was formed from porphyrin dyads bearing imidazole groups at either end. Bonding between porphyrin-bound zinc ions and imidazole groups causes a linear supramolecular complex to form spontaneously. Evidence was obtained showing that energy transfer within the array occurs. It was observed that when a manganese porphyrin unit was added, that this added to the ends of the array and acted as an electron or energy acceptor, and thus quenched the fluoroscence of the whole zinc porphyrin array.

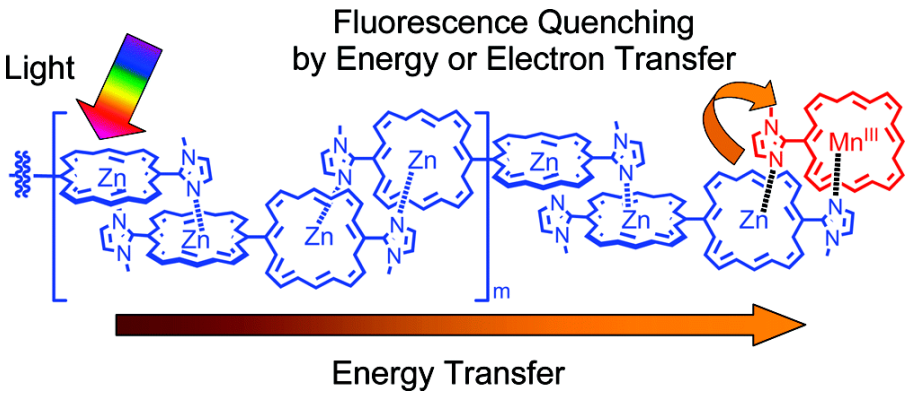

Figure 32: A functional self-assembled supramolecular linear array (fig. reproduced from Furutsu *et al.*[60])

The above are a sample of the variety of techniques that have been used to produce porphyrin arrays, but photochemical characterisation of these arrays has been relatively rare. When photochemical characterisation has been performed, it typically shows that arrays with conjugated linkers typically have broader absorption spectra, with increased absorption especially at longer wavelengths. Non-conjugated arrays typically exhibit transfer of photons between porphyrins, as long as the chromophores are sufficiently close.[57,60]

It may be seen from the published work reviewed above that there are a large number of porphyrin linking techniques available. In order for the array to bind to the maquette and be functional, it was expected that covalent linkages would be preferable because of their chemical stability and energy transfer characteristics.

In order to bind to a protein maquette, an array will likely require an amphiphilic character, but very few water-souble porphyrin arrays, and even fewer amphiphilic arrays have been produced. Therefore in order to produce an amphiphilic array that will bind to a protein maquette and function as a light harvesting antenna, the existing techniques for array synthesis and water solubilisation require adaptation. The general goal is to produce arrays with one hydophobic porphyrin linked to one or more hydrophilic porphyrins.

1.5 Thesis aims and structure

The aim of this thesis research was to make a wide range of amphiphilic porphyrins and porphyrin dyads and undertake preliminary investigations into their binding to protein maquettes. The most effective binders were then to be passed on to fellow researchers to undertake more detailed maquette binding studies and investigations into the porphyrin-maquette ensemble applications.

The work described in Chapter 2 was aimed at generating a library of porphyrins with properties ranging between highly hydrophobic and highly hydrophilic, and with amphiphilic compounds of various geometrical arrangements in between. Zinc and iron complexes were produced so that maquette ensembles could be created that would take advantage of the special properties of these particular complexes. An amphiphilic porphyrin bearing a ferrocene group as an electron donor was produced as a first step toward producing an electronically active maquette system and control over the electrochemical properties of amphiphilic porphyrins was explored through the production and characterisation of pre-amphiphilic porphyrins bearing pentafluorobenzene rings.

Chapter 3 contains a description of work performed using HPLC analysis in order to solve the problem of assessing the isomeric purity of the *ABAB* and *AABB* porphyrin isomers isolated from the statistical mixtures generated using mixed-aldehyde condensations in Chapter 2.

The work of Chapter 4 was aimed at synthesising amphiphilic porphyrin arrays linked by phenylene rings using mixed-aldehyde condensations. Two dyads, bearing carboxylic acids and quaternary ammonium salt groups were produced.

Chapter 5 contains a description of work undertaken aimed at modifying the existing Wittig-linking procedure to produce amphiphilic porphyrin arrays suitable for binding to

maquettes. Work towards using Knoevenagel condensations to produce porphyrin arrays was also undertaken.

Chapter 6 describes the development of a variety of strategies using the properties of different metal ions to aid the synthesis of porphyrin arrays of required metalation states and to facilitate the isolation of porphyrin arrays from the by-products of their synthesis.

Chapter 7 describes the preliminary investigations carried out into the binding of the members of the porphyrin library produced in Chapter 2, and also the dyads produced in Chapters 4 and 5. This was aimed at identifying those porphyrins which bound quickly and strongly to the maquettes so that they may be investigated further in the future.

Chapter 2: Amphiphilic porphyrins from mixed-aldehyde condensations

2.1 Introduction

The goal of the work described in this chapter was to produce a library of porphyrins in order to explore the construction of porphyrin-maquette ensembles using novel porphyrin materials and to identify the properties required of a synthetic porphyrin molecule in order to have it bind well to a maquette in aqueous solution. The strategy employed was to generate a diverse library of amphiphilic porphyrins so that their maquette-binding properties could be analysed and compared, with the results to be used to construct a general theory of the requirements for binding. Porphyrins were synthesised as statistical mixtures *via* mixed-aldehyde condensation and the individual products were isolated chromatographically. This had the advantage of producing up to six porphyrin products in each reaction, an efficient way of producing a library of compounds. The synthesis and characterisation of these compounds is described in this chapter, while the maquette-binding experiments are described in Chapter 7.

2.2 Choosing hydrophilic and hydrophobic groups for mixed-aldehyde condensation

The utility of the statistical mixture approach discussed in Section 1.4.2 of Chapter 1 depends on the porphyrin products being separable from one another. Flash chromatography on silica[70] is the method of choice for such separations, and the porphyrin products must therefore possess groups which interact favourably with the stationary phase *i.e.* neither too strongly, nor too weakly. The strongly hydrophilic functional groups required to endow a porphyrin with an amphiphilic character are *not* amenable to chromatography, and therefore must be generated *via* an intermediate group or a protected form of the hydrophilic group. Esters and dimethylamines were deemed suitable for this purpose, as they are amenable to chromatography on silica and may be converted to carboxylic acids and quaternary ammonium salts (QASs) respectively, both of which are hydrophilic, and have been used successfully to make hydrophilic porphyrins in the past.[71]

Carboxylic acids can act as water solubilising groups because of their ability to form hydrogen bonds with water, and also their ability to be ionised by deprotonation, thus becoming highly polarised. While carboxylic acids are not strong acids, especially when attached to a benzene ring (the pK_a of benzoic acid is 4.2[72]), they are predicted by the Henderson-Hasselbalch equation[73] to be practically fully ionised at pH 9, the pH at which maquette binding experiments were to be conducted (Figure 33).

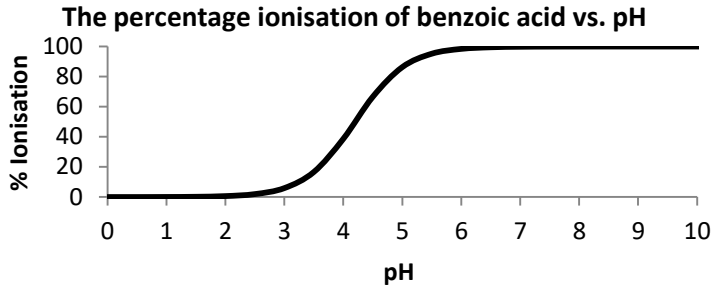

Figure 33: The percentage ionization of benzoic acid (pK_a 4.2) over a range of pH values calculated using the Henderson-Hasselbalch equation

QASs were chosen as an alternative water solubilising group, because in contrast to the negative charge of an ionised carboxylic acid, they possess a permanent positive charge. QASs lack the ability to hydrogen-bond, but due to their ionic character, offer good hydrophilicity over a wide range of pH conditions.

Benzene rings and butyl chains were chosen as the hydrophobic groups in order to test the effect of changing the groups that must enter the maquette core. Butyl chains, being more flexible than benzene rings, ought to be better able to conform to any available hydrophobic binding site. Benzene rings, however, are capable of participating in π stacking interactions with aromatic maquette amino acids, and it was unknown whether this effect would outweigh their greater steric bulk to produce stronger binding overall.

2.3 Synthesis of phenylporphyrin carboxylic acids

2.3.1 Porphyrin synthesis

The first series of porphyrins was synthesised *via* the condensation of a mixture of benzaldehyde and 4-formylbenzoic acid methyl ester with pyrrole in refluxing propanoic acid

according to the conditions of Adler[31] (Figure 34). The syntheses of these products have been published separately from one another previously, some from mixed-aldehyde condensations[74–78] and some using metal-catalysed biaryl couplings,[79–81] but no study presents a combinatorial approach in which all of these compounds are isolated from a single reaction.

The fact that these aldehyde precursors are robust enough to tolerate the high temperature of the Adler porphyrin synthesis allowed large quantities of these porphyrins to be produced in small solvent volumes compared to the alternative Lindsey synthesis conditions,[32] as described in Chapter 1.

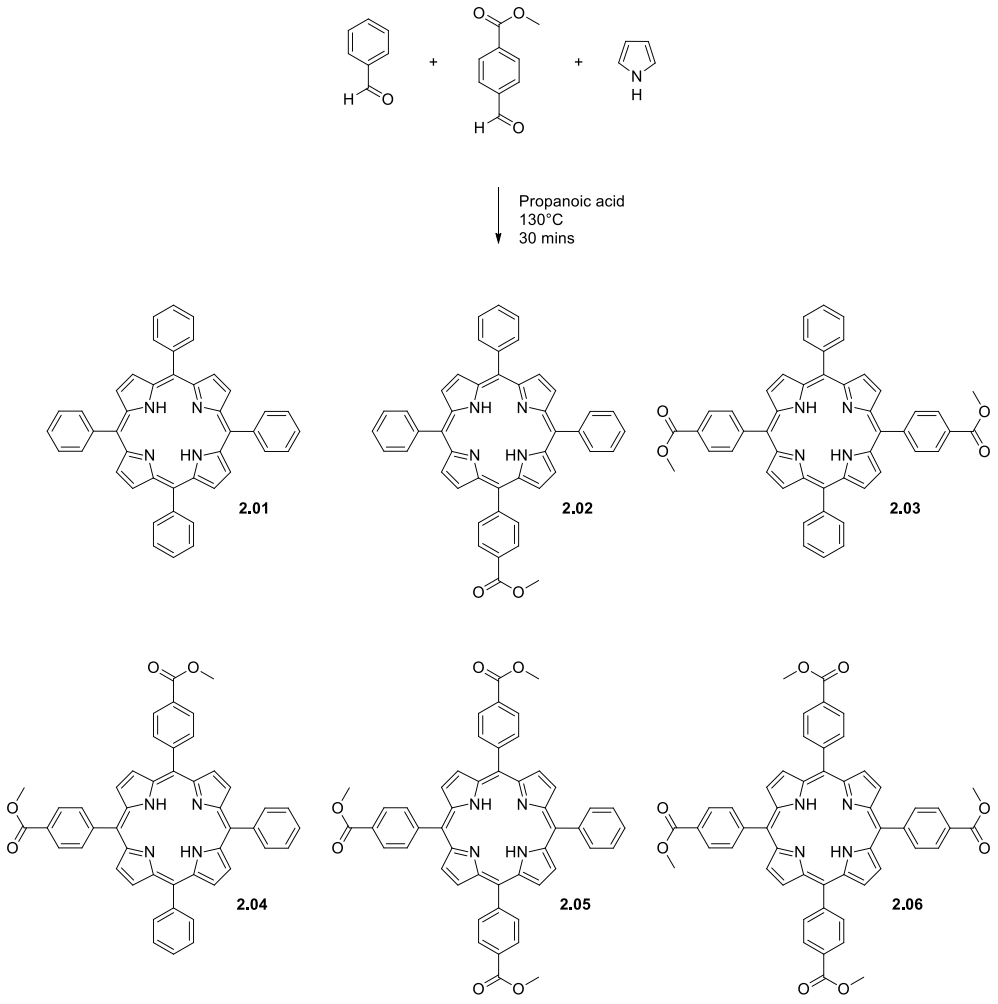

Figure 34: The mixed-aldehyde condensation used to generate the six porphyrins of this series

According to the conditions of Adler,[31] the aldehydes were added to refluxing propanoic acid followed by pyrrole, and stirred for 30 minutes before being exposed to atmospheric oxygen by bubbling air through the mixture. In many cases, porphyrins will crystallise from the propanoic acid on cooling, but in the case of these ester porphyrins, this did not occur. Therefore the propanoic acid was evaporated under reduced pressure and the individual porphyrins isolated from the residue by flash chromatography with DCM used as the eluent.

The fractions were analysed by TLC and it was evident that TPP **2.01**, the monoester **2.02** and both diesters **2.03** and **2.04** had emerged still mixed together. This was likely because the large quantity of black by-product material interfered with the proper interaction of the porphyrins with the silica. The triester **2.05** emerged uncontaminated with any other porphyrin, and following another round of chromatography to remove black material using 5% EtOAc as eluent, was found to be pure.

The mixture of TPP **2.01**, monoester **2.02** and diester porphyrins **2.03** and **2.04** were subjected to a second round of chromatography using DCM as eluent, after which only the diesters remained mixed with one another.

The diesters **2.03** and **2.04**, having similar retention properties, required progressive rounds of chromatography, according to the scheme shown in Figure 35, to purify them further. The diester-containing fractions, after emerging from a column, were analysed by TLC and sorted into two parts: "enriched *ABAB"* and "enriched *AABB"*. Each of these lots was then subjected to another round of chromatography, and the emergent fractions again sorted, according to TLC analysis, into "enriched *ABAB"* and "enriched *AABB"* but also into fractions containing sufficiently pure samples of each diester, which were set aside. After several repetitions of this process, adequate quantities of the diesters were brought to 95% purity, as estimated by TLC and confirmed by HPLC analysis (Chapter 3).

Each porphyrin, once uncontaminated by any other porphyrin, was concentrated by rotary evaporation and precipitated by the addition of methanol to remove non-porphyrin impurities. Yields are shown in Table 2. Although the tetraester **2.06** was formed in the reaction, it was not isolated and was instead synthesised in a single-aldehyde condensation according to a published procedure with a yield of 18%.[82]

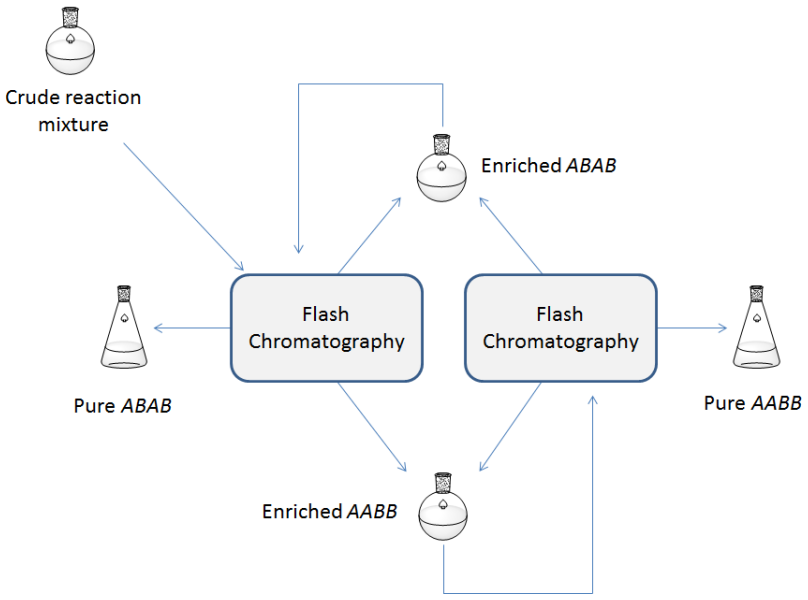

Figure 35: A schematic representation of the chromatographic process used to separate the *ABAB* and *AABB* isomers

Table 2: The percentage yield of each porphyrin isolated from the reaction and a comparison of the expected yield ratio and the actual yield ratio. The tetraester was not isolated from the mixture and so is not part of the analysis

	TPP **2.01**	Monoester **2.02**	ABAB diester **2.03**	AABB diester **2.04**	Triester **2.05**	Total
Yield %	1.8	5.4	1.0	2.0	6.2	16.4
Yield ratio	1.6	4.9	1.0	1.8	5.7	15
Statistical ratio	1	4	2	4	4	15

The ratio of yields of the porphyrin products was quite different to that expected from statistical distribution alone (Table 2). The largest deviation was for the diesters, which can be attributed to losses during purification; because of the difficulty in separating these compounds from one another, not all product material could be isolated in pure form. Other deviations of yield from the statistical prediction can be explained by differences in the reactivity of the two aldehydes and losses during purification *e.g.* by irreversible adsoption onto silica and incomplete crysallisation.

The crystalline products were analysed by ^{1}H NMR spectroscopy to confirm their identity and purity. Each porphyrin could be identified by comparing the integration of the β-pyrrolic peaks (8H) at around 8.5 ppm with the integration for the peak from the ester CH_3 groups at around 4.1 ppm and the multiplet at 7.8 ppm from the *meta* and *para* H nuclei on those benzene rings with no ester substitution. The two diesters could be distinguished by ^{1}H NMR spectroscopy only because of their different symmetry, which is manifested in their β-pyrrolic peak splitting patterns. While the *ABAB* diester has only two unique β-pyrrolic H nuclei which appear as two doublets, the *AABB* diester has four unique H nuclei which appear as two doublets and two singlets, which are superimposed to appear as two three-peak multiplets (Figure 36).

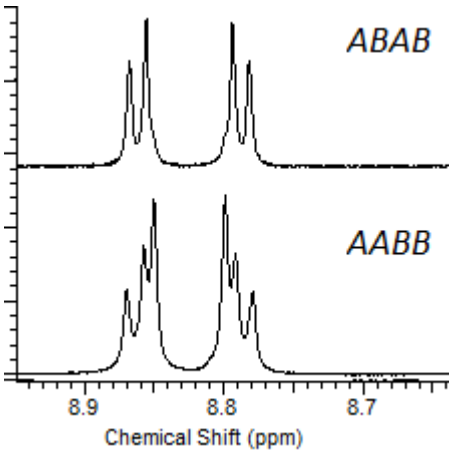

Figure 36: The β-pyrrolic signals from the phenylporphyrin diesters was the only way that the compounds could be distinguished

There was a problem however with using ^{1}H NMR spectroscopy to assess the *isomeric purity* of the *ABAB* and *AABB* diester isomers **2.03** and **2.04**. Their spectra differed only by the β-pyrrolic splitting pattern, with all the peaks clusters appearing in the same positions. Because of this peak overlap, there was no way to quantify the level of contamination of one with the other. To overcome this problem, a technique for analysing the porphyrins using HPLC was developed, and this is described in detail in Chapter 3. HPLC analysis also complemented ^{1}H NMR spectroscopy in assessing the purity of each member of the whole series of porphyrins. The results of both ^{1}H NMR spectroscopy and HPLC analysis indicated that flash chromatography had indeed been adequate to reach purities greater than 95% for each diester porphyrin, and much greater for the other porphyrins.

MALDI MS detected the molecular ion MH^{+} for each porphyrin. The UV-vis absorption spectrum for each compound was typical for a free base porphyrin, displaying four Q bands between 700 and 500 nm, and a B peak at around 419 nm. There was little variation in the spectra of the different compounds.

2.3.2 Formation of porphyrin metal complexes

Zinc complexes of **2.01** – **2.06** and iron complexes of **2.02** – **2.05** were prepared to provide a point of ligation in order to facilitate protein binding. The presence of a metal atom was also expected to influence the optical and electronic properties of the porphyrins. The metal complexes synthesised are shown in Figure 37.

Zinc complexes were chosen because of their good axial ligation properties for binding to a maquette, the ease of zinc insertion and their good stability under neutral and basic conditions. Zinc porphyrins have been shown to function well in solar cells requiring light-

induced electron donation, and are therefore likely to donate electrons well inside a maquette when paired with a suitable acceptor.

Iron complexes were chosen because of their excellent axial ligation properties and because they are a good model of heme, the ubiquitous natural porphyrin, which functions very well as an oxidation catalyst, O_2 binder and electron shuttle using the Fe(III) – Fe(II) couple. Synthetic iron porphyrins are therefore interesting as they may be similarly adapatable to perform a variety of roles when combined with maquettes.

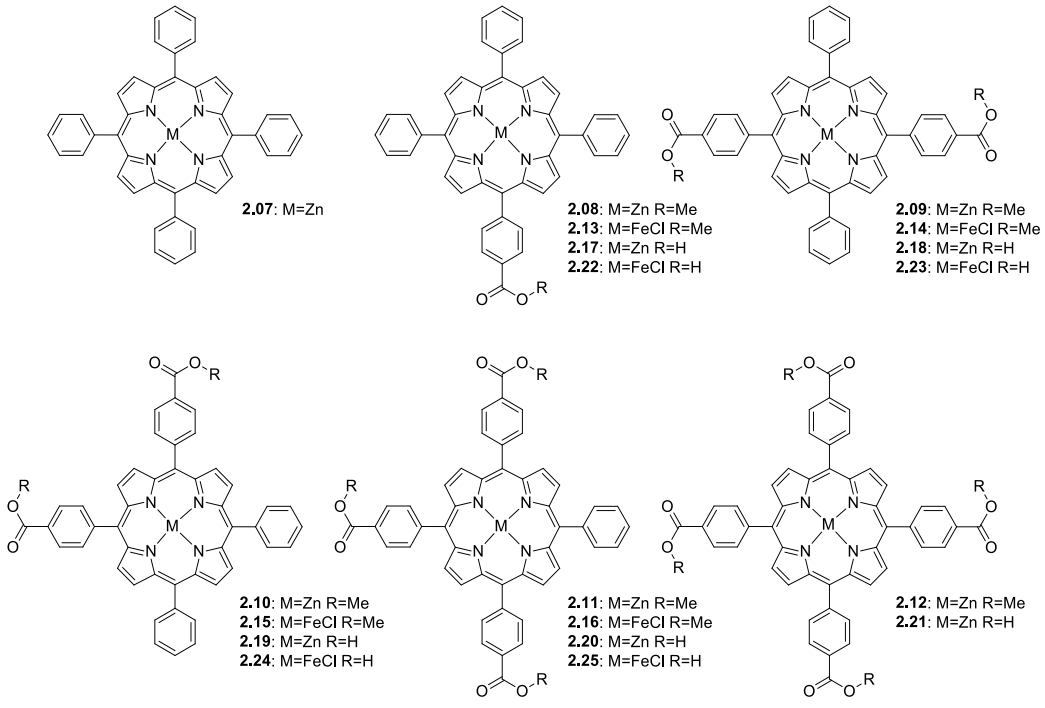

Figure 37: Metalated porphyrin esters (R = Me) and carboxylic acids (R = H)

Zinc insertion

Each ester porphyrin (**2.01 – 2.06**) was converted to its zinc complex (**2.07** – **2.12**) by dissolving it in DCM and adding a methanol solution of an excess of zinc acetate. The reaction was monitored by TLC analysis and MALDI MS, and when complete, the product was precipitated by concentration by rotary evaporation followed by the addition of methanol.

Yields were typically near-quantitative, with only minor losses occurring during the isolation process. Complete metalation was evidenced by MALDI MS analysis, which in each case detected the molecular ion MH^+ of the metalated product, and no ion for the non-metalated starting material. ^1H NMR spectroscopy confirmed this finding by the absence of any core NH signal below -2 ppm.

The UV-vis absorption spectra of the zinc porphyrins were typical of porphyrins metalated with zinc. There were two Q bands between 700 and 500 nm and a sharp B peak at around 425 nm, and there was little varation between the different compounds.

Iron insertion

Iron insertion was carried out in a similar manner to the zinc insertions, but with some important differences. Iron insertion into porphyrins requires a higher temperature and longer reaction time than is required for zinc insertion, but was achieved within a few hours and without the production of side products to produce porphyrins **2.13** – **2.16**.

Fe(II) is most often used for such metalation reactions because it is much more readily bound by the porphyrin than Fe(III), however Fe(III) has also been used successfully.[83] Once inside the porphyrin the Fe(II) ion is allowed to spontaneously oxidise to the (III) oxidation state by exposure to atmospheric oxygen.

DMF is the most commonly reported solvent for iron insertion reactions, however other solvents have been used successfully including acetonitrile[84] and chlorform.[85] In this work DCM was used and found to be quite effective, with the advantage that the isolation of the metalated porphyrin product was simplified because of the hydrophobicity and volatility of this solvent, which facilitates washing with aqueous HCl and subsequent evaporation.

The procedure used to effect iron insertion was as follows: the free base porphyrin was dissolved in DCM, the mixture heated to reflux, and a suspension of $FeCl_2$ in methanol was added. NaOAc dissolved in methanol was also added as a buffer to prevent acidification of the mixture due to the displacement of two H^+ ions from every porphyrin core that is metalated.

The reactions were monitored by TLC and the iron complexes were initially observed to form quickly. However, as each reaction neared completion it appeared to stall, with a pink porphyrin-coloured spot of high RF remaining on TLC. More iron(II) chloride was added, but it was not possible to eliminate this faint spot completely.

The mixture was then washed three times with 1% HCl solution or sat. NH_4Cl solution. This was because under basic or neutral conditions, iron porphyrins will bind to molecular oxygen to form peroxo dimers, which quickly convert to μ-oxo dimers.[5] These species were detected by TLC and in MALDI MS analysis prior to this treatment with acid to destroy them. Treatment with an acid catalyses the oxidation of the iron ion to the (III) state, and when chloride is present in excess, all of the iron cations bear chloride counterions.[28]

The iron porphyrin products were isolated by simply evaporating the organic solvent, or by precipitation *via* addition of hexane. Yields were between 60% and 80%. The porphyrin starting material was fully consumed according to TLC analysis and no side products appeared to form, but because the reactions were performed on small quantities of porphyrin (<20 mg) significant losses were incurred during isolation due to incomplete crystallisation and recovery from the filter.

^1H NMR spectroscopy is not applicable to iron porphyrins because of their paramagnetic nature (except in special states of oxidation state and ligation).[86] Therefore MALDI MS analysis was used to confirm the identity of the products. In each case the positive molecular ion was observed both with and without the chloride counterion. A weak signal for an ion with the

mass of the product with an oxygen radical or hydroxide ion attached was also detected. This was likely a fragment of a peroxo or μ-oxo dimer which was present in a trace quantity. No signal for the MH^+ ion of the unmetalated porphyrin was detected.

UV-vis absorption spectroscopy confirmed conversion to the iron complex because of the significant broadening of the B peak, whose maximum lay at 408 nm for each product. Also, only two Q bands were observed (at 609 and 569 nm), while the free base starting materials displayed four.

2.3.3 Hydrolysis of the ester groups

Hydrolysis of the zinc porphyrin ester groups

The ester groups of the zinc porphyrins were converted to carboxylic acids *via* base hydrolysis to form compounds **2.17** - **2.21** (Figure 37). The reagent solution consisted of a mixture of 10% water and 90% methanol containing 200 mmol/L KOH. The triester **2.11** and tetraester **2.12** were hydrolysed by dissolving them directly in this mixture and heating at reflux for three hours. The monoester **2.08** and diesters **2.09** and **2.10** required the addition of an equal volume of THF to the hydrolysis mixture in order to solubilise them.

It was not possible to monitor the progress of the reaction by TLC because of the high retention of the intermediate products bearing even a single carboxylic acid group (in the case of the monoester **2.08**, TLC was effective). However it was later confirmed by ^{1}H NMR analysis of the isolated products that three hours was sufficient to ensure that all ester groups were hydrolysed.

The zinc porphyrin products were precipitated without demetalation by adding water and then acidifying the solution with phosphoric acid. Phosphoric acid is a weak acid and thus may

be used to gradually reduce the pH of the unbuffered reaction mixture to protonate the carboxylic acids and induce precipitation without removing zinc from the porphyrin core. In some cases it was necessary to evaporate the organic solvents in order to effect complete precipitation.

Collection of the porphyrins proved challenging because of their tendency to precipitate in a microcrystalline form that would block a sintered glass filter. Therefore, each product was collected by serial centrifugation and supernatant replacement to remove practically all inorganic salt residue.

Yields were typically greater than 70% with no starting material remaining and no side products being detected. Losses ocurred only during supernatant removal at each round of centrifugation. The products were analysed using ^{1}H NMR spectroscopy. Hydrolysis was evident by the disappearance of the ester CH_3 signals. The spectra were otherwise similar to the esters. In the case of the zinc porphyrins it was noted that no NH peaks from the porphyrin core were detected indicating that the porphyrin remained metalated. MALDI MS detected the molecular ion MH^+ for each pophyrin.

The UV-vis absorption spectra were similar to those of the esters but shifted to shorter wavelengths by approximately 4 nm, but this was likely a negative solvatochromic effect, as they were recorded in DMSO rather than chloroform.

Hydrolysis of iron porphyrin ester groups

The iron porphyrin carboxylic acids **2.22** – **2.25** were generated in a manner similar to that employed for the free-base and zinc porphyrins. However it was necessary to treat the iron porphyrins slightly differently because of the tendency of the iron ion to bind oxygen. By

precipitating the carboxylic acid products with 3% HCl rather than H_3PO_4 and thus lowering the pH below 5, it was ensured that chloride was the counterion of every bound iron atom.

Because of the ionic nature of the Fe(III) ion, the iron porphyrins were less disposed to precipitate from aqueous solution, even when the organic solvents were completely removed by rotary evaporation. For this reason the yields were lower than those for the free-base and zinc porphyrins, and fell in a range between 50% and 70%.

Without ^{1}H NMR spectroscopy to characterise the products, it was necessary to rely on MALDI MS analysis alone to confirm complete hydrolysis. The positive molecular ion MH^+ for each product was detected, while no ions for the starting material or partially-hydrolysed products (for those starting materials bearing more than one ester group) were detected.

The UV-vis spectra indicated that iron remained bound and showed broad B peaks, typical of iron tetraphenylporphyrins, and distinct from free-base tetraphenylporphyrins which display sharper B peaks. They also displayed only two Q bands, while the free base precursors displayed four.

2.4 Synthesis of butylporphyrin carboxylic acids

Porphyrins bearing butyl chains instead of benzene rings were produced in order to test the effect of the different hydrophobic group on maquette binding. Aside from the tetraester **2.06** already discussed in Section 2.3, of this series, only the synthesis of the tetrabutylporphyrin **2.26** had been previously reported, albeit several times. In each case, it was synthesised *via* a variant of the Lindsey synthesis, as carried out by Oulmi *et al.* for example.[87] A variety of longer chain alkylporphyrin esters have been made, almost always by mixed-aldehyde condensation under Lindsey's conditions,[88] although an *AABB* alkylporhyrin diester has been prepared using a Suzuki coupling to introduce the aryl esters.[81]

Consequently, the preparation of the butylporphyrin series was carried out using Lindsey's conditions. These conditions likely avoid the oxidation of the electron-rich alkylporphyrins that can occur at the high temperature of the Adler conditions.

2.4.1 Butylporphyrin synthesis

Equimolar amounts of 1-pentanal and 4-formylbenzoic acid methyl ester were reacted with pyrrole using TFA as a catalyst, and the resulting porphyrinogen mixture was oxidised with DDQ. The porphyrins **2.26** – **2.31** (Figure 38) thus produced could be separated chromatographically in a similar manner to the phenylporphyrins (2.01 – 2.06) to give the isolated yields shown in Table 3. As occurred with the phenylporphyrins, the ratio of yields deviated from that which was expected from statistical probability alone (Table 1). The deviation can be explained by the different reactivities of the aldehydes and losses during purification, especially for the diesters, which required serial chromatography according to Figure 35 to separate satisfactorily.

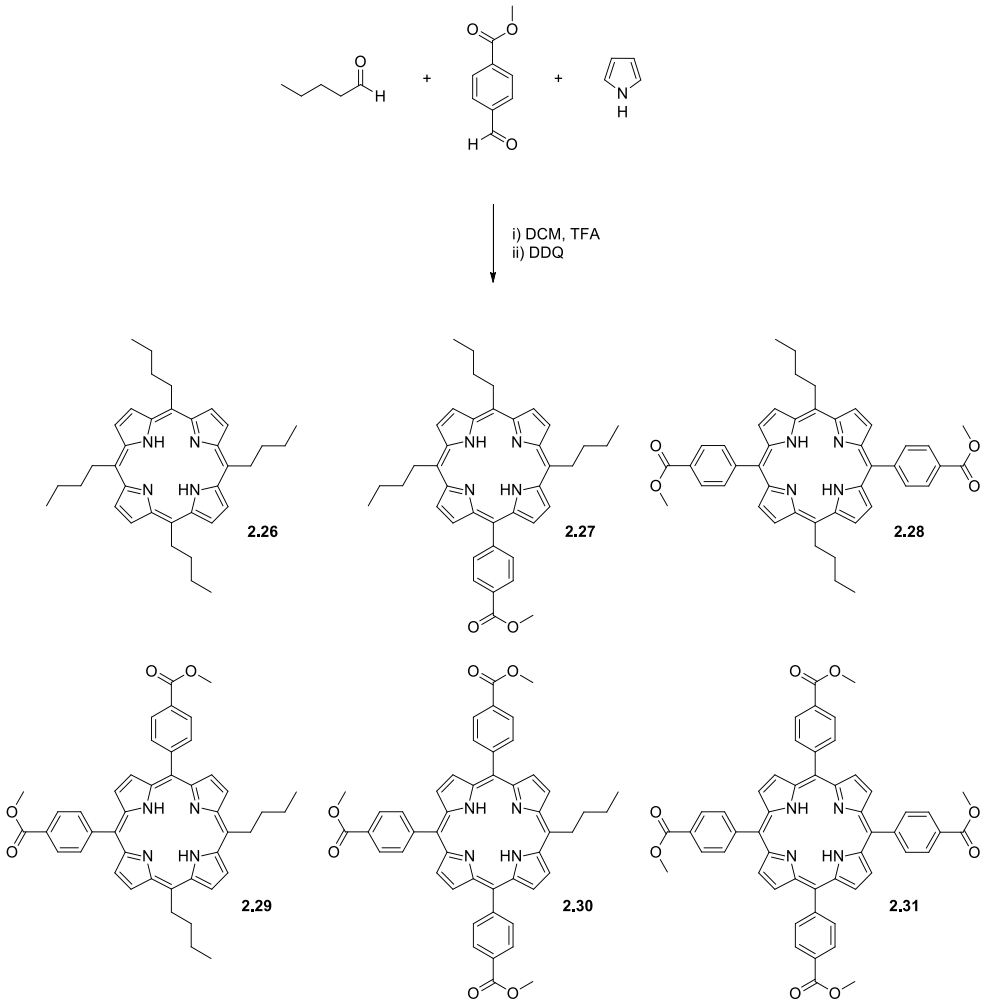

Figure 38: The mixed-aldehyde condensation to produce the statistical mixture of butylporphyrin esters

Table 3: The percentage yield of each porphyrin isolated from the reaction and a comparison of the expected yield ratio and the actual yield ratio. The tetraester was not isolated and so is not part of the analysis

	Tetrabutyl **2.28**	Monoester **2.29**	ABAB diester **2.30**	AABB diester **2.31**	Triester **2.32**	Total
Yield %	0.3	4.1	2.7	3.6	1.7	12.4
Yield ratio	0.4	5.0	3.1	4.3	2.1	15
Expected ratio	1	4	4	2	4	15

The products were characterised by ^{1}H NMR spectroscopy, MALDI MS and UV-vis absorption spectroscopy. In ^{1}H NMR, the integration of the the β-pyrrolic signals (8H) was

compared to that of the benzene ring H signals, which indicated the number of benzene rings contained within the compound. Unlike the aryl diesters **2.03** and **2.04**, the butyl diesters **2.28** and **2.29** could be assessed for isomeric purity by ^{1}H NMR spectroscopy because of their distinct β-pyrrolic peak positions in the region furthest downfield; they did not overlap when compounds were mixed.

MALDI MS detected the molecular ion MH^{+} for each product. The UV-vis absorption spectrum of each compound was typical for a free base porphyrin, and there was little variation between the different compounds. There were four Q bands between 700 and 500 nm and a single B band at around 420 nm. The spectra were similar to those of the phenylporphyrin esters **2.01** – **2.06**.

Initially the isolation of the *ABAB* isomer 2.28 of the diester was problematic because of the small difference in retention with the *AABB* diester 2.29 on a silica column, and so this compound was also synthesised via alternative means using 5-butyl dipyrromethane 2.32 as explained in the next section. The yields shown in Table 3 were isolated after several repetitions of the reaction and using improved chomatographic techniques such as careful equilibration of the column prior to loading and careful attention to the maintenance of a constant solvent ratio in the eluent.

2.4.2 ABAB butylporphyrin diester via a dipyrromethane

By synthesising the *ABAB* butylporphyrin diester via a 2+2 condensation, as discussed in Chapter 1, it was hoped that a higher concentration of this compound could be produced to facilitate chromatographic isolation. Firstly the appropriate dipyrromethane was synthesised followed by the condensation reaction to form the porphyrin.

Dipyrromethane synthesis

6-butyldipyrromethane **2.32** was synthesised *via* the reaction of pentanal and pyrrole in water, catalysed by HCl (Figure 39). The reaction produced a yield of 74% of the dipyrromethane **2.32**. The formation of the correct product was confirmed by the ^{1}H NMR spectrum, which matched a published spectrum.[89] No trace of tripyrrane was detected by TLC, supporting the assertion made in the publication that this technique does not form any higher pyrromethanes.[37]

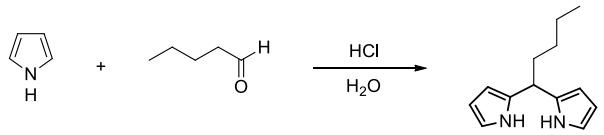

2.32

Figure 39: Synthesis of 6-butyldipyrromethane

Condensation of the dipyrromethane to form the porphyrin

The *ABAB* porphyrin diester **2.28** was formed under similar conditions to those used to produce the statistical mixture of butyl chain porphyrins, that is, *via* condensation in DCM with a catalytic quantity of acid, followed by oxidation of the porphyrinogens thus formed using DDQ according to Lindsey's conditions (Figure 40).[32] The progress of the reaction was monitored by observing the disappearance of the dipyrromethane in TLC analysis, with the dipyrromethane spot being stained with bromine vapour. After 10 minutes the dipyrromethane was fully consumed and DDQ was added to oxidise the porphyrinogens. TLC analysis revealed that while porphyrin **2.28** appeared to be the major product, several other porphyrins had formed, and MALDI MS analysis detected ions of m/z consistent with the MH^{+} ions of the tetrabutyl **2.26**, monoester **2.27**, diester **2.28** – **2.29** and triester **2.30** porphyrins. The presence of porphyrins besides the *ABAB* diester **2.28** can be explained by scrambling, a process which commonly occurs for electron rich, sterically unhindered dipyrromethanes such

as **2.32**.[38] By reducing the reaction time to a minimum (10 minutes) it was hoped that scrambling would not occur to any large extent, and the major product of the reaction was in fact the intended *ABAB* porphyrin **2.28**.

The *ABAB* diester **2.28** was isolated by chromatography in the same manner as for the products of the butylporphyrin statistical mixture. Being present in a much larger relative concentration than in the original statistical mixture, it was easier to isolate. It was crystallised from methanol and the yield was 6.3%. Its identity was confirmed by ^{1}H NMR in the same manner as that used for the statistical mixture of products in Section 2.4.1.

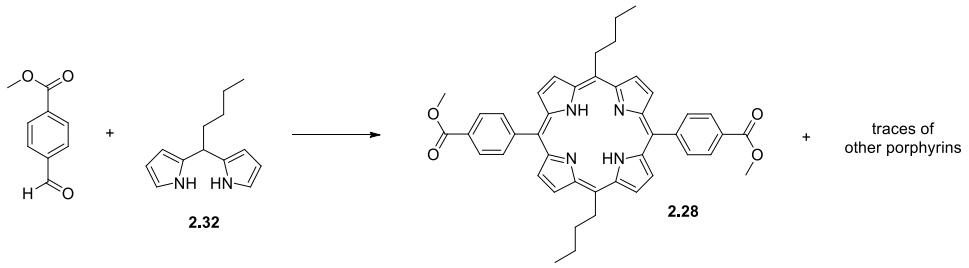

Figure 40: The condensation of the dipyrromethane with the ester aldehyde to produce predominantly the *ABAB* butylporphyrin diester 2.28

2.4.3 Zinc insertion

The butylporphyrin esters behaved similarly to the phenylporphyrin esters in that zinc insertion could be achieved by stirring at room temperature in DCM and adding zinc acetate dissolved in methanol. Products **2.33** – **2.37** (Figure 41) were precipitated by addition of methanol and collected by filtration. Yields were near quantitative, with the starting material being metalated completely and the only losses apparently occurring during crystallisation and collection by filtration. It is noteworthy that these compounds bearing butyl chains were significantly more soluble in methanol than the equivalent compounds bearing benzene rings.

Complete metalation was evidenced by MALDI MS analysis, which in each case detected the molecular ion MH^+ of the metalated product and no ions for the non-metalated starting material. ^{1}H NMR analysis confirmed this by the absence of a core NH signal below -2 ppm. The spectra were otherwise similar to that of the analogous free base butylporphyrin esters.

The UV-vis absorption spectrum for each compound was typical of a porphyrin metalated with zinc and there was little variation between the compounds. There were two Q bands between 700 and 500 nm and a B band at 425 nm.

2.4.4 Hydrolysis of the ester groups

The hydrolysis of the zinc butylporphyrin esters was accomplished similarly to that of the phenylporphyrin esters. As with the latter, it was necessary to add THF to the monoester and *ABAB* diester to induce these compounds to dissolve in order to react. The products were collected by precipitation by addition of phosphoric acid followed by serial centrifugation with supernatant replacement at each repetition. Products **2.39** – **2.43** (Figure 41) were analysed by ^{1}H NMR and complete hydrolysis was evidenced by the absence of the ester CH_3 signal at around 4.11 ppm. MALDI MS analysis detected signals consistent with the MH^+ ions of each compound. In the UV-vis absorption spectrum, the monoacid **2.39** displayed two Q bands with maxima at 608 and 566 nm.

The B peak of each compound lay between 428 and 430 nm, with all peaks being symmetrical except for the *ABAB* diacid, which displayed a shoulder on the blue side, probably indicative of aggregation of this compound.

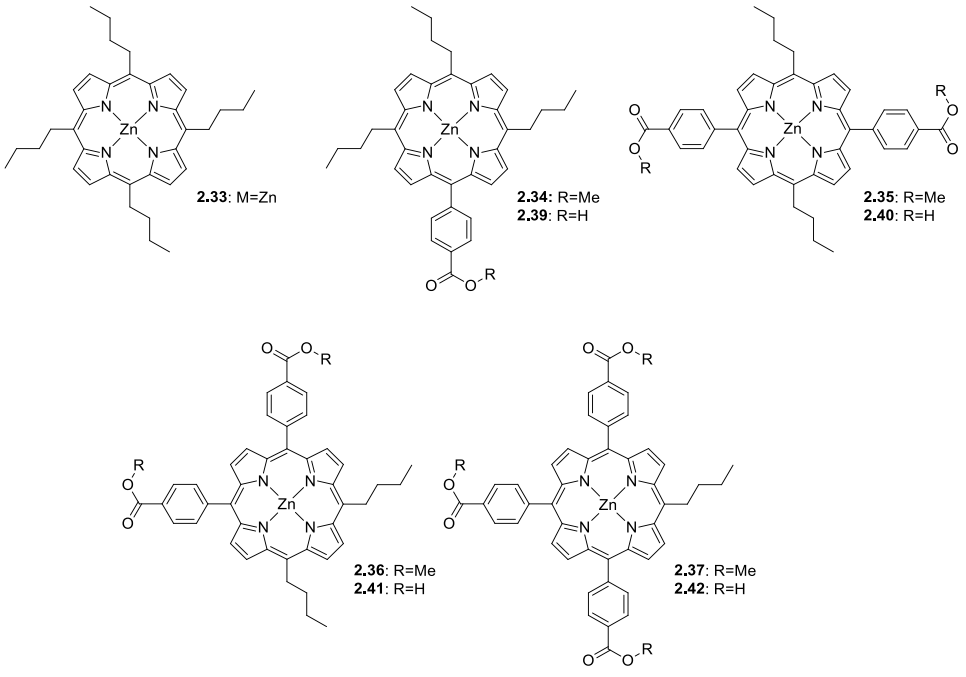

Figure 41: Metalated butyporphyrin esters (R = Me) and carboxylic acids (R = H)

2.5 Synthesis of phenylporphyrin quaternary ammonium salts

To test the effect of a positively-charged water solubilising group on the maquette-binding properties, a set of quaternary ammonium salt (QAS) porphyrins was prepared. The most important difference between the QAS and the carboxylic acid group is that the QAS group bears a positive charge in contrast to the negative charge of an ionised carboxylic acid.

QAS porphyrins have been most commonly formed using the pyridyl moiety, and a statistical mixture of pyridyl porphyrins has been produced and the individual porphyrin products isolated.[90] However, in order to exclude the electron-deficient quaternary nitrogen from the aromatic system and to have compounds more sterically similar to the carboxylic acid compounds, trimethylanilinium porphyrins were synthesised in this work.

The intermediate dimethylamino group was chosen for the porphyrin synthesis step over a primary phenylamine because the tertiary amino nitrogen cannot form an imine with the

aldehyde reagents present in a porphyrin synthesis, as a primary or secondary amine most probably would.

2.5.1 Porphyrin synthesis

The *p*-dimethylaminophenylporphyrin statistical mixture was prepared in a similar manner to that previously reported by Lindsey[91] (Figure 42). This paper reports the production of a statistical mixture of dimethylaminophenylporphyrins, however only the mono(dimethylaminophenyl)porphyrin and a mixture of the di(dimethylaminophenyl) porphyrins was isolated.[32] The procedure was improved by the identification of chromatographic conditions which enabled the separation and isolation of both di(dimethylaminophenyl)porphyrins **2.45** and **2.46**, and also the tri(dimethylaminophenyl)porphyrin **2.47**.

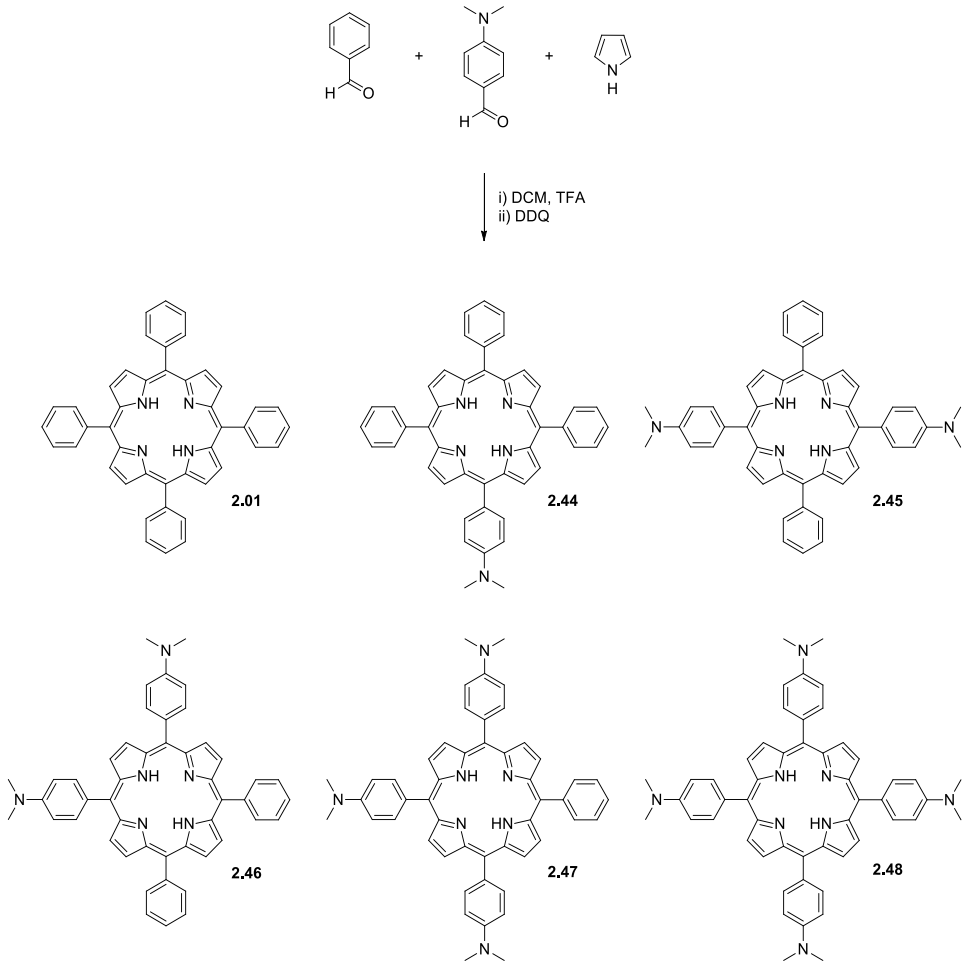

Figure 42: The synthesis of the dimethylamino porphyrins *via* mixed-aldehyde condensation

DCM was found to be an ineffective eluent for flash chromatography because only the monoamine **2.44** was eluted while the other porphyrins remained bound to the silica of the column despite a large volume of DCM being passed through it. Working under the assumption that the strong binding to the silica was a result of an interaction with the amine group, triethylamine was added to the eluent in order to compete for these binding interactions. This was quite effective and the triamine **2.47** was isolated in this manner. As was necessary for both sets of diester porphyrins in Sections 2.3.1 and 2.4.1, the diamines **2.45** and **2.46** required serial chromatography according to Figure 35 in order to separate them. Yields are shown in Table 4.

Table 4: The percentage yield of each porphyrin isolated from the reaction and a comparison of the expected yield ratio and the actual yield ratio. The tetraamine was not isolated and so is not part of the analysis

	Monoamine **2.44**	*ABAB* diamine **2.45**	*AABB* diamine **2.46**	Triamine **2.47**	Total
Yield %	3.1	1.0	0.2	0.8	5.1
Yield ratio	8.5	2.7	0.6	2.2	14
Expected ratio	4	4	2	4	14

The porphyrin tetraamine **2.48** did not elute from the column and was not detected by TLC it even though it was very likely present. Presumably it did not separate from the black polymeric by-product material which was present and is typically produced in such reactions.

Products were characterised by ^{1}H NMR spectroscopy, MALDI MS and UV-vis absorption spectroscopy. In the ^{1}H NMR spectrum, the integration of the β-pyrrolic peaks (8H) was compared with that of the NCH_3 signal at 3.2 ppm to ascertain the number of dimethylamino groups within the molecule. Like the aryl porphyrin diesters **2.03** and **2.04**, the two porphyrin diamines **2.45** and **2.46** could not be assessed for isomeric purity by ^{1}H NMR spectroscopy and it was necessary to use HPLC analysis for this purpose, as described in Chapter 3. MALDI MS detected the MH^+ molecular ion for each compound.

The UV-vis absorption spectra were typical of free base porphyrins, displaying four Q bands between 700 and 500 nm. The mono(dimethylaminophenyl)porphyrin **2.44** displayed peaks in similar positions to those of TPP with the B band appearing at 420 nm. However, the *ABAB* and *AABB* di(dimethylaminophenyl) porphyrins **2.45** and **2.46** displayed their peaks at 425 and 426 nm respectively, and the tri(dimethylaminophenyl)porphyrin **2.47** at 434 nm. This tendency to shift the B peak with different substitution patterns was not observed for the phenylporphyrin or butylporphyrin esters described in Sections 2.3.1 and 2.4.1 respectively, and is likely due to the electron donating effect of the dimethylamino groups.

2.5.2 Tetraamine via tetranitro TPP

Although it is reported in the literature,[92,93] none of the porphyrin tetraamine **2.48** could be isolated from a mixture generated by the condensation of 4-dimethylaminobenzaldehyde with pyrrole. An alternative synthesis *via* tetranitro TPP **2.49** has also been published,[94] and this was the technique pursued (Figure 43).

Using the published conditions of condensation in propanoic acid, tetranitro TPP **2.49** was isolated in a yield of 20%. This is slightly lower than the published yield of 25%, which may be a reflection of a higher purity because of thorough washing with pyridine to remove black by-product material. MALDI MS found the molecular ion MH^+ and ^1H NMR spectroscopy produced a spectrum identical to that which had been published.

Reduction to the tetraamine **2.50** with $SnCl_2$ in HCl produced a yield of 68%, lower but similar to the published yield of 79%. MALDI MS analysis found the molecular ion MH^+ and ^1H NMR spectroscopy produced a spectrum identical to that published.

The UV-vis absorption spectrum of **2.50** displayed four Q bands between 700 and 500 nm and a B band at 439 nm. This is significantly red-shifted relative to TPP **2.01** (418 nm) but since the spectrum was recorded in DMSO rather than chloroform the results are not comparable. This result does however continue the red-shift trend observed with increasing numbers of amino groups described above.

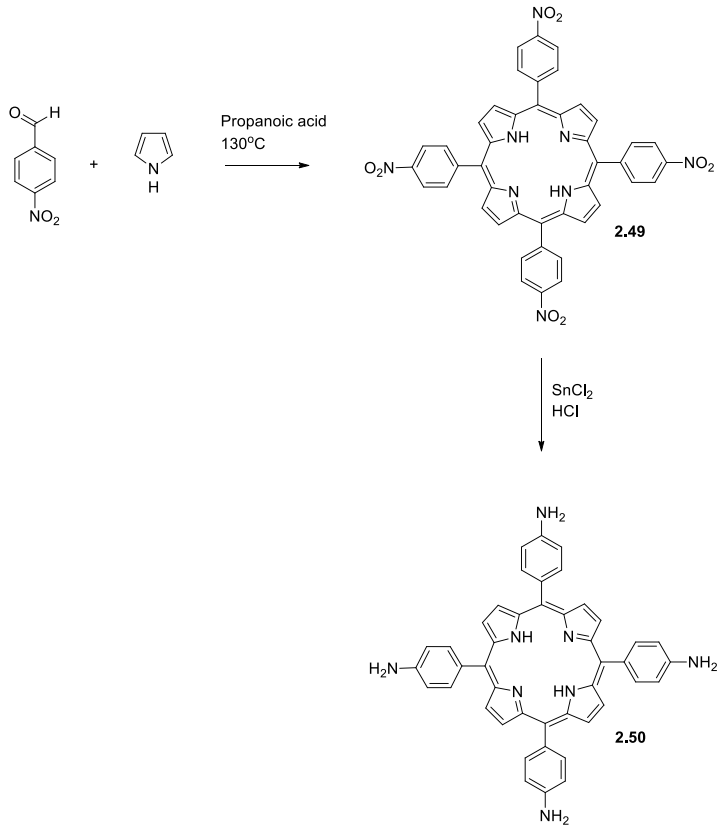

Figure 43: The procedure used to synthesise tetraamino TPP

2.5.3 Zinc insertion

Zinc was inserted into the dimethylaminophenylporphyrins **2.44** – **2.47** in a similar manner as for the phenylporphyrin esters and butylporphyrin esters in sections 2.3.2 and 2.4.3 (Figure 44). They were each dissolved in DCM and a solution of zinc acetate in methanol was added. The products **2.51** – **2.54** were isolated by adding methanol to induce precipitation. The zinc complexes were obtained in quantitative yields.

Zinc insertion for the tetraaminophenylporphyrin was problematic however because of its low solubility in DCM. In order to obtain a pure product, porphyrin **2.50** was mixed in DCM and was treated with a methanol solution of excess zinc acetate. The solution was filtered to remove undissolved material and stirred until MALDI MS analysis indicated that no non-

metalated starting material remained. The solution was washed with aqueous ammonia to remove remaining zinc acetate, and the product isolated by evaporation. A yield of 24% was obtained.

The ^{1}H NMR spectrum of the zinc porphyrin tetraamine **2.55** displayed broad peaks, likely because of ligation between the amine N atoms and the bound zinc ions. The addition of 10 mg of triethylamine to the NMR tube improved the spectrum, likely by breaking the N-Zn ligation between porphyrins. Metalation was evident by the absence of an NH signal below -2 ppm.

MALDI MS analysis of all of the zinc complexes detected the molecular ion MH^{+} and the UV-vis absorption spectrum of each compound was typical for a zinc porphyrin with two Q bands between 700 and 500 nm. The B bands lay at 439 nm, significantly shifted towards red relative to the analogous carboxylic compounds of Section 2.3.2.

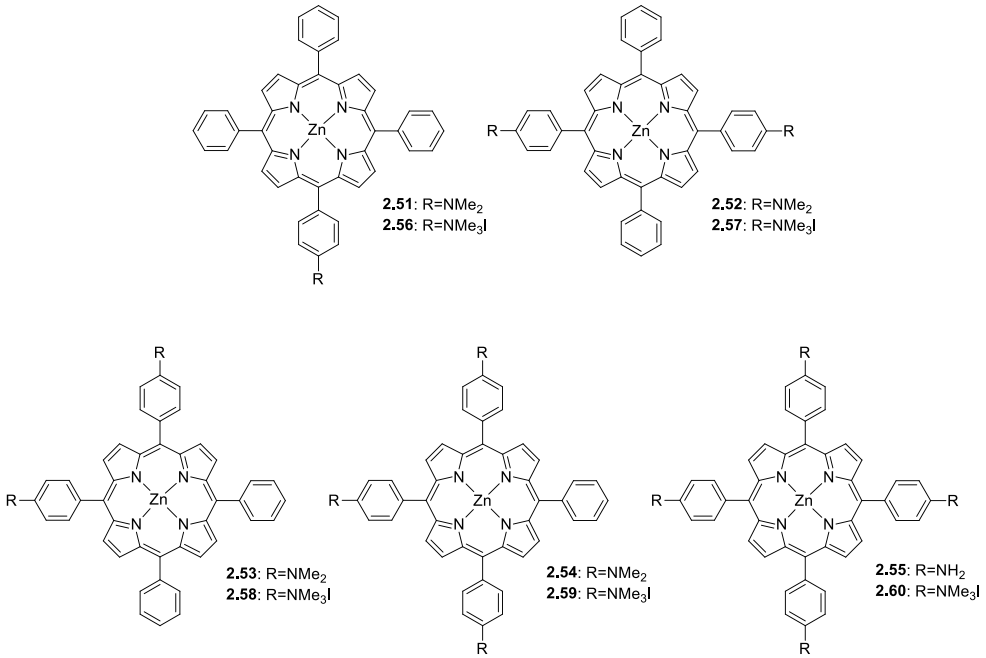

Figure 44: Metalated porphyrin dimethylamines (R = NMe_2) and QASs (R = NMe_3I)

2.5.4 Methylation of dimethylaminophenylporphyrins

Synthesis of a phenylporphyrin tetra QAS from the analogous tetraamine and tetra(dimethylamine) has been reported in the literature, but porphyrins with fewer than four appended QAS groups have not been produced. The zinc complex of the tetra QAS porphyrin **2.60** has also been prepared, but with metalation taking place after the methylation step.[95,96] Metalation had been performed by treating the QAS porphyrin with one equivalent of zinc acetate in water.

In order to simplify the process, it was decided that metalation with zinc should be carried out prior to methylation to form the QAS. This was because it was expected that isolation of a QAS product from a solution containing a zinc salt could be problematic, especially for the small quantities (~10 mg) of porphyrin compounds involved. No methylation of zinc-metalated aminophenylporphyrins has been published previously, and in order to investigate the required methylation conditions, experiments were conducted using the methylation of the mono(dimethylamino)phenyl porphyrin **2.51**.

The reaction was trialled under microwave irradiation. With methyl iodide in THF heated to 100 °C for 15 minutes, much methylation occurred as evidenced by TLC, but demetalation was also evident. Complete methylation without demetalation, according to TLC and ^{1}H NMR analysis, was achieved by microwave heating at 50 °C for 3 hours in a mixture of 2:1 acetonitrile/methyl iodide. It appeared that demetalation occurs more slowly at this temperature, and with a large excess of methyl iodide, methylation occurs relatively rapidly. The product was isolated by simply evaporating the acetonitrile and excess methyl iodide. Each dimethylaminophenylporphyrin was methylated in this manner. Yields were quantitative.

Under the same conditions in a round bottom flask, the methylation of zinc mono(4-dimethylamino)TPP **2.51** was monitored by TLC. It was found that after one hour the reaction was not complete, but after three hours it was. MALDI MS analysis however showed only a

very strong ion for the starting material. Under MALDI MS conditions, methyl iodide is apparently eliminated from a porphyrin QAS, giving the appearance that no methylation has taken place. This was true even of the zinc porphyrin tri QAS **2.59**, which lost three molecules of methyl iodide during laser desorption. Electrospray ionisation was used later to obtain high resolution results, and ions were observed with m/z ratios consistent with multiple charges from the loss of iodide ions. Once this was realised, ^{1}H NMR was relied upon instead to indicate completion of the reactions and to characterise the products. Complete methylation was evident by the integration of the NMe_3 peak at 3.9 ppm compared to the β-pyrrolic peak integration of 8H.

The UV-vis absorption spectra of the products in DMSO each displayed two Q bands at around 604 and 562 nm, with the peaks of the compounds with more QAS groups appearing at slightly longer wavelengths. The B bands appeared at between 427 and 430 nm, again with the compounds with more QAS groups displaying the peaks at longer wavelengths. This was unexpected, as the electron donation properties of a QAS should be much less than for a tertiary amine, as the lone pair of electrons is not utilised in a chemical bond.

2.5.5 Methylation of the tetra amino porphyrin

The zinc tetraaminophenylporphyrin **2.55** was slower to methylate to form the QAS, likely because each nitrogen required methylation three times. The microwave procedure developed for the dimethylamines did not go to completion. Complete methylation was still not achieved even after 40 hrs at 45 °C according to ^{1}H NMR analysis, and these conditions would remove zinc from the porphyrin core and produce a green solution which was possibly a core *N*-methylated product. Core *N*-methylation has been reported using methyl iodide under more extreme, but similar conditions.[97]

In order to make sure that, if a porphyrin became demetalated it would be immediately re-metalated, a large excess of zinc acetate was added to the reaction mixture. Microwave heating at 50 °C for 60 hrs fully methylated the aniline nitrogens while the porphyrin remained metalated with zinc, as indicated by ^{1}H NMR spectroscopy.

This resulted in an acetonitrile and methanol solution of excess methyl iodide, zinc acetate and the tetraaminophenylporphyrin QAS. The excess zinc acetate could not be removed by water washing, as the porphyrin was water soluble and therefore, in order to remove the excess zinc acetate, the mixture was treated with a DCM solution of TPP **2.01** to chelate the excess zinc ions. The mixture was then filtered to collect the methylated porphyrin, while the ZnTPP and excess TPP passed through. In this way, the fully methylated porphyrin product **2.60** was obtained in a quantitative yield.

The ^{1}H NMR spectrum of **2.60** showed a singlet at 8.80 ppm with an integration of 8H that was assigned to the β-pyrrolic protons and which indicated that all *meso* substituents were identical. A singlet at 3.9 ppm with an integration of 36H was assigned to the NMe_3 groups and this was further evidence of complete methylation. There was no NH peak below 0 ppm, indicating that the porphyrin remained fully metalated.

MALDI MS analysis detected an ion at m/z = 850, consistent with the MH^+ ion of the tetra dimethylamino compound. This was consistent with the finding in Section 2.5.4 that the ionization process removes MeI from each QAS group.

The UV-vis absorption spectrum displayed Q bands at 606 and 565 nm and a B peak at 432 nm, continuing the trend toward longer wavelengths with more QAS groups which was observed in Section 2.5.4.

2.6 Synthesis of a ferrocene porphyrin carboxylic acid

The zinc porphyrins described thus far would be expected to donate an electron to a suitable acceptor upon photoexitation. This would leave behind a porphyrin radical cation, a highly oxidative species which will reoxidise the electron acceptor with no net gain, a process called recombination. Ferrocene has been used as an electron donor to quench such radical cations and generate long-lived charge separated states, which are important for energy storage.[98–100] An amphiphilic ferrocene-appended porphyrin was therefore synthesised aimed at producing the same result in a porphyrin-maquette ensemble.

Maquette-binding studies had revealed that the zinc tetraphenylporphyrin tricarboxylic acid **2.20** and *AABB* dicarboxylic acid **2.19** (Figure 37) bound quickly and strongly to the maquette being tested (Chapter 7). It was envisioned that by modifying these compounds to include a ferrocene group in the 4-position of the unsubstituted benzene rings, that the resulting compounds would likely function as ferrocene-bearing, maquette-binding porphyrins. However, in order that the molecule have only a single electron acceptor so as to simplify the interpretation of experimental observations of its behaviour, the initial target was **2.63** (Figure 45), the porphyrin bearing a single ferrocene group, as well as three carboxylic acid groups for water-solubilisation. It was envisioned that this compound could be synthesised *via* the ester intermediate **2.61**. Similar compounds lacking ester or acid groups had been prepared using a mixed-aldehyde condensation with 5-ferrocenylbenzaldehyde and a second aromatic aldehyde being condensed with pyrrole[101] or dipyromethane.[102]

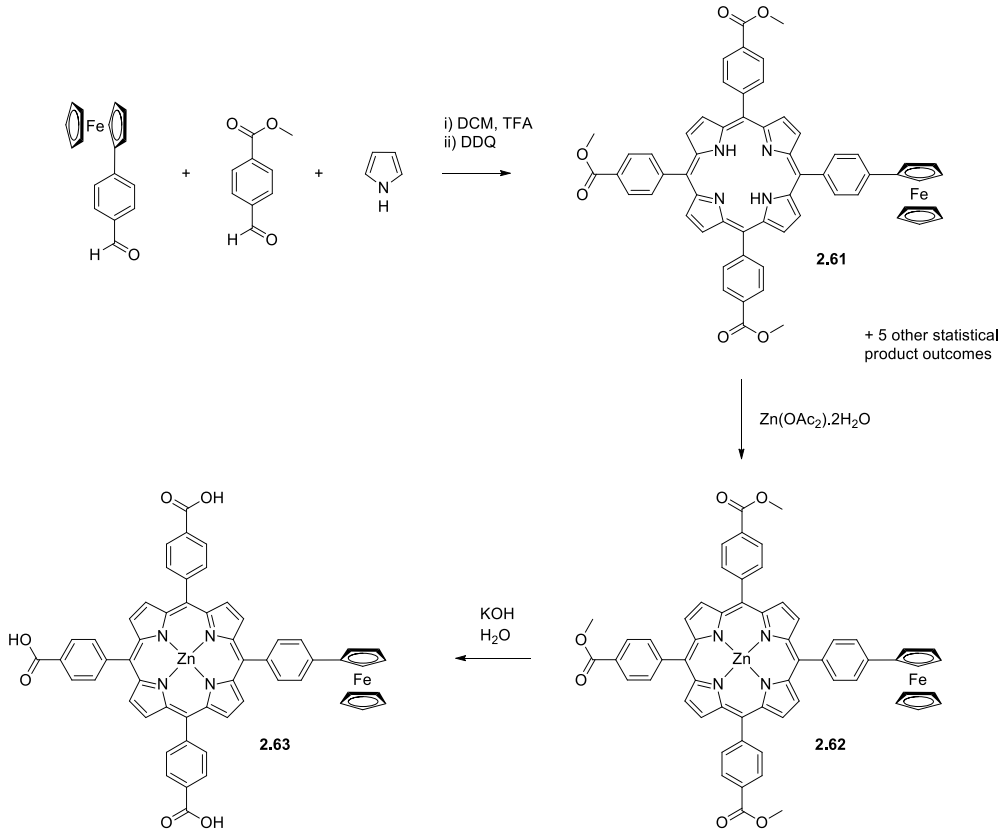

Figure 45: Preparation of the ferrocene porphyrin tricarboxylic acid 2.63

2.6.1 Porphyrin synthesis

To produce porphyrin **2.61** the strategy of mixed-aldehyde condensation with subsequent chromatographic separation was continued (Figure 45). One equivalent of 4-ferrocenylbenzaldehyde was condensed with three equivalents of 4-formylbenzoic acid methyl ester and four equivalents of pyrrole. The ratio of aldehydes was chosen to favour the formation of the monoferrocenyl porphyrin over the other five statistical possibilities. This depended on the assumption that the reactivities of the aldehydes were approximately equal. The condensation was performed in DCM with a TFA catalyst according to Lindsey's conditions.[32]

Two rounds of flash chromatography produced the pure ferrocenylporphyrin triester **2.61** in a yield of 16%. The product was characterised by MALDI MS analysis which detected an ion of m/z 973.26 which was attributed to the molecular ion MH^+.

Although the compound contains iron, ^{1}H NMR spectroscopy was applicable because unlike the porphyrin iron complexes of Section 2.3.2, ferrocene compounds are diamagnetic.[103] ^{1}H NMR spectroscopy (Figure 46) detected a single, symmetrical NH peak at -2.76 ppm (a), an indication that only a single porphyrin compound was present. A singlet at 4.14 ppm with an integration of 9H (b) was assigned to the ester CH_3 groups. The symmetrical unsubstituted cyclopentadiene anion protons appeared as a singlet at 4.27 ppm with an integration of 5H (c), while the asymmetry of the ferrocene cyclopentadiene anion bonded to the benzene ring was reflected in the appearance of its protons as two triplets at 4.51 and 4.95 ppm (d and e) with an integration of 2H each, typical of a monosubstituted ferrocene.[104]

The aromatic region displayed a pair of multiplets at 7.87 and 8.13 ppm, each with an integration of 2H (f and g), and these were assigned to the aromatic H nuclei of the ferrocene-bearing benzene ring. Two multplets at 8.28 - 8.33 ppm (h) and 8.42 – 8.48 ppm (i), each with an integration of 6H, were assigned to the aromatic H nuclei of the ester-bearing benzene rings.

The β-pyrrolic H nuclei appeared as a pair of doublets at 8.82 and 8.97 ppm, with the lower shift doublet being superimposed with a singlet, a similar pattern to that observed for the phenylporphyrin triester **2.05** (j and k). The total integration of these peaks was 8H. The compound was also characterised by UV-Vis absorption spectroscopy which showed a typical free base porphyrin spectrum. There were four Q bands at 648, 591, 554 and 517 nm. The B peak was sharp and lay at 421 nm.

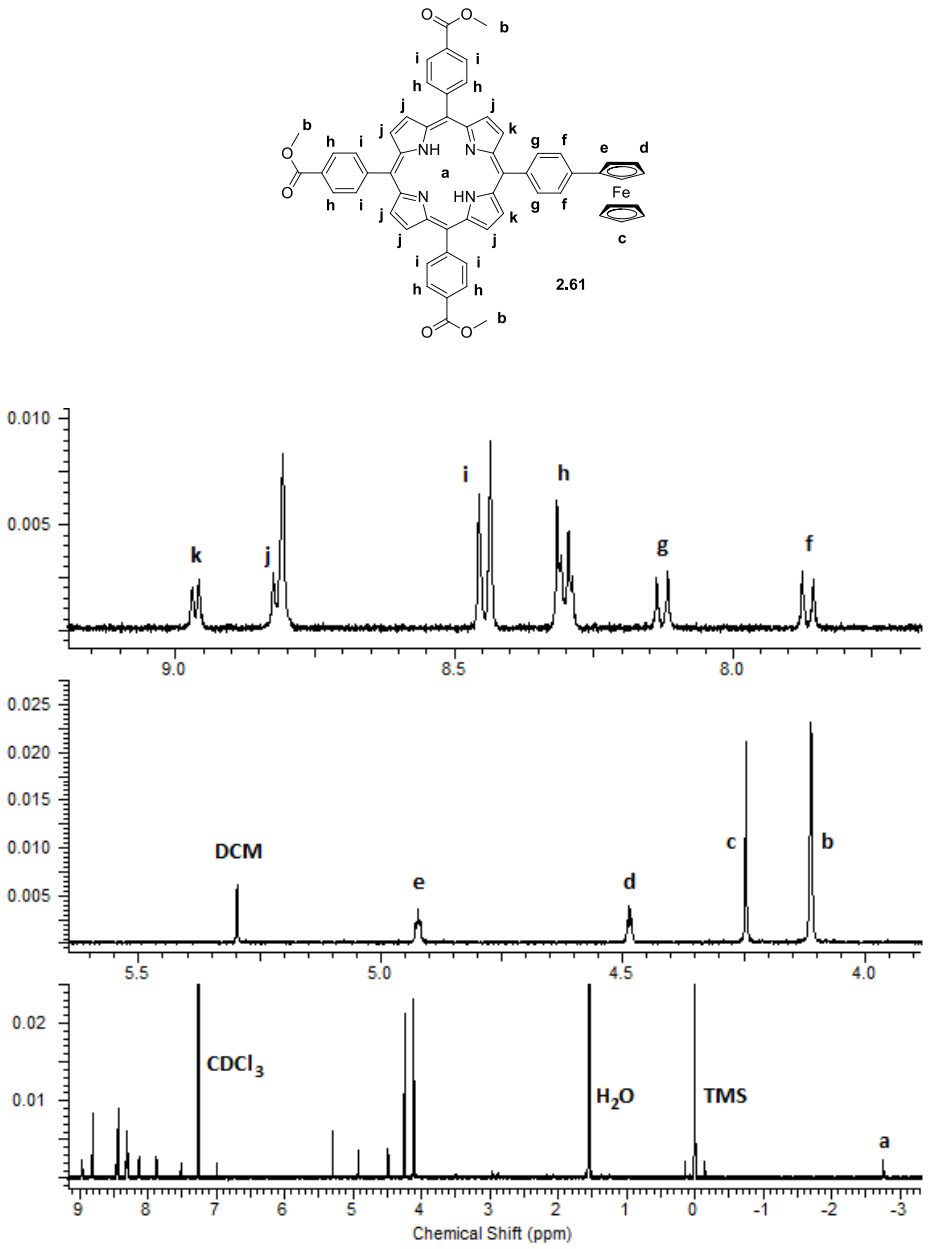

Figure 46: The ^{1}H NMR spectrum of the ferrocene porphyrin triester 2.61

2.6.2 Zinc insertion

Zinc insertion was achieved by treating a DCM solution of the ferrocene porphyrin triester **2.61** with zinc acetate in methanol. The product **2.62** was precipitated *via* the addition of methanol, and it is worth noting that this porphyrin precipitated very thoroughly and formed

sparkling crystals. It seemed that ferrocene contributes to this compound a strong tendency to crystallise.

MALDI MS analysis detected the molecular ion MH^+ of the zinc complex of the monoferrocenyl porphyrin. ^1H NMR spectroscopy detected no signal below -2 ppm for core NH peaks, indicative of complete metalation, and the spectrum was otherwise similar to the non-metalated starting material.

The UV-vis absorption spectrum was typical of a zinc porphyrin, displaying two Q bands at 598 amd 557 nm. The B peak maximum lay at 427 nm, slightly red-shifted relative to the 425 nm of the analogous non-ferrocene appended compound.

2.6.3 Hydrolysis of the ester groups

The hydrolysis of the of the zinc ferrocenyl porphyrin **2.62** was attempted using the usual conditions *viz.* 200 mmol/L KOH in 5% water, 45% methanol and 50% THF, which was added to improve the solubility. However, the porphyrin was still incompletely dissolved after the addition of the THF. After heating for 16 hours, TLC analysis indicated that very few of the ester groups had hydrolysed at all. This was attributed to the porphyrin's previously-observed poor solubility in methanol, and so the reaction was attempted in a solvent mixture containing 1 mmol/L KOH in 95.5% THF with only 0.05% water and 0.45% methanol. After 1.5 hours TLC found that no triester remained and a precipitate had formed. Water was added and the precipiate dissolved. After 2 more hours the porphyrin **2.63** was isolated *via* precipitation with H_3PO_4 and repeated suspension and centrifugation. The product was isolated in a quantitative yield.

The ^{1}H NMR spectrum indicated that all of the ester groups had been hydrolysed by the absence of any ester CH_3 signal at 4.1 ppm. The spectrum was otherwise similar to the ester starting material.

MALDI MS analysis detected an ion at m/z 993, consistent with the MH^+ ion of the triacid product. The UV-vis absorption spectrum was typical of a zinc porphyrin and similar to the ester starting material, with two Q bands appearing at 603 and 562 nm and a sharp B band at 430 nm.

2.7 Synthesis of pentafluorophenylporphyrin esters

The midpoint potential of the Fe(II) – Fe(III) couple of an iron porphyrin is an important factor in its functionality. It describes the voltage at which Fe(II) and Fe(III) are at equilibrium and is a measure of its reductive power when in the the (II) state and oxidative power in the (III) state. It has been found that the midpoint potential of a porphyrin-bound iron atom can be influenced by substituents on the porphyrin ring and Fe F_{20}TPP, in which all of the phenyl hydrogens are replaced by fluorine, has been measured to have a midpoint potential 300 mV more positive than Fe TPP.[105] This extra oxidising power may be useful in the realization of a water oxidizing porphyrin-maquette ensemble.

From maquette binding studies (Chapter 7) it was demonstrated that the iron phenylporphyin *AABB* diacid **2.19** and triacid **2.20** (Figure 37) bind well to the maquette. It was envisioned that by replacing the phenyl substituents of these compounds with the sterically-similar pentafluorophenyl group to produce compounds **2.64** and **2.65** that these compounds would still bind to the maquette but have a more positive midpoint potential.

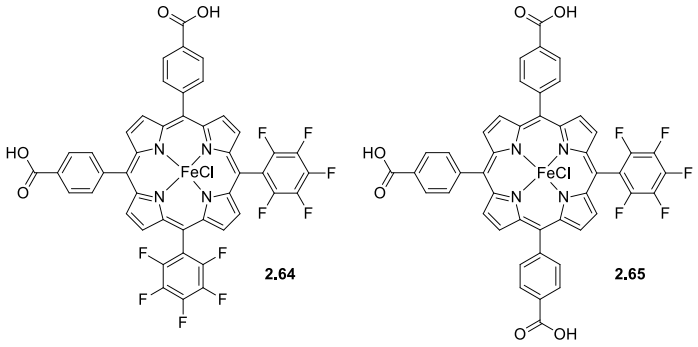

Figure 47: The target pentafluorobenzene-bearing iron porphyrin carboxylic acids

2.7.1 Porphyrin synthesis

F_{20}TPP can be produced by condensation of pentafluorobenzaldehyde with pyrrole, and therefore a mixed-aldehyde condensation was the obvious choice for preparing compounds **2.66** and **2.67** (Figure 48), which could be later converted to the metalated and hydrolysed products **2.64** and **2.65**. One equivalent of pentafluorobenzaldehyde and three equivalents of 4-formylbenzoic acid methyl ester were reacted with pyrrole with a TFA catalyst according to the conditions of Lindsey.[32] Chloranil was added to oxidise the resulting porphyrinogens, but TLC monitoring indicated that the porphyrinogens did not oxidise fully even after 1 hr of heating at reflux. This is despite published reports of the oxidation of the F_{20}TPP porphyrinogen with chloranil.[106] This was likely a result of the expected electron-poor nature of the macrocycle, which resulted in a raised oxidation potential. The porphyrinogens were finally oxidised by adding an excess of the stronger quinone oxidant DDQ.

The porphyrin products were separated using flash chromatography in the same manner as for the phenylporphyrins described in Section 2.3.1, and then precipitated by addition of methanol. The *AABB* diester **2.66** was isolated in a yield of 1% and the triester **2.67** in a yield of 7%.

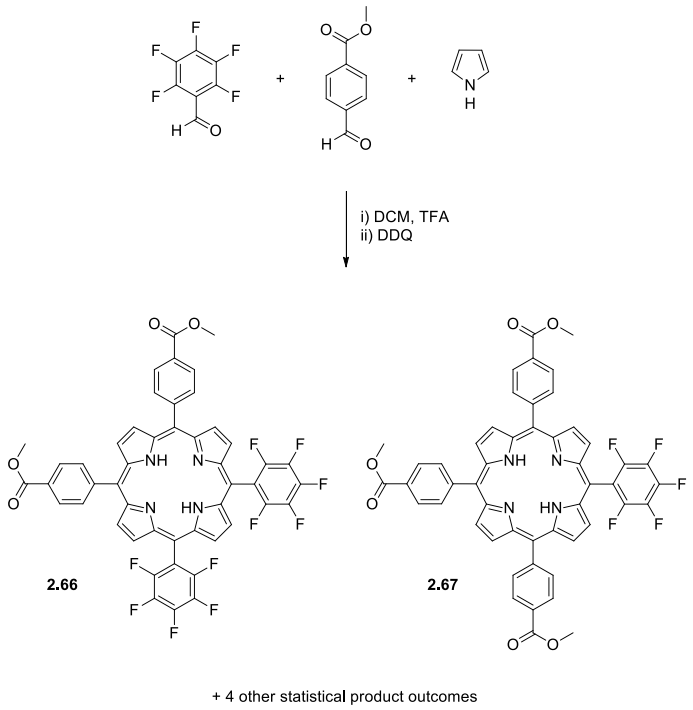

Figure 48: The synthesis of the pentafluorobenzene porphyrin esters

The ^{1}H NMR spectrum of the diester **2.66** displayed a single, symmetrical NH peak at -2.80 ppm. A singlet at 4.12 ppm with an integration of 6H (relative to the NH peaks 2H) was attributed to the ester CH_3 groups. The aromatic region displayed two doublets at 8.29 and 8.46 ppm, each with *J* = 8.24 Hz and each integrating to 4H. These peaks were attributed to the H nuclei of the benzene rings bearing the ester groups. The β-pyrrolic H nuclei appeared as two multiplets between 8.77 and 8.93 ppm with a total integration of 8H.

The ^{1}H NMR spectrum of the triester **2.67** displayed a single, symmetrical NH peak at -2.77 ppm. Two superimposed singlets between 4.11 and 4.18 ppm with a total integration of 9H were assigned to the ester CH_3 groups. The H nuclei of the benzene rings appeared as two multiplets at between 8.27 – 8.35 ppm and 8.45 and 8.52 ppm, each of which integrated to 6H. The β-pyrrolic H nuclei appeared as a multiplet between 8.79 – 8.87 ppm with an integration

of 6H, and as a doublet at 8.91 ppm with an integration of 2H, a similar pattern to that observed for the non-fluorinated triester **2.05**.

MALDI MS analysis of the diester and triester detected ions of m/z 911.06 and 879.22, which were attributed to the molecular ion MH^+ of each compound.

The UV-vis absorption spectra for the *ABAB* diester and triester products were similar to one another and were typical of free base porphyrins. Each displayed four Q bands at approximately 643, 588, 546 and 513 nm. The B peak for the diester lay at 417 nm while that of the triester lay at 418 nm.

2.7.2 Iron insertion

Iron insertion into the porphyrins **2.66** and **2.67** was achieved by heating at reflux with iron(II) chloride in DCM. Sodium acetate was added as a buffer to prevent acidification. The reaction was monitored by TLC and extra iron(II) chloride added as required to complete metalation. The mixture was washed with 10% HCl in order to convert all the iron complexes to the (III) oxidation state and pair them with chloride counterions. Yields were 91% for the diester **2.58** and 73% for the triester **2.59**.

MALDI MS analysis detected the molecular ion including chloride, $MClH^+$, the molecular ion without chloride, MH^+, and a trace of the molecular ion with chloride replaced with hydroxide MOH_2^+. The UV-vis absorption spectra confirmed the conversion to the iron complexes by the broadness of the B peak, typical of iron tetraphenylporphyrins, and distinct from free-base tetraphenylporphyrins which display sharp B peaks.

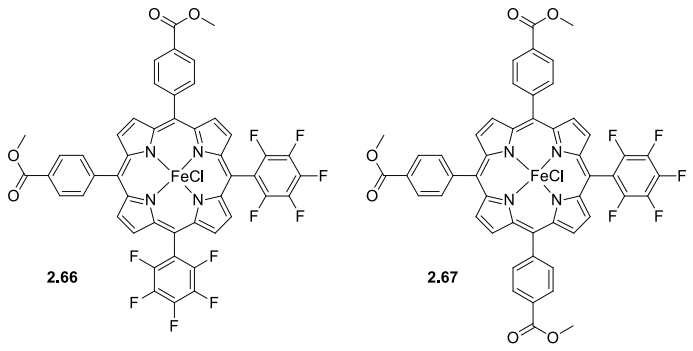

Figure 49: The iron complexes of the fluorinated porphyrins

2.7.3 Hydrolysis

Hydrolysis of the ester groups of the FeCl diester porphyrin **2.58** was carried out under the usual conditions using KOH in methanol (see Section 2.3.3). After 3 hours, the mixture was acidified with HCl which caused the porphyrin to precipitate. MALDI MS analysis of the product detected a strong ion at m/z 965 only, and this was attributed to the nucleophilic substitution of F atoms with methoxide groups (Figure 50). Indeed, it is reported that such nucleophilic aromatic substitution of perfluorinated benzene ring with alkoxide ions occurs under similar conditions.[107] This meant that the intended carboxylic acid products could not be obtained by this hydrolysis method. They could perhaps be obtained *via* an alternative method, *e.g.* acid hydrolysis, but due to time constraints this was not pursued.

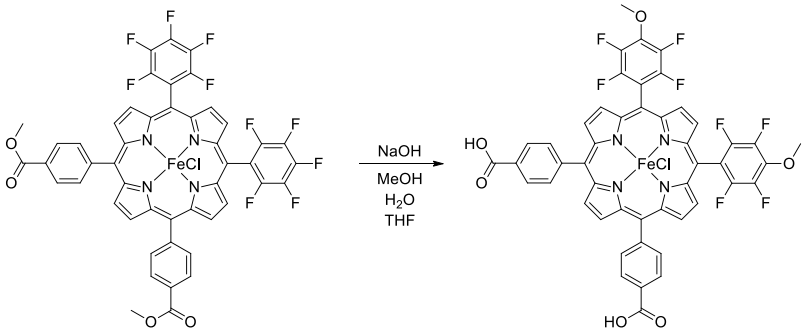

Figure 50: Treatment of the fluorinated diester porphyrin with the hydrolysis conditions resulted in the hydrolysis of the ester groups but also the nucleophilic substitution of a fluorine atom from each ring with a methoxide group

2.7.4 Electrochemical analysis

The iron pentafluorobenzene porphyrins were produced with the intention that the midpoint potential of the Fe(II) – Fe(III) transition would be influenced. The midpoint potentials of the two pentafluorobenzene ester porphyrins **2.66** and **2.67** were therefore measured using square wave voltammetry by a fellow PhD student, Chris Hobbs. The measurement was also performed for the analogous non-fluorinated porphyrins **2.15** and **2.16** to provide a comparison (Figure 51).

Square wave cyclic voltammetry was used because of its speed and easily-interpreted results[108] and this technique has been applied effectively to porphyrins in the past.[109] By scanning in the reductive direction, peaks were obtained which represented the midpoint potentials of the first three reductions of the porphyrin molecules.

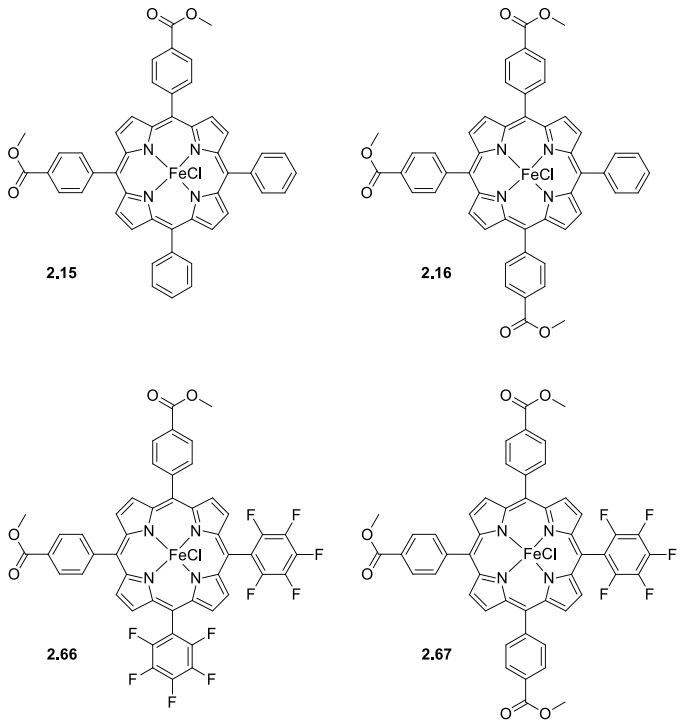

Figure 51: The compounds submitted to electrochemical analysis

The traces shown in Figure 52 show the reduction peaks. Moving from the positive end in the negative direction, the peaks represent the reduction of the bound Fe ion from the air-stable Fe(III) oxidation state first to Fe(II), then to $Fe(I)^{-}$ and finally $Fe(0)^{2-}$.[110] All voltages are relative to NHE.

The diester **2.15** requires a more negative potential (E_h = -0.045 V) to reduce the Fe ion than does the triester **2.16** (E_h = -0.006 V). This is reflective of its relative electron deficiency because of having two, rather than three, electron-withdrawing ester substituents. The diester **2.66,** bearing two pentafluorobenzene rings, accepts electrons much more readily (E_h = -0.081 V) than do either of the non-fluorinated compounds while the triester **2.67**, bearing only one pentafluorobenzene substituent, accepts electrons slightly less readily (E_h = -0.072 V), indicating that the pentafluorobenzene substituent withdraws electrons more strongly than the phenylester.

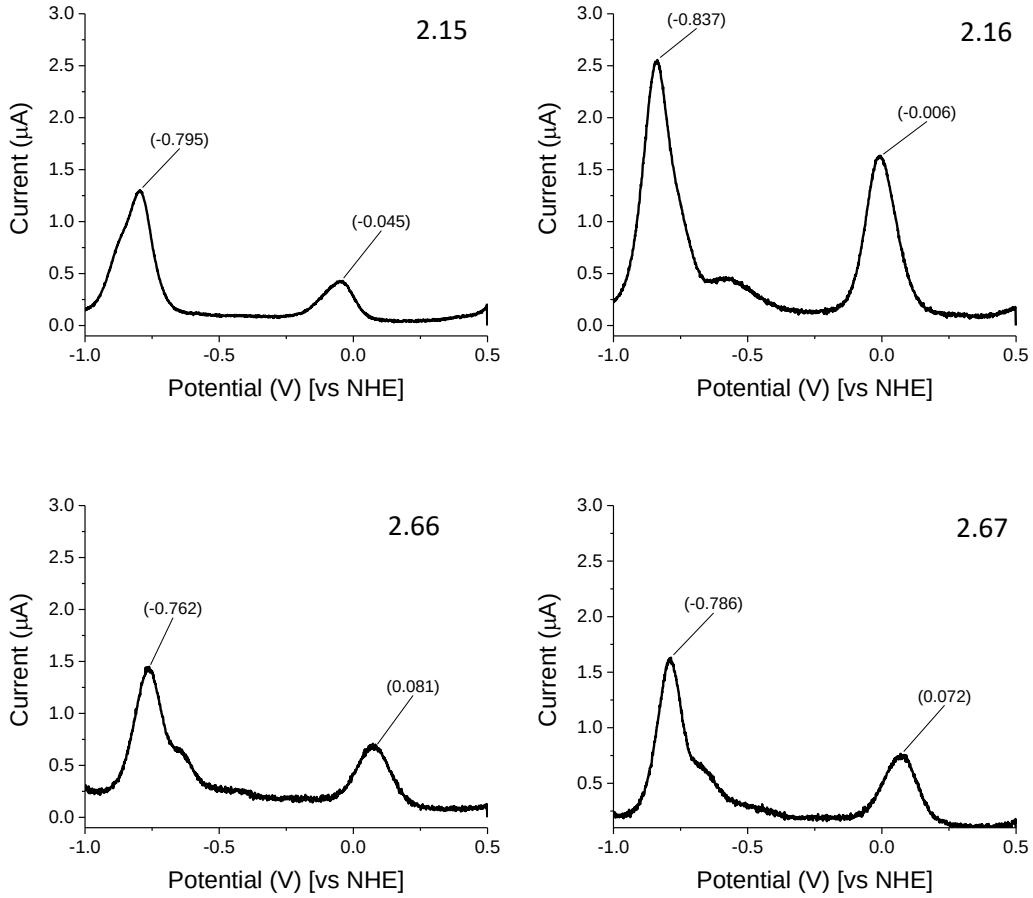

Figure 52: Square-wave voltammetry traces from the analyses of the porphyrins

By comparing the Fe(II) – Fe(III) midpoint potential of the non-fluorinated diester **2.15** (E_h = -0.045 V) and non-fluorinated triester **2.16** (E_h = -0.006 V), one can see that the addition of the extra ester group has shifted the potential by 0.039 V in the positive direction. Similarly, by comparing the non-fluorinated triester **2.16** to the fluorinated triester **2.57** (E_h = 0.072 V), one can see that in this case the addition of five fluorine atoms has shifted the potential by 0.066 V in the positive direction. Based on these values, in comparing the diester **2.15** to the fluorinated triester **2.57** (a conversion that could be made by adding one ester group and fluorinating one benzene ring), one would expect that the midpoint should be shifted by 0.105 V. The measured traces indicate that the real value is 0.117 V, only 0.012 V different from the

predicted value. Similarly, by comparing the Fe(II) – Fe(III) midpoint potential of the non-fluorinated diester **2.15** (E_h = -0.045 V) with that of the fluorinated diester **2.66** (E_h = 0.081 V), a difference of 0.126 V is observed: 0.063 V in the positive direction per fluorinated benzene ring. This is very similar to the result of the 0.066 V positive shift observed for the fluorinated *vs* non-fluorinated triesters. This value is also similar to the published midpoint value of Fe tetra pentafluorophenylporphyrin, 0.300 V higher than for Fe TPP: a 0.075 V shift in the positive direction per fluorinated benzene ring. Taken together, these results indicate that substituting a benzene ring for a pentafluorobenzene group produces a shift in midpoint potential only approximately 1.7 times as great as a single ester-bearing benzene ring.

The second iron reduction, from Fe(II) to $Fe(I)^-$ in each case occurs at voltages between 0.75 and 0.85 V more reductive than the Fe(II) – Fe(III) midpoint. The shoulder observed at -0.7 V in the traces for **2.16**, **2.66** and **2.67** may be attributed to the reduction of oxygen, present in trace amounts.

These results demonstrate control over the midpoint potential of the the Fe(II) and (III) couple of porphyrins using pentafluorobenzene substituents. While this method does not control the midpoint potential over as wide a range as might be desired, the compounds produced are a useful step towards the tailoring of both the maquette-binding and redox properties of porphyrins.

2.8 Chapter conclusion

This chapter presented the synthesis of a number of porphyrins of a variety of properties to provide a library for exploring maquette binding. The later chapters are in large part built on this work. Also produced was an amphiphilic porphyrin bearing a ferrocene substituent, a compound which may form a functional unit of a charge-separating molecular device.

Fluorinated porphyrins were produced to explore the tuning of the redox properties of porphyrins. This work lays a foundation for the production of porphyrins, tailor made with the desired redox properties, which will spontaneously bind to a protein scaffold to form a functional molecular device for performing artificial photosyntheis.

Chapter 3: Analysis of ABAB and AABB isomers

3.1 Introduction

Although there are reports of the isolation of *ABAB* ester[77,111,112] and *AABB*[112] ester porphyrins from statistical mixtures, there has been no mention of the problem of assessing the regioisomeric purity of the isolated products.

During the synthesis of the phenylporphyrin esters and phenylporphyrin QASs described in the previous chapter, it was difficult to both purify and assess the purity of the *ABAB* and *AABB* compounds. The isomers had very similar retention properties on a silica column and it was therefore not possible to be sure of achieving 100% isomeric purity in the isolated products. This problem was compounded by difficulties in actually determining the isomeric ratio in the samples that were produced. There was no significant difference in their UV-vis absoption spectra and mass spectrometry is of no use because of their identical molecular masses.

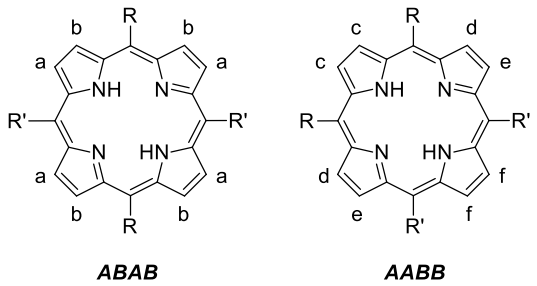

Figure 53: A comparison of the structure of the ABAB and AABB isomers with equivalent H nuclei labelled

^{1}H NMR spectroscopy did display distinct peak patterns for the β-pyrrolic protons because of their different symmetries and numbers of equivalent H nuclei (Figure 53), which enabled

the identification of each isomer. However, if the two disubstituted isomers were mixed together, the splitting patterns of the peaks from each compound were superimposed to form complex peak clusters (*vide infra*). Although it is possible to *distinguish* the two compounds by the ^{1}H NMR splitting patterns, it is not possible to determine the *isomeric ratio* in a mixed sample by this method.

During chromatographic separation the compounds were analysed by TLC, and this qualitative technique indicated that the isomers were separated to a reasonable extent. This however gave insufficient information on purity to be confident enough to carry them forward into further experiments.

For example, in the aromatic section of the spectra of the phenylporphyrin diesters **2.03** and **2.04** shown in Figure 54, it may be seen that the spectrum of the *ABAB* isomer is very similar to that of the *AABB* isomer. The peak clusters are in the same positions and differ only in their splitting patterns. The pair of doublets between 8.75 and 8.90 ppm is the only feature which clearly distinguishes the *ABAB* from the *AABB*. For the *AABB* compound, a pair of multiplets consisting of two doublets and overlapping singlets is observed in the same position. When the two compounds are mixed in approximately equal proportions the peaks are superposed to produce peak clusters from which it is not possible to confidently extract quantitative information about the isomeric ratio present in the mixture.

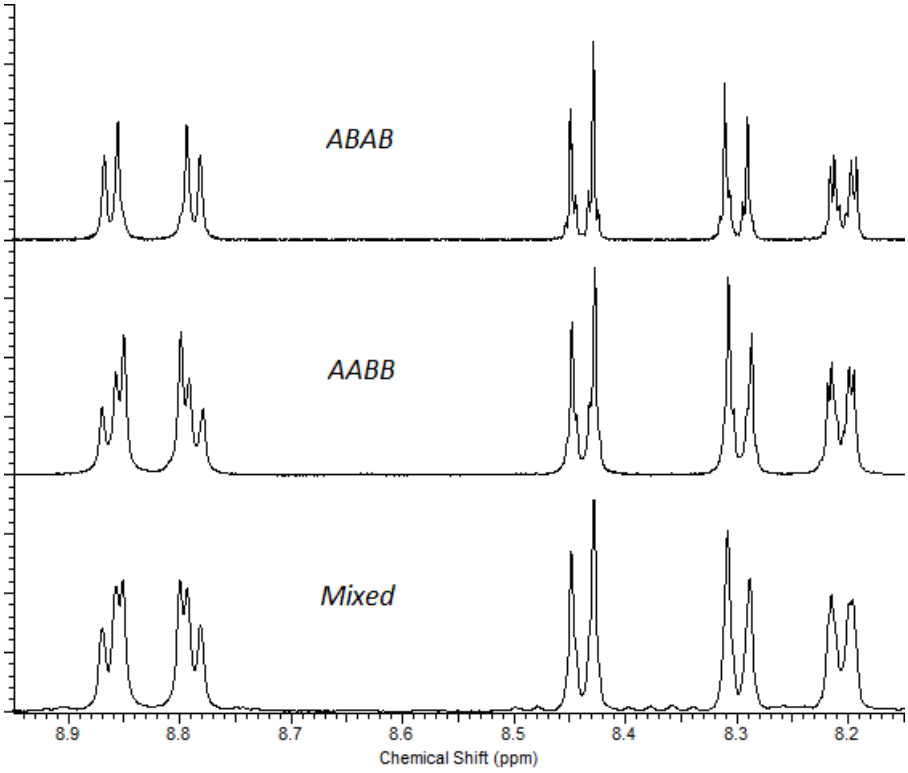

Figure 54: The overlapping signals from the β-pyrrolic H nuclei of the phenylporphyrin diesters 2.03 and 2.04, confounded the determination of the isomeric ratio in a mixed sample

Faced with this problem, and with qualitative TLC information that indicated that the compounds were almost isomerically pure, zinc was inserted into the core of each isomer in the hope that their ^{1}H NMR spectra would then diverge. It can be seen in Figure 55 that this did not occur. Although the peaks are sharpened, and one might expect less prone to superposition, the peak clusters are again superimposed for the mixed sample and no quantitative information on isomeric purity can be garnered.

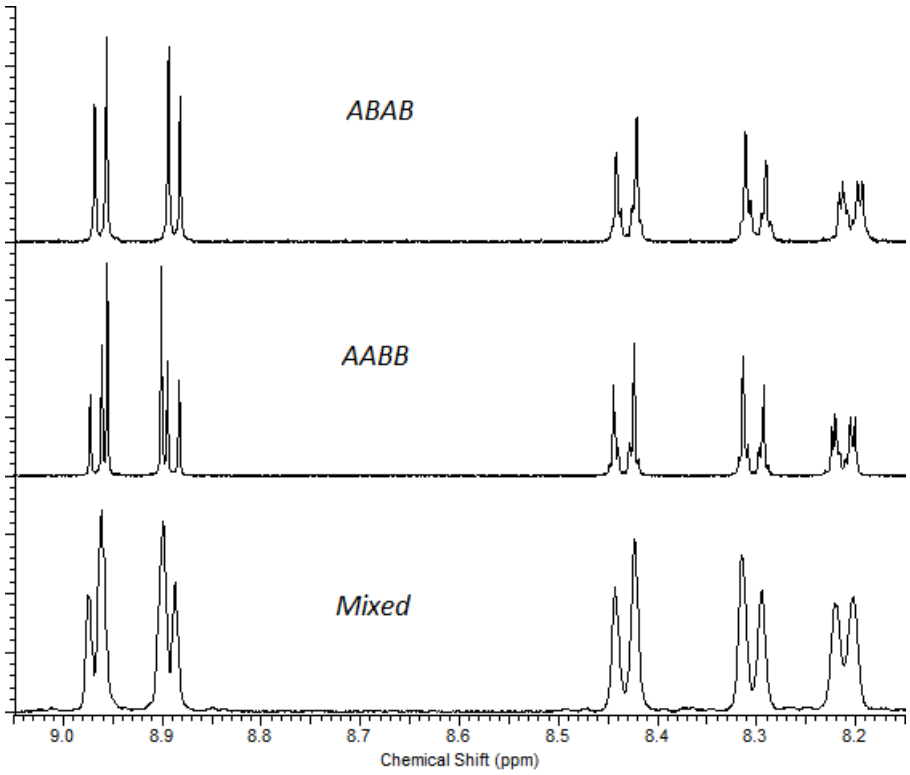

Figure 55: ^{1}H NMR spectra of the zinc phenylporphyrin diesters 2.09 and 2.10

Again the decision was made to carry the compounds to the next stage of synthesis, ester hydrolysis, in the hope that their ^{1}H NMR spectra would at last diverge. Figure 56 shows the spectra of the dicarboxylic acid products, and again it can be seen that the spectra are of no use for quantifying isomeric purity.

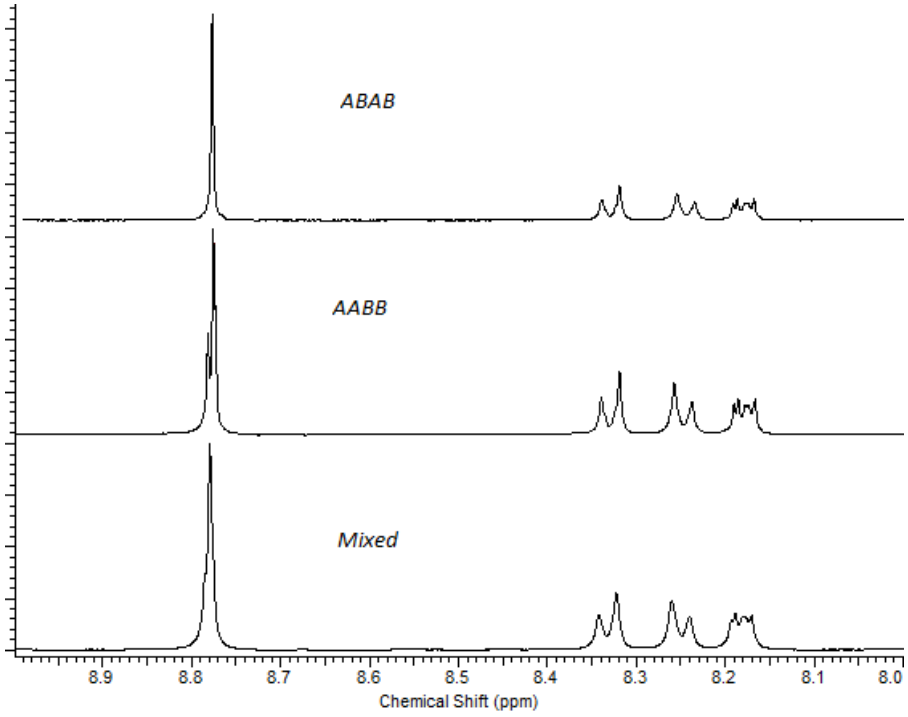

Figure 56: ^{1}H NMR spectra of the zinc phenylporphyrin diacids 2.18 and 2.19

The same problem was encountered for the di(dimethylamino)phenylporphyrins **2.47** and **2.48**. In both their free-base and zinc-metalated state, isomeric purity could not be quantitatively assessed by ^{1}H NMR. Methylation to form the QAS also failed to make the spectra of the isomers diverge. Clearly a different method of quantifying the isomeric purity of the compounds was required.

3.2 HPLC analysis

To determine the isomeric ratio of the disubstituted porphyrin products, HPLC analysis was employed. Reverse-phase HPLC was used initially to analyse the final products of the reaction scheme, that is, the carboxylic acids and quaternary ammonium salts. TLC analysis of the

original esters and amines had indicated that they were quite pure, and HPLC analysis was seen as a method of confirming this.

Conditions were also developed for normal-phase analaysis of the esters and amines produced in the porphyrin synthesis reaction so that in future the isomeric ratio of a mixed sample can be determined before further synthetic steps are taken.

3.2.1 Reversed-phase HPLC

HPLC analysis of porphyrins has typically been undertaken for the diagnosis of the disease porphyria by the analysis of urine samples, for example by Li *et al.*[113] There are also publications concerning the HPLC analysis of paleoporphyrins in order to study ancient life.[114] These analyses are of natural porphyrins, which typically bear carboxylic acid groups. It was therefore expected that the conditions identified as suitable for the analysis of natural porphyrins would also be suitable for the synthetic compounds described in Chapter 2.

These analyses typically utilise two solvent mixtures, one more-polar aqueous solvent and one less-polar organic solvent. These are then mixed in a ratio which varies during elution to enable the separation and analysis of compounds with quite different retention properties. The aqueous eluent is typically buffered with ammonium acetate and the organic eluents used are acetonitrile and methanol.[113,115,116]

Based on the conditions from the literature, trials were conducted to identify suitable conditions to analyse the synthetic porphyrins. The goal was to develop a method that would have the disubstituted porphyrins elute completely separate from one another and in a reasonable amount of time. Because of the acidity of the carboxylic acid compounds being analysed, the aqueous solvent needed to be buffered to maintain a constant level of ionisation between samples. With the assumed pK_a of approximately 4.2, the vast majority of the

carboxylic acid groups were expected to be ionised at pH 7. A more basic pH would have ionised the acid groups more completely but may have caused damage to the column.[117] Acetonitrile was chosen as the less-polar solvent.

Suitable conditions were identified as follows: the column was initially equilibrated with a mixture of 60% acetonitrile, 40% 20 mM ammonium acetate buffer set at pH 7. Over the course of 17 minutes the solvent was linearly varied to 20% acetonitrile, 80% buffer.

It was found to be necessary to dissolve the analytes in an aqueous buffer solution rather than in acetonitrile prior to injection. If the latter was used, no porphyrins would elute from the column. It seems that although these compounds appeared to dissolve in acetonitrile, they formed aggregates which could not pass through the pre-column filter.

The UV absorbance at 420 nm was used to detect the elution of porphyrins as this wavelength lies at the Soret peak of all of the porphyrins being analysed. Although there are differences between the spectra of the porphyrins bearing different numbers of acid groups, the difference between the absorbance of the two diacid isomers (in an almost isomerically pure state according to TLC analysis) at this wavelength was minimal, and so comparison of the integration of their peak areas gives a quantitative measurement of the relative proportions of these compounds.

The zinc tetraphenylporphyrin *ABAB* diacid **2.18** and *AABB* diacid **2.19** were initially investigated using a 250 mm C18 HPLC column and the eluent conditions described above. The *ABAB* diacid was eluted at 12.9 minutes and the *AABB* diacid at 13.9 minutes, with their peaks being separated completely (Figure 57, a and b). The trace from the analysis of the *ABAB* diacid (a) displays a peak for the residual quantity of *AABB* diacid. The same is true for the trace from the *AABB* diacid (b); a residue of *ABAB* is visible. In both traces the *ABAB* and *AABB* compounds consistently eluted at 12.9 and 13.9 minutes respectively. Integration of the peaks revealed

the isomeric purities of the *ABAB* diacid **2.18** and the *AABB* diacid **2.19** as 96% and as 98% respectively.

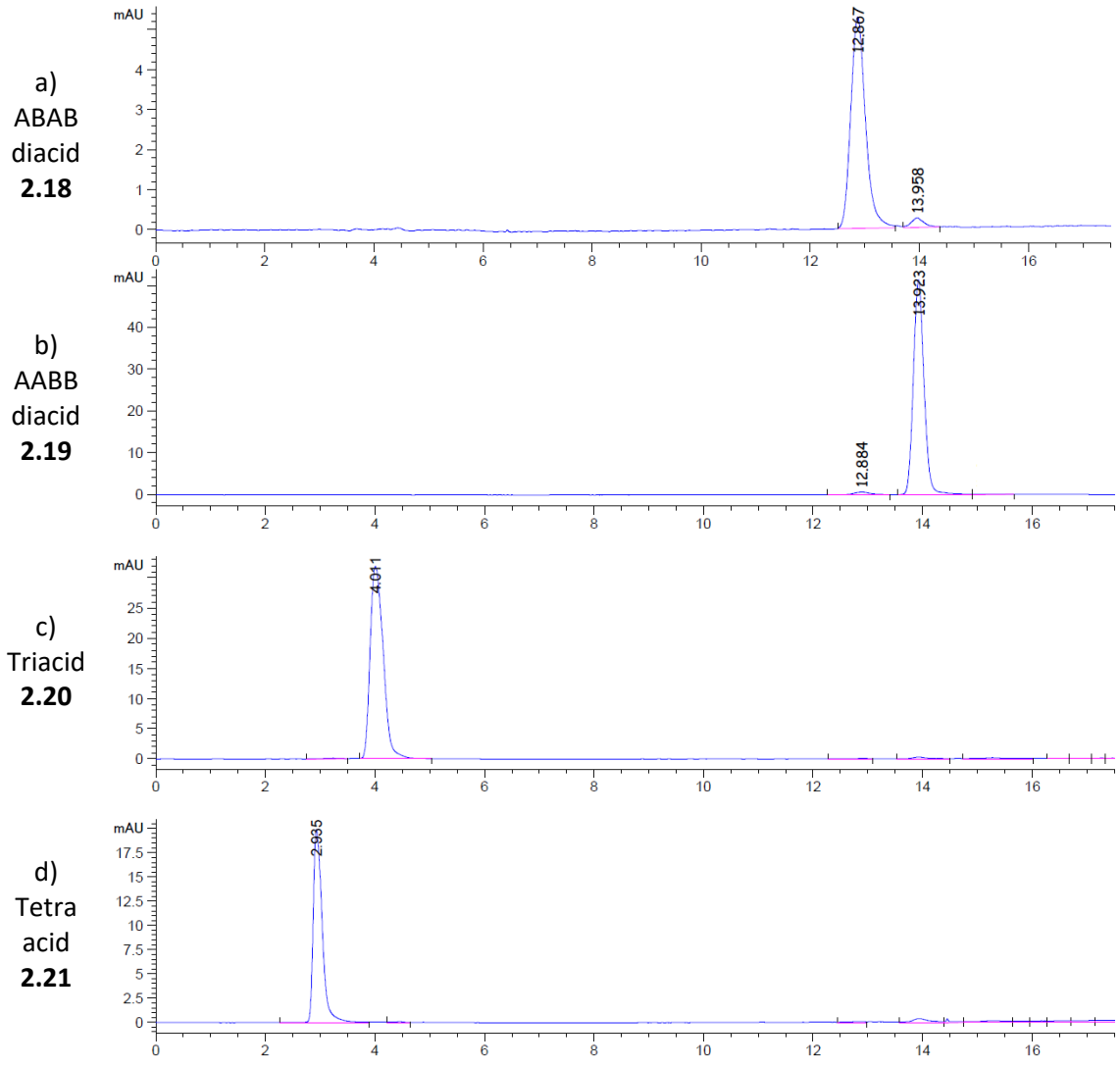

Figure 57: HPLC traces of the zinc phenylporphyrin carboxylic acids

The technique was also applied to the other members of the zinc phenylporphyrin carboxylic acid series **2.17**, **2.20** and **2.21**. As was expected in reversed phase chromatography, the most polar compound, the tetraacid **2.21**, eluted earliest at 2.9 minutes and the triacid

eluted at 4.0 minutes (Figure 54, c and d). The monoacid **2.17** did not elute after 1 hour of continued solvent flow, likely because of aggregation due to its greater hydrophobicity.

The porphyrin di QASs **2.57** and **2.58** also would not elute at all, although HPLC analysis of QAS compounds has been reported.[118–120] It is possible that because the eluent was buffered at a pH above the pK_a of any residual silanol groups on the column that the cations paired with siloxy anions and thus became anchored to the column.[121]

This technique provided a confirmation of the isomeric purity of the porphyrin dicarboxylic acids and is a useful tool for the analysis of porphyrin carboxylic acids in general. It does however have some limitations. Although it was useful to be able to confirm the purity of the amphiphilic porphyrins before they were used in further experiments, if their purity had been found to be inadequate it would be very difficult to purify them because they are not amenable to chromatography on silica, and preparative reverse phase chromatography is slow and expensive. Also problematic is that this technique was not applicable to all porphyrin types, namely the porphyrin monoacid and all of the QASs. It is desirable that the purity of the diesters and diamines be determined when they are first isolated from their respective porphyrin synthesis reactions, and normal-phase HPLC was pursued to this end.

3.2.2 Normal-phase HPLC

In order to assess the isomeric purity of the *ABAB* and *AABB* isomers directly after their synthesis, and therefore at a stage when further purification by flash chromatography may be undertaken, methods for normal-phase HPLC analysis were developed. With a view to developing a general method which could be applied to a range of porphyrin syntheses to be undertaken in the future, the three complete series of porphyrins were analysed and not only the disubstituted compounds.

There is very little literature surrounding the normal phase HPLC analysis of porphyrins, but solvents could be chosen based on those found to work well during flash chromatography. For porphyrin esters, initially 20% hexane in DCM was used as the eluent because of the high degree of solubility of most porphyrins in that solvent mixture, and because of its proven effectiveness in flash chromatography. The addition of hexane had been necessary to separate the tetraphenylporphyrin monoester **2.02** from tetraphenylporphyrin **2.01** in flash chromatography but was unnecessary for HPLC, as 100% DCM was effective in separating these compounds.

Detection was achieved by monitoring UV absorbance at 410 nm, a wavelength strongly absorbed by the B bands of all the porphyrins tested. The B peaks of the disubstituted porphyrins of each type lay in the same positions and had similar extinction coefficients, and this allowed the quantitative determination of the isomeric ratio of mixed samples. This was successful in separating the phenylporphyrin diesters **2.03** and **2.04** as shown in Figure 58. The *ABAB* diester **2.03** eluted at 2.932 minutes, while the *AABB* isomer **2.04** eluted at 3.326 minutes. Integration of the peaks revealed isomeric purities of 99% and 98% respectively.

ABAB phenylporphyrin diester **2.03**

AABB phenylporphyrin diester **2.04**

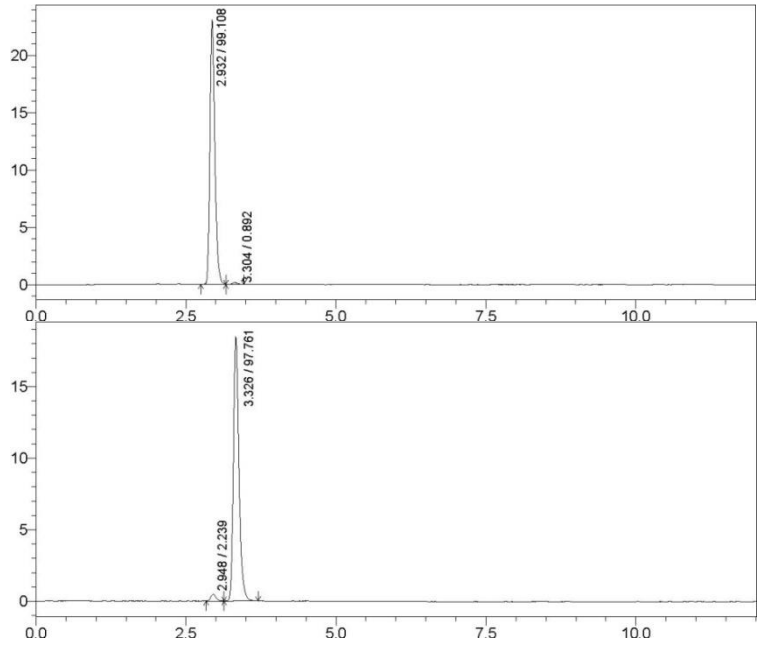

Figure 58: HPLC analysis of phenylporphyrin diesters in 100% DCM showing complete separation

These conditions were also applied to a mixture of porphyrins made by mixing approximately equal amounts of each member of the phenylporphyrin series **2.01** – **2.06**. Using 100% DCM, the phenylporphyrin triester and the tetraester took more than 30 minutes to elute, and 0.1% methanol was added to reduce their elution time. Much less methanol was required for HPLC than for flash chromatography. In flash chromatography solvents mixtures containing up to 1% methanol were effective but on the HPLC column 0.1% methanol was sufficient to reduce the tri and tetraester elution times to 3.4 and 5.0 minutes respectively, and this solvent system was applied to the whole series of phenylporphyin esters including TPP (Figure 59). The same solvent mixture was also applied to the butylporphyrin esters.

While effective in analysing the porphyrin purity, this solvent system did not completely separate the two diester isomers as well as did 100% DCM. Also, in order to transfer the column to the methanol-containing eluent a long period of equilibration was required. Complete equilibration required 100 mL of solvent, which completely negated the solvent savings from having the porphyrins elute more quickly. Therefore, unless many samples of porphyrin triesters or tetraester are to be analysed, methanol is best not used.

Phenylporphyrin *ABAB* diester **2.03**

Phenylporphyrin *AABB* diester **2.04**

All phenylporphyrin ester series **2.01** – **2.06**

All butylporphyrin ester series (inc. tetrabutyl but not tetraester) **2.26** – **2.30**

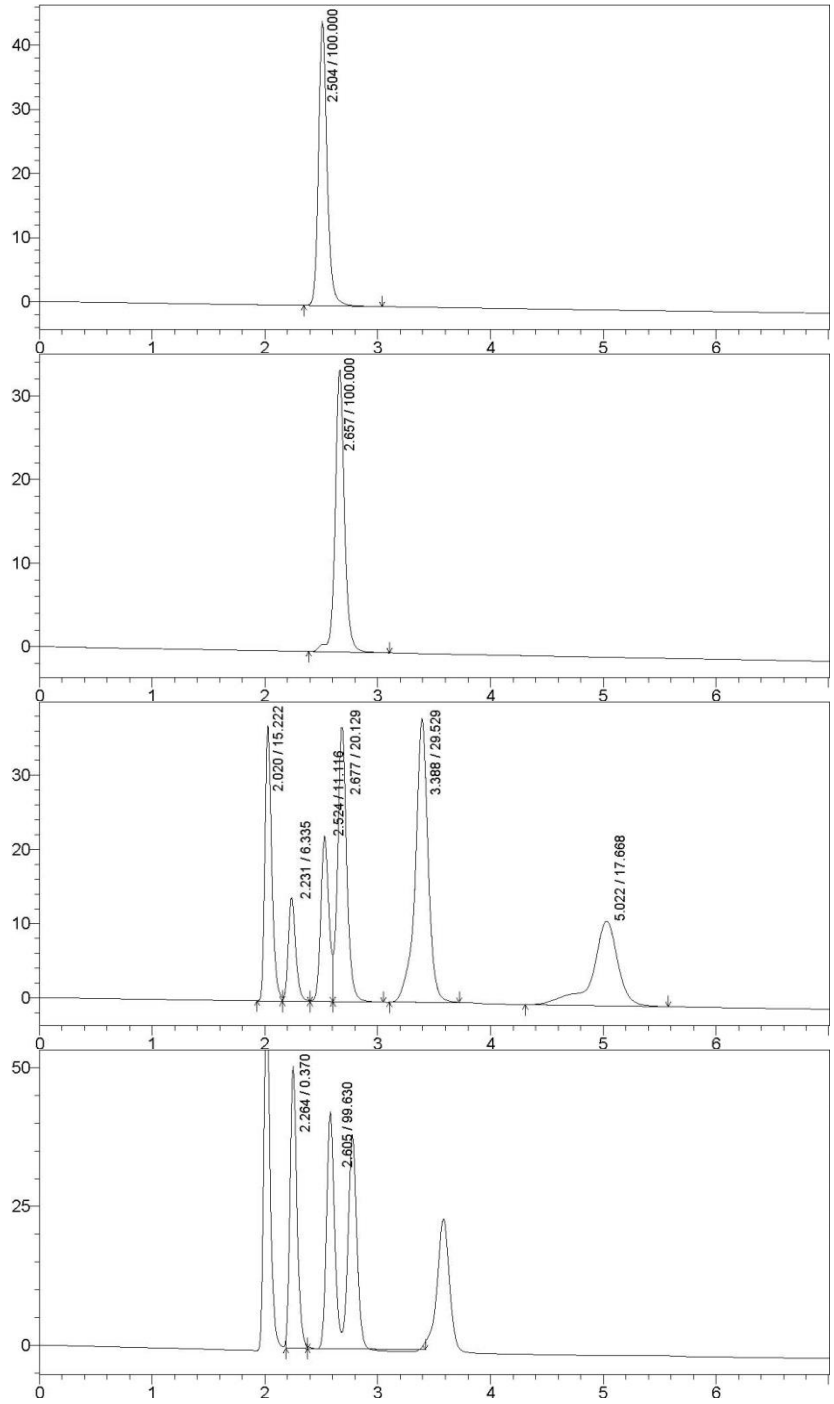

Figure 59: Normal phase HPLC analysis of the phenylporphyrin esters in 0.1% methanol in DCM

A mixture of the aminophenylporphyrins **2.44** – **2.47** was prepared and analysed, but none of them eluted from the column unless 0.1 % triethylamine was added to the solvent mixture. This was in line with what was encountered during flash chromatography. Using 0.1 % triethylamine in DCM, the dimethylaminophenyl porphyrins were separated effectively (Figure 60).

The traces for the disubstituted porphyrins show that they were effectively separated from one another, allowing assessment of their isomeric purity. The *ABAB* di(dimethylaminophenyl)porphyrin **2.45** eluted at 2.57 minutes, while the *AABB* isomer **2.46** eluted at 2.79 minutes. The integration of the peaks shows isomeric purities of 92% for the *ABAB* isomer and 93% for the *AABB* isomer.

ABAB di(dimethylaminophenyl) porphyin **2.45**

AABB di(dimethylaminophenyl) porphyin **2.46**

Mono, *ABAB* di, *AABB* di and tri(dimethylaminophenyl) porphyrins **2.44** – **2.47**

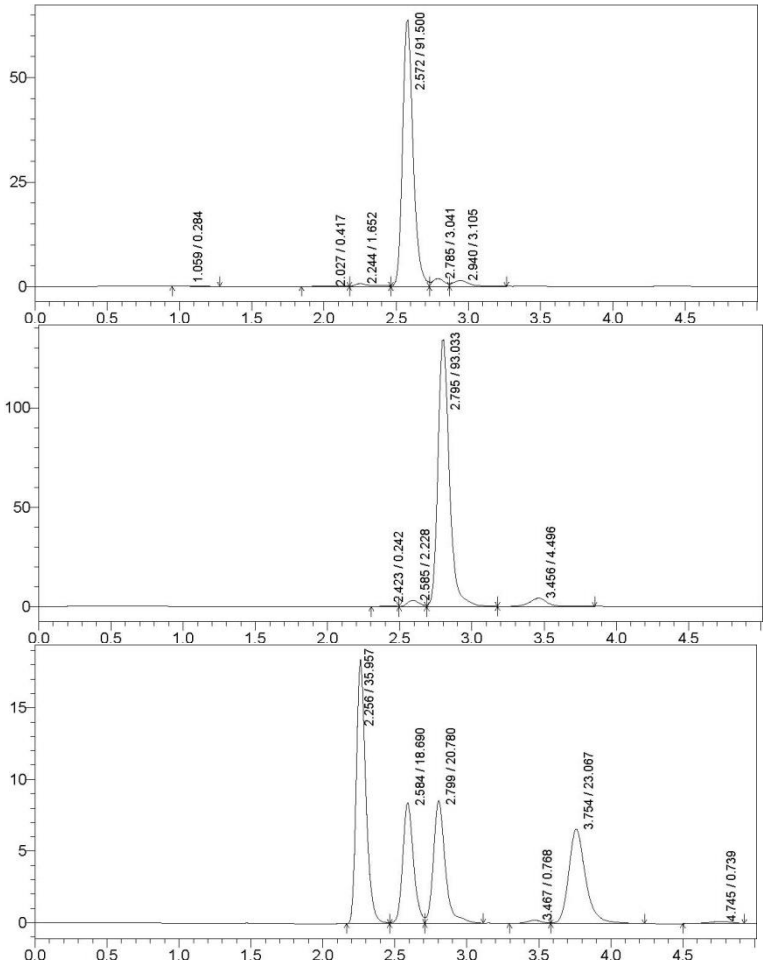

Figure 60: HPLC analysis of the aminophenylporphyrins using 0.1% triethylamine in DCM

3.3 Chapter conclusion

HPLC was proven as an efficient technique for analysis of complex porphyrin mixtures. Conditions for porphyrin esters and dimethylamines were developed and used to assess the purity of porphyrin samples, especially the isomeric purity of disubstituted porphyrin samples. Both reversed-phase and normal phase conditions were developed. These analytical techniques are a useful tool for future syntheses, especially where ^{1}H NMR spectroscopy data can be difficult to interpret because of spectral complexity and overlapping peaks.

Chapter 4: Phenylene-linked porphyrin arrays

4.1 Introduction

As discussed in Chapter 1, multiporphyrin arrays offer the possibility of delivering photonic energy to a reaction centre at a higher rate than can be achieved using a single chromophore. Natural photosynthesis makes use of a non-covalently bound chromophore array to deliver photons to its water oxidising catalyst at a high rate to minimise the amount of time that reactive intermediates must exist. It is therefore an important challenge to produce a porphyrin array that will form an ensemble with a protein maquette with a similar goal in mind.

Following the success of the experiments using single porphyrins to investigate binding requirements (see Chapter 7), work commenced to synthesise porphyrin arrays based on the principles of amphiphilicity which had proven successful in achieving maquette binding. Many different methods of porphyrin array formation have been employed in the past, as discussed in Chapter 1.[58] One of these methods is to use mixed-aldehyde condensation to form an array as part of a statistical mixture. This chapter will present the investigations undertaken to synthesise arrays by extension of the statistical mixture approach employed successfully to form the amphiphilic single porphyrins described in Chapter 2.

4.1.1 Porphyrin arrays from statistical mixtures

Porphyrin arrays have been constructed in the past by building a porphyrin ring on an aldehyde group already attached to a porphyrin. This approach had been used by Wennerström *et al*. to make a dyad and a pentad[66] and by Officer *et al.* to make a nine-porphyrin array.[69] The pentads and nine-porphyrin array were made by condensing a single aldehyde-bearing porphyrin with pyrrole in a porphyrin synthesis reaction. The symmetrical dyad of Wennerström, however, was produced by the condensation of a mixture of an aldehyde-bearing porphyrin and benzaldehyde with pyrrole, and was therefore a mixed-aldehyde condensation. It was envisioned that similar mixed-aldehyde condensations could be used to form an asymmetrical amphiphilic porphyrin dyad (Figure 61), and that the process could be extended to produce larger arrays.

The synthesis was undertaken in two stages; first the precursor aldehyde-bearing porphyrins were produced, also using the statistical mixture method, and then these reagents were used in condensation reactions to produce the arrays.

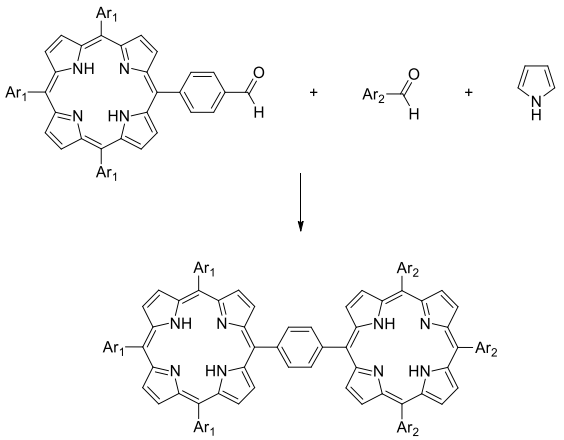

Figure 61: The synthesis of an asymmetrical porphyrin dyad *via* mixed-aldehyde condensation

4.2 Synthesis of meso-aldehyde bearing porphyrins

Syntheses of porphyrins bearing *meso*-benzaldehyde functionality had been published in the past. This had been done by oxidation of a porphyrin benzyl alcohol produced by reduction of the analogous carboxylic acid[122] or ester,[123] Bouveault formylation[66] and *via* a monoprotected phthalaldehyde.[124] Several options were therefore available for the synthesis of aldehyde-bearing porphyrins.

Bouveault formylation of bromophenyl porphyrins appeared to be the best method because it involves fewer steps than the alcohol reduction method and does not require the synthesis of a monoprotected phthalaldehyde starting material, instead using the commercially available 4-bromobenzaldehyde.

4.2.1 Porphyrin aldehydes via Bouveault formylation

Bromophenyl porphyrin synthesis

According to the procedure of Wennerström *et al.*[66] a statistical mixture of porphyrins bearing various numbers of *meso* p-bromophenyl groups can be produced from a mixed-aldehyde condensation. Following this procedure, a mixture of one equivalent of 4-bromobenzaldehyde and three equivalents of benzaldehyde was condensed with four equivalents of pyrrole. The aldehyde molar ratio of 1:3 was chosen in order to favour the formation of the monobromo product (it was assumed that the aldehydes had approximately equal reactivity). The condensation was performed by mixing the reagents in refluxing propanoic acid according to the conditions of Adler.[31]

The mixture of porphyrins was isolated from the crude reaction mixture, but the individual porphyrin components were not separated because of their very similar chromatographic retention properties. In order to gain some insight into the outcome of this statistical

synthesis, ^{1}H NMR analysis was performed on this mixture. The NH peak of TPP was assigned from a known sample and by assuming that the NH peaks further upfield belonged to porphyrins with increasing numbers of electron-withdrawing bromine substituents (as was observed for the porphyrins bearing electron-withdrawing ester groups: **2.01** – **2.06** and **2.26** – **2.31**), integration of these NH peaks indicated that the porphyrin products were present in the following molar ratio: TPP **2.01** (28%), monobromo **4.01** (39%), dibromo **4.02** and **4.03** (24%), tribromo **4.04** (8%), tetrabromo **4.05** (<1%) (Figure 62). This equates to 39% monobromoporphyrin by mass.

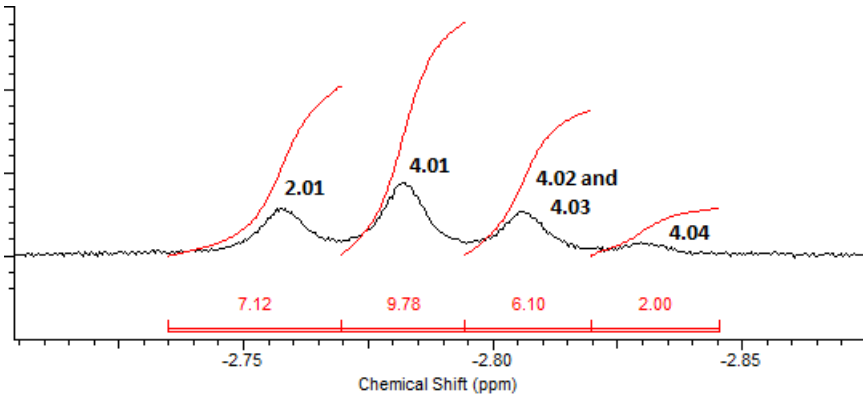

Figure 62: The NH signals in the ^{1}H NMR spectrum of the bromoporphyrin statistical mixture showing the molar ratios of TPP 2.01, monobromo 4.01, dibromo 4.02 and 4.03 and tribromo 4.04 porphyrins to be 7.12 : 9.78 : 6.10 : 2.00, simplifying to 28%, 39%, 24% and 8% respectively

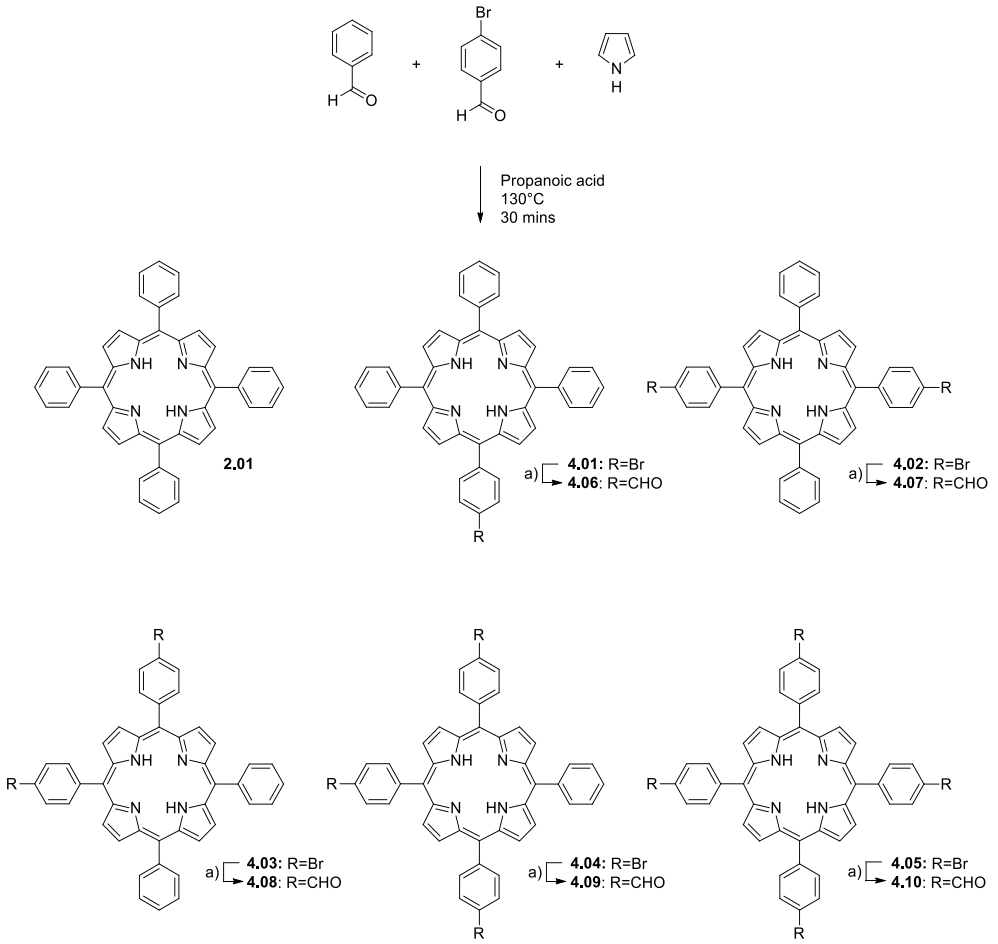

Figure 63: The mixed-aldehyde condensation and Bouveault formylation used to form p-formylphenylporphyrins. Reaction conditions: a) n-BuLi followed by DMF

Bouveault formylation of bromophenylporphyrins

The bromine substituents were then replaced with formyl groups *via* Bouveault formylation to form the compounds **4.06** – **4.10** shown in Figure 63. This was carried out by treating a diethyl ether solution of the mixture of bromophenyporphyrins at -84 °C with *n*-BuLi followed by DMF in an adaptation of the conditions of Wennerström *et al.*[66]

The mixture of formylporphyrins thus generated was submitted to flash chromatography. TLC analysis indicated that the separation had been very effective and the second porphyrin fraction, expected to contain the monoaldehyde **4.06**, was concentrated and treated with

methanol to precipitate the porphyrin product. MALDI MS analysis of this product revealed however that in addition to the expected ion at m/z 643.25, the porphyrin monoaldehyde molecular ion MH^+, there were also ions at m/z 615, 671, 699 and 727, which could be assigned to TPP **2.01**, the dialdehydes **4.07** and **4.08**, the trialdehyde **4.09** and tetraaldehyde **4.10** compounds respectively. ^{1}H NMR analysis showed two overlapping NH peaks and seemed to indicate a mixture of compounds. Careful repeated TLC analysis indicated a minor contamination with TPP, but there was no trace of dialdehyde or tetraaldehyde present (these had significantly lower rf values and were detected in later fractions from flash chromatography, confirmed by MALDI MS). It seemed unlikely that the compounds could bear extra aldehyde groups and yet not be distinguishable chromatographically.

This result may be explained when it is realised that a butyl substituent plus a hydrogen atom has a very similar mass (58.12 Da) to two formyl groups (58.01 Da). The anomalous masses could then be explained by the lithiated benzene rings having reacted with the *in situ*-generated bromobutane to place a butyl chain where the bromine atom had been before as shown in Figure 64, a previously recognised process.[125] The anomalous masses could be therefore explained by the compounds shown in Figure 65.

Because these butyl chain-bearing porphyrin aldehydes could not be chromatographically separated from the porphyrin monoaldehyde **4.06**, the product mixture was not used for further synthesis and this approach was not pursued further.

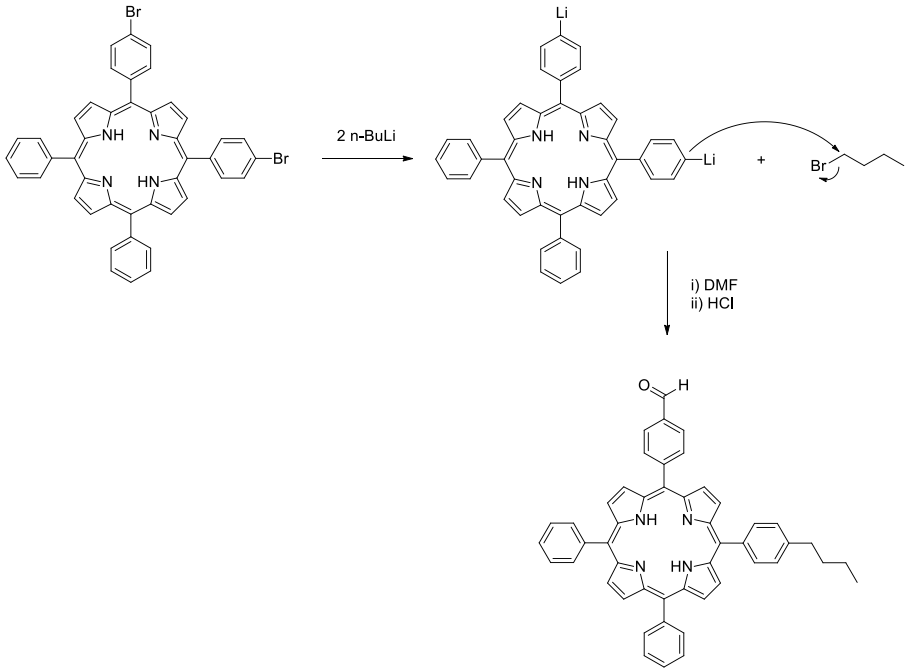

Figure 64: The mechanism *via* which butyl chain-bearing porphyrins were likely generated

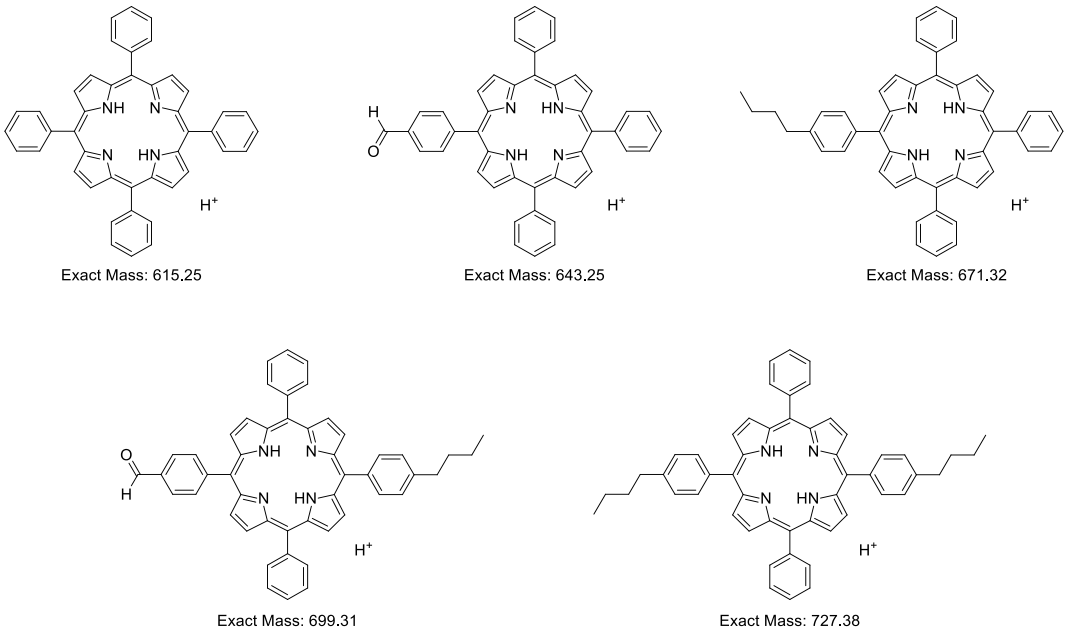

Figure 65: Structures of ions likely detected during MALDI MS analysis

4.2.2 Porphyrin aldehydes via monoprotected phthalaldehyde

Following the failure of Bouveault formylation to produce pure aldehyde-bearing porphyrins, an alternative strategy was pursued. A monoprotected phthaladehyde was prepared, from which the required aldehyde porphyrin statistical mixture was then produced.

Synthesis of monoprotected phthalaldehyde

The monoprotected phthaladehyde **4.12** was prepared in two steps according to the procedure of Hong *et al.*[126] (Figure 66). 4-Bromobenzaldehyde was protected with 2,2-dimethylpropaneglycol (DPG) catalysed by *p*-toluenesulfonic acid. The product **4.11** was purified *via* flash chromatography and was isolated in a yield of 99%. The ^{1}H NMR spectrum matched the published spectrum.[126]

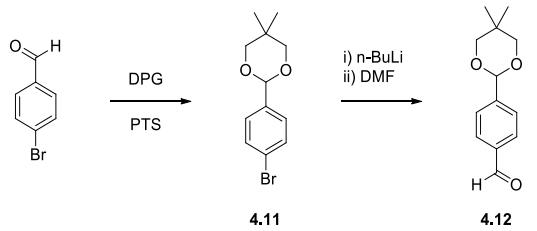

Figure 66: The synthesis of a monoprotected phthalaldehyde in two steps from 4-bromobenzaldehyde

The bromine substituent was then replaced with a formyl group *via* Bouveault formylation. A solution of the protected 4-bromobenzaldehyde in THF was treated with *n*-BuLi followed by DMF. The product **4.12** was purified by flash chromatography and isolated in a yield of 71%. The ^{1}H NMR spectrum was fully consistent with the published spectrum.[126]

Condensation and deprotection to form an aldehyde porphyrin statistical mixture

Using a method similar to that employed by Bhat *et al*.,[124] a statistical mixture was produced from monoprotected pthalaldehyde **4.12** and benzaldehyde according to the conditions of Lindsey[32] (Figure 67). Initially, an attempt was made to chromatographically separate the porphyrins in their protected form, but this was confounded by the fact that some deprotection had occurred during the porphyrin synthesis process, evident from TLC and MALDI MS analysis. The presence of TFA and a trace of water in the reaction likely caused the hydrolysis of some of the protecting groups. Because of the different retention properties of a protected *vs.* unprotected aldehyde and the large number of products generated by this random partial deprotection, no useful separation could be performed. Instead the porphyrins were purified from the non-porphyrinic reaction products *via* flash chromatography and, as a mixture, submitted to deprotection. This was carried out by treatment with a 5:2:8 v/v/v mixture of TFA, water and DCM. The resulting porphyrin aldehydes could now be successfully separated from one another *via* flash chromatography to give monoaldehyde **4.06** 1.5%, *ABAB* dialdehyde **4.07** 0.5%, *AABB* dialdehyde **4.08** 1.1% and trialdehyde **4.09** 2.8%. The tetraaldehyde **4.10** was not isolated.

These yields are lower than can usually be expected from a porphyrin synthesis reaction under Lindsey's conditions. This was likely due to the occurrence of deprotection of the aldehyde groups and subsequent formation of polymeric products *via* reaction of the now-unprotected aldehyde groups with pyrrole and pyrromethane oligomers.

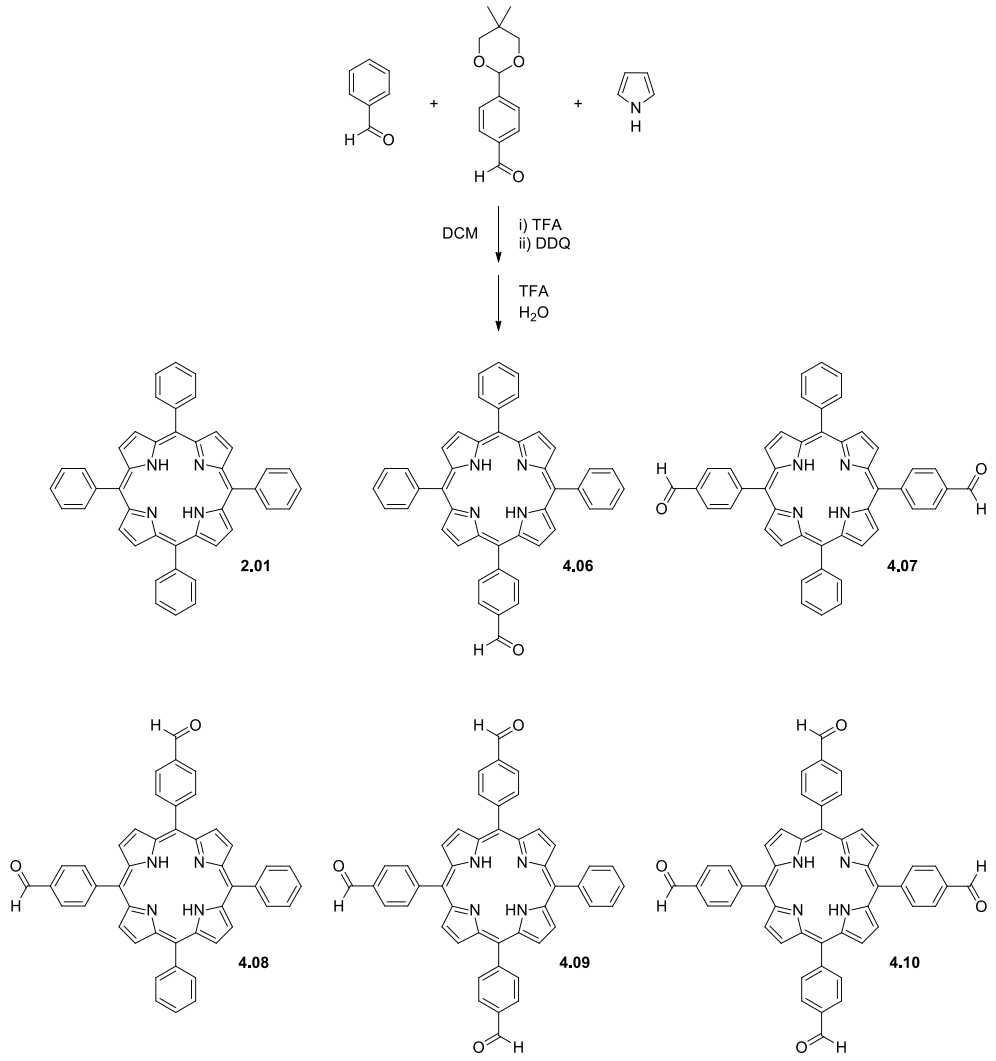

Figure 67: The synthesis of a porphyrin aldehyde statistical mixture *via* a monoprotected phthaladehyde

The ^{1}H NMR spectra of the products enabled their identification. They each displayed NH signals at around -2.75 ppm and benzene-ring and β-pyrrolic signals, depending on their substitution pattern, which were very similar to those of the analogous members of the phenylporphyrin ester series **2.02- 2.05** in Chapter 2. Furthest downfield, at around 10.4 ppm, the signal from the aldehyde protons appeared. The integration of this peak confirmed the number of aldehyde groups in the molecule and therefore the identity of each product. The ^{1}H

NMR spectrum for the monoaldehyde matched the spectrum from the literature[124] but the spectra of the other compounds were not available.

The UV-vis spectra were typical of free base tetraphenylporphyrins, displaying four Q bands and a sharp B band at around 421 nm. MALDI MS analysis detected the MH^+ ion for each compound.

4.3 Synthesis of porphyrin arrays

4.3.1 Ester porphyrin dyad formation in a statistical mixture

With the porphyrin aldehydes at hand, the next step was to construct a dyad by forming a second porphyrin ring from the attached formyl group of the porphyrin monoaldehyde **4.06**. This was accomplished *via* the statistical mixture method as shown in Figure 68.

In order to promote the maximum dyad yield and limit the production of other arrays in the statistical product mixture, a large excess of the benzaldehyde ester and pyrrole (10 eq. of pyrrole and 9 eq. of ester) were initially used in the condensation reaction with porphyrin aldehyde **4.06** using a TFA catalyst under Lindsey's conditions.[32] This strategy is analogous to the skewing of the statistical outcome used for the synthesis of bromoporphyrins in Section 4.2.1. The resulting porphyrinogen mixture was oxidised with p-chloranil. Products were isolated by flash chromatography. A yield of 12% of the dyad **4.11** was obtained. However, MALDI MS analysis of an earlier chromatography fraction detected an ion of m/z 1805. This corresponds to the MH^+ ion of the porphyrin triad **4.12**, a result of two molecules of porphyrin aldehyde **4.01** being incorporated into the same product. Therefore to further optimise the formation of the dyad product **4.11**, the reaction was repeated twice using 15 equivalents of pyrrole and 14 equivalents of 4-formylbenzoic acid methyl ester, and this produced dyad yields

of 23% and 28% and much smaller quantities of the triad. This demonstrated the effective control of the product ratio that can be achieved by varying the ratio of aldehyde reagents.

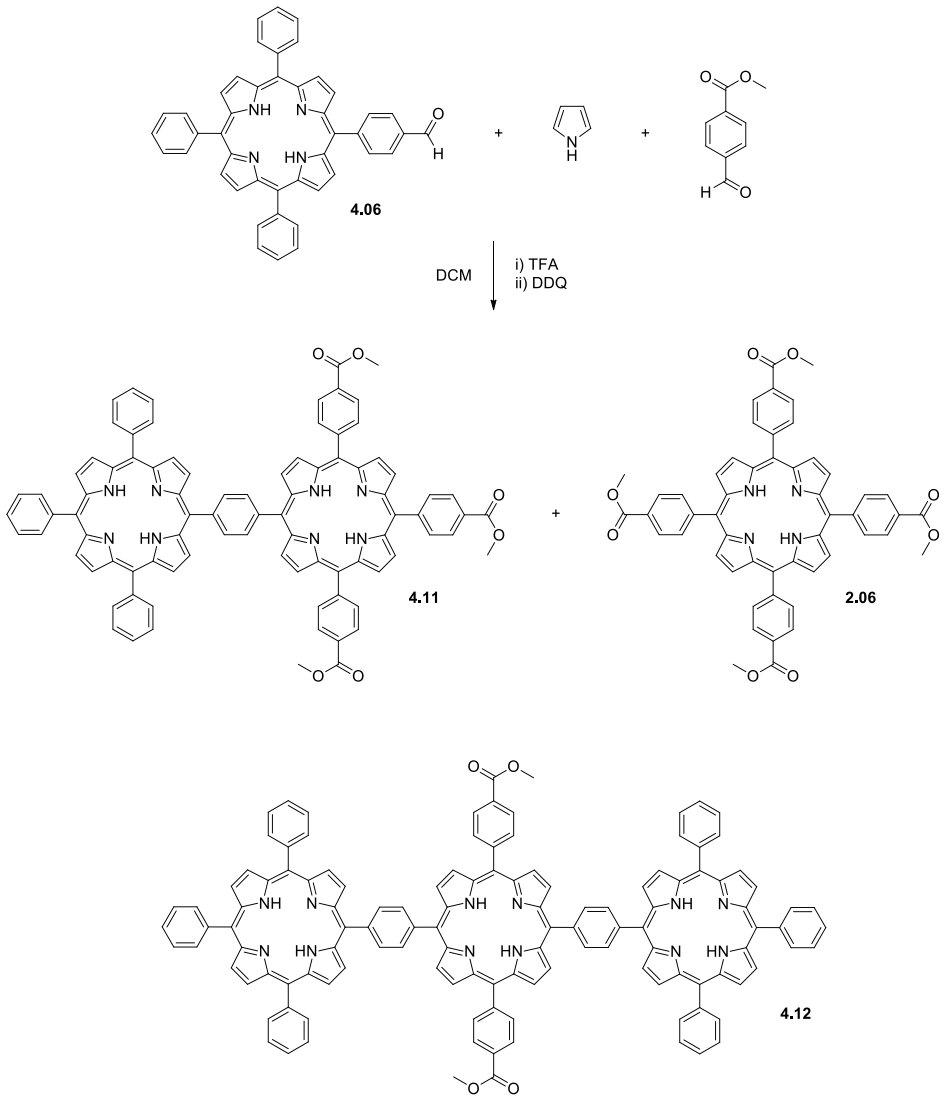

Figure 68: The synthesis of the phenylene-linked ester dyad

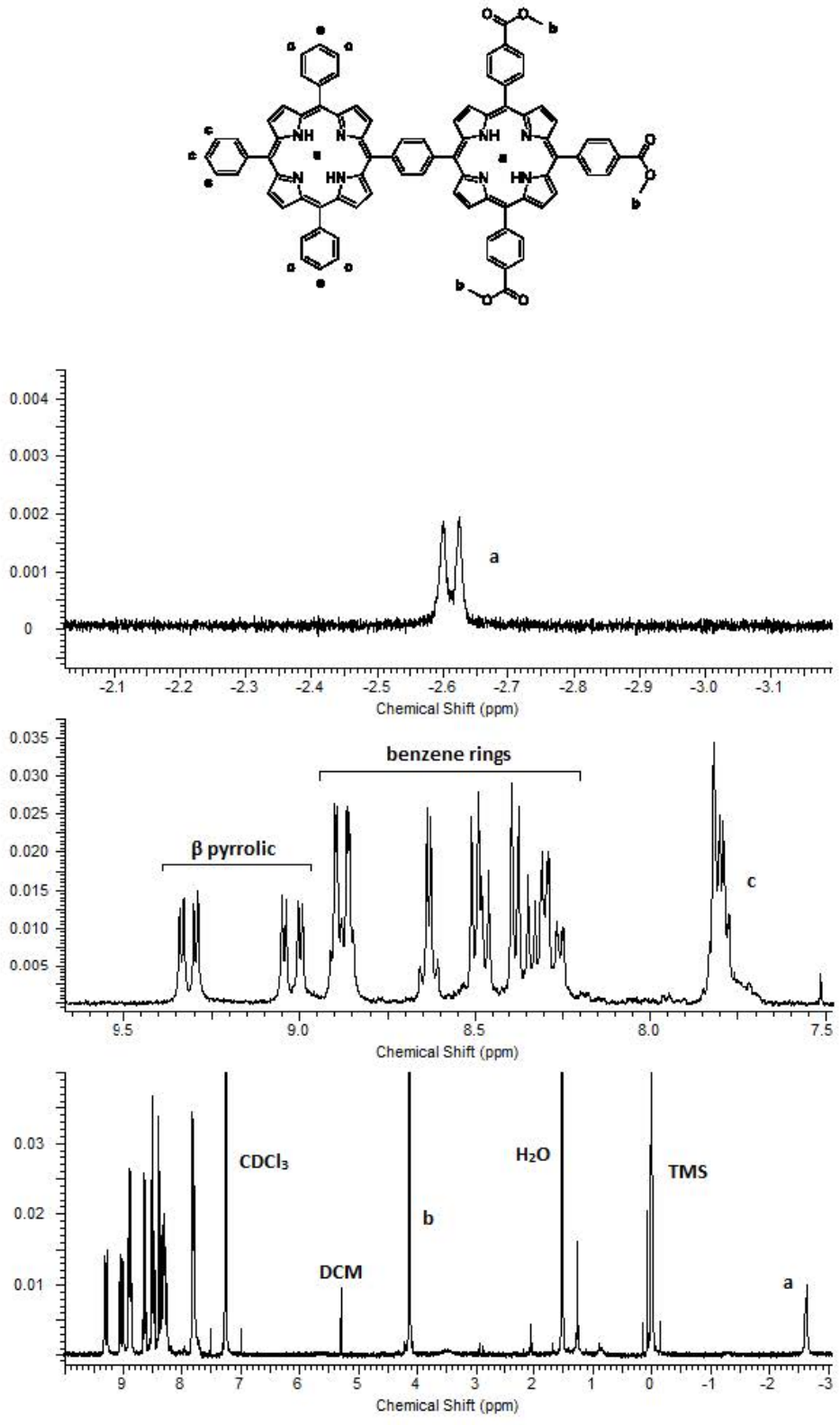

Figure 69: The ^{1}H NMR spectrum of the porphyrin dyad 4.11

The ^{1}H NMR spectrum (Figure 69) of the dyad **4.11** displayed two NH peaks of equal integration at -2.61 and -2.63 ppm. This was a good indication that the product contained two porphyrin rings with different electronic structure. Two singlets at 4.13 and 4.14 ppm, which integrated to 3H and 6H respectively were attributed to the three ester CH_3 groups. A multiplet between 7.70 and 7.85 ppm integrated to 9H and was attributed to the *meta* and *para* protons of the three unsubstituted *meso* benzene rings. Several multiplets between 8.20 and 8.95 ppm with a total integration of 22H were attributed to the remaining benzene ring H nuclei. Four overlapping doublets between 8.82 and 8.93 ppm with a total integration of 8H were attributed to the β-pyrrolic protons of the non ester-substituted porphyrin. Four 2H doublets at 9.00, 9.04, 9.30 and 9.34 ppm were attributed to the β-pyrrolic protons of the ester-substituted porphyrin. MALDI MS analysis of the dyad detected an ion of m/z 1325, which was attributed to the molecular ion MH^+ of the dyad.

The UV-vis absorption spectrum is interesting in that it displays two B peaks at 428 nm and 420 nm (Figure 70). This would not be expected if the spectrum was a simple superposition of the absorption of the two porphyrin halves; the B peak of tetraphenylporphyrin **2.03** appeared at 418 nm, and that of tetraphenylporphyrin triester **2.05** appeared at 420 nm. This outcome may be attributed to electrostatic interaction between the porphyrin chromophores and is known as Davydov splitting.[127] This means that the two peaks do not come one from each porphyrin, but that both are produced by both porphyrins because of their interaction with one another while remaining separate chromophores due to the out-of-plane orientation of the phenylene linker. There were also four Q bands at 647, 590, 552 and 516 nm, typical of free base porphyrins.

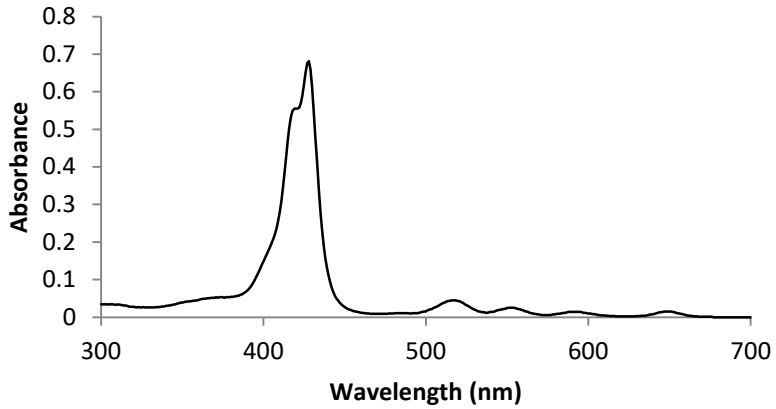

Figure 70: The UV-vis absorption spectrum of the phenylene-linked porphyrin triester dyad 4.11 (in $CHCl_3$, 1.2 μM)

4.3.2 Dimethylamine porphyrin dyad

The same process as in the previous section was adapted to produce a dimethylaminoporphyrin dyad **4.13** (Figure 71). The monoaldehyde **4.06** was condensed with 14 equivalents of 4-*N*,*N*-dimethylaminobenzaldehyde and 15 equivalents of pyrrole with a TFA catalyst according to the conditions of Lindsey.[32] The porphyrinogens thus generated were oxidised with p-chloranil and the mixture submitted to flash chromatography. Fractions were analysed by MALDI MS. Signals with m/z ratios corresponding to MH^+ ions for the dyad (1280 Da) as well as a triad **4.14** (1774 Da) and the tetra dimethylamine **2.48** (787 Da) were detected. The dyad product **4.13** was precipitated by addition of methanol and was isolated in a yield of 12%. The triad and the tetra dimethylamine were not isolated.

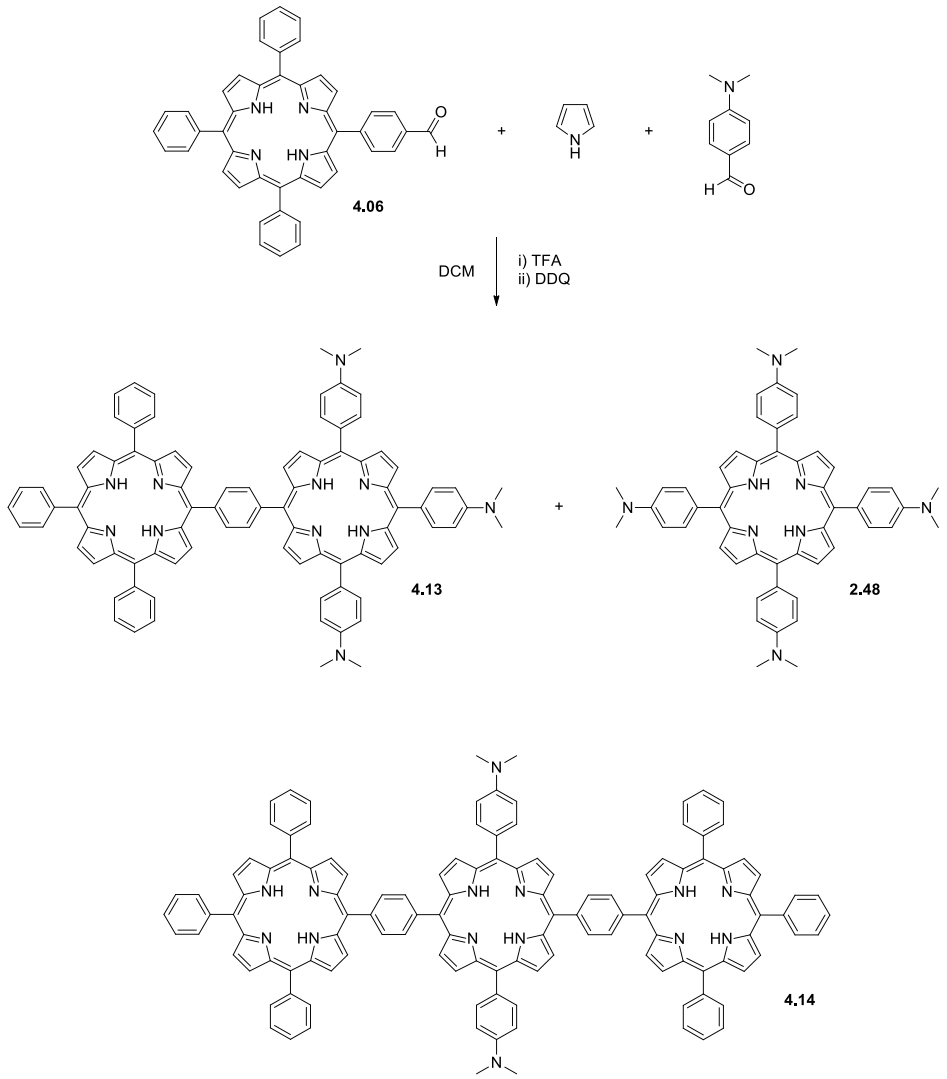

Figure 71: The synthesis of the phenylene-linked dimethylamine dyad 4.13

The ^{1}H NMR spectrum (Figure 72) of the dyad **4.13** was similar to that of the triester dyad **4.11** and displayed two NH peaks of equal integration, one from each porphyrin. These were assigned to each porphyrin ring (**a** and **b**) based on the less-negative shift of the analogous signal of the porphyrin triamine **2.47** (-2.62 ppm) than that of TPP **2.01** (-2.76 ppm). Two overlapping singlets at 3.26 and 3.27 ppm integrating to a total of 18H were assigned to the $N(CH_3)_2$ groups (**c**). A multiplet between 7.10 and 7.20 ppm with an integration of 6H was assigned to the aromatic H nuclei adjacent to the N atoms (**d**). A multiplet between 7.70 and

7.85 ppm with an integration of 9H was assigned to the *meta* and *para* H nuclei of the unsubstituted *meso* benzene rings (**e**). A multiplet between 8.10 and 8.20 ppm with an integration of 6H was assigned to the *ortho* H nuclei on the NMe_2-substituted benzene rings (**f**). A similar multiplet between 8.24 and 8.33 ppm with an integration of 6H was assigned to the *ortho* H nuclei on the unsubstituted benzene rings (**g**). A multiplet between 8.59 and 8.66 ppm with an integration of 4H was assigned to the H nuclei of the bridging benzene ring (**h**). Eight doublets between 8.85 and 9.35 ppm with a total integration of 16H were assigned to the β-pyrrolic H nuclei.

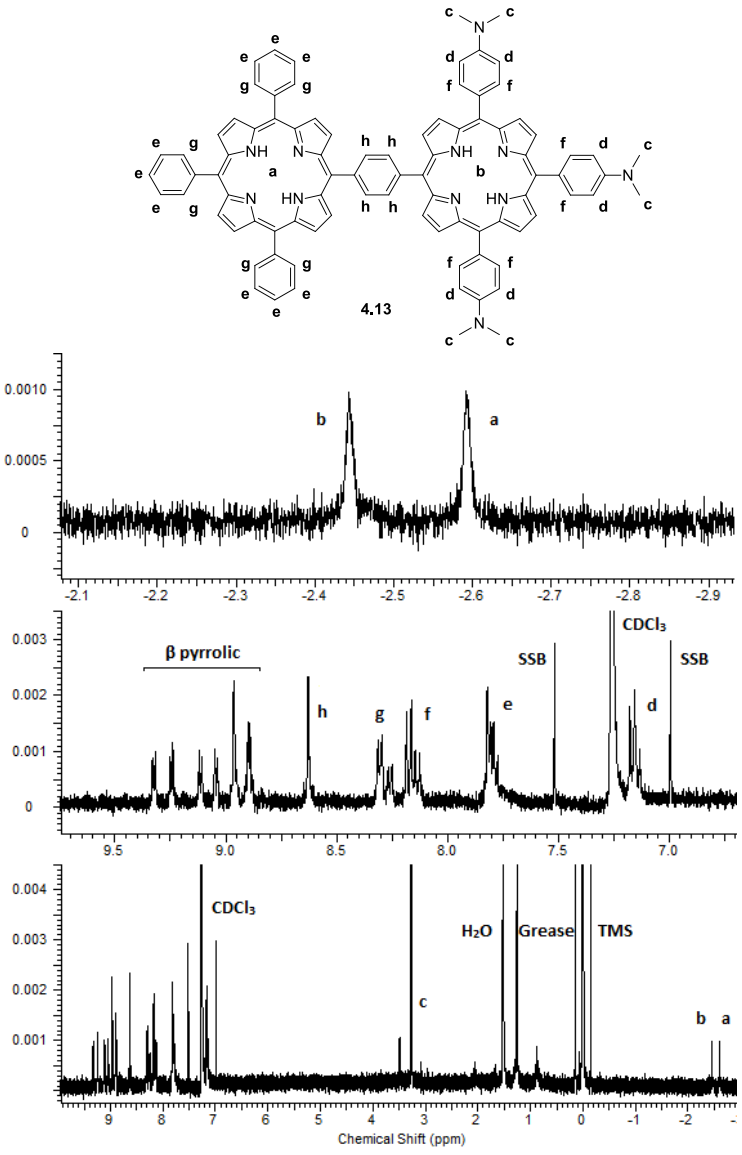

Figure 72: The ^{1}H NMR spectrum of the porphyrin dyad 4.13

The UV-vis absorption spectrum of **4.13** was similar to that of the analogous triester compound **4.11** (Figure 73). There were three Q bands evident at 653, 572 and 517 nm but they were not symmetrical and were likely a result of superposition of several peaks. There was a split B peak, with maxima at 433 and 419 nm. This split peak was attributed to Davydov splitting, as described in Section 4.3.1.

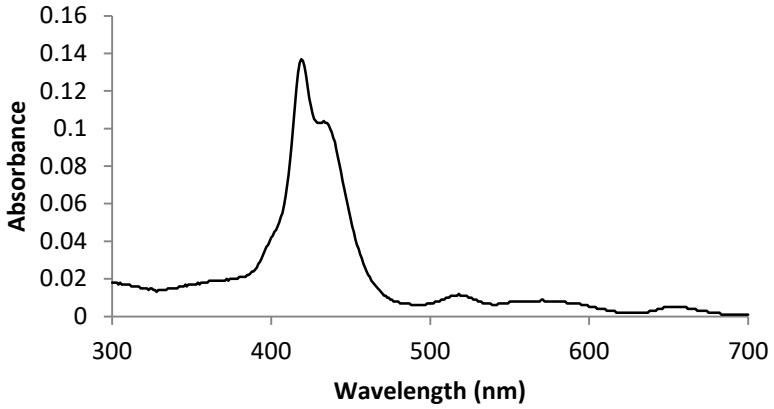

Figure 73: The UV-vis absorbance spectrum of the phenylene-linked dimethylamine dyad 4.13 (in $CHCl_3$, 3.5 μM)

4.3.3 Zinc complexes of porphyrin dyads

The zinc complexes **4.15** and **4.16** (Figure 74) of both the ester dyad **4.11** and the dimethylamino dyad **4.13** were prepared. Each free base dyad was dissolved in DCM and a methanol solution of zinc acetate was added. The progress of each reaction was monitored by TLC analysis. For the ester dyad, two intermediate products were observed as well as the starting material and ZnZn product. These were presumed to be the two possible mono-metalated states. The observed separability of these compounds was utilised later, as described in Chapter 6. With continued stirring for 17 hours each dyad was completely converted to the ZnZn product and was precipitated by addition of methanol.

Complete metalation was evident by the absence of NH peaks in the ^{1}H NMR spectrum for each compound. Spectra were otherwise similar to those of the free base compounds. MALDI MS detected ions at m/z 1453 for the ester dyad and m/z 1280 for the dimethylamine dyad, consistent with the respective MH^{+} ions.

The UV-vis absorption spectrum of the ZnZn triester dyad **4.15** displayed two major Q bands at 598 and 556 nm and two weaker ones at 623 and 517 nm. The simplification of the Q band region is typical of zinc porphyrins due to the increase in symmetry of the porphyrin core on metal binding. The split B peak was still evident, with maxima at 433 and 423 nm.

The UV-vis absorption spectrum of the ZnZn triamine dyad **4.16** was similar, with two major Q band peaks appearing at 605 and 557 nm, with a shoulder on the red side of the peak at 605 and another small peak at 518 nm. The B peak was split, with two maxima at 439 and 424 nm.

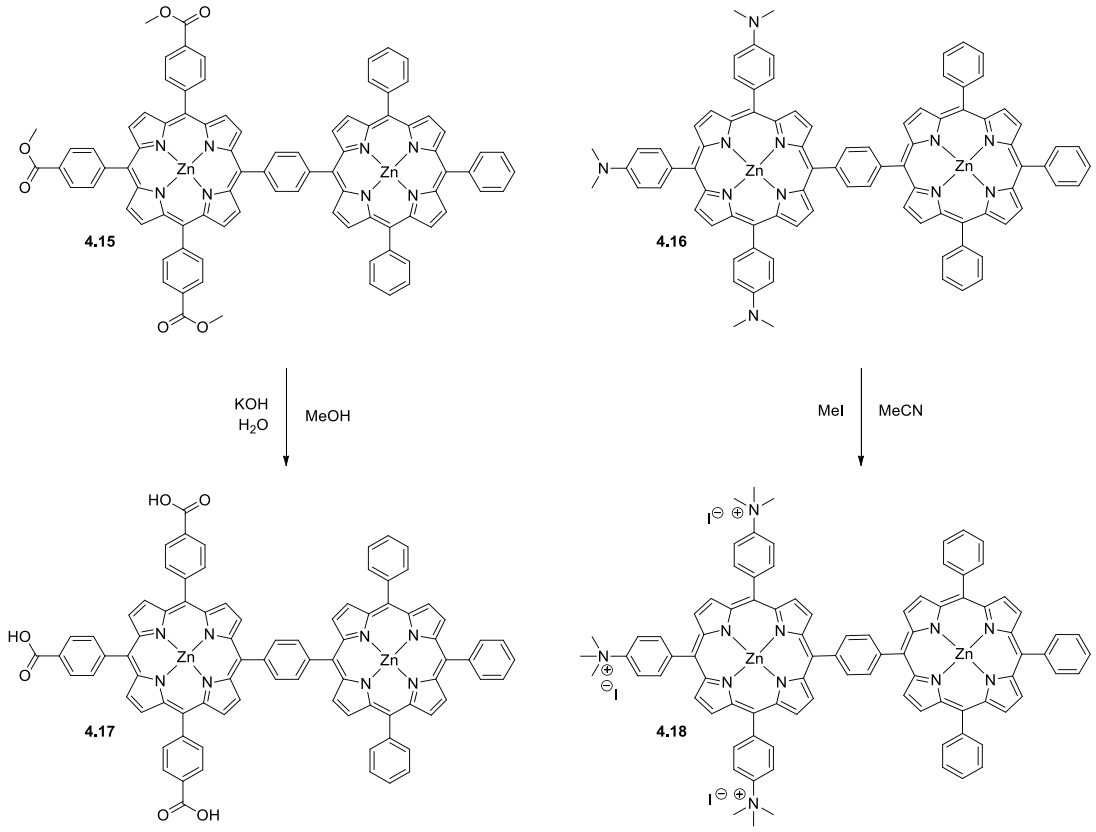

Figure 74: The conversion of the ZnZn ester dyad 4.15 and the ZnZn amine dyad 4.16 to their respective amphiphilic carboxylic acid 4.17 and QAS 4.18 forms

4.3.4 Hydrolysis of zinc porphyrin ester dyad

The ester groups of the ZnZn porphyrin dyad **4.15** were hydrolysed by treatment with a solution of 0.2 M KOH in a mixture of 5% water, 45% methanol and 50% THF (Figure 74). The product **4.17** was collected by precipitation *via* addition of H_3PO_4 and collected by repeated centrifugation and re-suspension to remove inorganic residues. The product was isolated in 94% yield. Complete hydrolysis of the ester groups was evident by the absence of any ester signal at 4.15 ppm in the ^{1}H NMR spectrum.

The UV-vis absorption spectrum was similar to the ester starting material and displayed two Q bands at 604 and 562 nm and a split B peak with maxima at 437 and 426 nm. MALDI MS analysis detected the MH^+ ion of the dyad triacid.

4.3.5 Methylation of zinc porphyrin dimethylamine dyad

The ZnZn dimethylamino dyad **4.16** was converted to the QAS **4.18** by treatment with a large excess of MeI in acetonitrile. The product failed to precipitate following concentration and addition of DCM and was isolated by complete evaporation of solvents and unreacted MeI. Formation of the correct product was confirmed by the integration of the NMe peak at 5.8 ppm in the ^{1}H NMR spectrum. This peak integrated to the expected value of 27H compared to the 8H of the β-pyrrolic peaks.

The UV-vis absorption spectrum was similar to the dimethylamine starting material and displayed two Q bands at 602 and 561 nm and a split B peak with maxima at 437 and 426 nm.

MALDI MS analysis detected an ion at m/z 1408, and this was assigned to the MH^+ of the dyad minus three molecules of methyl iodide. This loss of methyl iodide from QAS compounds was observed for the single porphyrins in Chapter 2.

4.3.6 Triad formation in statistical mixtures

The technique of producing porphyrin dyads *via* mixed-aldehyde condensations using a porphyrin monoaldehyde was highly successful. Using porphyrin dialdehydes, the same method was used to pursue the synthesis of the analogous porphyrin triads.

The yield of each porphyrin-forming reaction was expected to be less than 40% as can typically be expected for any porphyrin ring-forming reaction. The technique becomes less

appealing for larger arrays because the more porphyrin rings that must be formed, the more the low yield for each ring is compounded. Despite this, triads were successfully formed and were detected by MALDI MS, but their isolation from the statistical mixture proved impractical.

Formation of ABAB triad

The synthesis of the *ABAB* triad **4.19** (Figure 75) was carried out by the condensation of the *ABAB* dialdehyde **4.07** with 24 equivalents of *p*-formylbenzoic acid methyl ester and 25 equivalents of pyrrole. The condensation was carried out under Lindsey's conditions with the porphyrinogens being oxidised with DDQ.[32] The crude reaction mixture was submitted to flash chromatography and the fractions analysed by MALDI MS. For each of the porphyrin-containing fractions an ion of m/z 2037 was detected and was attributed to the MH^+ ion of the expected triad. An ion of m/z 847 was also detected and was attributed to the MH^+ ion of the porphyrin tetraester **2.06**. Despite repeated attempts to purify the triad from the tetraester (eluent was 3% ethyl acetate in DCM), it could not be isolated in pure form.

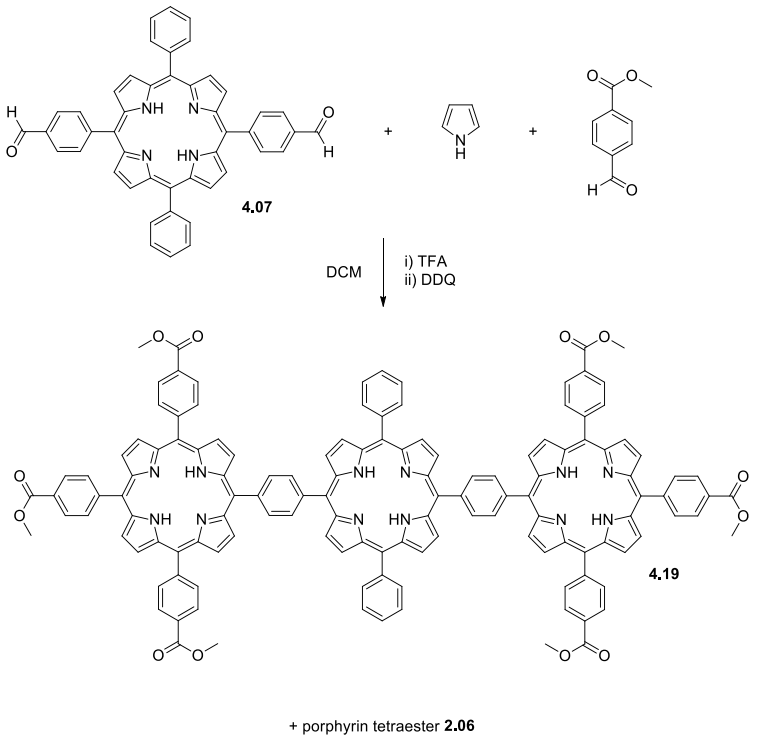

Figure 75: Synthesis of a *ABAB* porphyrin triad from a porphyrin dialdehyde

Formation of AABB triad

The synthesis of the *AABB* triad **4.20** was also carried out under similar conditions. It was expected that the bent shape of this molecule would produce a stronger dipole than the *ABAB* form, and that this might facilitate chromatographic separation. However the product could not be isolated *via* flash chromatography, with MALDI MS detecting a mixture of triad and tetraester in all porphyrin-containing fractions. Repeated attempts to purify the triad *via* flash chromatography were not successful.

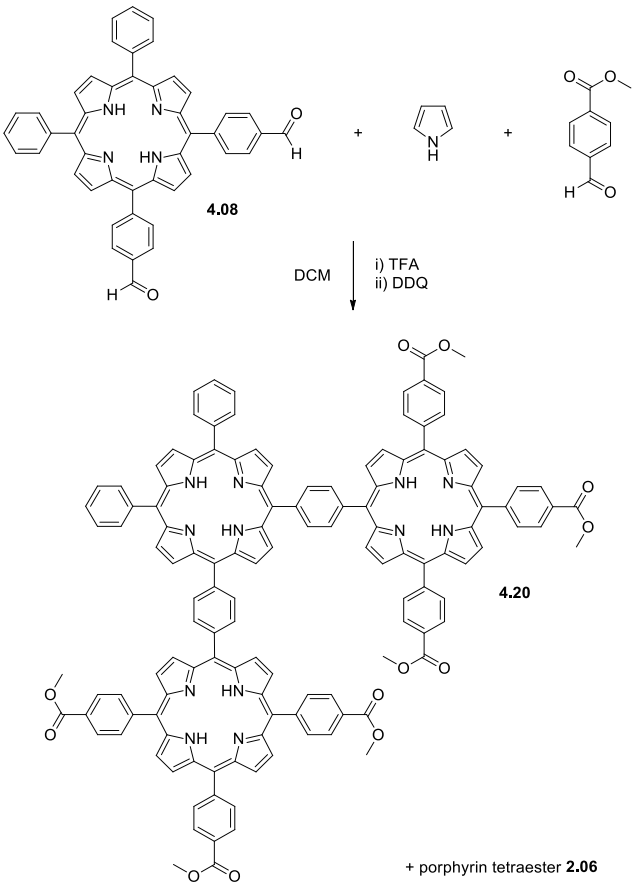

Figure 76: Synthesis of the *AABB* porphyrin triad from a porphyrin dialdehyde

4.4 Chapter conclusion

The process of synthesising amphiphilic porphyrin arrays *via* mixed-aldehyde condensation was developed and found to be convenient and highly effective in producing dyads bearing carboxylic acids and QAS groups. The process was also applied to triads and the synthesis appeared to proceed as expected. Unfortunately the fact that they could not be isolated in pure form means that a new synthetic approach must be found in order to obtain these compounds for use in further experiments. Attempts to achieve this using metal tagging are described in Chapter 6.

Chapter 5: Vinyl-linked porphyrin arrays

5.1 Introduction

The phenylene linking method for producing porphyrin arrays described in Chapter 4 was only partially successful (resulting only in producing dyads). Triads proved difficult to isolate, and the yields of these compounds were expected to be low because of the generally low yields of the aldehyde condensation reactions involved. An alternative strategy, offering the potential for higher yields and more easily-purified products, is the β-pyrrolic linking technique using the Wittig reaction described by Bonfantini *et al.*[128] Alkene linkage at the β-pyrrolic position offers the added advantage of better electronic coupling between porphyrins because of the conjugation of the linker with the aromatic system, and porphyrins with surface-binding linkers of this type have produced some of the highest efficiencies in porphyrin dye-sensitised solar cells.[129] Arrays containing up to nine porphyrins[69] have been produced using β-pyrrolic linkages, however these have been mostly fully hydrophobic in nature. Mozer *et al.* reported porphyrin dyads produced *via* Wittig coupling of a porphyrin β-pyrrolic phosphonium salt with a porphyrin *meso* benzaldehyde[130] (Figure 77), and this chapter describes the adaptation of this technique to the synthesis of amphiphilic arrays.

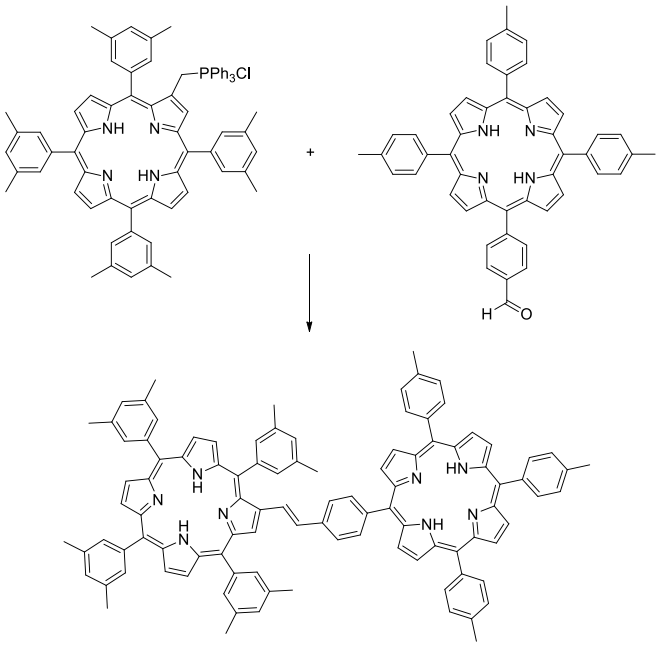

Figure 77: The synthesis of a porphyrin dyad *via* Wittig coupling reported by Mozer *et al.*[130]

The Wittig coupling consists of the reaction of an aldehyde with a phosphonium ylide, formed from a phosphonium salt. It was envisioned that amphiphilic porphyrin arrays could be constructed by reacting a pre-hydrophilic (ester-bearing) porphyrin phosphonium salt with a hydrophobic porphyrin aldehyde. A synthesis of a hydrophobic porphyrin β phosphonium salt was developed by Bonfantini *et al.*,[69] and this compound had been used as a key building block to produce hydrophobic arrays. This phosphonium salt synthesis was adapted to produce the pre-hydrophilic porphyrin tetraester **5.01** (Figure 78) by Campbell,[131] who used it to produce an amphiphilic array. This porphyrin phosphonium salt appeared to be ideal for generating the desired amphiphilic multiporphyrin arrays by combining it with hydrophobic porphyrin aldehydes in the same manner as Mozer *et al.*[130]

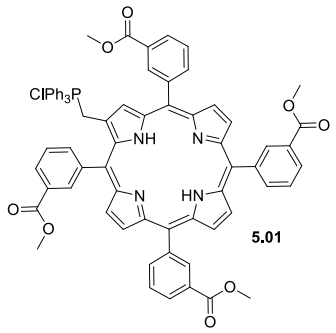

Figure 78: The porphyrin tetraester phosphonium salt whose synthesis was developed by Campbell[131]

5.1.1 Synthesis of starting materials

Meso-disubstituted porphyrin aldehyde

Prior to the maquette-binding experiments with singular porphyrins, it was believed that steric hindrance would be an important issue influencing binding. All previously published porphyrin-maquette bindings had used porphyrins with unsubstituted *meso* positions, and it was anticipated that for a dyad to bind it must also follow this pattern. A *meso* disubstituted aldehyde-bearing porphyrin was therefore produced, and this synthesis is described below.

5, 15 Meso disubstituted porphyrin aldehyde

The protected porphyrin aldehyde **5.03** (Figure 79) was prepared by condensing dipyrromethane **5.02** (synthesised *via* a literature procedure[132]) with benzaldehyde and the monoprotected phthaladehdye **4.12**. The condensation was performed under the conditions of Lindsey[32] with DDQ being used to oxidise the porphyrinogens thus generated. The product **5.03** was isolated *via* flash chromatography and crystallised *via* addition of methanol to the concentrated pure fractions to afford a yield of 4.6%. The diphenyl and di-protected dialdehyde porphyrins were also isolated in yields of 8.6% and 3.3% respectively.

The protected monoaldehyde ^{1}H NMR spectrum displayed a single symmetrical NH peak at -3.11 ppm. This was a good indication that only one porphyrin compound was present in the

sample. Two singlets at 0.93 and 1.49 ppm were assigned to the CH_3 substituents of the protecting group. These groups are non-equivalent because of the symmetry-breakage imposed by the carbon atom bonded to the two oxygen atoms. The H atom bonded to this carbon appeared as a singlet with an integration of 1H at 5.79 ppm. The H nuclei of the two CH_2 groups of the protecting group were also non-equivalent because of the symmetry breakage, and in addition to this were split by geminal coupling to appear as two doublets at 3.38 and 3.99 ppm, each with *J* = 11.1 Hz (reasonable for a geminal coupling) and each with an integration of 2H. A multiplet between 7.75 and 7.83 ppm with an integration of 3H was assigned to the *meta* and *para* H nuclei of the unsubstituted phenyl substituent. The *ortho* H nuclei of this ring appeared as a multiplet between 8.25 and 8.29 ppm with an integration of 2H. Two doublets at 7.97 and 8.29 ppm and *J* = 8.01 Hz each with an integration of 2H were assigned to the H nuclei of the benzene ring bearing the protected aldehyde group. The β-pyrrolic H nuclei appeared as two overlapping doublets at 9.07 and 9.08 ppm, each with *J* = 4.69 Hz and with a integration of 2H each, as well as two overlapping doublets (that looked like a triplet) at 9.38 ppm and 9.39 ppm with *J* = 4.88 Hz, and integrations of 2H each. The *meso* H nuclei, highly deshielded by the ring current of the porphyrin ring, appeared as a singlet at 10.30 ppm with an integration of 2H. MALDI MS analysis detected only an ion of m/z 577, which was assigned to the MH^+ ion of the product. The UV-vis absorption spectrum was typical for a free base porphyrin, displaying four Q bands and a sharp B band with its peak at 407 nm.

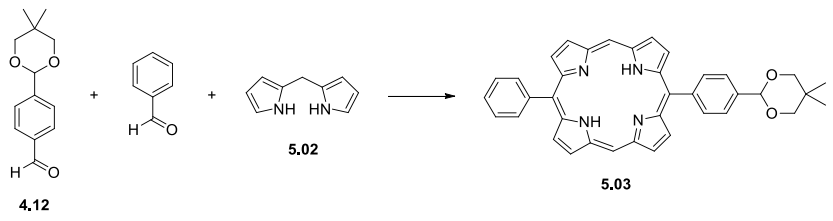

Figure 79: The synthesis of the mono protected aldehyde *meso* free porphyrin 5.03

The protecting group of the aldehyde of **5.03** was then removed *via* treatment with a 5:2:8 v/v/v mixture of TFA, water and DCM to produce **5.04** (Figure 80). TLC analysis indicated that the reaction was complete after 25 mins and the product was isolated in a yield of 85%. ^{1}H NMR analysis confirmed complete conversion by the absence of any protecting group signals and the appearance of a singlet for the aldehyde H nucleus at 10.43 ppm with an integration of 1H. The spectrum was otherwise similar to the protected compound. MALDI MS analysis did not detect any of the MH^{+} of the starting material, only that of the product, at m/z 492. The UV-vis absorption spectrum was similar to that of the protected starting material, but with the B band now shifted to 410 nm.

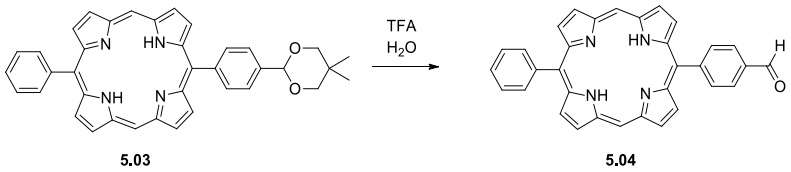

Figure 80: Deprotection of the mono protected aldehyde *meso* free porphyrin 5.03

5.2 Synthesis of vinyl-linked dyads

5.2.1 Meso-free dyad

Given that fellow student Rhys Mitchell had already synthesised porphyrin ester phosphonium salt **5.01**, porphyrin aldehyde **5.04** was provided to him to undertake the Wittig coupling for the synthesis of the dyad **5.05**. However, the dyad proved to be unstable, with baseline material appearing when analysed by TLC. This was attributable to the presence of unsubstituted and reactive *meso* positions. Consequently, no further work was pursued with this compound.

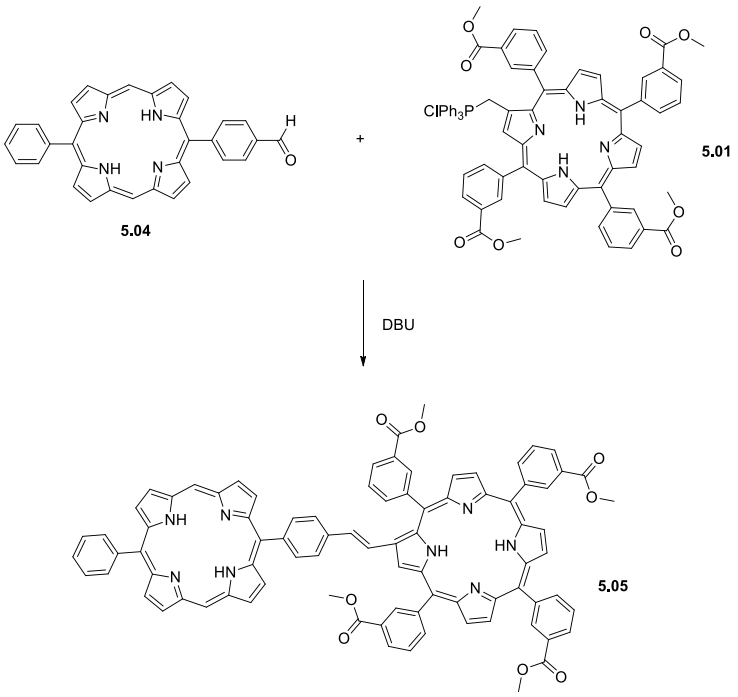

Figure 81: Wittig coupling to form the dyad 5.05 carried out by fellow PhD student Rhys Mitchell

Later however, it was demonstrated by the success of the maquette-binding of singular *meso*-substituted porphyrins (Chapter 7) that such subsituents do not hinder binding at all, and in fact offer the advantageous effect of hindering aggregation in solution. Following this finding, the more easily-produced porphyrin aldehydes from Chapter 4, **4.06** – **4.09**, were deemed to be suitable for producing maquette-binding arrays and were used in all further syntheses.

5.2.2 Fully meso-substituted arrays

The synthesis of a variety of porphyrin aldehydes in Chapter 4 opened up the possibility of making various dyads and larger arrays (represented as **5.07** in Figure 82) *via* Wittig reaction with the porphyrin tetraester phosphonium salt. By reacting the monoaldehyde **4.06** (Figure 82, R_1, R_2 = H) with the phosphonium salt **5.01**, kindly supplied by Rhys Mitchell, a dyad could

be produced (R_3, R_4 = H, R_5 = ester porphyrin). If instead the *ABAB* dialdehyde **4.07** (R_1 = CHO, R_2 = H) was was used then an *ABAB* triad could be formed (R_3, R_5 = ester porphyrin, R_2 = H). Similarly, by using the *AABB* diester porphyrin **4.08** (R_1 = H, R_2 = CHO), an *AABB* triad (R_3 = H, R_4, R_5 = ester porphyrin) could be formed.

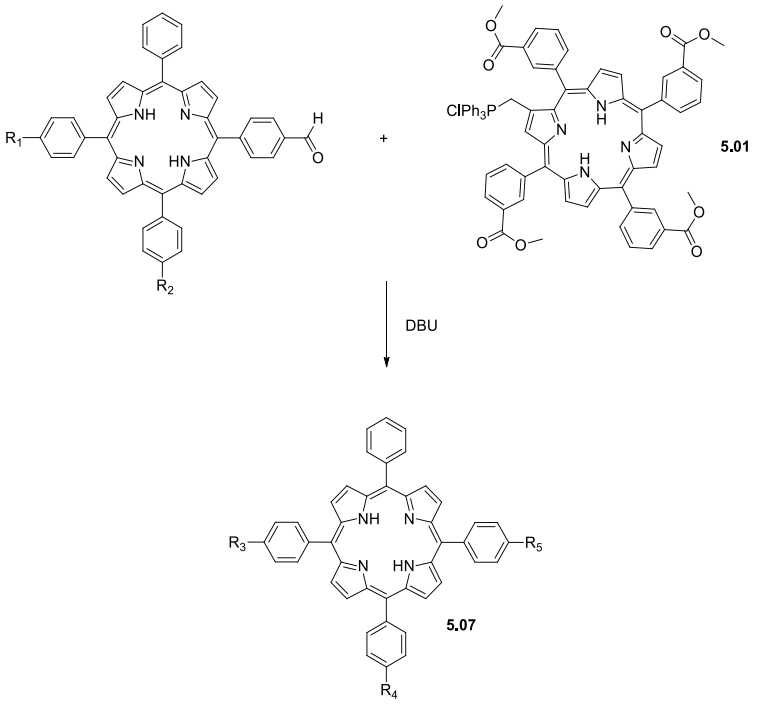

Figure 82: Potential array syntheses using the porphyrin aldehydes from Chapter 4

5.2.3 Vinyl-linked dyad

The porphyrin monoaldehyde **4.06** was reacted with the porphyrin phosphonium salt **5.01** to form the dyad **5.08** (Figure 83)**.** This was carried out by dissolving the porphyrin starting materials in chloroform at room temperature and adding the organic base DBU. The reaction was monitored by TLC which showed the formation of several products and the consumption of much of the porphyrin aldehyde starting material. The mixture was submitted to flash chromatography and the fractions analysed by MALDI MS and ^{1}H NMR spectroscopy to ascertain their contents.

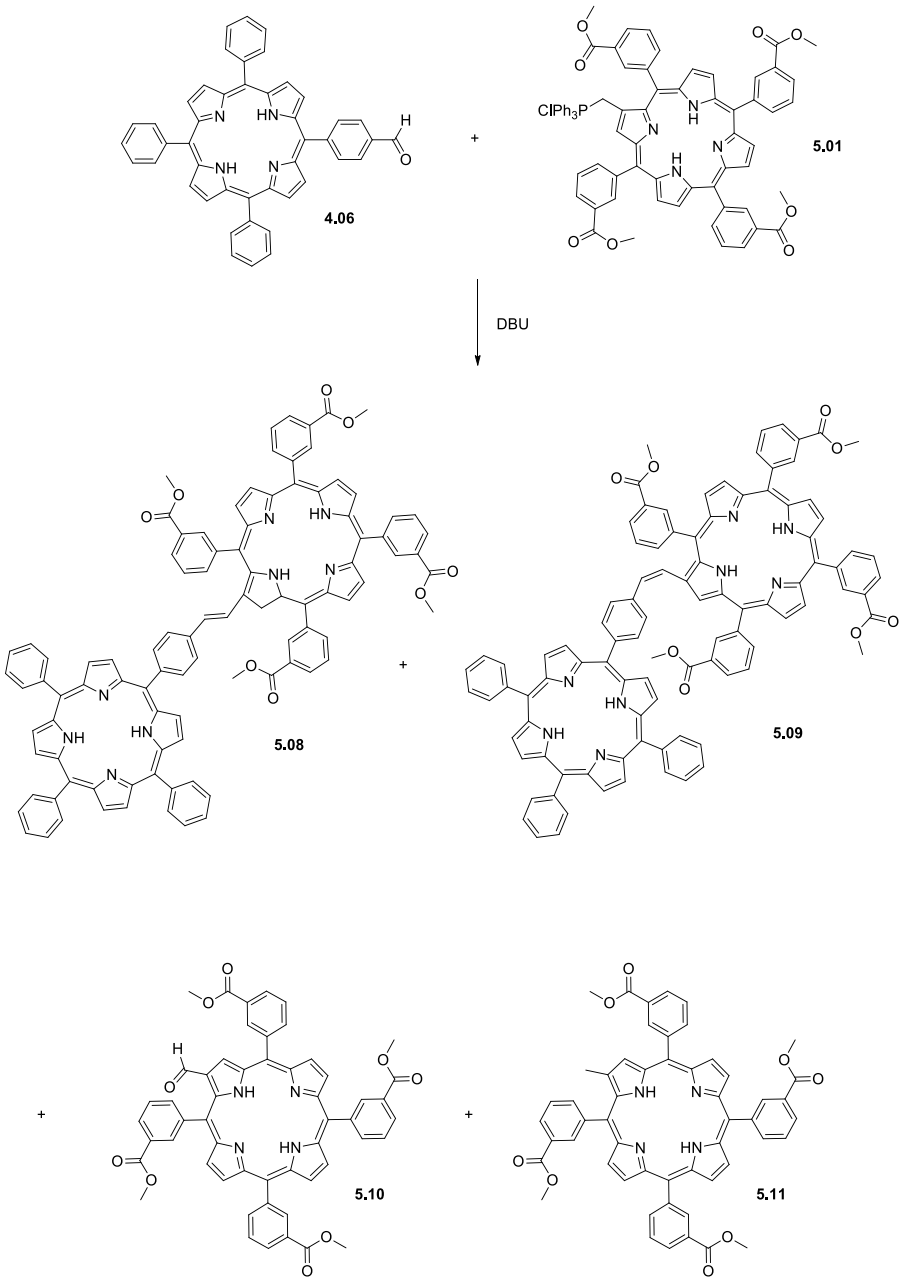

Figure 83: Wittig coupling to form the dyads 5.08

A considerable quantity of the porphyrin aldehyde starting material **4.06** was recovered (52%) but some dyad **5.08** was also collected (48%). These yields were based on the aldehyde starting material, which was the limiting reagent for these products. Also identified were the β formyl and β methyl tetraester porphyrin compounds **5.10** and **5.11**, which were isolated in

yields of 25% and 12% respectively (based on the phosphonium salt starting material). These products resulted from the degradation of the phosphonium salt *via* oxidation and hydrolysis respectively, and were reported previously by Reid[133] with similar porphyrin phosphonium salts. The fact that only 48% of the aldehyde was converted to the dyad was likely due to the degradation of the phosphonium salt into these two by-products.

Also detected by MALDI MS were, surprisingly, the copper complexes of both **5.10** and **5.11**, and mono copper-metalated dyad **5.08**. This can be explained by the fact that the synthesis of the phosphonium salt requires metalation of the porphyrin tetraester with copper to facilitate β formylation. The copper is usually completely removed later, however evidently the sample of porphyrin phosphonium salt that was provided still contained some bound copper ions. Fortunately, the copper-containing product could be removed during chromatographic purification.

The dyad product of the Wittig coupling consisted of a mixture of two isomers. The *Z* isomer was converted to the more thermodynamically favourable *E* isomer *via* treatment with TFA according to the conditions of Campbell.[131] MALDI MS analysis detected an ion of m/z 1486, which was assigned to the MH^+ ion of the dyad.

The ^{1}H NMR spectrum of the dyad **5.08** (Figure 84) was very complex owing to the asymmetry imposed on the tetraester porphyrin by its β-pyrrolic substitution. There were two NH peaks, each of which integrated to 2H. These were assigned to each of the two porphyrin rings based on the NH peak positions observed for aldehyde porphyrin starting material and the β formyl tetraester. These peaks were a good indication that there was a single pure dyad present. Several peaks between 3.85 and 4.10 ppm with a total integration of 12H were assigned to the ester CH_3 signals. A doublet at 7.17 ppm (J = 16.8 Hz) was assigned to the alkene proton closer to the more electron deficient ester porphyrin. The J-value 16.8 Hz is evidence that the product was the *E* isomer (expected J = 11 – 18 Hz as opposed to 6-14 Hz for

Z). The other alkene proton signal was mixed in a multiplet between 7.50 and 7.62 ppm with a total integration of 5H. This multiplet also contained signals from four benzene ring protons. The remaining benzene ring protons appeared as several multiplets between 7.67 and 8.63 ppm which had a total integration of 33H. A cluster of signals between 8.73 and 9.05 ppm with an integration of 16H was assigned to the β-pyrrolic proton signals. There was nothing to indicate the presence of any of the *cis* isomer **5.09** despite such products sometimes being formed during Wittig condensation reactions.[131]

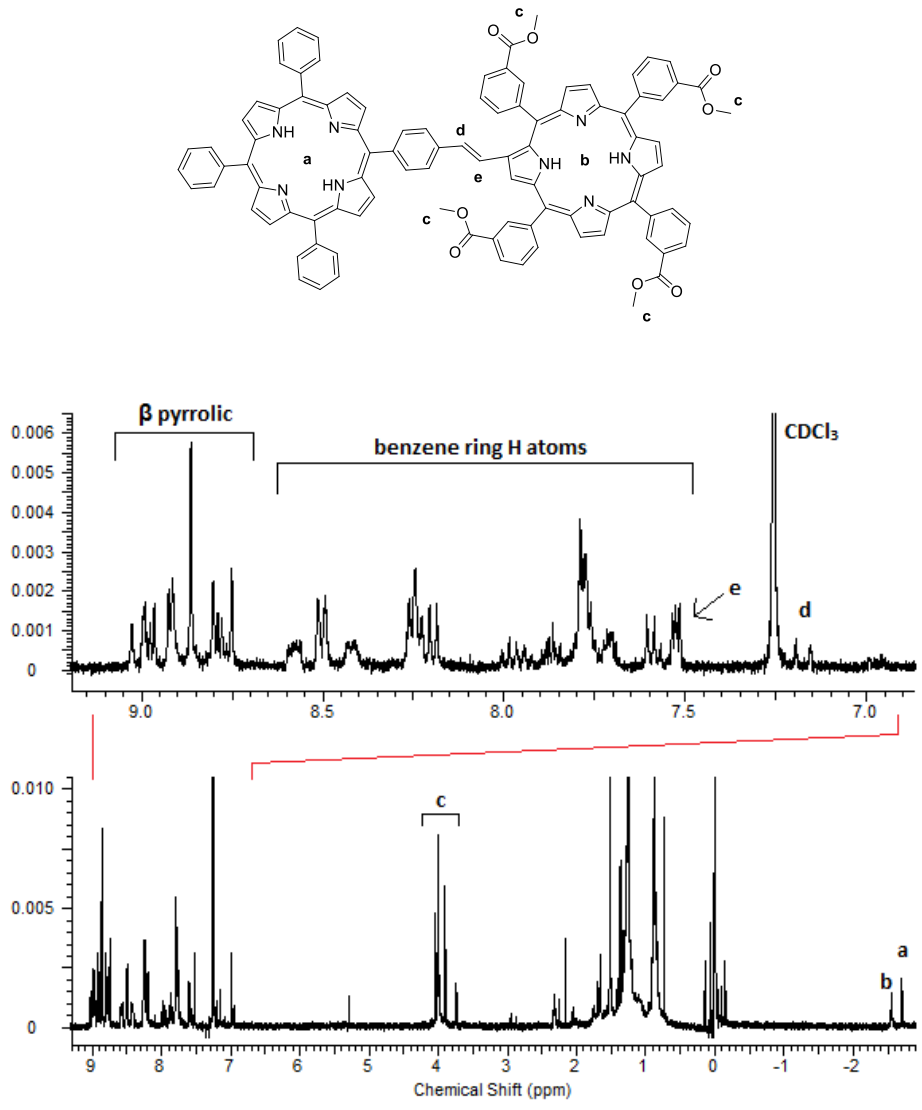

Figure 84: The ^{1}H NMR spectrum of the dyad 5.08 with assignments

The UV-vis spectrum of the dyad (Figure 85) was similar to that of a typical free base tetraphenylporphyrin in that it displayed four Q bands and a single B band. The B band was however significantly broadened. This broadening may be attributable to the extension of the conjugation of the porphyrin ring by the conjugated linker in the β-pyrrolic position, as it is often observed with porphyrins of this type.[40] MALDI MS analysis detected the MH^+ ion of the dyad.

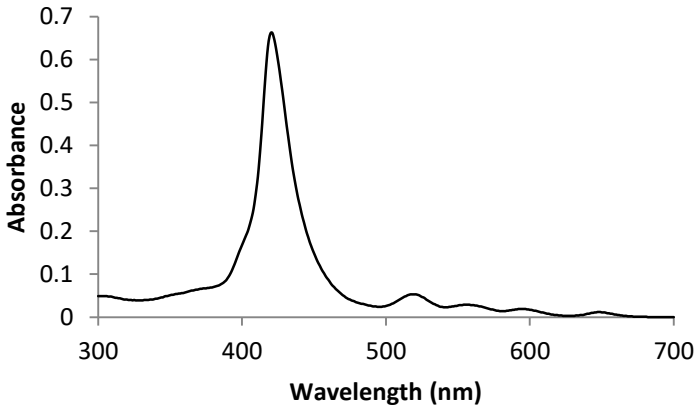

Figure 85: UV-vis absorbance spectrum of the dyad 5.08

Zn insertion

In order to facilitate maquette binding *via* axial ligation, the zinc complex **5.12** of the dyad (Figure 86) was produced. The free base dyad **5.08** was dissolved in DCM and a solution of zinc acetate in methanol was added. The progress of the reaction was monitored by TLC and when complete, the product was precipitated by evaporation and addition of methanol in a yield of 79%.

MALDI MS analysis of the product detected an ion of m/z 1612 which was assigned to the MH^+ ion of the dimetalated dyad. There were no ions detected at m/z 1486 or 1548 which

would correspond to the MH^+ ions of the non-metalated and monometalated dyad respectively.

The ^1H NMR spectrum displayed no NH peaks, indicating that no free base porphyrins were present. The spectrum was otherwise similar to the free base dyad but the peaks were significantly sharpened.

The UV-vis spectrum only displayed two Q bands instead of the four displayed by the starting material. Zinc tetraphenylporphyrins typically do display only two Q bands. Like the starting material, the B band is significantly broadened compared to a typical zinc tetraphenylporphyrin.

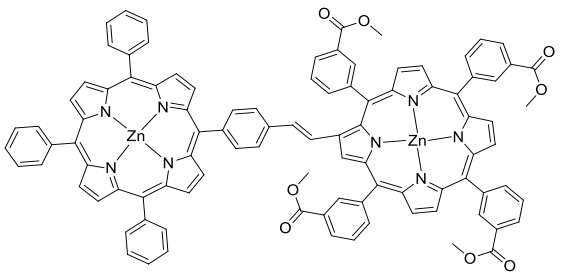

5.12

Figure 86: The zinc metalated vinyl-linked dyad 5.12

Hydrolysis

The ester groups of the zinc dyad **5.12** were hydrolysed to form the analogous tetracarboxylic acid product **5.13**. This was carried out *via* the same method used for the single porphyrins and for the phenylene-linked dyad *i.e.* treatment with a solution of 0.2 M KOH in a mixture of 5% water, 45% methanol and 50% THF. The product was precipitated by neutralisation with acetic acid and collected by centrifugation to afford a yield of 45%. Complete hydrolysis was evident by the absence of any ester signals in the ^1H NMR spectrum.

The UV-vis absorbance spectrum was very similar to the ester starting material. MALDI MS analysis detected an ion at m/z 1612, assigned to the MH^+ ion of the tetraacid product.

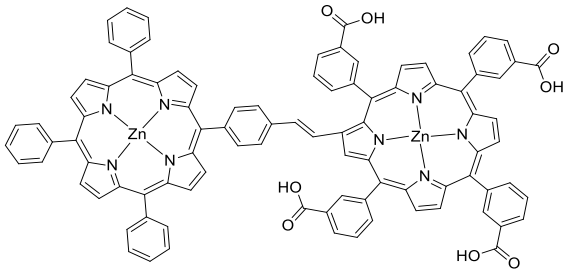

5.13

Figure 87: The tetracarboxylic acid amphiphilic porphyrin dyad

5.2.4 Vinyl-linked ABAB triad syntheses

With the success of the synthesis of the vinyl-linked dyad *via* Wittig reaction, the next step was to extend the technique to produce porphyrin triads from porphyrin dialdehydes. The *ABAB* porphyrin dialdehyde **4.07** was mixed with the porphyrin tetraester phosphonium salt **5.01** in DCM at room temperature with DBU added as a catalytic base. The reaction was monitored by TLC analysis and although it appeared that products had formed, additional portions of both phosphonium salt and DBU were added when it was observed that dialdehyde consumption had stalled; TLC analysis indicated that these additions did not result in the consumption of any more dialdehyde. The mixture was submitted to flash chromatography and the fractions analysed by TLC and MALDI MS. The first band to elute was identified as the porphyrin dialdehyde starting material **4.07**. There were no more clear bands and the remaining compounds eluted as a mixture. Products identified by MALDI MS by their MH^+ ions (Figure 88) were the intended triad product **5.14** M_1, M_2 = 2H (m/z = 2357), mono copper metalated triad **5.14** M_1 = Cu, M_2 = 2H (m/z = 2418), di-copper metalated dyad **5.14** $M_1 = M_2$ = Cu (m/z = 2485) as well as a dyad resulting from a single Wittig condensation reaction **5.15** M = 2H (m/z = 1514) and its copper-metalated counterpart **5.15** M = Cu (m/z =

1576). Also detected were the β methyl and β formyl tetraester products **5.10** and **5.11** as well as their copper-metalated versions.

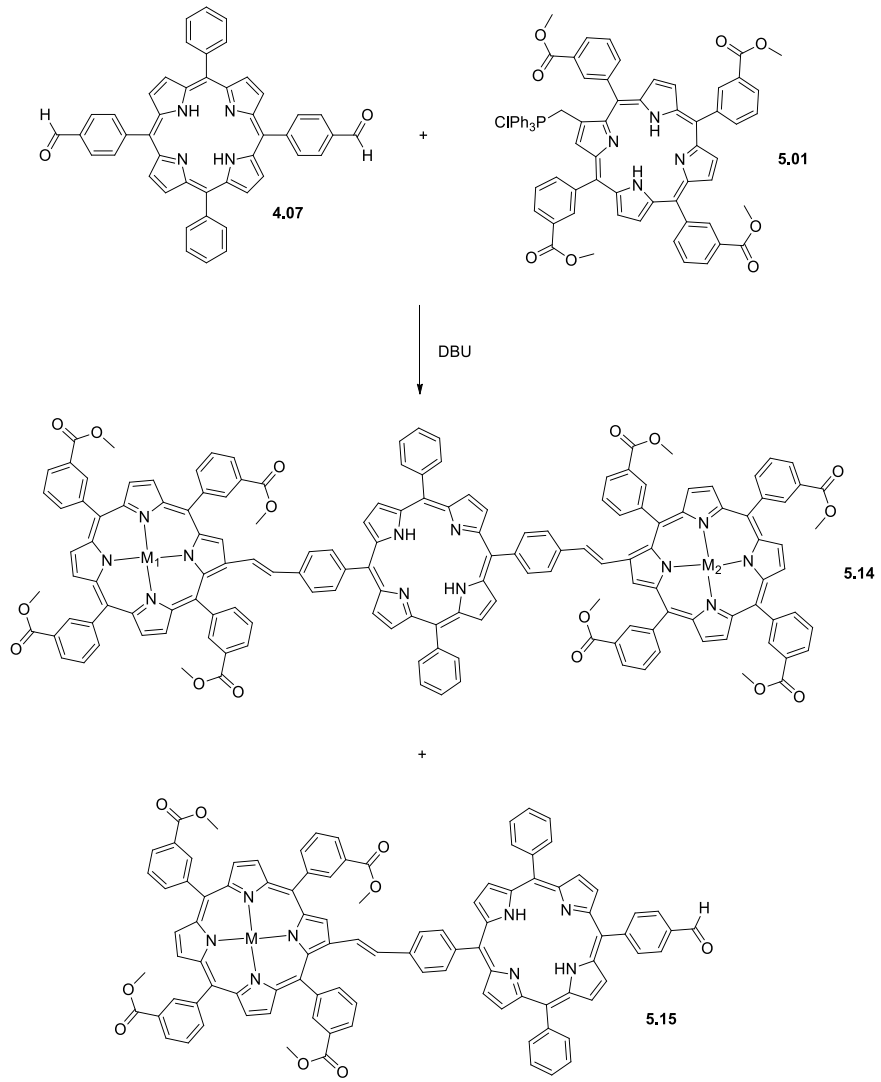

Figure 88: The products of the Wittig condensation aimed at forming the triad 5.14

Repeated attempts to separate these compounds to isolate the triad proved futile. The products did not elute as tight bands but as mixed streaks, likely because of intermolecular interactions between the several polar ester groups that they carried. In addition to this, the presence of copper-metalated products made the isolation of any one product from the complex mixture very challenging. The analogous reaction to form the *AABB* triad from the

AABB dialdehyde **4.08** was also trialled with a similar result. Because of the inadequacy of flash chromatography for isolating the triad from the reaction products and the unavailability of copper-free phosphonium salt starting material, this line of investigation was not pursued further.

5.3 Knoevenagel condensation

In order to explore alternative methods for the formation of unsymmetrical amphiphilic porphyrin arrays using the porphyrin aldehyde materials **4.06** – **4.10** already at hand, produced in Chapter 4, and that would permit the use of pre-metalated porphyrin building blocks, Knoevenagel condensations were trialled. The Knoevenagel condensation is similar to the Wittig condensation in that it forms a carbon-carbon double bond between two reactants. It involves the reaction of a nucleophilic carbon with an aldehyde, followed by elimination of H^+ and OH^-, which can go on to form water (Figure 89). The usual method of generating a nucleophilic carbon is to deprotonate an electron-poor carbon to produce a carbanion. This requires that the proton be somewhat acidic, and this may be achieved *via* stabilisation of the carbanion by adjacent electron-withdrawing groups. The original Knoevenagel reaction utilised a diketone, but reactions utilising other carbanions are also commonly referred to as Knoevenagel condensations.[134] Alpha-cyanomethylbenzene compounds have been found to be effective in this role,[135] and work was undertaken to produce porphyrins bearing this moiety.

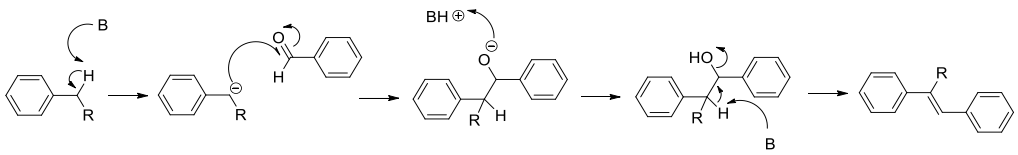

Figure 89: An example Knoevenagel condensation using a cyanomethylbenzene and a benzaldehyde, where R is an electron withdrawing group and B is a base

Knoevenagel condensations have been used to append porphyrins with other functional molecules *e.g.* by Moser *et al.* for binding to TiO_2 for use in a DSSC[130] (Figure 90).

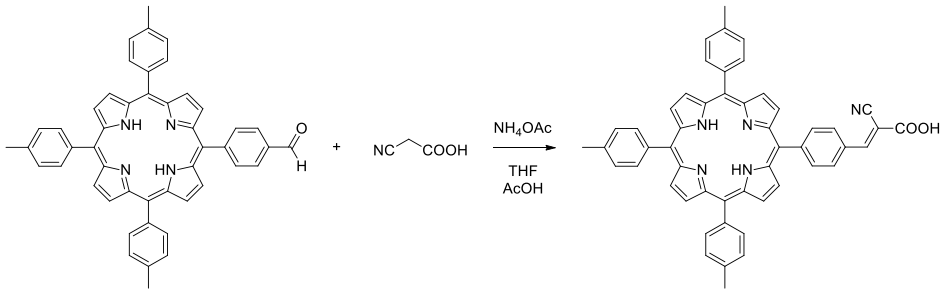

Figure 90: The procedure used by Moser *et al.*[130] to append a porphyrin with a surface-binding group *via* Knoevenagel condensation

Jiang *et al.*,[136] used a di(cyanomethyl)benzene bridging unit to produce polymeric porphyrin materials from a porphyrin dialdehyde. It seemed that this type of reaction would be suitable for the construction of pure-material multiporphyrin arrays, but to the author's knowledge there have been none synthesised *via* Knoevenagel condensation. The basic conditions of the condensation reaction were also expected to permit the use of porphyrin reagents with co-ordinated acid-sensitive metal ions.

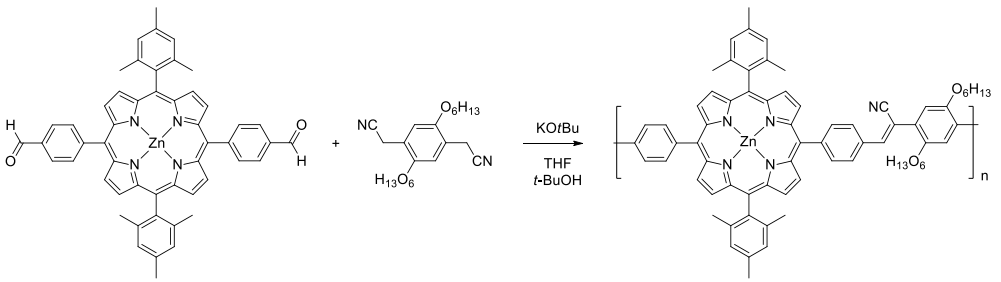

Figure 91: The procedure used by Jiang *et al.*[136] to produce a polymeric porphyrin material

To generate arrays, a benzyl cyanide porphyrin reagent was required. In a similar manner to that in which the tetraester phosphonium salt was used as a hydrophilic porphyrin building block for the production of porphyrin arrays *via* Wittig reaction, it was envisioned that the benzylcyanoporphyrin triester **5.16** (Figure 92) could fill a similar role for producing arrays using Knoevenagel condensations.

The mixed-aldehyde condensation approach appeared to be an efficient method for producing the benzylcyanoporphyrin triester **5.16**. There were two options for producing the benzylcyanoporphyrin: it could be synthesised directly using α-cyanomethylbenzaldehyde or it could instead be produced *via* the analogous porphyrin benzyl bromide **5.17**. It was anticipated that it would be difficult to isolate the α-cyanomethylporphyrin product from a statistical mixture because of the similar retention properties of nitrile and methyl ester groups. The synthesis *via* the bromoporphyrin **5.17** appeared more favourable, as it was expected that the monobromoporphyrin could be isolated from the statistical mixture before the replacement of the bromine atom with nitrile group *via* nucleophilic substitution.

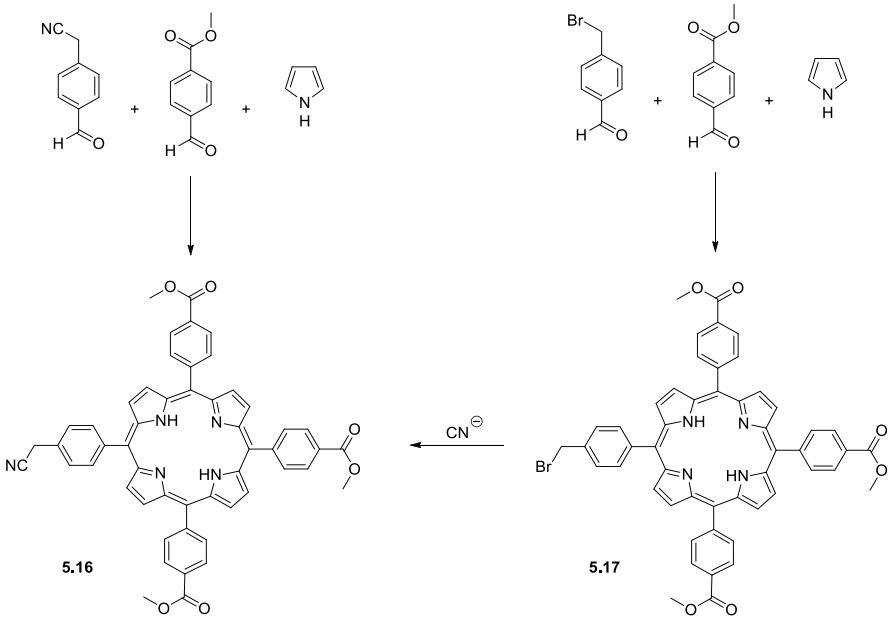

Figure 92: The two proposed syntheses of the cyanoporphyrins

Cyanide substitution reactions were initially tested on bromomethylporphyrins, which had been previously prepared by the author for unrelated experiments. The synthesis of the hydrophobic cyanomethylporphyrin **5.19** was pursued via **5.18**, and the preparation of these compounds is described below.

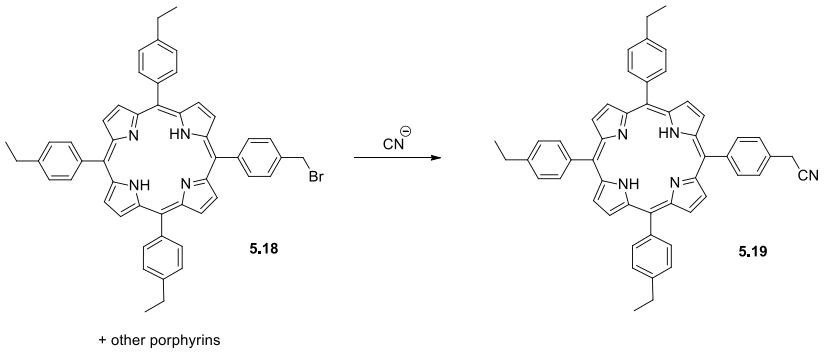

Figure 93: The cyanide substitution reaction was tested on a statistical mixture containing 5.18

5.3.1 Preparation of cyanoporphyrins

4-Formylbenzyl bromide

The synthesis of porphyrins bearing benzyl bromide substituents using a mixed-aldehyde condensation required the synthesis of the appropriate aldehyde precursor, 4-formylbenzyl bromide. This compound was prepared from 4-tolunitrile in two steps according to the procedure of Wen *et al.*[137] (Figure 94). Initially 4-tolunitrile was brominated to produce 4-cyanobenzyl bromide **5.20** *via* treatment with NBS, initiated with benzoyl peroxide, in yield of 57%. This was significantly higher than the 48% reported in the literature, possibly due to a better crystallisation yield during purification. The identity and purity of the product was confirmed by the ^{1}H NMR spectrum, which matched the reported spectrum.[137] Nitrile **5.20** was then treated with DIBAL in toluene to produce 4-formylbenzyl bromide **5.21** in a yield of 64%, significantly lower than the reported yield of 85%. The identity and purity of the product was confirmed by the ^{1}H NMR spectrum, which was identical to that published in the literature.

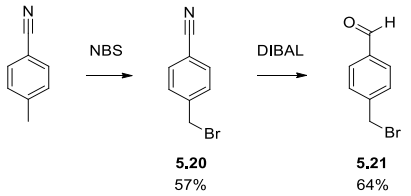

Figure 94: Synthesis of 4-formylbenzyl bromide

4-(Ethylphenyl)porphyrin benzyl bromides

A statistical mixure of porphyrins bearing benzyl bromide and 4-ethylphenyl groups was produced by condensing 4-ethylbenzaldehyde, 4-formylbenzyl bromide **5.21** and pyrrole under the conditions of Lindsey,[138] with the porphyrinogens thus generated being oxidised with DDQ. The porphyrin mixture was separated from the black by-product material *via* flash chromatography, but because of the very similar retention properties of the six porphyrin products, they could not be separated from one another.

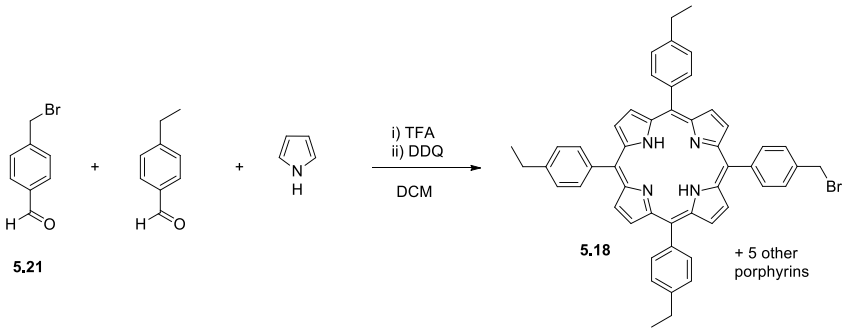

Figure 95: Mixed-aldehyde condensation to produce a statistical mixture containing the porphyrin mono benzyl bromide

The mixture was analysed *via* MALDI MS, which detected ions with m/z ratios of 726, 792, 857 and 923 in decreasing order of intensity. These were attributed to the tetraethyl, triethyl, diethyl and monoethyl bromoporphyrin MH^+ ions. No MH^+ ion was detected for the

tetrabenzylbromide, but this was not surprising as the signal was likely simply too weak based on the trend of decreasing intensity observed for the other MH^+ ions. Ions of m/z ratios of 712, 776 and 842, attributable to the homolytic loss of a Br radical from the triethyl, diethyl and monoethyl porphyrins respectively (MH^+-$Br^\cdot$), were also detected (Figure 96).

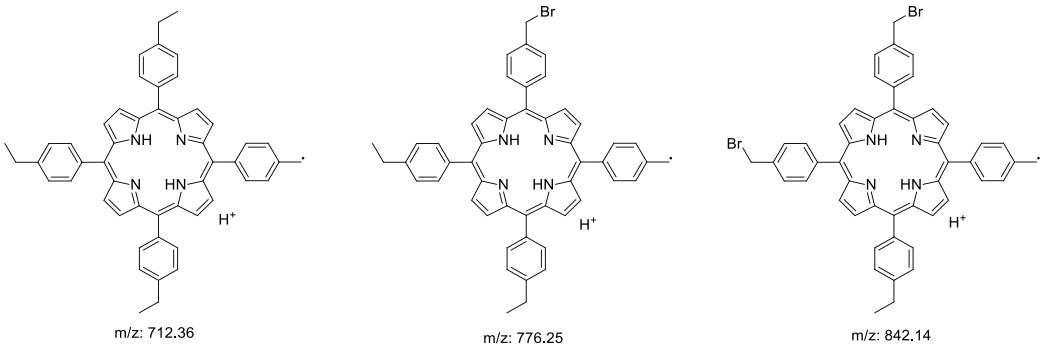

Figure 96: The proposed structures of the ions detected by MALDI MS. The m/z ratios are for the highest isotopic abundance

The ^{1}H NMR spectrum of the mixture (Figure 97) did not allow for the relative yields of each of the components of the mixture to be measured, as the NH peaks (a), the best features for accomplishing this, were superimposed. However, the spectrum did allow an assessment of the relative abundance of ethyl and bromomethyl substituents. A triplet at 1.54 and a quartet at 3.01 ppm (b and c) with relative integrations of 3H and 2H and both with *J* = 7.69 Hz were attributed to the CH_3 and CH_2 groups of the ethyl substitutents respectively. A singlet at 4.85 ppm (d) was attributed to the CH_2 of the benzyl bromide substituents. The integration of the CH_2 protons of the ethyl groups and the benzyl bromine groups revealed that they were present in a ratio of 1:1. This indicated that the aldehydes had had very similar reactivity and that the porphyrins were likely present in a purely statistical ratio, as shown in Table 1 in Chapter 2. This meant that the intended product, the monobromo porphyrin, should be present in a molar percentage of 25% (23% by mass). The aromatic region displayed a pair of

multiplets at 7.58 and 7.78 ppm (e and f), each which integrated to 2H relative to the 2H of the CH_2 signal of the ethyl group at 3.01 ppm (peak c). Another pair of multiplets at 8.12 and 8.19 ppm (g and h), each of which also integrated to 2H relative to the 2H of the CH_2 signal of the benzyl bromide substituents at 4.85 ppm (c). The relative integration of the aromatic proton signals of the two substituent types confirmed the 1:1 ratio. Signals from β-pyrrolic H nuclei appeared 8.78 and 8.91 ppm (peak cluster i) and integrated to 8H relative to the total integration of the benzene ring protons of 16H.

Although the intended product was formed as part of an inseparable mixture, the substitution of bromine with cyanide was undertaken with the expectation that the nitrile products would then be chromatographically separable.

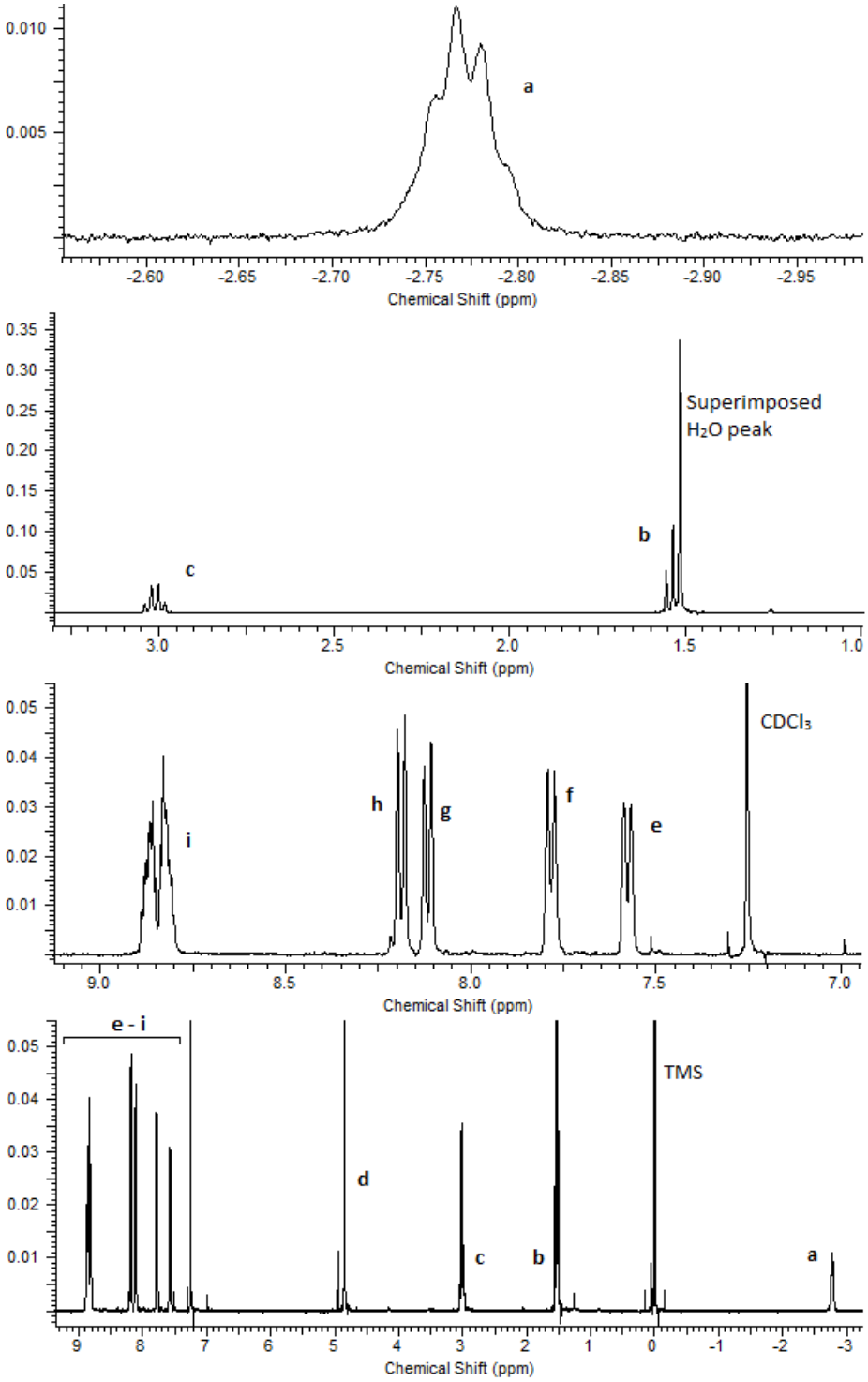

Figure 97: The ^{1}H NMR spectrum of the statistical mixture of bromomethyl porphyrins

CN substitution on bromobenzyl porphyrin mixture

Cyanide substitutions of benzyl bromides have been performed under a wide variety of conditions. Most often a two-phase solvent system is employed with a phase transfer catalyst and the cyanide salt of sodium or potassium. Common phase-transfer catalysts are the quaternary ammonium halides, *e.g.* tetrabutylammonium chloride. Organic solvents employed with these phase transfer catalysts include DCM,[139] toluene[140] and DMF.[141] However, success has also been reported with polar solvents such as THF,[142] dioxane,[143] ethanol,[144] methanol[145] mixed with water and employing a cyanide salt.

Because of the simplicity of the polar solvent single-phase conditions, a similar method was trialled for the CN substitution of the bromoporphyrins (Figure 98). The porphyrin mixture was dissolved in THF and treated with NaCN and water. Tetrabutylammonium chloride was also added to improve the solubilty of CN^- in the predominantly-THF solvent mixture. After 24 hours TLC indicated that some nitrile products had formed but that the reaction was far from complete. MALDI MS analysis of the mixture detected an ion of m/z 739, likely the MH^+ ion of the intended mononitrile porphyrin product **5.19**.

The reaction was trialled with dioxane in place of THF in the hope of improving the reaction rate. After 24 hours TLC indicated that very little non-nitrile porphyrin remained but MALDI MS analysis still detected ions of porphyrins bearing bromine atoms. After 48 hours TLC indicated that the reaction was complete and the products were separated by column chromatography. The monocyanoporphyrin product **5.19** was isolated in a yield of 82% based on the assumption that the monobromoporpyrin did indeed form 23% of the starting material by mass (as calculated previously). The di-, tri- and tetracyano compounds were not isolated.

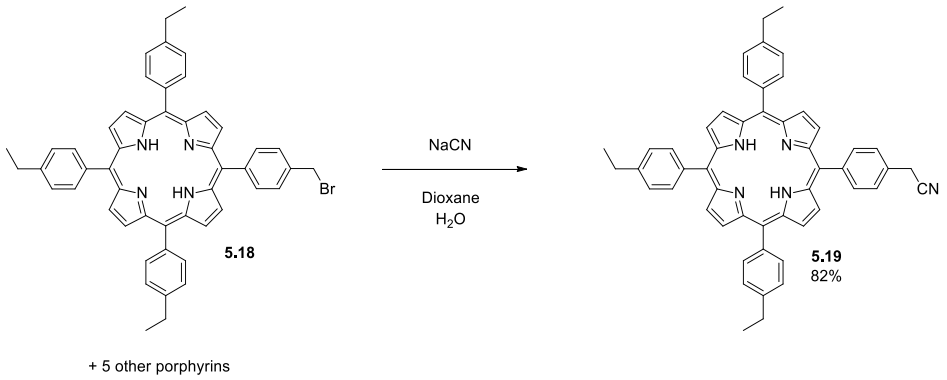

Figure 98: Nucleophilic substitution to produce the monocyanoporphyrin 5.19

The ^{1}H NMR spectrum displayed a single symmetrical NH peak at -2.78 ppm, an indication that only one porphyrin compound was present. A triplet at 1.53 ppm with *J* = 7.69 Hz and an integration of 9H was assigned to the three CH_3 groups of the ethyl substituents. A quartet at 3.01 ppm with the same *J* value and an integration of 6H was assigned to the CH_2 groups. A singlet at 6.55 ppm with an integration of 2H was assigned to the CH_2 group of the α-cyanomethylbenzene substituent. The aromatic H atoms of the ethylbenzene groups appeared as two doublets at 7.58 and 8.12 ppm, each with *J* = 7.88 Hz and an integration of 6H. The aromatic H atoms of the cyanomethylbenzene group appeared as two doublets at 7.71 and 8.23 ppm, each with *J* = 8.06 Hz and an integration of 2H. The β-pyrrolic H nuclei appeared as two doublets at 8.76 and 8.88 ppm with *J* = 4.76 Hz and a superimposed singlet at 8.86 Hz. The total integration of these peaks was 8H.

MALDI MS analysis of the isolated product detected the MH^+ ion. The UV-vis absorption spectrum was typical of a free base tetraphenylporphyrin, displaying four Q bands and a sharp B band with its maximum at 420 nm.

With these conditions for cyanide substitution having been developed, the same chemistry was applied to the bromoporphyrin triester **5.17,** whose synthesis is described below. The

hydrophobic cyanoporphyrin produced during the development of the substitution conditions was also a potentially useful synthon for the production of porphyrin arrays *via* Knoevenagel condensation.

Bromoporphyrin triester

Bromoporphyrin triester **5.17** (Figure 99), was produced *via* the statistical mixture approach with three equivalents of 4-formylbenzoic acid methyl ester and one equivalent of 4-formylbenzyl bromide condensed with pyrrole under Lindsey's conditions and the resulting porphyrinogens oxidised with DDQ. The aldehyde ratios were chosen to maximise the formation of the triester monobromoporphyrin as discussed in Section 4.2.1. Unlike the ethylphenyl porphyrin statistical mixture (*vide supra*), the ester porphyrin products were separable *via* flash chromatography and the triester product was purified in this manner. The fractions were analysed by MALDI MS and the triester-containing fractions were identified by the detection of an ion of m/z 881, which was attributed to the MH^+ ion. The product was precipitated by addition of methanol to afford a yield of 8.7%.

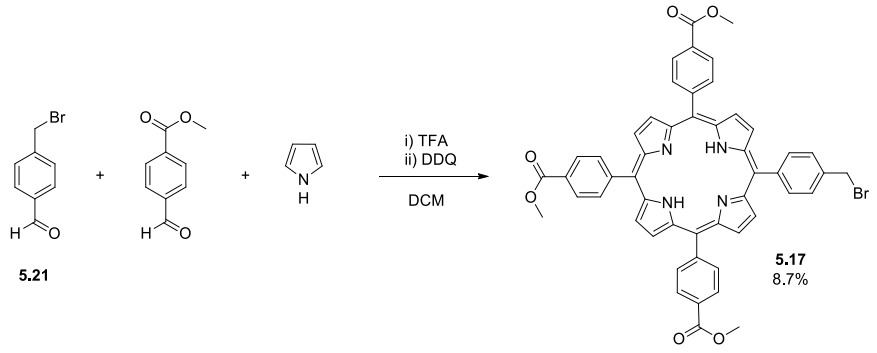

Figure 99: The synthesis of the bromoporphyrin triester building block 5.17

The ^{1}H NMR spectrum displayed a single symmetrical NH peak at -2.80 ppm which integrated to 2H. A singlet at 4.11 ppm integrated to 9H and was assigned to the three ester CH_3 groups. Another singlet at 4.85 ppm integrated to 2H and was assigned to the benzylic H atoms. In the aromatic region there was a pair of doublets at 7.80 and 8.19, which integrated to 2H each with *J* = 8.10 Hz. These were assigned to the H atoms of the benzene ring bearing the bromomethyl group. Another pair of doublets at 8.29 and 8.44 ppm had a *J* = 8.30 Hz and integrated to 6H each. These were assigned to the H atoms of benzene rings bearing ester groups. The β-pyrrolic H atoms appeared as a pair of doublets at 8.80 and 8.87 ppm with a superimposed singlet at 8.10 ppm. The total integration of these peaks was 8H. The UV-vis spectrum was typical of a free base tetraphenylporphyrin, displaying four Q bands and a sharp B band with its maximum at 420 nm.

CN substitution of bromoporphyrin triester

The conditions that had proven sucessful for the cyanide substitution of the bromoporphyrin statistical mixture were applied to the bromoporphyrin triester **5.17** in an attempt to generate the porphyrin mononitrile triester **5.16**. The porphyrin was treated with NaCN in dioxane and water and the progress of the reaction monitored by TLC. After 1 hour a significant quantity of porphyrin-coloured baseline material had appeared and very little other porphyrin material was detected. This was surprising, as the rf of the cyanoporphyrin product was expected to be only moderately lower than that of the starting material. The result was attributed to the hydrolysis of the ester groups catalysed by the basicity of the cyanide ions. The reaction was trialled with no water present and progress monitored by TLC analysis, but it was found that the cyanide substitution did not proceed at all under these conditions. Alternative conditions were therefore required for the nitrile substitution of the triester porphyrin **5.17**.

The nucleophilic substitution of benzyl bromides with cyanide using DMF as the solvent under anhydrous, single phase conditions has been reported in the literature, for example by Lee *et al.*[146] Under these anhydrous conditions, it was expected that the ester groups would remain intact through the cyanide substitution.

A sample of the bromoporphyrin triester **5.17** was dissolved in DMF and sodium cyanide added. Progress of the reaction was monitored by TLC anaylsis, and under these conditions the nucleophilic substitution proceeded much faster than in dioxane. After 30 mins TLC analysis indicated that no starting material remained. Ammonium acetate was added to neutralise the solution, water was also added, and the product extracted with DCM. The product was submitted to flash chromatography and the fractions analysed by MALDI MS. Analysis of the first band to elute detected an ion of m/z 828 which was assigned to the MH^+ ion of the cyanoporphyrin product **5.16**. Precipitation with methanol afforded a yield of 53%.

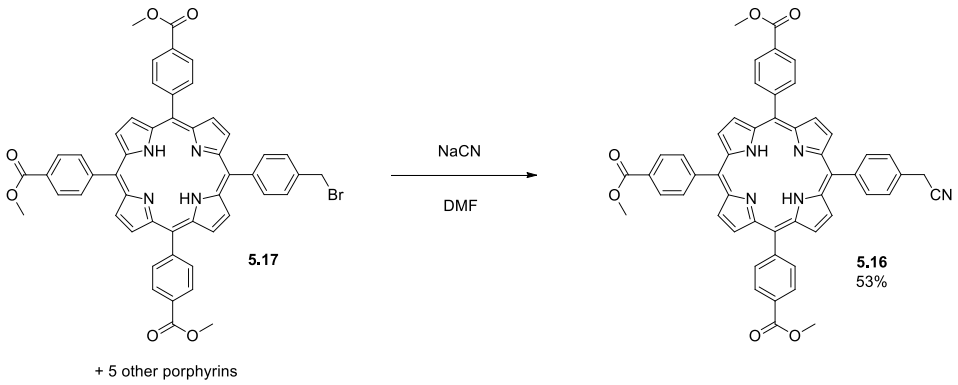

Figure 100: The substitution of a bromine for a nitrile group in a nucleophilic substitution reaction

The ^{1}H NMR spectrum displayed a single symmetrical NH peak at -2.80 ppm, an indication that only one porphyrin was present. Two superimposed singlets at 4.11 and 4.12 ppm with a total integration of 11H were assigned to the ester CH_3 groups and the benzylic CH_2. Two doublets at 7.74 and 8.23 ppm with *J* = 8.24 Hz and an integration of 2H each were assigned to

the aromatic H atoms of the cyanomethylbenzene substituent. Two doublets at 8.29 and 8.44 ppm, each with *J* = 8.24 Hz and each with an integration of 6H, were assigned to the aromatic H atoms of the ester-bearing benzene rings. A multiplet between 8.78 and 8.85 ppm was assigned to the β-pyrrolic H atoms.

The UV-vis spectrum was typical of a free base tetraphenylporphyrin, displaying four Q bands and a sharp B band with its maximum at 420 nm. MALDI MS analysis of a second chromatography band detected an ion of m/z 1630, which was tentatively identified as the dyad **5.22**, formed by the base-catalysed nucleophilic reaction of a molecule of the cyanoporphyrin product with a molecule of the bromoporphyrin starting material *via* the mechanism shown in Figure 101. This demonstrated that the benzylic protons could be removed under basic conditions to generate a nucleophilic carbon, as is required for the Knoevenagel condensation. Although this reaction was not repeated, dyad formation could likely be minimised in future by conducting the reaction at a lower porphyrin concentration.

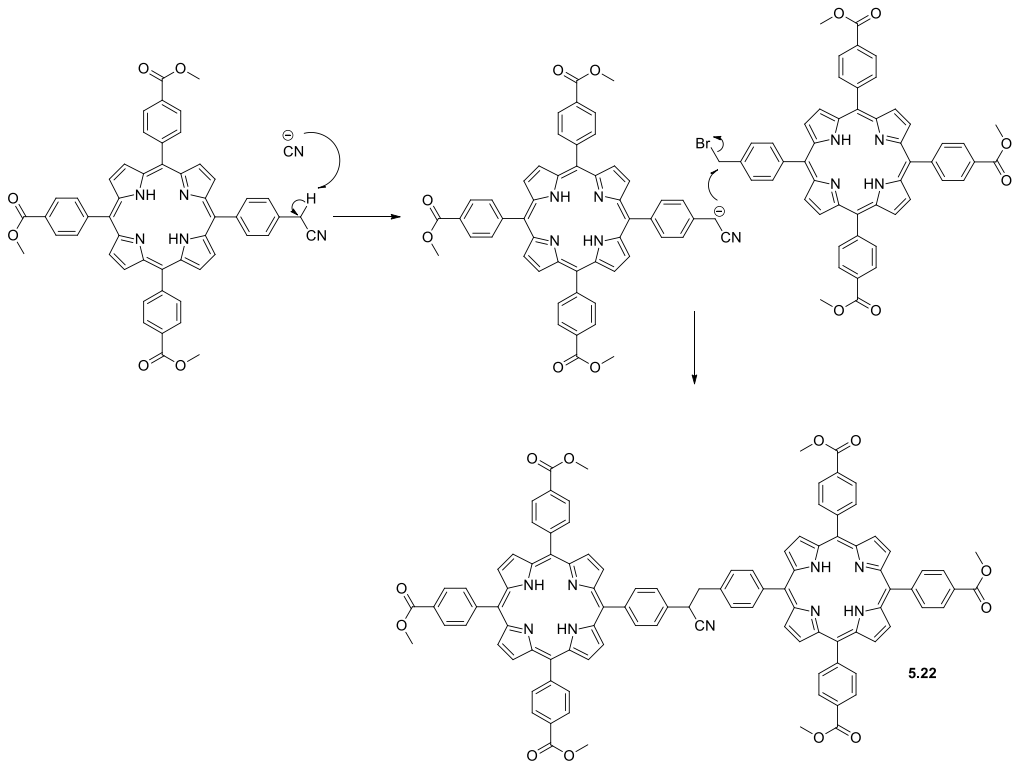

Figure 101: The proposed mechanism of dyad formation during the cyanide substitution reaction

5.3.2 Knoevenagel condensation

With the cyanomethylporphyrin triester building block **5.16** in hand, a Knoevenagel condensation could then be attempted. DBU has been used successfully as a base catalyst to couple a benzaldehyde with a benzyl cyanide[147,148] and was used in initial attempts at the condensation of the porphyrin monoaldehyde **4.06** with **5.16** (Figure 102). DCM was used as the reaction solvent because of the good solubilty of the reagents in this solvent and the ease of workup because of its volatility.

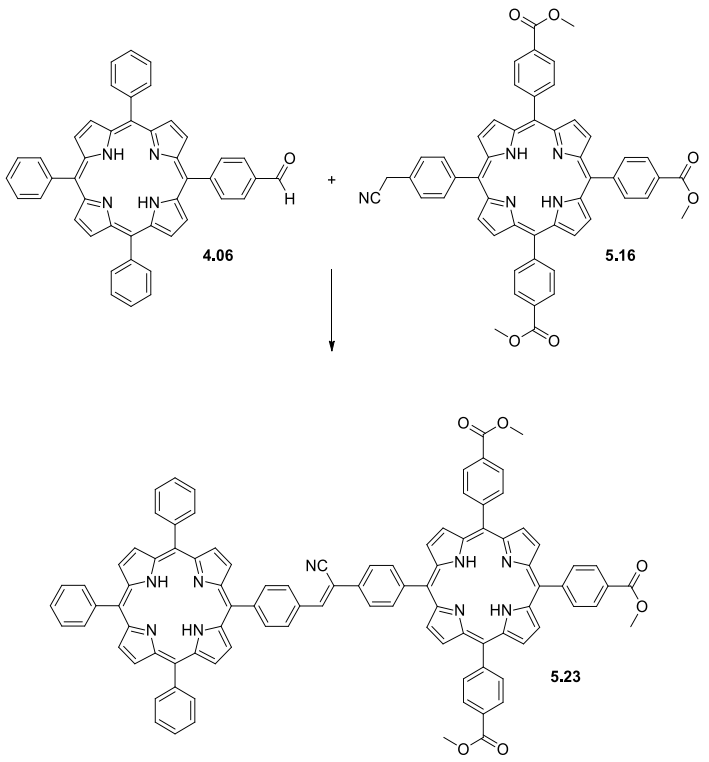

Figure 102: Knoevenagel condensation to form the porphyrin dyad 5.23

The reagents were mixed and stirred at room temperature and the progress of the reaction monitored by TLC analysis. After 30 mins the presence of a product was observed. MALDI MS analysis of the mixture detected an ion at m/z 1454, assigned to the MH^+ ion of the intended dyad product. The mixture was submitted to flash chromatography and the fractions

analysed by MALDI MS, which revealed that most of the starting materials remained unreacted, but a small amount (<1 mg) of dyad was isolated.

The ^{1}H NMR spectrum (Figure 103) displayed two symmetrical NH peaks at -2.74 and -2.71 ppm, each with equal integration. This was a good indication that a dyad was present and not contaminated with any other porphyrin. Two superimposed singlets at 4.12 and 4.13 ppm with a total integration of 9H were assigned to the CH_3 signals of the ester groups. A singlet at 7.31 ppm with an integration of 1H was assigned to the vinyl H. This is similar to the shift reported for the analogous proton of the same moiety (7.54 ppm) between two phenyl groups by Taha *et al.*[149] A multiplet between 7.70 and 7.85 was assigned to the *meta* and *para* H nuclei of the unsubstituted phenyl substituents. Several superimposed multiplets between 8.20 and 8.55 ppm with a total integration of 26H were assigned to the remaining H nuclei of the benzene rings. Several superimposed multiplets between 8.80 and 9.00 ppm with a total integration of 16H were assigned to the β-pyrrolic H nuclei.

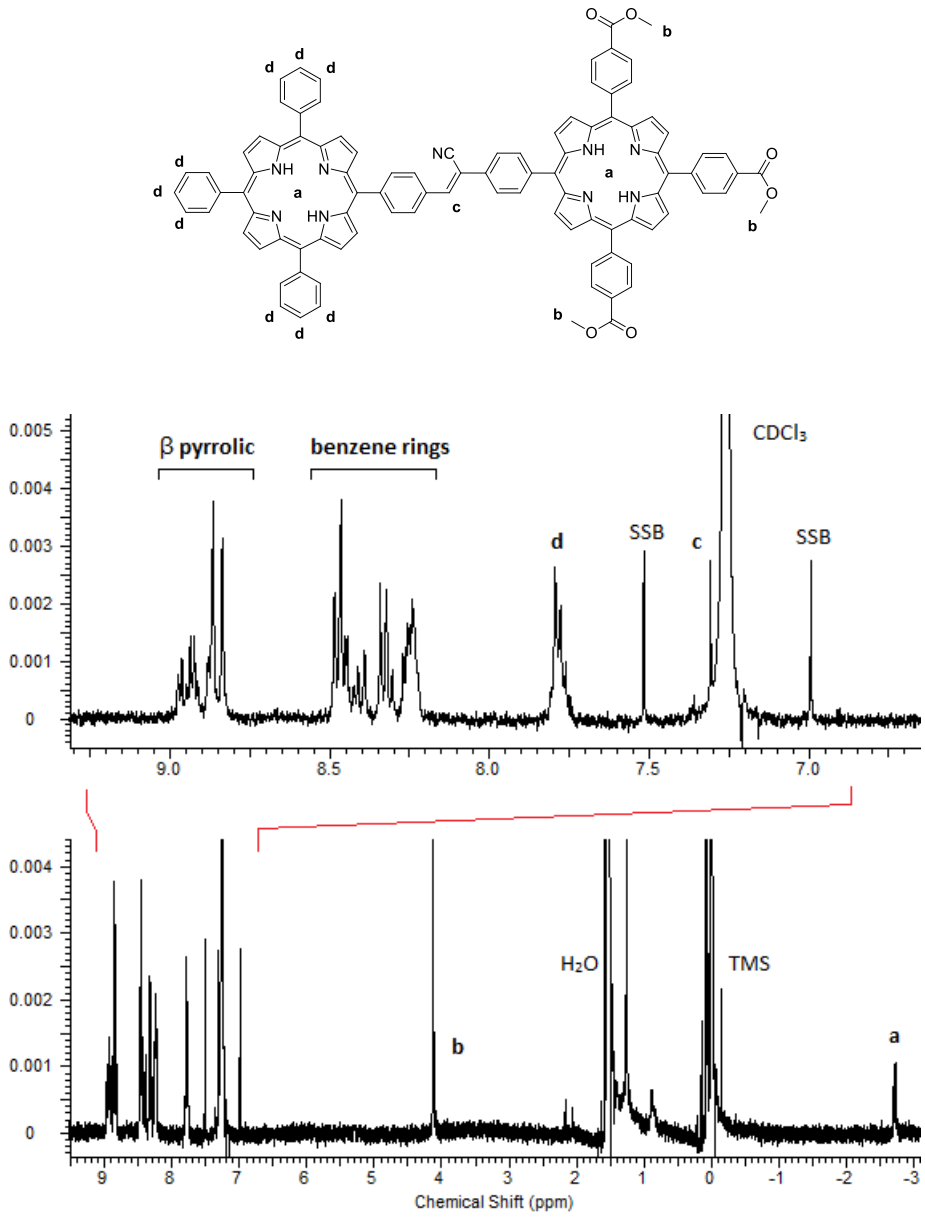

Figure 103: The ^{1}H NMR spectrum of the dyad 5.23

The UV-vis absorption spectrum (Figure 104) was similar to a single free base tetraphenylporphyrin in that it displayed four Q bands and a (somewhat broadened) B peak with its maximum at 422 nm. This is distinctly different from the phenyene-linked dyads of Chapter 4, which displayed dual B peaks. It is more similar to the Wittig-linked porphyrins in that the B peak is somewhat broadened, and no Davydov splitting occurs.[127]

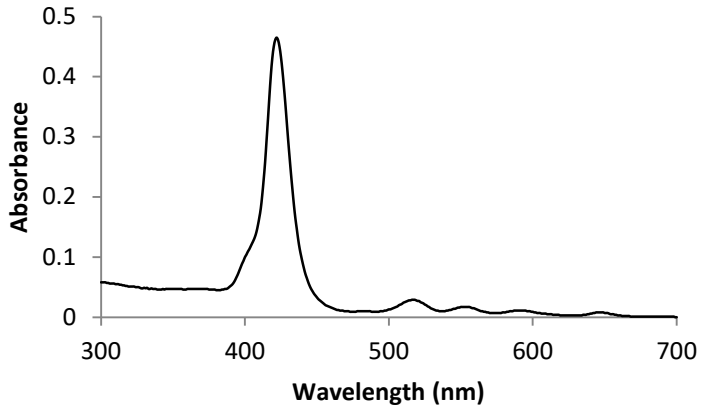

Figure 104: The UV-vis absorption spectrum of the dyad 5.23

While successful in generating the dyad product, the low yield of this reaction clearly needed improvement. The reaction was repeated under similar conditions, but this time heated at reflux. TLC indicated that most of the triester starting material had been consumed and the reaction was submitted to flash chromatography. As with the reaction conducted at room temperature, mostly starting material was recovered and only a small amount of the dyad, seemingly in contradiction of the TLC analysis. Also noted was a faint band which eluted after the triester starting material. MALDI MS analysis of this band detected an ion of m/z 1472. This was attributed to the dyad compound **5.24** (Figure 105), an intermediate of the reaction which had been expected to spontaneously undergo elimation of water to produce the alkene product **5.23**. The presence of this product and the observed consumption of the CN triester during the reaction by TLC analysis indicates that the low yield may be attributed to the slow elimination of water and reversibility of the initial C-C bond forming step, causing the reformation of the starting material upon workup of the reaction.

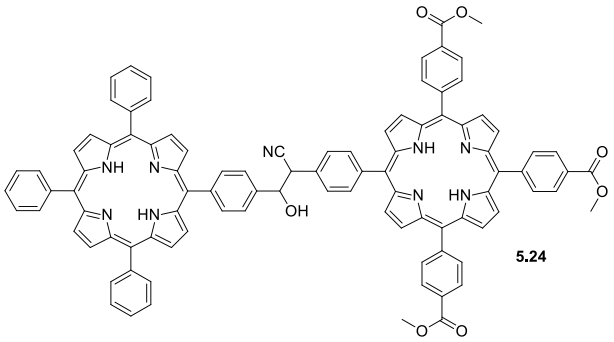

Figure 105: An intermediate product of Knoevenagel condensation which was detected by MALDI MS

The reaction was trialled in toluene, THF, ethanol and DCE with DBU as the catalytic base and in each case only a small quantity of dyad product and OH intermediate was observed in TLC analysis. Sodium methoxide was tested as the catalytic base in THF, toluene and DCE but this again produced only a trace of dyad product and hydrolysed the ester groups. Microwave irradiation was trialled with DBU in DCE but this failed to increase the conversion of the starting materials to the product.

The consistent low yield of the product and the presence of the alcohol intermediate suggested that the reaction proceeded but formed an equilibrium favouring the starting materials, and equilibrium behaviour of Knoevenagel condensations has been reported previously.[150] A sample of the dyad product was isolated and characterised but in a quantity too small to carry through further synthetic steps to produce the target amphiphilic dyad. No attempt was made to make a triad because it would have likely had a very low yield due to the compounding low yields of the individual condensations.

5.4 Chapter conclusion

The technique of Wittig condensation to form amphiphilic porphyrin arrays was used successfully in producing an amphiphilic dyad. This compound is suitable for experiments with maquette binding, and a binding test with this compound is described in Chapter 7.

As for the phenylene-linked compounds of Chapter 4, the isolation of a triad proved elusive because of the difficulty of chromatographic isolation. This seems to indicate that this may be a general problem with the isolation of ester-bearing porphyrin arrays from the by-products of their formation. The reaction may yet prove useful for the production of triads and larger ester-bearing arrays if a better product-isolation technique can be developed.

A dyad was also successfully formed *via* the Knoevenagel linking technique, however, the product was produced in a low yield, seemingly because of a reversibility of the linkage reaction. Characterisation data for the dyad was obtained, but there was not enough of the product for it to be carried through metal insertion and hydrolysis for maquette-binding testing.

Chapter 6: Using porphyrin metalation to facilitate array synthesis and purification

6.1 Differential dyad metalation of phenylene-linked dyad

The synthetic strategy described in Chapter 4 was effective in producing the porphyrin dyads **4.11** and **4.13**, but as it stood it lacked any provision for differential metalation of the porphyrin rings, *i.e.* binding a different metal ion in each side of the dyad. It would be beneficial if the two rings of the dyad could be differentially metalated in order to provide a means of tuning the redox and photonic properties to suit their application as light harvesting antennas. In particular, the creation of zinc-iron dyads was desirable because of the demonstrated electron transfer from a photoexcited zinc porphyrin to a nearby iron porphyrin.[151] The initial targets were both metal isomers of zinc-iron complexes, but with the aim of developing a general method that could be applied to any pair of metal ions.

The simplest way to achieve differential metalation would be to pre-place a metal ion in the porphyrin aldehyde prior to the formation of the second ring (Figure 106). Unfortunately zinc cannot be pre-placed because it would be displaced by the acidity of both the Adler and Lindsey's porphyrin synthesis conditions. On the other hand, if iron were to be pre-placed, it would likely survive the acidic conditions of the porphyrin synthesis, but because of the highly polar nature of the spontaneously-formed Fe(III) complexes, the products would be difficult to separate from the by-products of the reaction. However, if an alternative metal without these limitations could be identified, it could allow the effective ring protection of a dyad.

It was reported by Collman *et al.*[152] that a silver ion can be used as a place-holder and protection group for the first-formed porphyrin ring in the synthesis of a dyad. Silver is more acid tolerant than zinc, but unlike iron, does not cause strong retention on silica during chromatography. It was shown that the silver ion could be later removed *via* treatment with $NaBH_4$ in THF-H_2O without displacing zinc ions also present, bound in the second-formed porphyrin ring.

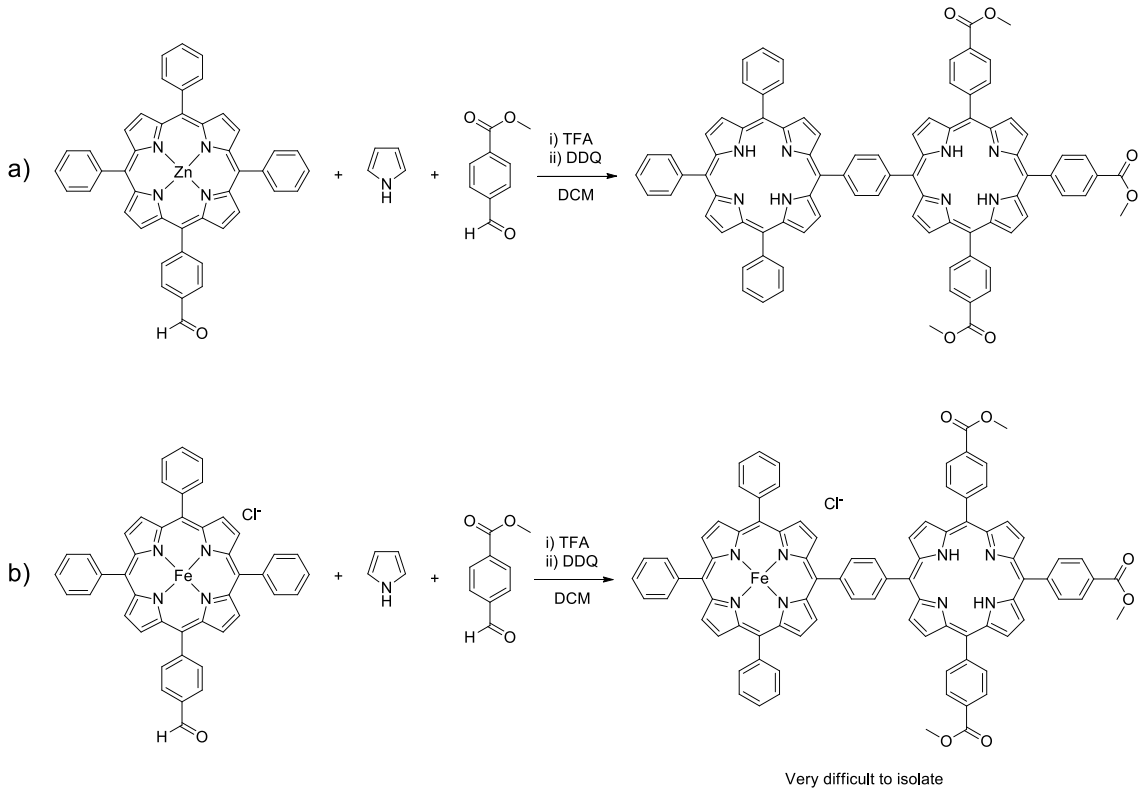

Figure 106: a) Pre-metalation of the porphyrin aldehyde with an acid-labile metal such as zinc would likely result in a fully unmetalated dyad following the synthesis of the second porphyrin ring b) Pre-metalation with a metal which spontaneously adopts the (III) oxidation state results in a dyad which is very difficult to isolate from the reaction mixture

6.1.1 Silver protection of porphyrin aldehyde

A process using the previously described silver protection[152] to produce a zinc-iron dyad was envisioned and is shown in Figure 107. First a silver porphyrin aldehyde **6.01** was to be condensed with 4-formylbenzoic acid methyl ester and pyrrole to produce the mono silver-metalated phenylene-linked dyad **6.02** in a similar manner to that used in Chapter 4 to produce the unmetalated dyad **4.13**. The work of Collman *et al.*, however, did not take a silver-metalated porphyrin through a porphyrin synthesis reaction, and therefore it was neccessary to test if the silver ion would remain bound under the necessary acidic conditions of such reactions.

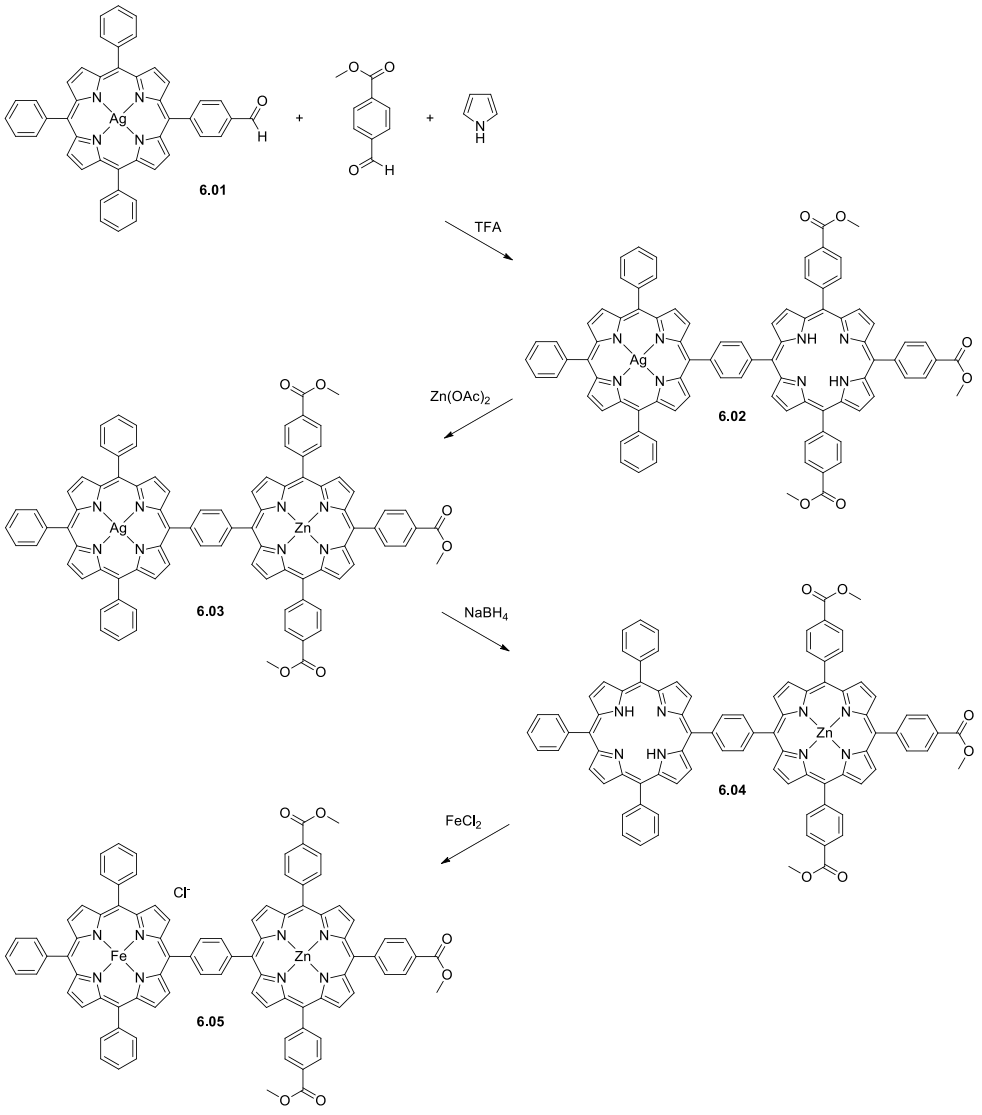

Figure 107: The proposed synthesis of a FeZn phenylene-linked dyad

Testing of acid tolerance of silver porphyrins

The limit of the acid tolerance of porphyrin-bound silver was investigated by treating Ag tetra-(4-ethylphenyl)porphyrin (TEPP) (provided by Dr Pawel Wagner) **6.06** (Figure 108) with 22 mM TFA in DCM, the same concentration used in Lindsey's porphyrin synthesis. TLC analysis did not detect any demetalated porphyrin. The concentration of TFA was increased more than 10-fold to 284 mM, and left to react for 1 hour, but still no demetalated porphyrin was detected. It appeared that a bound silver ion should remain in place during a porphyrin synthesis under Lindsey's conditions.

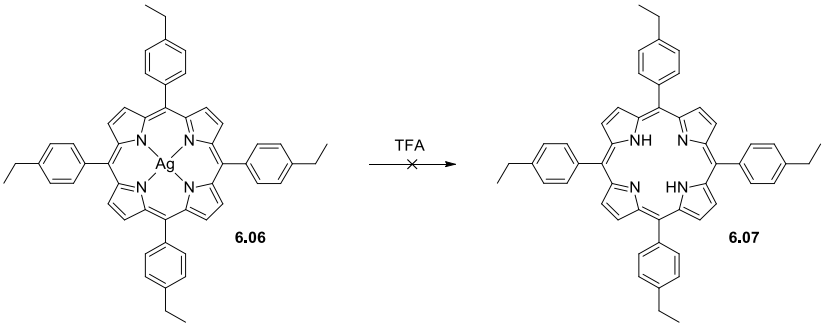

Figure 108: Investigation into silver porphyrin stability when exposed to TFA found that the metal ion was not removed

Test for the selective removal of silver

It had been reported by Collman *et al.*,[152] for β-alkyl *meso*-unsubstituted porphyrins that by reducing porphyrin-bound silver to its (I) oxidation state and treating it with a dilute acid, that the silver ion could be easily removed. In their publication this was achieved with an AgZn dyad without removing zinc. Trials were conducted using AgTEPP **6.06** to test the applicability of this process to tetraphenylporphyrins before attempting to use it on a dyad.

In similar conditions to those used by Collman *et al.*,[152] a mixture of AgTEPP **6.06** in DCM and isopropanol was treated with $NaBH_4$ followed by aqueous ammonium chloride (Figure 109

a). A stronger acid was not used to quench the reaction to avoid the loss of zinc when the conditions were applied to the dyad. MALDI MS analysis detected a strong signal for an ion of m/z 727, which was assigned to the demetalated TEPP. A weaker signal at m/z 832 was also detected, which was assigned to the still metalated AgTEPP. This result indicated that while the silver removal conditions were effective to a great extent, some silver ions remained bound.

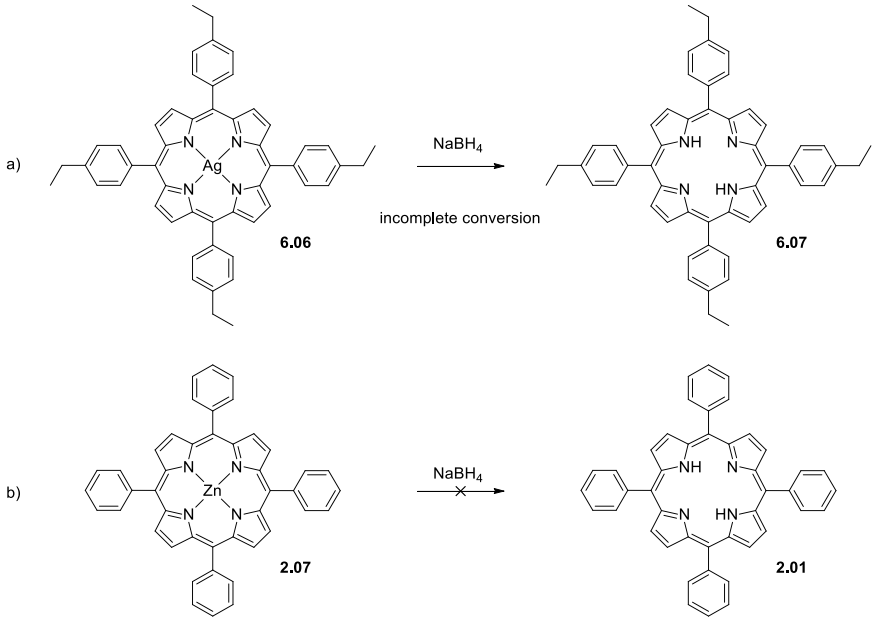

Figure 109: Testing of conditions for the removal of silver from a porphyrin

To test the resistance of bound zinc ions to the silver removal conditions, the same conditions were applied to ZnTPP **2.07** and MALDI MS analysis detected no demetalated porphyrin (Figure 109 b). With this, the effectiveness of the conditions for the removal of silver without removing zinc had been confirmed. However, since the silver porphyrin was not completely demetalated and because complete demetalation was required to make the reaction useful, the conditions required improvement.

Alternative reducing agents were therefore trialled. Hypophosphorous acid, dithiothretol, $NaCNBH_4$ and EDTA failed to produce any demetalated porphyrin. Trimethylphosphine produced some demetalated porphyrin but was very slow-acting and produced unidentified side-products. Hydrazine or dithiothretol with acetic acid produced some demetalation but were slow-acting.

In contrast, while *N*,*N*-diethylhydroxylamine demetalated **6.06** slowly at room temperature, the demetalation rate could be considerably increased by using acetonitrile and heating at reflux, conditions which produced complete demetalation in 1 hour. In addition, no acid was required for the work up. As a result, this method appeared to be superior to Collman's method, giving complete demetalation with short reaction times and without the need for any strong acid, base or water. This is the first reported use of the reductive demetalation of silver porphyrins with *N*,*N*-diethylhydroxylamine.

Preparation of silver porphyrin monoaldehyde

With the knowledge that a silver porphyrin complex is resistant to the TFA concentration of a porphyrin synthesis reaction, work commenced to synthesise a dyad pre-metalated with silver. A portion of the porphyrin monoaldehyde **4.06** was metalated with silver by dissolving it in a mixture of 1:1 DCM:THF and adding $AgOOCCF_3$ (Figure 110). In this process, it has been proposed that initially Ag(I) becomes bound to the porphyrin, with the bound silver ion then being oxidised to the (II) state by excess Ag(I) in solution in a disproportionation reaction.[153] NaOAc was also added to prevent acidification of the solution. The product **6.01** was isolated *via* flash chromatography and the product-containing fractions were identified by TLC and by MALDI MS. Pure fractions were combined and evaporated to give a yield of 78%.

The ^{1}H NMR spectrum displayed no NH peak in the negative region, indicating complete metalation. The aromatic region contained three broad and superimposed peaks at 7.63, 7.74 and 8.16 ppm. There was also a singlet at 10.35 ppm which was attributed to the aldehyde H nucleus. The broadness of the peaks in ^{1}H NMR spectra of silver porphyrins can be attributed to the paramagnetism of the bound Ag(II) species.[28]

MALDI MS analysis detected an ion of m/z 748, consistent with the MH^{+} ion of the expected silver complex **6.01**. No ion was detected for the starting material **4.06**. The UV-vis absorption spectrum was typical for a silver porphyrin,[154] and displayed four Q bands at 610, 575, 542 and 513 nm. The B peak was at 427 nm, significantly shifted toward longer wavelengths relative to the analogous zinc compound, which displays a B peak at 419 nm.

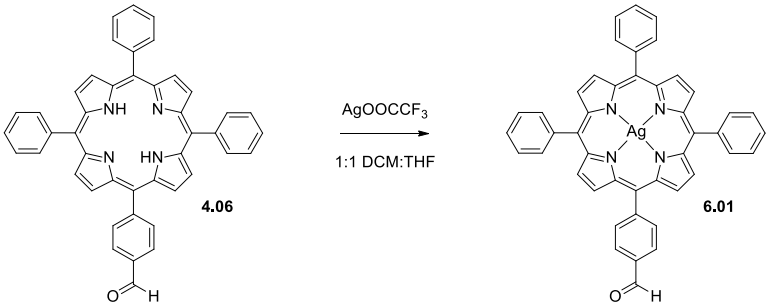

Figure 110: Metalation of the porphyrin aldehyde with silver

Dyad formation from silver porphyrin monoaldehyde

The silver porphyrin aldehyde **6.01** was condensed with pyrrole and 4-formylbenzoic acid methyl ester to produce a dyad, but MALDI analysis revealed that it was completely demetalated and that **4.11** was the sole dyad product (Figure 111).

Although silver porphyrins are resistant to demetalation by TFA alone, it is likely that the reductive power of the pyrrole present in the porphyrin synthesis reaction resulted in the reduction of the silver ions to the (I) state in which they are highly prone to displacement by

protons. The oxidative polymerisation of pyrrole using Ag(I) has been reported[155] and one might reasonably expect that the Ag(II) ion bound in the porphyrin might oxidise pyrrole even more readily, being as it is at a higher oxidation state. This would reduce the silver ion to the (I) state where it is highly prone to displacement by acid. This method was therefore not pursued further and alternative approaches were trialled.

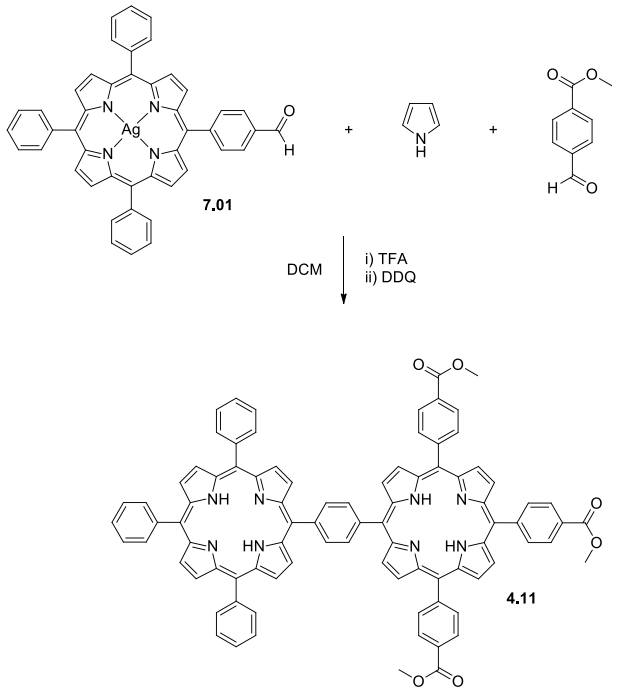

Figure 111: During the formation of the dyad, the silver atom was displaced from the core of the porphyrin ring in which it was bound

Because of the intolerance of silver porphyrins of porphyrin synthesis conditions, this particular line of investigation had to be abandoned. The silver tagging method however remains a promising technique which may be applicable in the synthesis of porphyrin arrays that do not require silver porphyrins to endure aldehyde condensation reactions. A new technique of producing the mixed-metal dyad was required however, and the isolation of partially metalated states was pursued instead.

6.1.2 Separation of partially-metalated dyads

Partial metalation with zinc

While metalating the dyad **4.11** with zinc, described in Chapter 4, it was observed that the two intermediate monometalated states were distinguishable by TLC. This seemed surprising as one could expect that the chromatographic retention due to the presence of a zinc ion would be the same irrespective of which of the two rings it was bound in. If these mono metalated states could be separated on a preparative scale then it would offer the possibility that iron could be bound in the unmetalated ring to produce both the target zinc-iron dyads.

A sample of the dyad **4.11** was therefore submitted to metalation with zinc, but with only one equivalent being added to ensure that the monometalated products would be generated, albeit in a mixture with unmetalated starting material and the dimetalated product. TLC analysis displayed two porphyrin spots of intermediate rf between the starting material and dimetalated dyad spots (Figure 112). MALDI MS analysis detected ions of m/z 1325, 1387 and 1453, the expected MH^+ molecular ions of the starting material, monometalated products and dimetalated products respectively. The mixture was submitted to flash chromatography with 2% ethyl acetate in DCM as eluent (the same eluent as for TLC). The fractions were analysed by TLC to determine if the separation had been successful. Although the dimetalated product was isolated from the mixture, the unmetalated starting material and the two monometalated products were not separated from one another.

Although this technique was unsuccessful, it was proposed that perhaps using a different metal might produce metalation states that were separable in flash chromatography. During related experiments it had been observed that the rf of a porphyrin in TLC analysis increased when a silver (II) ion is bound in its core. This is in contrast with zinc which decreases the rf. This can be attributed to the fact that unlike zinc, silver does not tend to coordinate axially but simply eliminates any H-bonding possibility from the porphyrin core by replacing the H atoms.

If a sample of the dyad could be partially metalated and the singularly-metalated silver complexes isolated, this would offer the potential to then metalate the other porphyrin with iron or zinc before removing the silver ion with the conditions of Collman *et al.*[152]

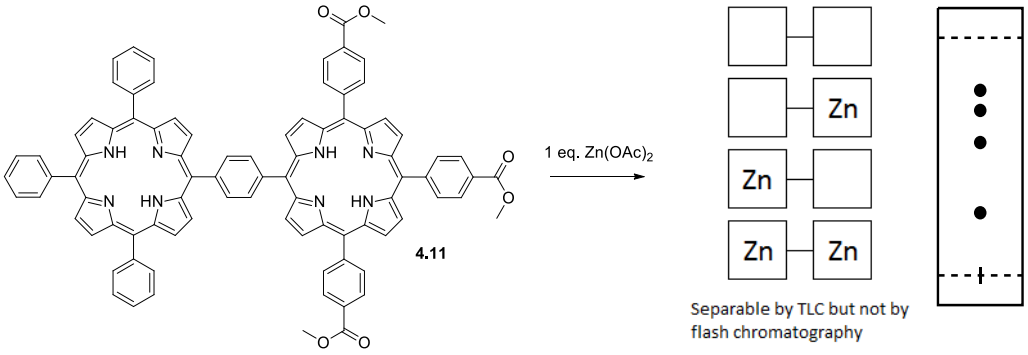

Figure 112: Partial metalation of the dyad to produce a mixture of metalation states separable by TLC with 2% ethyl acetate in DCM as eluent

Partial metalation with silver

A similar partial metalation process to that used with zinc was therefore applied to a sample of the dyad **4.11** with one equivalent of silver trifluoroacetate to produce a mixture of the three metalation states as well as starting material (Figure 113). TLC analysis indicated that the starting material and AgAg dyad were separable, but that the two Ag2H compounds were not. Flash chromatography was performed on the mixture and the fractions analysed by TLC and MALDI MS, but the singularly-metalated dyads were not separated from one another.

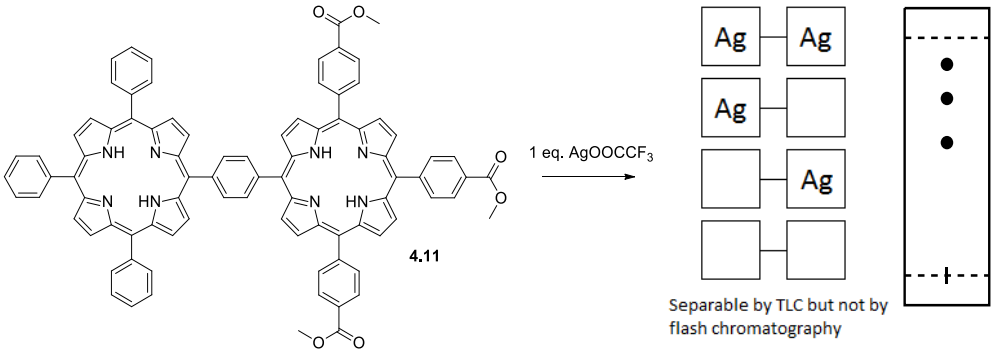

Figure 113: Partial metalation with silver also failed to produce a separable mixture

With the knowledge that zinc increases chromatographic retention of a porphyrin while silver decreases it, it was proposed that by metalating the dyad with a mixture of zinc and silver that the metals' respective retention-modifying properties might combine to increase the separability of the two expected AgZn isomers. If the AgZn dyads could be isolated, it was expected that they could be converted to ZnFe dyads *via* exclusive removal of silver and replacement with iron (Figure 114).

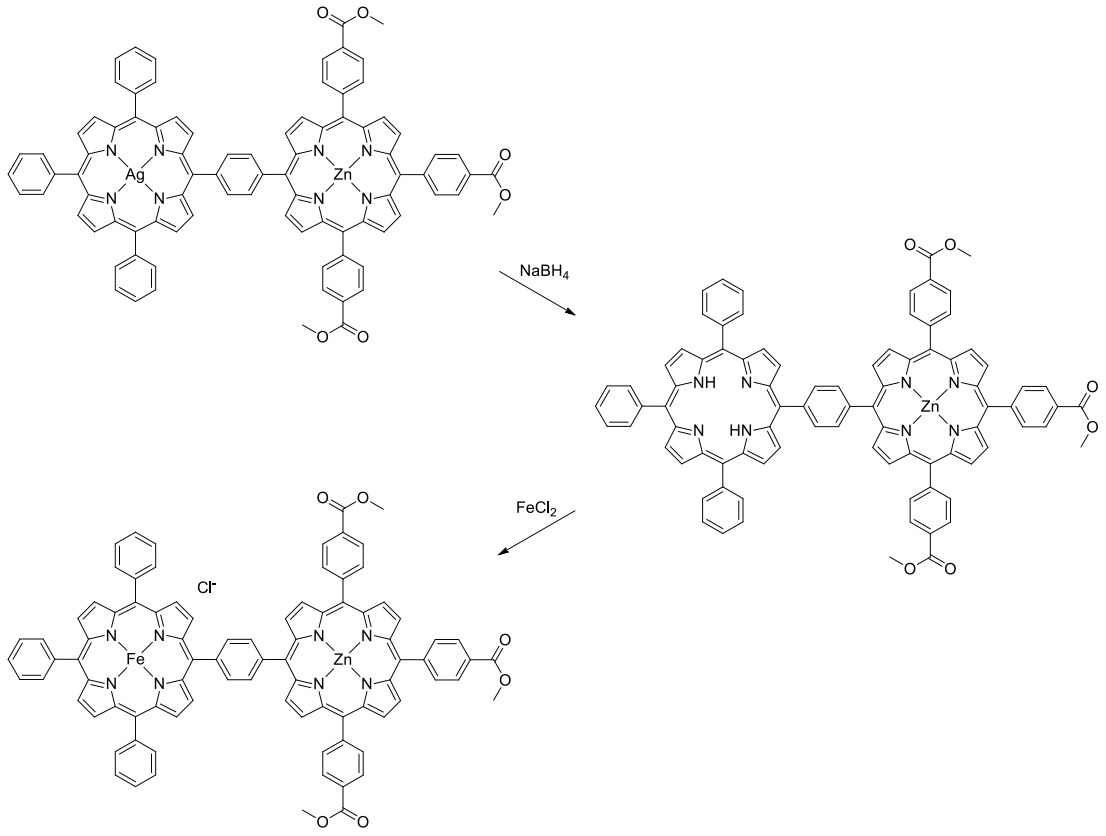

Figure 114: The proposed pathway to obtain ZnFe dyads *via* mixed metalation

Combined zinc and silver metalation

In order to investigate the separation of a mixed metal dyad, a solution of the dyad **4.11** was treated with one equivalent of zinc acetate and one equivalent of silver trifluoroacetate to provide a mixture of the four possible metalation states (Figure 115). MALDI MS confirmed that each metalation state was present in the mixture, with ions of m/z 1453, 1495 and 1538 being detected. These were assigned to the MH^+ ions of the ZnZn, ZnAg and AgAg metalation states respectively.

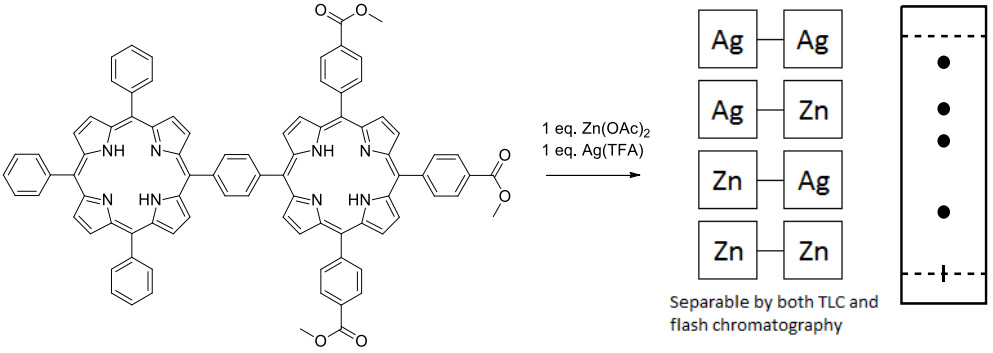

Figure 115: Dual-metal metalation to produce a mixture of metalation states with increased differences in retention properties facilitate chromatographic separation

TLC analysis indicated that the metalation states were all separable from one another and that separability was improved compared to partial metalation with either metal alone. The mixture was submitted to flash chromatography using DCM to elute. The fractions were analysed by TLC, which indicated that the AgAg product and the first AgZn product (AgZn-A) had eluted mixed together. These compounds did however elute separate from the second AgZn product (**AgZn-B**) and the ZnZn product, which were also mixed with one another. MALDI MS analysis confirmed the TLC result.

A second round of flash chromatography resulted in good separation of the AgAg and **AgZn-A** products. Because of the stronger retention of the **AgZn-B** and ZnZn products, further purification was attempted using 3% ethyl acetate in DCM. Separation was incomplete but pure fractions of each compound were obtained.

^{1}H NMR spectroscopy was used to identify and characterise the two AgZn dyads (Figure 116). The aromatic region of each dyad contained some broad and some sharp peaks. Since the ^{1}H NMR spectrum of the ZnZn dyad **4.15** contained only sharp peaks, and the spectrum of the Ag porphyrin monoaldehyde **6.01** had broad peaks (because of its paramagnetism),[28] the

broad peaks were attributed to the H nuclei of the half of the dyad with silver bound inside. This gave sufficient information to determine the arrangement of the metal ions in the dyad.

The spectra of the two dyads and the assignments of some of the peaks are shown in Figure 116. The signal from the *meta* and *para* H nuclei of the unsubstituted phenyl substituents was sharp for **AgZn-A** (peak a), indicating that the zinc ion was in the non-ester ring and the silver ion was in the ester ring. For **AgZn-B**, there was only a broad peak in this position, indicating the opposite metal arrangement.

This is consistent with the appearance of the two doublets (b and c) with integrations of 2H and 4H respectively (relative to the 9H of peak a), which may be assigned to the *ortho* H nuclei of the phenyl substituents of the zinc-metalated half of **AgZn-A**. The peaks i and j in the spectrum of **AgZn-B** are the analogous *ortho* peaks of the ester-bearing benzene rings. The *meta* peaks of these rings appear as two overlapping doublets (k and l). In the spectra of both compounds, the H nuclei of the linking benzene ring appear as two overlapping doublets, peaks e and m.

The broad peaks (d, f, g, h, n and o) are attributable to the H nuclei of the silver-metalated half of the molecule, but not enough information was available to make specific assignments. It is noteworthy that no sharp β-pyrrolic signals are visible for either compound, and the cause of this effect is unclear.

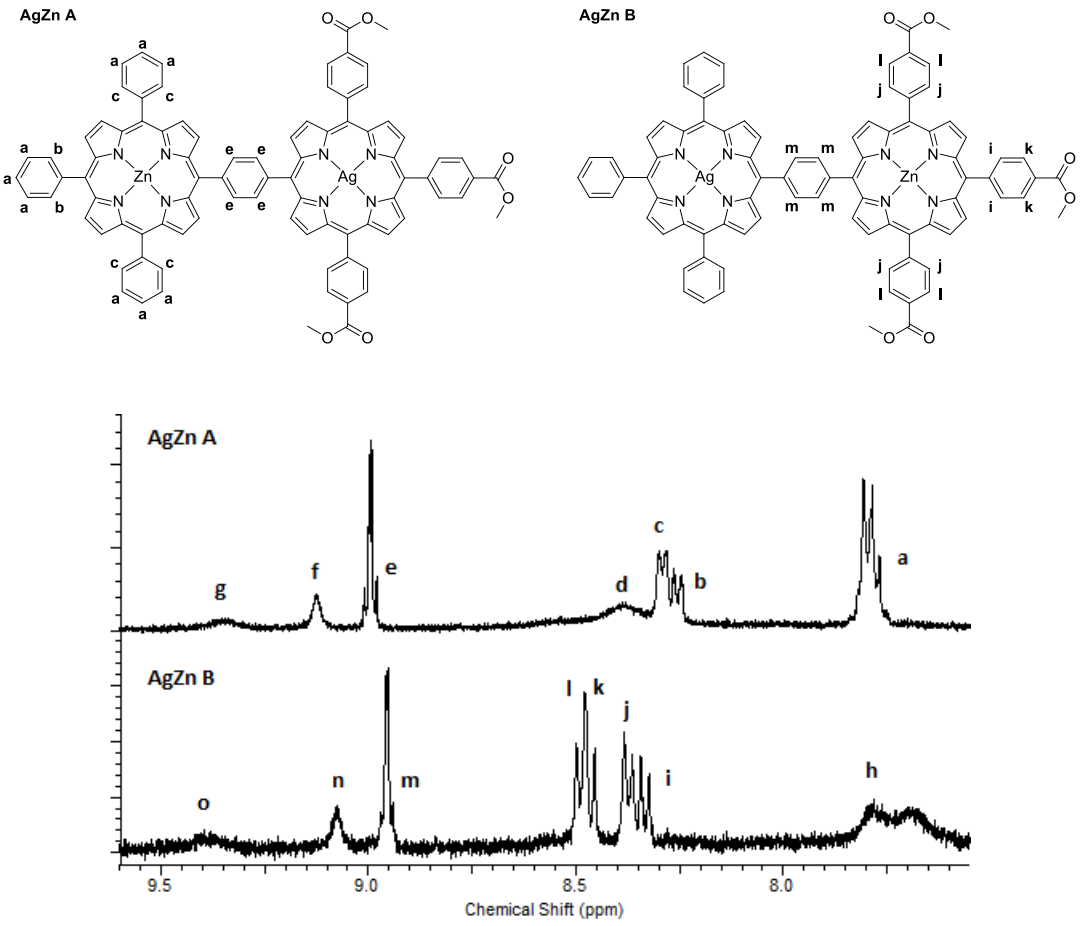

Figure 116: The aromatic region of the ^{1}H NMR spectra of the two AgZn dyads with peak assignments

Silver removal from AgZn dyads

Treatment of the dyad **AgZn-A** with the conditions described in 6.1.1 resulted in incomplete demetalation as determined by MALDI MS. Additional portions of *N*,*N*-diethylhydroxylamine were added however, and after 20 hours MALDI MS indicated that the reaction was complete; no ions for dyads metalated with silver were detected. There was however an ion detected at m/z 1325, the mass of the MH^+ ion of the 2H2H dyad. The mixture was purified *via* flash chromatography and fractions containing only 2HZn dyad were identified by TLC and MALDI MS.

Similarly, treatment of **AgZn-B** with the same conditions required extra portions of *N*,*N*-diethylhydroxylamine to effect complete silver removal. After 20 hours MALDI MS detected no ions of silver metalated dyads, only those of a 2HZn dyad.

Singular demetalation was evident by ^{1}H NMR spectroscopy because of the appearance of a single NH peak at -2.60 ppm for **2HZn-A** and at -2.61 ppm for **2HZn-B** (Figure 117). There were two singlets for the ester CH_3 groups of both compounds at 4.2 ppm. The aromatic region of the spectra is shown in Figure 117, and by using the spectra of the AgZn starting materials as a guide, it was possible to directly assign all of the signals for the benzene ring H nuclei.

A multiplet between 7.7 and 7.9 ppm (peaks a and m) was typical of the *meta* and *para* nuclei of the unsubstituted *meso* phenyl substituents of each compound. Two doublets at 8.29 and 8.33 ppm (peaks b and c, n and o) with integrations of 2H and 4H respectively were assigned to the *ortho* H nuclei of the same rings for both compounds. These signals had been present in the spectrum of the **AgZn-A** starting material but not in that of **AgZn-B**. Another two doublets at 8.37 and 8.41 ppm (peaks d and e, p and q) were assigned to the *ortho* nuclei of the ester-bearing benzene rings. These signals had been present in the spectrum of **AgZn-B** but not that of **AgZn-A**. Two overlapping doublets at 8.5 ppm of integration 2H and 4H respectively were assigned to the *meta* H nuclei of the ester-bearing rings. These signals also had been present for **AgZn-B** but not **AgZn-A**.

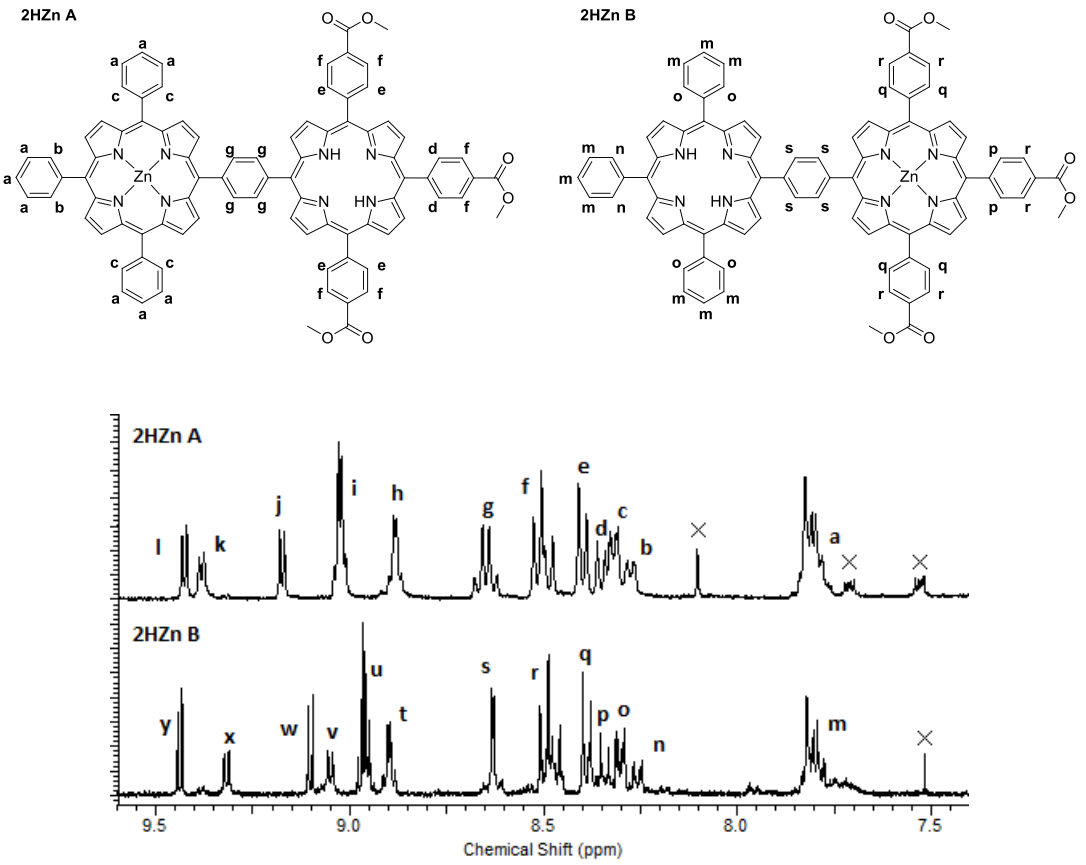

Figure 117: The aromatic region of the ^{1}H NMR spectrum of the two 2HZn compounds with peaks assigned

These silver-removal reactions were conducted on a scale of less than 5 mg, and the product quantities obtained were therefore very small and ^{1}H NMR indicated the presence of significant aliphatic impurities. Because of this fact, no attempt at iron insertion was made. However, the synthetic steps taken up until this point were successful, and future investigations carried out on a larger scale offer the promise of success.

6.2 Manganese tagging to produce phenylene-linked porphyrin triads

The method developed in Chapter 4 was effective in synthesising the phenylene-linked porphyrin triads **4.19** and **4.20**, however it was not possible to isolate them chromatographically.

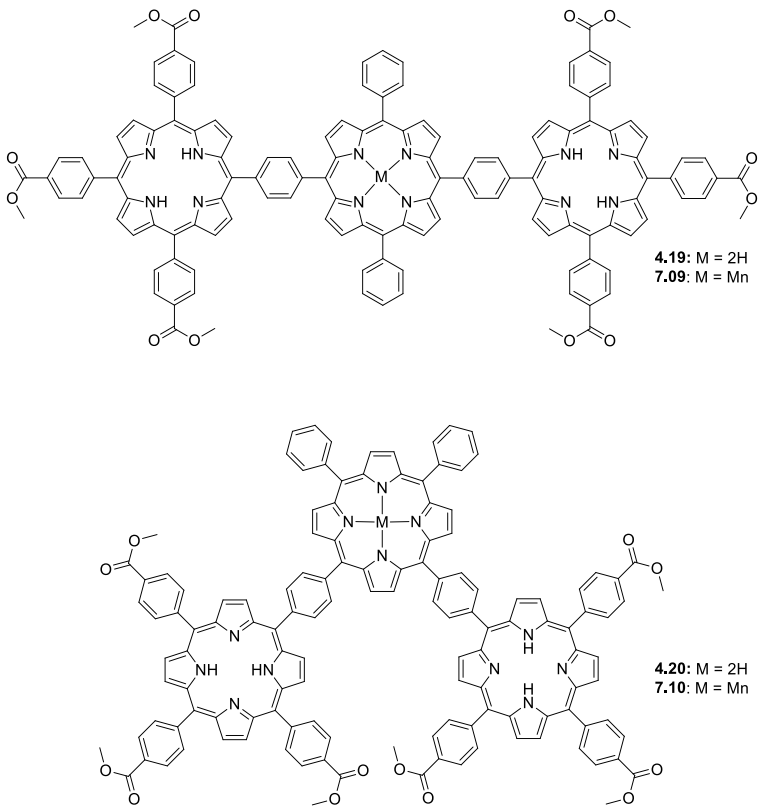

Figure 118: The phenylene-linked triads synthesised, but not isolated, in Chapter 4

Attempts to isolate the phenylene-linked triads synthesised in the previous chapter from the tetraester by-product **2.06** were unsuccessful. It was envisioned that by tagging the porphyrin dialdehyde with a metal prior to the formation of the two new porphyrin rings that the product might be isolable by taking advantage of the added chromatographic retention of the metal ion.

Iron would be an effective tag as its more-stable (III) oxidation produces strong retention on silica which would make it separable from the tetraester by-product. It would be hard to isolate from the black by-product material however and would require demetalation to facilitate this, requiring strong acidic conditions.

Manganese is similar to iron in that it will spontaneously adopt a highly-retained (III) oxidation state when exposed to the oxygen of atmosphere. It is resistant to displacement from the porphyrin core by acid in this state too, and could be expected to remain bound through a porphyrin synthesis reaction. Unlike iron however, its (II) oxidation state is quite acid-labile and can be quickly removed from the porphyrin core with HCl. Manganese porphyrin demetalation *via* reduction and acid displacement is reported in the literature.[156]

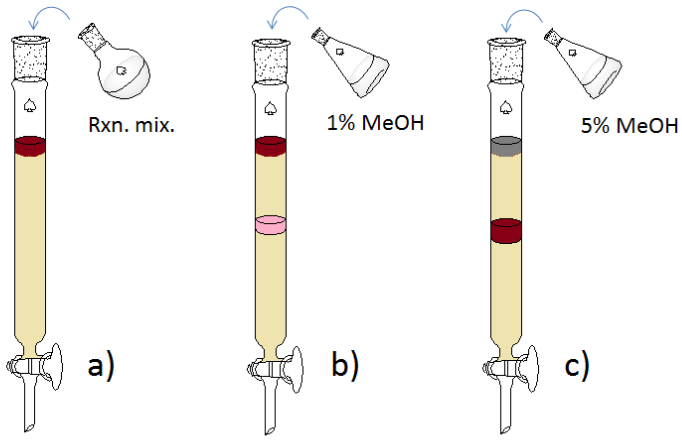

Figure 119: The procedure used to isolate manganese-tagged porphyrins a) the crude reaction mixture containing manganese porphyrins is loaded onto the column b) 1% methanol in DCM is used to elute the porphyrins not tagged with manganese c) 5% methanol elutes the manganese-tagged porphyrins from the column, but also some of the polymeric by-products of the reaction

6.2.1 Mn tagged porphyrin aldehyde

The manganese complex of the *AABB* porphyrin dialdehyde **4.08** was produced to form **6.11** (Figure 120). This was carried out by stirring with $MgCl_2$ in DMF. The product was obtained in a quantitative yield.

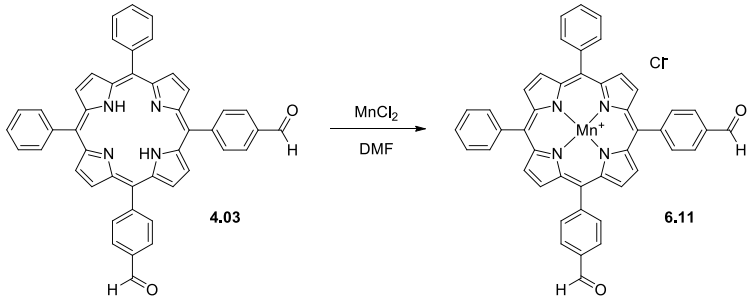

Figure 120: Insertion of manganese into the *AABB* porphyrin dialdehyde

6.2.2 Triad synthesis

The Mn *AABB* aldehyde was condensed with 24 equivalents of 4-formylbenzoic acid methyl ester and 25 equivalents of pyrrole under the same conditions as for the synthesis of the phenylene-linked dyad **4.11** in Chapter 4. The black crude reaction mixture was analysed by MALDI MS and an ion of m/z 2089 was detected and attributed to the $M\text{-}Cl^-$ ion of the Mn triad **6.10**.

The mixture was submitted to flash chromatography, initially using 1% methanol in DCM. As expected, a red band eluted and this was identified as the tetraester by-product by MALDI MS. The solvent mixture was changed to 5% methanol and a lot of dark material eluted. MALDI MS analysis indicated that the triad was present in this fraction.

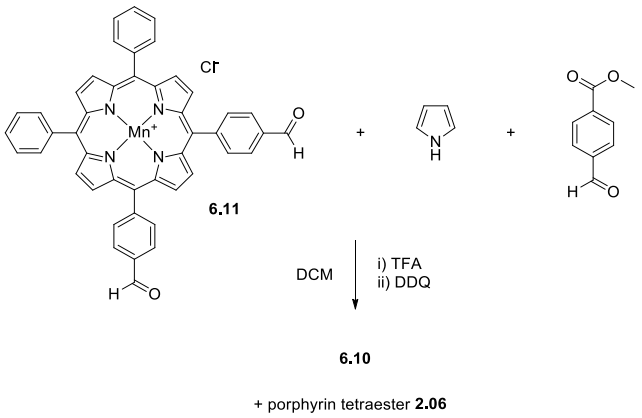

Figure 121: Synthesis of the *AABB* porphyrin triad from the manganese-tagged porphyrin dialdehyde

6.2.3 Manganese removal

The triad-containing fraction was treated with $NaBH_4$ in THF followed by HCl to remove manganese. MALDI MS analysis revealed that the demetalated triad was now present but that some Mn triad remained. The mixture was submitted to flash chromatography and a red band eluted. MALDI MS analysis revealed that, as expected, this was the demetalated triad **4.20**. It was precipitated from methanol to afford an overall yield of 7% (for triad formation and metal removal).

The ^{1}H NMR spectrum with assignments is shown in Figure 122. It shows two NH peaks at -2.52 and -2.68 ppm (peaks a and b), which integrate to 2H and 4H respectively. This was just what was expected from the 2:1 ratio of porphyrin types within the triad. Two superimposed singlets at 4.06 and 4.08 ppm (peak c) had a total integration of 18H and were assigned to the ester CH_3 groups. In the aromatic region, a multiplet between 7.68 and 7.82 (peak d) with an integral of 6H was typical of the *meta* and *para* H nuclei of *meso*-bound phenyl substituents, and was assigned to the 6 such H nuclei in the molecule.

Two superimposed doublets at 8.27 ppm with a total integration of 8H were assigned to the *ortho* H nuclei of the unsubstituted benzene rings and the benzene rings opposite the

linking porphyrin. The assignment was made firstly because this is the usual position of the *ortho* H nuceli of the unsubstituted phenyl substituents, and secondly because the *ortho* substituents of the rings opposite the linking porphyrin are the only H nuclei in the molecule that should form a 4H doublet, with the exception of the *meta* substituents on the same ring which were expected to appear further downfield because of the adjacent ester groups. A doublet at 8.33 ppm (peak f), with an integration of 8H, was assigned to the *ortho* substituents of the four other ester-bearing benzene rings. From experience with ester-bearing single porphyrins and with the ester-bearing phenylene-linked dyad, it was known that the *ortho* H nuclei of an ester-bearing benzene ring will appear further upfield than the *meta* H nuclei. The integration of the peak was also correct for these nuclei. A doublet at 8.41 ppm (peak g) was assigned to the *meta* substituents of the ester-bearing benzene rings opposite the linking porphyrin. Of the unassigned *meta* H nuceli within the molecule, these were expected to appear the furthest upfield because of their separation from the linking porphyrin ring. The integration of the peak, 4H, was also as-expected for these nuclei. A doublet at 8.44 ppm (peak h), with an integration of 8H, was assigned to the *meta* H nuclei of the four ester-bearing rings *syn* to the linking porphyrin. Of the ester-bearing benzene ring H nuclei, these were expected to appear the furthest downfield because of their proximity to the ring current of all three porphyrin rings. The integration was also as-expected for the peak from these H nuclei. Two doublets at 8.61 and 8.66 ppm (peak i), with an integration of 4H each, were assigned to the H nuclei of the linking benzene rings. The position and appearance of these peaks was typical for such phenylene linkages and the integration was as-expected. Two overlapping doublets at 8.79 and 8.81 ppm (peak j), with a total integration of 8H and with J = 4.76 Hz were assigned to the β-pyrrolic H nuclei furthest from the linking porphyrin. Being the most removed from the ring current of the linking porphyrin meant that these nuclei should appear furthest upfield of the β-pyrrolic H nuclei.

A singlet at 8.89 ppm (peak k) with an integration of 2H was assigned to the two β-pyrrolic H nuclei of the linking porphyrin furthest from the ester-bearing porphyrins. These two H nuclei are equivalent and therefore not split by coupling. A singlet at 9.44 ppm (peak p), also integrating to 2H, was assigned to the opposite pair of H nuclei for the same reason. Two doublets at 9.02 and 9.28 ppm (peaks m and n), each integrating to 2H, were assigned to the remaining β-pyrrolic H nuclei of the linking porphyrin ring. The assignment was made based on the symmetry of the molecule: the linking porphyrin is the only one expected to produce β-pyrrolic peaks with integrations of 2H.

This left only the two sets of β-pyrrolic H nuclei of the ester porphyrin rings closest to the linking ring unaccounted for. These were expected to appear as two doublets coupled to one another. There was one apparent doublet at 8.95 ppm (peak l) which integrated to 4H and could account for one set of H nuclei, but there was no other doublet for the other set of peaks. Instead there was only a broad singlet at 9.30 ppm (peak o). This peak had the correct integration value of 4H.

This lead to the conclusion that the double peak at 8.95 ppm was not a doublet at all, but was in fact two singlets. These were assigned to the β-pyrrolic H nuclei as labelled in Figure 122, but these nuclei would only be non-equivalent (and therefore appear as two singlets) if they are in different environments due to the adoption of a stable conformation about the phenylene linker. The broadness of peak o can be similarly explained.

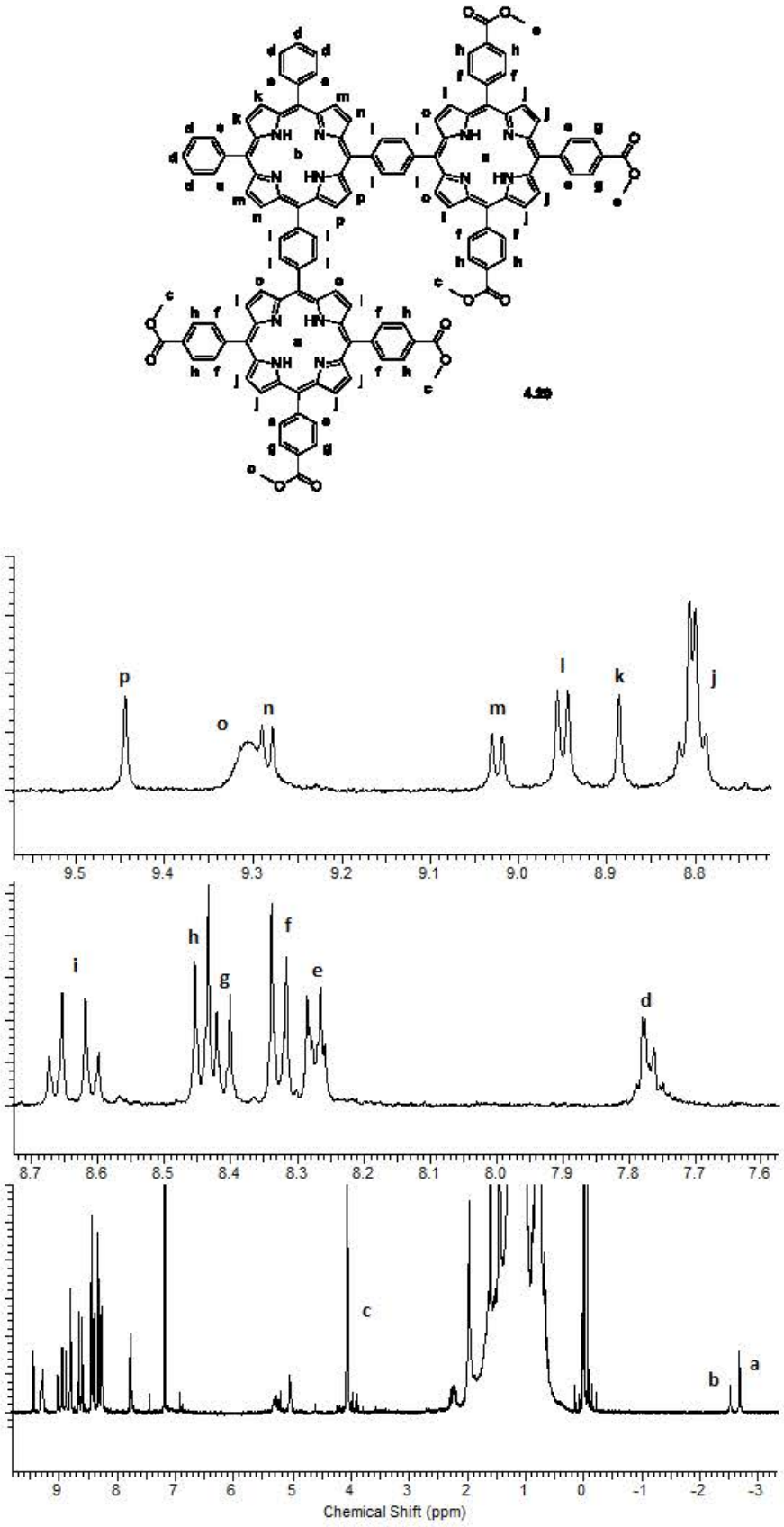

Figure 122: The ^{1}H NMR spectrum of the phenylene-linked *AABB* triad 4.20 with assigned peaks

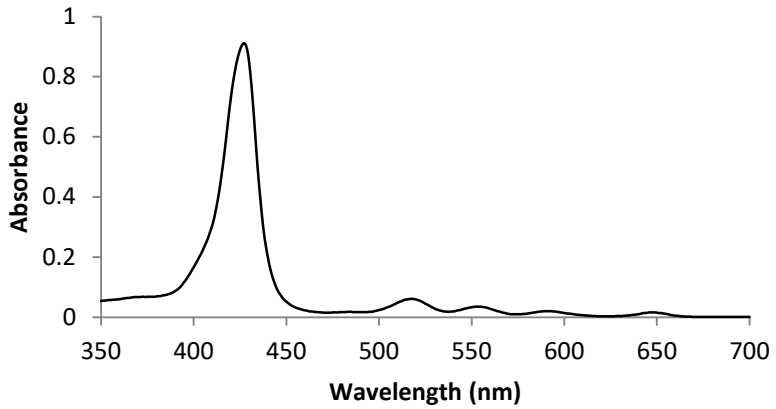

Figure 123: The UV-vis absorption spectrum of the triad

The UV-vis absorption spectrum displayed four Q bands, at 647, 592, 554 and 518 nm. There was a B band with a single maximum at 428 nm. This contrasted with the split B peaks of both phenylene-linked dyads **4.11** and **4.13**.

No further synthetic steps were carried out with this compound because of the small quantity obtained. Although this procedure is effective in producing this triad, it is quite low yielding and the process should be repeated on a larger scale to produce a useful quantity of the triad product.

6.3 Silver redox tagging chromatography

The potential for silver redox tagging was serendipitously identified when a sample of AgTTPP was analysed by TLC. It was expected to be only weakly retained on the silica when DCM was applied as eluent, but in fact it was observed to remain on the baseline of the plate. It was discovered that treating the material with triethylamine changed its colour from bright orange to the usual porphyrin red and that it now displayed a very high rf on TLC in DCM.

It has been reported that porphyrin-bound silver ions can be oxidised to the (III) oxidation state, and this was proposed as an explanation of the observed chromatographic behaviour.[28] This behaviour offered the possibility of achieving control over chromatographic retention, which could be used to selectively isolate porphyrin compounds tagged with a silver ion if the silver ion could be oxidised and reduced at will. The silver removal conditions previously developed in Section 6.1.1 could then be used to completely remove the silver tag. If this process could be developed it could be applied to any reaction of porphyrins to facilitate the isolation of products. In particular, it could be applied to the isolation of the porphyrin arrays with vinyl linkages formed *via* Wittig reactions described in Chapter 5. In that work, a dyad was isolated but it was not possible to isolate either of the triads from the by products of the reaction, a problem that silver tagging could potentially solve.

6.3.1 Development of oxidation conditions

In order to identify conditions suitable for the selective isolation of silver tagged porphyrins, experiments were conducted using silver TEPP **6.06**. Various oxidants were trialled with samples of AgTEPP dissolved in THF. Treatment with atmospheric oxygen, hydrogen peroxide and benzoyl peroxide did not produce baseline material when the mixture was analysed by TLC. A sample treated with 4.4 mM DDQ however displayed significant baseline material immediately following the treatment.

The process was then applied to flash chromatography. A column was packed with silica in the usual manner except that the top few centimeters were treated with a 4.4 mM soliution of DDQ in DCM. Elution commenced using 0.4 mM DDQ solution in DCM. No porphyrin moved through the column despite extensive elution. The eluent was then changed to 2% NEt_3 in DCM and a porphyrin band eluted from the column (Figure 124). MALDI MS analysis detected an ion of m/z 832, the mass of the MH^+ ion of AgTEPP.

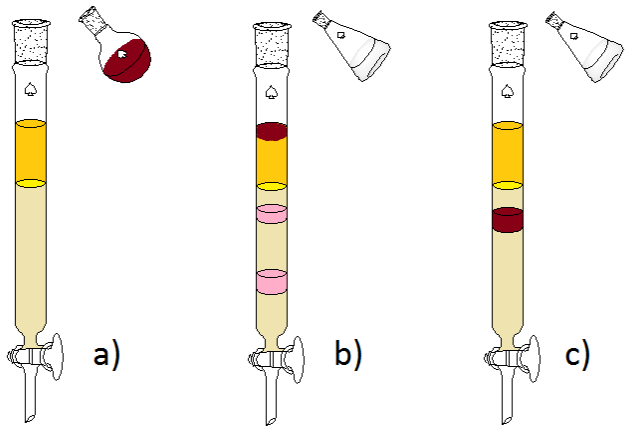

Figure 124: The procedure used to isolate silver-tagged porphyrin compounds a) the crude reaction mixture is treated with DDQ and loaded onto the column whose upper portion has also been treated with DDQ b) non-tagged compounds are eluted from the silica c) eluent containing triethylamine is added to the column and the silver-tagged porphyrins are eluted

The process was then tested in the separation of AgTEPP **6.06** and ZnTPP **2.07**, compounds which, because of their minimal retention on silica, would normally be difficult to separate chromatographically. A column was prepared with the top 10 cm being packed using a 0.6 mM solution of DDQ in DCM. A mixture of 3.6 mg AgTEPP **6.06** and 1.2 mg ZnTPP **2.07** was treated with 4.4 mM DDQ solution in DCM and allowed to react at room temperature for one minute before being loaded onto the column. Elution commenced using 0.6 mM DDQ solution and a pink band was eluted and collected. TLC analysis and MALDI MS analysis indicated that this was ZnTPP **2.07**, uncontaminated with AgTEPP **6.06**.

The eluent was then changed to 2% triethylamine in DCM. A red band eluted, and TLC and MALDI MS analysis indicated that this was AgTEPP **6.06** uncontaminated with ZnTPP **2.07**. The separation had been highly effective and the technique appeared to be promising for the isolation of otherwise difficult-to-isolate porphyrin arrays.

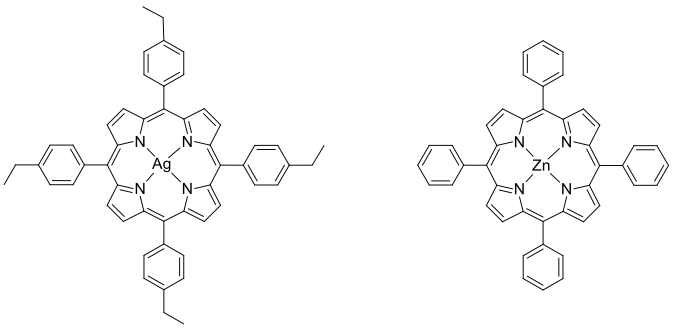

Figure 125: The silver redox-tagging method enabled the separation of the two compounds AgTEPP 6.06 and ZnTPP 2.07, which would normally be very difficult to separate chromatographically

6.3.2 Application in the isolation of Wittig-linked arrays

In order to test the applicability of the process to Wittig linked arrays, first a silver tagged dyad was produced. A Wittig coupling of the silver-tagged porphyrin monoaldehyde **6.01** with the porphyrin phosphonium salt **5.01** was carried out (Figure 126) according to the same procedure used in Chapter 5 to produce the free base compound. MALDI MS analysis of the crude reaction mixture revealed the presence of the intended Ag2H dyad **6.12**, but also the 2H2H dyad. This meant that the reaction conditions had removed silver from the porphyrin core.

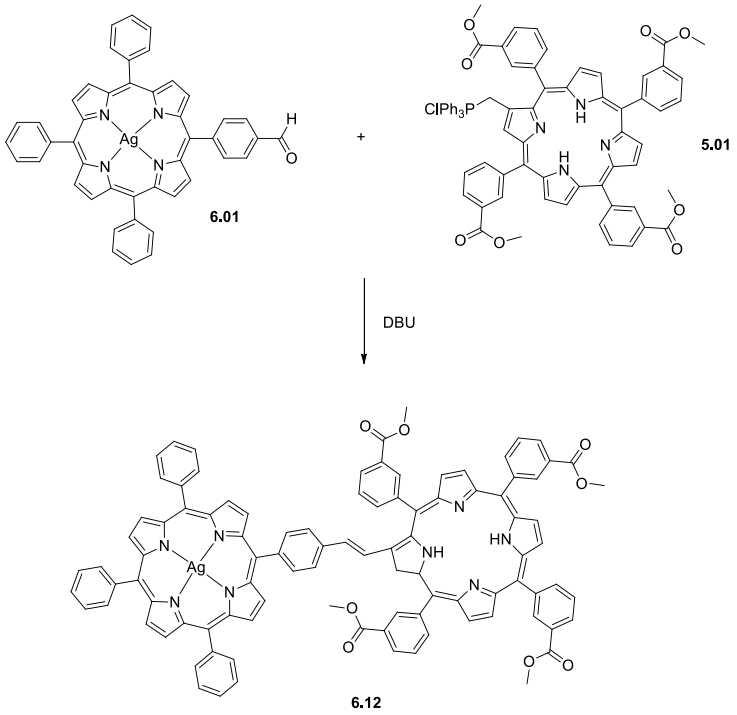

Figure 126: The silver tagged vinyl-linked dyad 6.12 was produced in order to test the applicability of the silver tagging method to the isolation of porphyrin arrays of this type

The crude reaction mixture was submitted to the DDQ oxidation flash chromatography procedure described in the previous section. Non-tagged compounds were eluted from the column before the eluent was changed to 1% triethylamine in DCM. A porphyrin band then eluted. MALDI MS analysis of this band revealed that it was a mixture of the Ag2H and 2H2H dyad compounds, also containing some 2HCu dyad. The purification procedure was repeated, and MALDI MS analysis of the product indicated that it contained only Ag2H dyad. ^{1}H NMR analysis of the product however revealed two NH peaks, showing that in fact two types of free base porphyrin were present. This indicated that while the process is promising, that the conditions tended to remove silver from the tagged compounds and the tagging chromatography was not completely effective. Futher work may improve this technique and transform it into a useful synthetic tool.

6.4 Chapter conclusion

Three different methods of using metal ions to facilitate the chemistry of porphyrin arrays were developed. Mixed metalation and silver protection allowed the isolation of required metalation states of the phenylene-linked dyad **4.11**. Manganese tagging was used to isolate the *ABAB* phenylene linked triad, a process which has not previously been reported. Silver redox tagging chromatography was developed and used successfully in the separation of single porphyrins, and remains promising for facilitating the isolation of porphyrin arrays, subject to further development.

Chapter 7: Maquette binding of amphiphilic porphyrins and porphyrin arrays

7.1 Introduction

The porphyrins and porphyrin arrays synthesised in the preceding chapters were designed to possess a range of hydrophilic and hydrophobic properties in order to explore their effects on the binding to protein maquettes. Binding light-absorbing cofactors to protein maquettes is an important step toward building molecular devices to produce fuel and high-energy materials directly using the power of sunlight. In this chapter, the creation of porphyrin maquette complexes will be investigated, and the characteristics of the binding interactions probed in a preliminary study. Binding experiments with protein maquettes have in the past used almost exclusively natural porphyrins and derivatives thereof, *e.g.* by Rabanal *et al.*[19] This work represents one of the first attempts to bind synthetic porphyrins.

The maquettes were kindly supplied by the group of Professor P. Leslie Dutton at the University of Pennsylvania as part of an ongoing collaboration. Two different maquettes were used in the experiments, one for binding zinc porphyrins and another for iron porphyrins. The sequences of the two maquettes are shown in Figure 127.

A zinc porphyrin is typically pentacoordinate, and so will only accept ligation at one face at a time to form a square pyramidal compex, while a hexacoordinate iron porphyrin will accept simultaneous axial ligation from both faces, forming an octahedral compex. For zinc porphyrins, the maquette BT H7H112 was used. It has histidine residues in positions 7 and 112

in the sequence (hence the name) and these are designed to sit in such a way as to accept two porphyrin cofactors, one at each end of the maquette block. For iron porphyrins, the maquette BT bis his was used, which is the same as BT H7H112, only with two alanine residues replaced with histidine to create two binding sites, each with a pair of histidine residues to ligate iron porphyrin cofactors.

BT H7H112

α helices	Loop regions
N - G E I W K Q H E D A L Q K F E E A L N Q F E D L K Q L	G G S G S G S G G
E I W K Q A E D A L Q K F E E A L N Q F E D L K Q L	G G S G S G S G G
E I W K Q A E D A L Q K F E E A L N Q F E D L K Q L	G G S G S G S G G
E I W K Q H E D A L Q K F E E A L N Q F E D L K Q L - C	

BT bis his

α helices	Loop regions
N - G E I W K Q H E D A L Q K F E E A L N Q F E D L K Q L	G G S G S G S G G
E I W K Q H E D A L Q K F E E A L N Q F E D L K Q L	G G S G S G S G G
E I W K Q H E D A L Q K F E E A L N Q F E D L K Q L	G G S G S G S G G
E I W K Q H E D A L Q K F E E A L N Q F E D L K Q L - C	

Figure 127: The structure and amino acid sequence of the maquettes BT H7H112 and BT bis his used in the porphyrin binding experiments. Histidine is marked in red

7.2 Formation of porphyrin-maquette complexes

To ensure the integrity of the maquette structure, binding of a porphyrin needs to take place in a pH-buffered aqueous solution, a less than ideal medium for porphyrin solubility. The porphyrins to be tested were therefore dissolved in DMSO in order to suppress aggregation. This solution was then added to the maquette or buffer solution according to the experiment being performed. A solution of pH 9, buffered with *N*-cyclohexyl-2-aminoethanesulfonic acid (CHES) was used, with KCl added to increase ionic strength. The maquette solution consisted of the same buffer solution containing 1 μM maquette, with its concentration measured by the absorbance at 280 nm using the known extinction coefficient of the maquette of 22400 L mol^{-1} cm^{-1}.[157]

Characterisation of porphyrin binding was carried out using UV-vis absorption spectroscopy. Zinc porphyrins generally display their B peak maximum at around 420 nm in aqueous solution in the absence of any ligand. When they are ligated to histidine however, the peak shifts toward longer wavelengths by around 10 nm,[28] and this was the main method of assessing whether a porphyrin bound to a maquette or not. The binding process takes some time to reach equilibrium. By recording the spectrum at regular intervals, one can observe how it changes over time and at what point it reaches equilibrium *i.e.* when the spectrum is stable.

7.2.1 Binding strength: K_d measurement

The strength of binding can be expressed by the dissociation constant K_d, which is the equilibrium constant of the binding reaction. The binding equilibrium is illustrated in Figure 128. The two reactants are the unbound maquette (M_u) and the unbound porphyrin (P_u), while the product (P_b) is the complex of the two species.

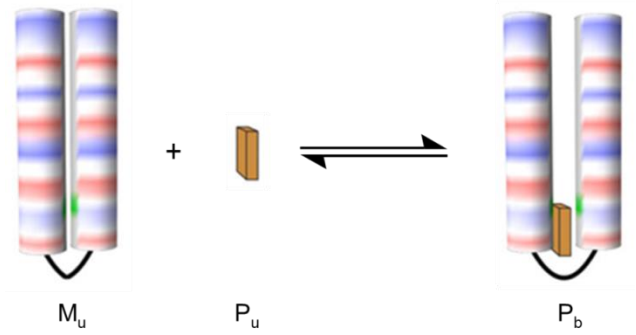

$$K_d = \frac{[M_u][P_u]}{[P_b]}$$

Figure 128: An illustration of the porphyrin maquette binding equilibrium reaction, which can be described by the dissociation constant K_d defined by the equation as shown

The K_d value of the equilibrium can be determined spectroscopically by utilising the fact that axial ligation of a porphyrin-bound metal ion with the histidine residues of the maquette results in a significant change to the porphyrin spectrum.

Experimentally, this measurement is performed using a titration. A solution of the maquette is put into a cuvette, and portions of porphyrin solution are added and the UV-vis absorption spectrum recorded after each addition (Figure 129). The porphyrin is practically all bound initially, as there is a large excess of maquette present. This is apparent as the spectrum of the bound porphyrin grows in intensity in direct proportion to the amount of porphyrin added. However, as more porphyrin is added, and its concentration approaches that of the maquette binding site, the effect of the equilibrium means that some of the porphyrin is now unbound, and this is evident by the appearance of a new B band absorption maximum at a wavelength 10 nm less than that which was observed previously.

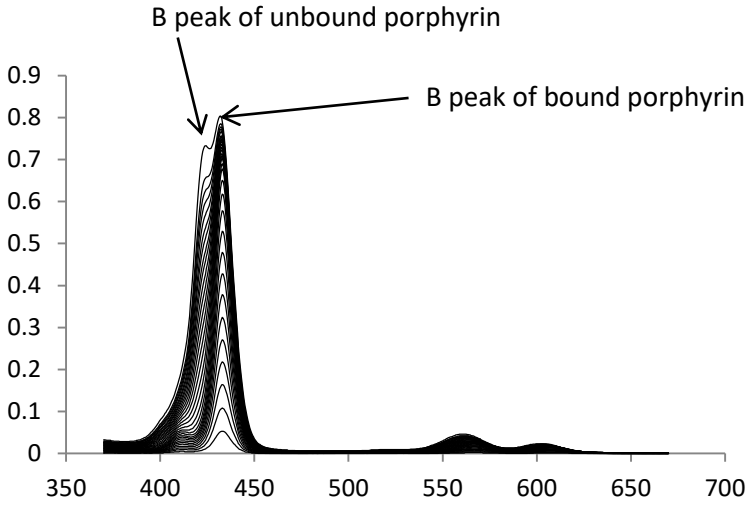

Figure 129: UV-visible spectra collected during a typical titration to measure the K_d of a porphyrin maquette binding interaction. This data is from the Zn phenylporphyrin *AABB* diacid 2.19 (*vide infra*)

When the absorbance A_t (total absorbance that includes any contribution from the unbound porphyrin) at the wavelength of the absorbance maximum of the B band of the bound porphyrin is plotted against the total porphyrin concentration [P_t], the curve generated has two linear regions connected by a curved region (Figure 130). The first linear region represents that part of the experiment when the maquette is in excess over the porphyrin and practically all of the porphyrin is bound. The curved region is the part where the equilibrium effect becomes significant and not all of the porphyrin is in the bound state. The second linear region is where the porphyrin is in excess over the maquette and the addition of more porphyrin to the mixture does not produce a significant increase in the amount of porphyrin in the bound state. All further additions of porphyrin then go into solution in the unbound state.

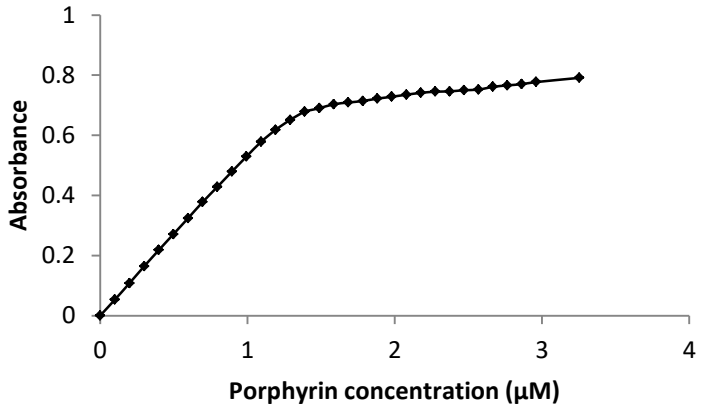

Figure 130: A typical plot of the absorbance A_t *vs* total porphyrin concentration [P_t] (the data from the Zn *AABB* phenylporphyrin diacid 2.19 shown in Figure 129) from which the K_d of the binding interaction can be determined

If it is assumed that there are indeed only two porphyrin states in the system, bound and unbound, then Equation 1 may be derived. By using an algorithm and the computer program Fityk,[158] the values of E_b, E_u and K_d are iteratively adjusted so as to produce the best fit to the experimental data. E_b is determined from the slope of the first linear region, E_u from the slope

of the second linear region and K_d from the sharpness of the "kink" connecting the two linear regions. For the sake of simplicity, an arbitrary K_d value of 100 nM was set as the threshold at which a porphyrin can be said to bind strongly to the maquette.

$$\frac{A_t}{l} = (E_b - E_u)\frac{[M_t]+[P_t]+K_d-\sqrt{([M_t]+[P_t]+K_d)^2-4[P_t][M_t]}}{2} + E_u[P_t]$$

A_t = total absorbance
l = path length
E_b = extinction coefficient of bound porphyrin
E_u = extinction coefficient of unbound porphyrin
$[M_t]$ = total concentration of maquette binding sites
$[P_t]$ = total concentration of porphyrin
K_d = dissociation constant

Equation 1: The equation that can be used to find the Kd value of the binding interaction based on the assumption of the two porphyrin states, bound and unbound

If the time required to reach equilibrium is too long, then titration becomes impractical. In such cases its necessary to use a parallel equilibration method. Several equal portions of maquette solution are taken, and a range of quantities of porphyrin solution are added to them. They are then left for a pre-determined period to allow the binding to reach equilibrium before their spectra are recorded, and the data is analysed in the same way as for a titration experiment.

To fully describe the maquette binding, the rate of binding *i.e.* how long it takes to come to equilibrium, must be considered in addition to the K_d. Given limited time, this work is a preliminary investigation into both of these properties, and is limited in scope. More extensive investigations were performed by fellow PhD student Chris Hobbs and will be reported in his thesis.

7.3 Maquette-binding of amphiphilic zinc porphyrins

7.3.1 Zinc phenylporphyrin benzoic acids 2.07, 2.17 – 2.21

The phenylporphyrin benzoic acids synthesised in Chapter 2, Section 1.4 (Figure 131) were the first compounds investigated for maquette binding. This included the two extremes in hydrophobicity and hydrophilicity, and compounds with a range of amphiphilic properties in-between.

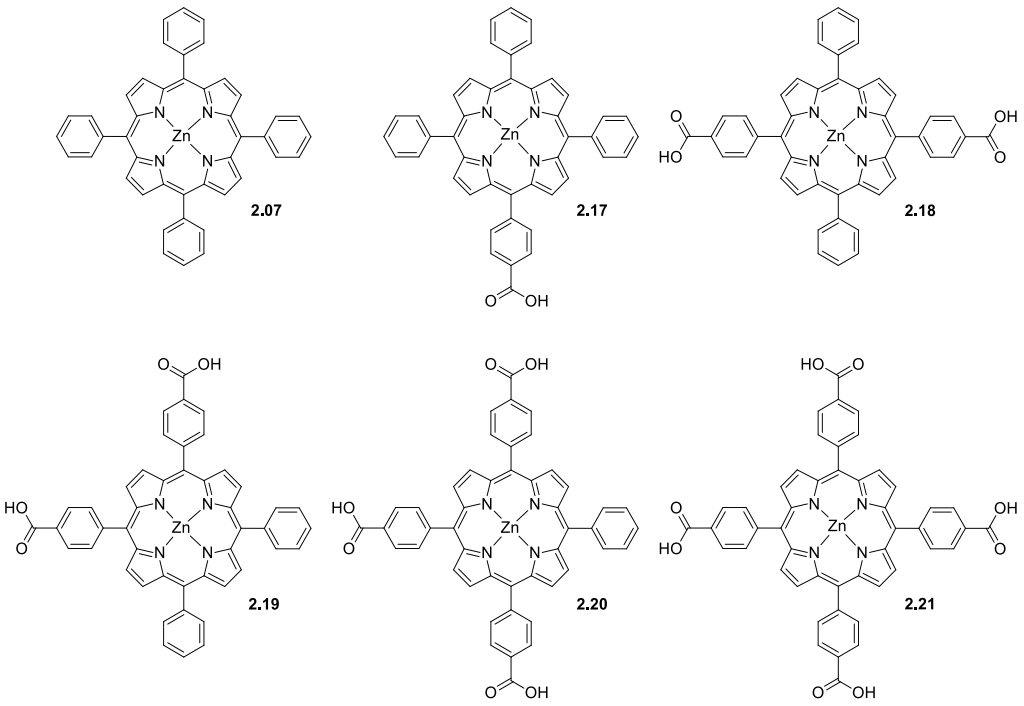

Figure 131: The zinc phenylporphyrin benzoic acid series that was tested for maquette binding

Zinc tetraphenylporphyrin 2.07

Zinc tetraphenylporphyrin (ZnTPP) **2.07** was not soluble in DMSO, and so was instead dissolved in isopropanol. This substitution of DMSO for isopropanol was not expected to have any major effect on the binding behaviour, because it would be present in such a small proportion (0.5 %) relative to water.

A qualitative binding experiment was initially conducted to test for binding and to measure the equilibration time. When a portion of the ZnTPP **2.07** solution was injected into a solution of buffer to produce a concentration of 0.3 µM, it displayed a broad B band with its peak at 421 nm (Figure 132). It also displayed two broad Q bands at 552 and 596 nm. The spectrum did not change significantly over the course of the 5 minutes for which it was observed.

When the same experiment was performed with a solution of 1.0 µM maquette, the spectrum was similar, with a broad B band with a peak at 420 nm and two Q bands with peaks at 553 and 596 nm. There was a slight shoulder on the red side of the B peak in buffer, which may reflect aggregation which the maquette may supress (Figure 132), however the spectra were very similar and because of the broadness of the B peak, seem to indicate minimal interaction between the maquette and this porphyrin, and rather that the porphyrin aggregates. This was not unexpected because of the fully hydrophobic nature of this porphyrin; it was expected that a degree of hydrophilicity would be required to suppress aggregation for binding to occur.

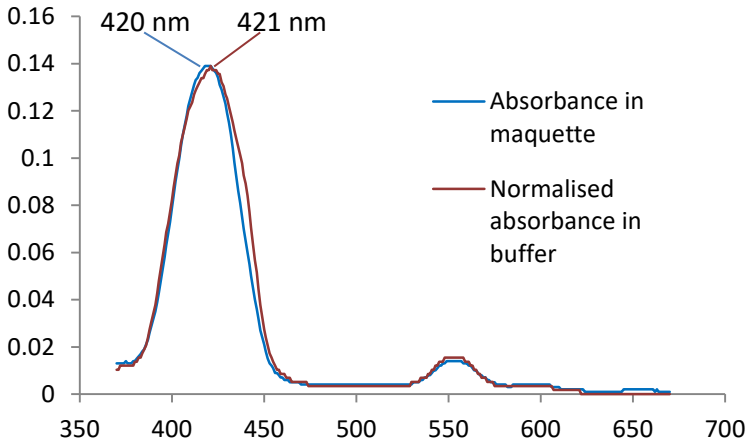

Figure 132: Comparison of the normalised ZnTPP 2.07 (0.3 µM) spectra with and without the maquette (1.0 µM)

Zn phenylporphyrin monoacid 2.17

Zn phenylporphyrin monoacid **2.17** was tested for binding by dissolving it in DMSO and adding it to 1.0 µM maquette and buffer solutions to produce concentrations of 1.0 µM in each case. In buffer, the B peak appeared at 409 nm, with two Q bands at 568 and 609 nm, and this spectrum did not change over the 5 minutes for which it was monitored. The appearance of the B peak in this position was unusual for this series of porphyrins (*vide infra*). In DMSO solution, this porphyrin is most likely in a non-aggregated state and displays its B peak at 428 nm, and in the absence of aggregation one would expect that the peak in aqueous solution would shift 3 nm towards longer wavelengths, to 431 nm. The fact the the peak is at 409 nm is therefore an indication that it is in fact aggregated in the buffer solution.

In the maquette solution, the spectrum initially displayed a B peak at 432 nm and two Q bands at 562 and 603 nm (Figure 133). The sharp B band with its peak at 432 nm is typical of a maquette-bound porphyrin (Figure 129). There was also a shoulder on the side of the B peak at 410 nm, with an extinction coefficient of approximately 10% of that of the B peak. Over time, the peak at 432 nm grew, while the shoulder at 410 nm disappeared. This indicated a transition from an aggregated state into a maquette-bound state.

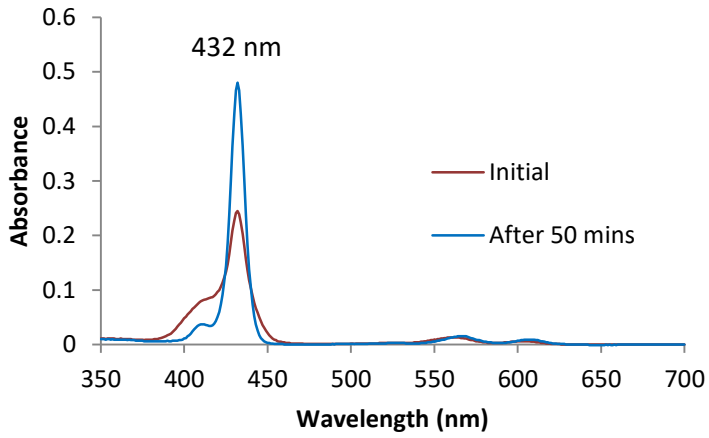

Figure 133: The spectrum immediately after addition of porphyrin 2.17 to the 1.0 µM maquette solution and then again 50 minutes later

To observe the time that the porphyrin takes to reach binding equilibrium, a portion of the porphyrin was added to a 1.0 μM maquette solution, again to produce a porphyrin concentration of 1.0 μM, and the spectrum recorded every 30 seconds. During the course of the 50 minutes over which it was observed, the B peak at 432 nm grew in extinction while the shoulder at 410 became less intense, eventually becoming a distinct peak at 410 nm. The Q bands shifted from 562 and 603 nm to 566 and 606 nm respectively.

The spectral changes likely indicate a transition from an aggregated state with a B band maximum at 410 nm to the maquette-bound state with the maximum at 432 nm. By plotting the absorbance at 432 nm over 50 minutes (Figure 134), one can see that the binding was complete after 20 minutes.

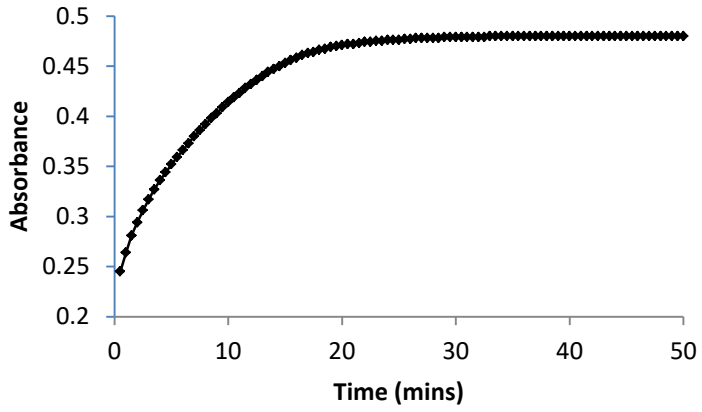

Figure 134: Plot of absorbance at 432 nm over time for the binding of the Zn phenylporphyrin monoacid 2.17

A titration experiment was performed to determine the dissociation constant for the binding interaction. After the addition of each portion of porphyrin the mixture was left for 40 minutes before the spectrum was recorded to ensure complete equilibration. The absorbance at 432 nm was plotted against porphyrin concentration to obtain the curve in Figure 135.

One can see two linear regions which meet one another at a porphyrin concentration of about 0.8 μM. Because the maquette was present in a concentration of 1.0 μM, this indicates that the porphyrin binds to the maquette in a ratio of less than 1:1. This was unexpected because the maquette BT H7H112 posesses two binding sites. The fact that the binding ratio was approximately 1:1 may indicate the the binding of one porphyrin to the maquette distorts its structure so that the second binding site will not accept a porphyrin or binds a porphyrin more weakly. This appears similar to the results of Zeng et. al.[159] who obtained non-integer binding ratios from 0.7 – 0.9 in the binding of a zinc porphyrin to a maquette that contains two binding sites, suggesting the presence of one high affinity binding site. A K_d value for this binding experiment could not be determined with any degree of reliability due to an inadequate number of data points.

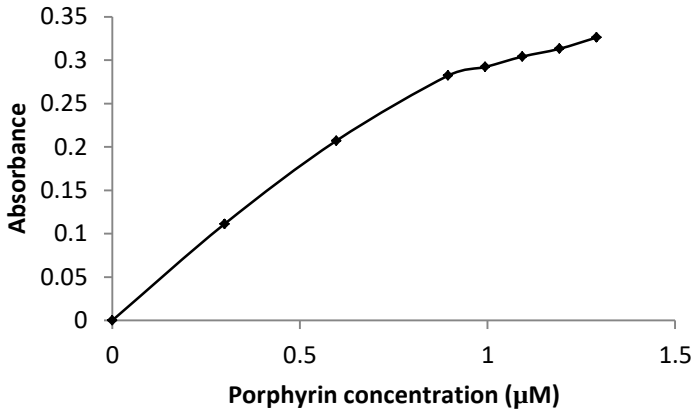

Figure 135: Plot of absorbance at 432 nm against porphyrin concentration for the binding titration of Zn phenylporphyrin monoacid 2.17. The maquette concentration is 1.0 μM

Zn phenylporphyrin ABAB diacid 2.18

To test for binding and to measure the timescale of equilibration, a portion of porphyrin **2.18** was added to a solution of maquette to make concentrations of 1.5 μM for the porphyrin and 1.0 μM for the maquette. This is an excess of maquette if indeed both binding sites can

participate in binding. The absorption spectrum was recorded (Figure 136). The B peak appeared at 432 nm, indicative of binding. There were also two Q bands at 566 and 607 nm. The spectrum was stable after the initial mixing, which showed that the porphyrin reached binding equilibrium before the first spectrum was recorded 30 seconds after the addition of the porphyrin.

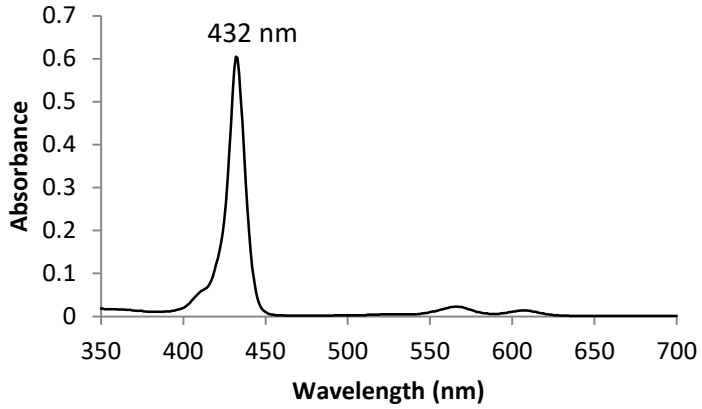

Figure 136: The spectrum of the Zn *ABAB* phenylporphyrin diacid 2.18 in a 1.0 µM maquette solution

A titration was carried out in order to measure the dissociation constant K_d. The mixture was allowed to equilibrate for 15 minutes between additions. At low concentrations the spectrum appeared as it had in the initial qualititative binding test, but at around 1.0 µM of porphyrin (0.5 equivalents per maquette binding site), a shoulder began to appear at 412 nm. When the absorbance at 432 nm was plotted against porphyrin concentration, the curve shown in Figure 137 was obtained. It shows two linear regions linked by a curved region at 0.8 µM porphyrin concentration. As previously discussed for the zinc phenylporphyrin monoacid **2.07**, this suggests that one of the two binding sites has a higher porphyrin affinity than the other.

A curve was fitted to the data based on Equation 1. The K_d of the binding interaction was 60 nM, a strong binding that is better than the arbitrarily-set requirement of 100 nM. The apparent extinction coefficient for the porphyrin was ~560000 L mol^{-1} cm^{-1}, reasonable for a porphyrin of this type and indicating that there had been no large error in measuring porphyrin quantities.

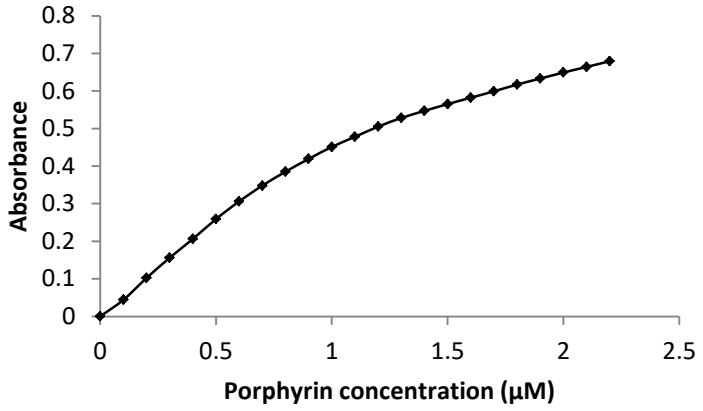

Figure 137: The absorbance at 432 nm plotted against porphyrin 2.18 concentration in a 1.0 µM maquette solution

Zn phenylporphyrin AABB diacid 2.19

A qualitative binding and equilibration experiment was conducted. The spectrum of the porphyrin (1.0 µM) in the 1.0 µM maquette solution is shown in Figure 138. The B peak is at 433 nm and there are two Q bands at 567 and 609 nm. The spectrum was stable for 10 minutes after the initial recording, indicating that this porphyrin reached binding equilibrium in the ~30 seconds between the initial mixing and the recording of the spectrum.

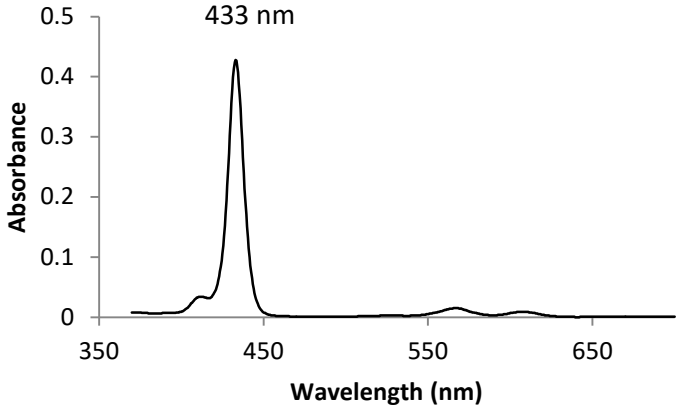

Figure 138: The spectrum of the Zn *AABB* phenylporphyrin diacid 2.19 with 1.0 µM maquette. The B peak is sharp and lies at 433 nm, indicating that the porphyrin is bound to the maquette

A titration was carried out to measure its binding ratio and the K_d of the binding interaction. The absorbance at 433 nm was plotted against porphyrin concentration to obtain the curve shown in Figure 139. It shows two distinct linear regions linked by a curved section. Fitting Equation 1 to the data revealed a K_d of 10 nM. The apparent extinction coefficient was 550000 L mol^{-1} cm^{-1}. The apparent maquette binding site concentration was 1.3 µM, likely indicating that this porphyrin binds only once to the maquette, despite its two binding sites, as discussed previously.

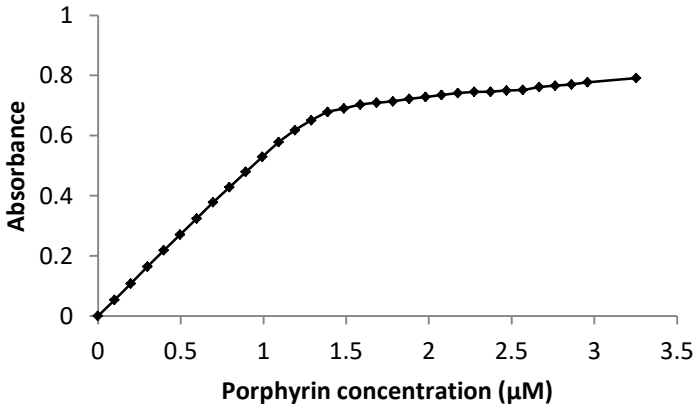

Figure 139: The extinction at 433 nm plotted against the porphyrin 2.19 concentration

Zn phenylporphyrin triacid 2.20

A qualitative test for maquette binding and equilibration time was carried out. The spectrum of the porphyrin triacid **2.27** (1.0 μM) in the maquette solution (1.0 μM) immediately after mixing is shown in Figure 140. The B peak appears at 433 nm and is sharp, indicating that the porphyrin is ligated to the histidine of the maquette. The spectrum was stable after the initial recording, indicating that the porphyrin reached binding equilibrium in less than the ~30 seconds between mixing it with the maquette and recording the spectrum.

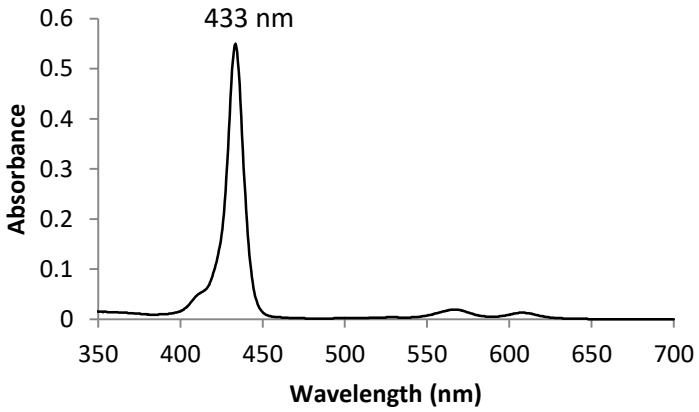

Figure 140: The spectrum of the porphyrin 2.20 (1.0 μM) in a solution of 1.0 μM maquette

A titration was carried out in order to measure the K_d of the binding interaction. The absorbance at the bound porphyrin B peak at 433 nm was plotted against the porphyrin concentration to give the result shown in Figure 141. The data followed the expected behaviour for the most part; there was a linear region and then a transition through a curve to a second region. However, the second region was not linear as expected, and the absorption of the B peak of the porphyrin in the bound state actually decreased in intensity following maquette saturation. This titration was repeated three times, and in each case the "dip" in the B peak intensity was observed after maquette saturation.

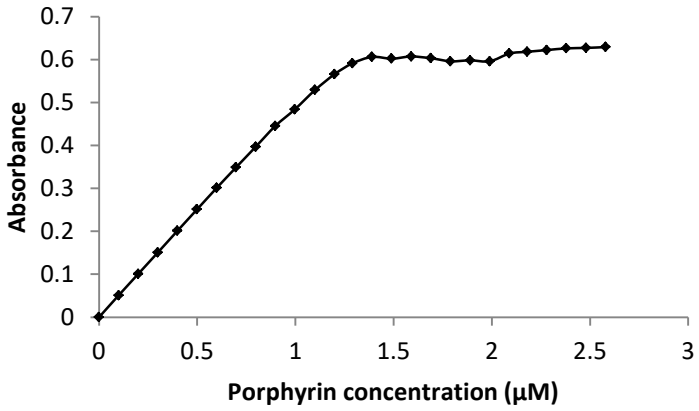

Figure 141: The plot of absorbance at 433 nm vs porphyrin 2.20 concentration in the titration with the maquette (1.0 µM)

The origin of the "dip" might be that non-specific binding of the porphyrin to the maquette, driven by hydrophobic partitioning, warps the structure to weaken the histidine ligation and thus shifts the bound porphyrin B peak towards shorter wavelengths. Because of this dip, no K_d could be calculated from the data. The porphyrin appeared to bind to the maquette in the ratio 1.2:1, which most likely indicates that it binds to the maquette in a 1:1 ratio as discussed previously.

Zn phenylporphyrin tetraacid 2.21

A qualitative test was performed to measure the binding affinity of porphyrin **2.28**. It was mixed into a solution of buffer and a solution of 1.0 µM maquette to produce concentrations of 0.5 µM) and their spectra recorded. The spectra are shown in Figure 142, and it can be seen that they are virtually identical. This was not surprising; because of the hydrophilicity of the acid groups, it would be thermodynamically costly to bury one of these groups in the hydrophobic core of the maquette because of the necessity of breaking interactions between

at least one acid group and water. Therefore this porphyrin does not bind to the maquette at all. The spectrum of the porphyrin in each case didn't change over the 60 minutes that it was observed. The B peak was at 423 nm and there were two Q bands at 558 and 597 nm.

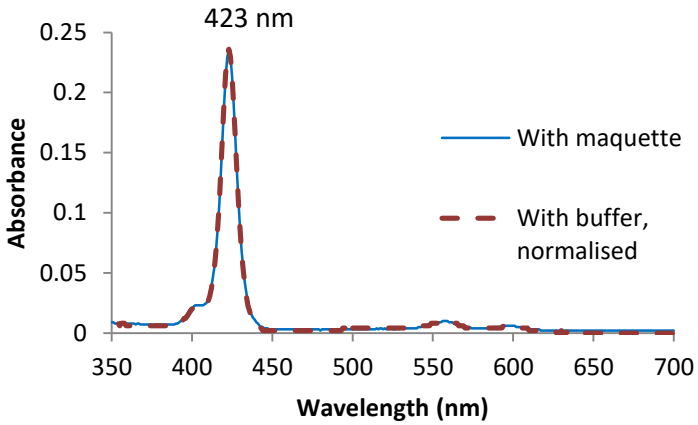

Figure 142: Spectra of the Zn phenylporphyrin tetraacid 2.21 (0.5 µM) immediately after addition to a buffer and 1.0 µM maquette solution. The spectra are practically identical and are therefore overlaid

Conclusion

The results for this series of porphyrins (summarised in Table 5) show that extremes in hydrophobicity and hydrophilicity are not conducive to maquette binding. The porphyrin with no acid groups, **2.07**, showed no sign of binding to the maquette. Being completely hydrophobic, it aggregated in solution, and this is reflected in the broad B peak of its spectrum (Figure 132). While the monoacid **2.17** bound, it required 20 minutes to reach equilibrium. The *ABAB* **2.18** and *AABB* **2.19** diacids and the triacid **2.20** bound immediately. It seems that these compounds had enough hydrophilic character that they did not aggregate in the solution, but had a suitable hydrophobic area for binding to the maquette. The fact that each of these three compounds bound indicates that the specific arrangement of hydrophilic and hydrophobic groups is not critical to binding, at least for this porphyrin series.

The K_d values measured for the the *ABAB* **2.18** and *AABB* **2.19** diacids are both below the arbitrarily-set threshold of 100 nM, meaning that these porphyrins bind strongly enough to be deemed suitable for future experiments.

The "dip" observed in the plot from the titration experiment of the triacid **2.20** still requires an explanation, but indicates that a porphyrin may be in more states in the system than simply bound and unbound. A more complex model and/or analysis method is required to interpret the result for this compound.

Following this preliminary study, a more detailed study of the binding of these porphyrins with the same maquette was undertaken by fellow PhD student Chris Hobbs and collaborators at the University of Pennsylvania.[160]

Table 5: The results of the maquette binding experiment for the Zn phenylporphyrin benzoic acid series

Porphyrin	Acid groups	Equilibration time	K_d
2.07	0	Doesn't bind	N/A
2.17	1	20 mins	Not calculable
2.18	2	<30 sec.	6×10^{-8} M
2.19	2	<30 sec.	1×10^{-8} M
2.20	3	<30 sec.	Not calculable
2.21	4	Doesn't bind	N/A

7.3.2 Zinc butylporphyrin benzoic acids 2.33, 2.39 – 2.42

This series (Figure 143) was similar to the phenylporphyrin acid series in that the compounds bore p-benzoic acid groups for water-solubilisation. The hydrophobic groups however were butyl chains instead of benzene rings, and it was expected that by comparing the results of the two series, the effect of the properties of the hydrophobic group on binding could be assessed.

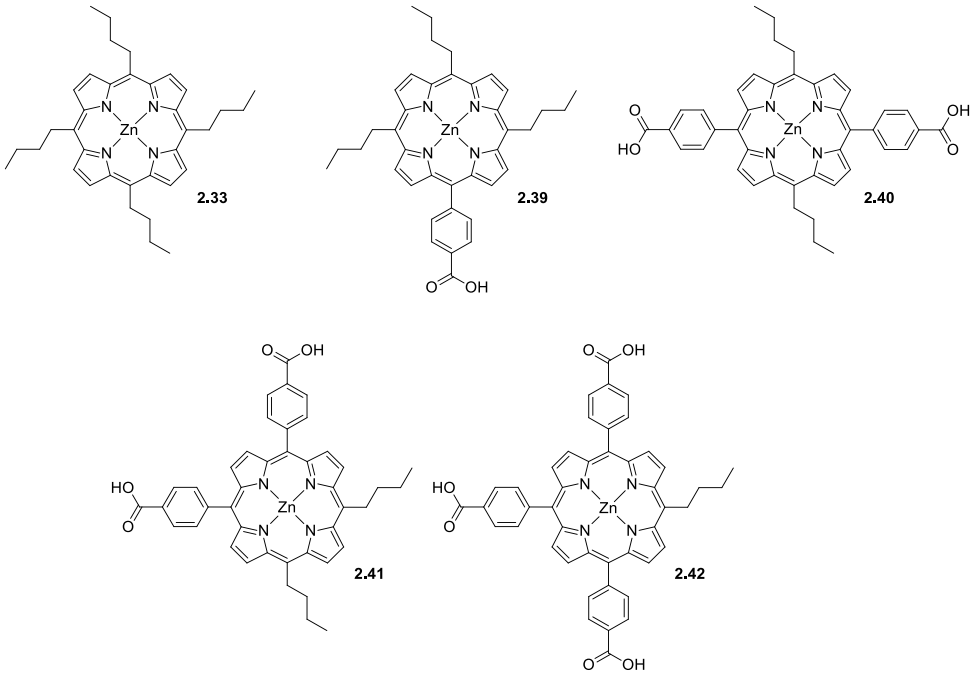

Figure 143: The zinc butylporphyrin benzoic acid series that was tested for maquette binding

Zn tetrabutylporphyrin 2.33

A qualitative binding experiment was undertaken to test for binding of porphyrin **2.33** and equilibration time. The spectra in buffer and with the 1.0 µM maquette are shown in Figure 144 (porphyrin concentration is 0.5 µM). The spectra are similar, and in each case the B band is very broad, a sign of aggregation. The presence of the maquette did have an effect however; the B peak was actually shifted toward blue by 4 nm (from 405 to 401 nm). This may be attributed to the supression of aggregation by the maquette. The absence of a red shift and the fact that, even in the presence of the maquette, the B band is broad, indicates that no histidine ligation is occurring and therefore the porphyrin is unlikely to have penetrated into the maquette core.

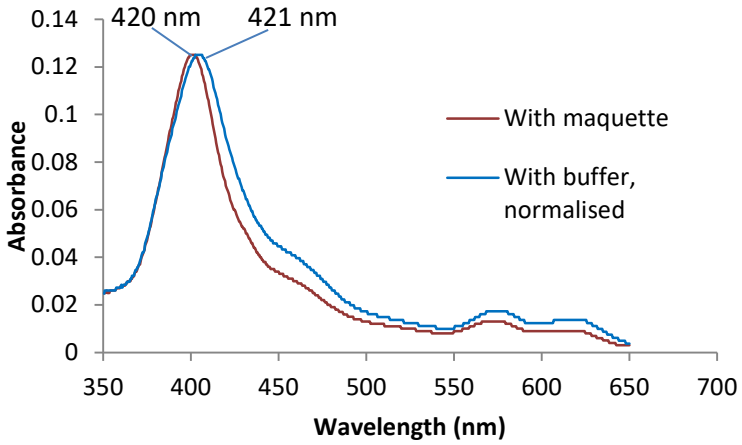

Figure 144: Spectra of the Zn tetrabutylporphyrin 2.33 (0.5 µM) immediately after addition to a 1.0 µM solution of maquette and to a buffer solution

Zn butylporphyrin monoacid 2.39

A qualitative binding experiment was performed to test for binding of porphyrin **2.39** and for equilibration time. Immediately after the injection of the porphyrin solution into the 1.0 µM maquette solution (porphyrin concentration 0.5 µM), a broad band with two peaks at 408 and 431 nm was evident (Figure 145). The peak at 408 nm was attributed to porphyrin in an aggregated state, while the peak at 431 nm was attributed to the porphyrin bound to the maquette and ligated to histidine.

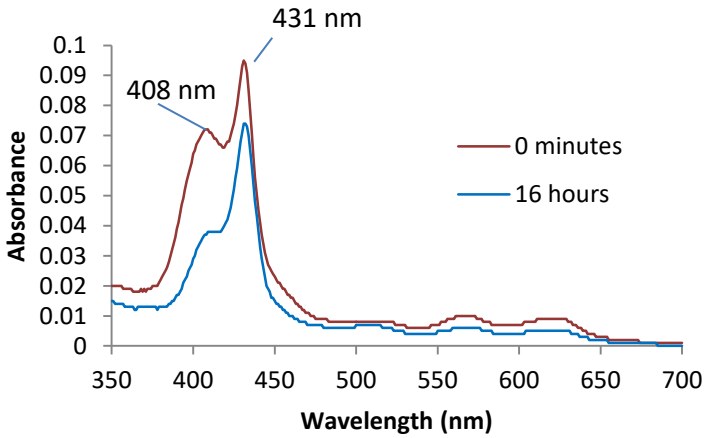

Figure 145: The absorbance of the Zn butylporphyrin monoacid 2.39 immediately after addition to the 1.0 µM maquette solution and again after 16 hours

The spectrum was monitored for 16 hours, over which time the peak at 431 nm grew relative to the peak at 408 nm, indicative of porphyrin coming out of the aggregated state and binding to the maquette. The overall intensity of the bound porphyrin B peak however decreased significantly over the 16 hours as shown in Figure 146. This indicated that the porphyrin was leaving the solution, probably *via* aggregation, but the mechanism of this process was not identified.

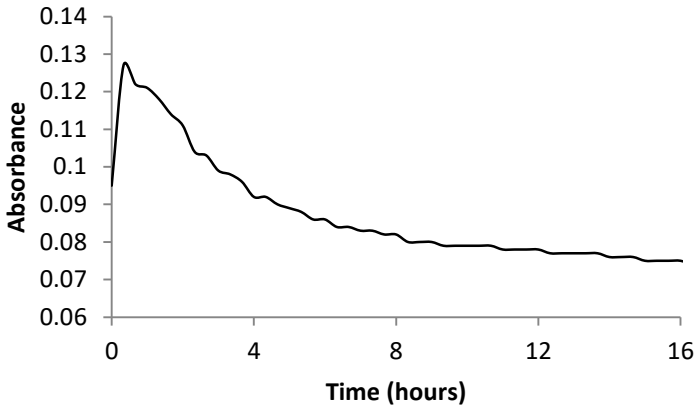

Figure 146: The absorbance at 431 nm of a solution of porphyrin 2.39 (0.5 µM) in 1.0 µM maquette solution, showing an initial increase in intensity and then a decline over the 16 hours for which it was monitored

Zn butyl ABAB diacid 2.40

A qualitative binding experiment was undertaken for porphyin **2.40** to test for binding and to measure equilibration time. The porphyrin solution was injected into a 1.0 µM maquette solution and the spectrum recorded (porphyrin concentration 0.2 µM). Initially the spectrum displayed a very broad B band with a peak at 434 (Figure 147). After 20 minutes this peak had *increased* in intensity. This may indicate that the porphyrin was in an aggregated state when it was injected into the maquette solution, and that the aggregation partially broke apart over time. By plotting the increase in absorption over time, it can be seen that equilibrium was reached after 7 minutes (Figure 148). The result seems to indicate that this porphyrin

aggregates rather than binds to the maquette. The analogous porphyrin from the phenylporphyrin benzoic acid series *did* bind to the maquette, and this is evidence that phenyl substituents are superior to butyl chains for facilitation of maquette binding.

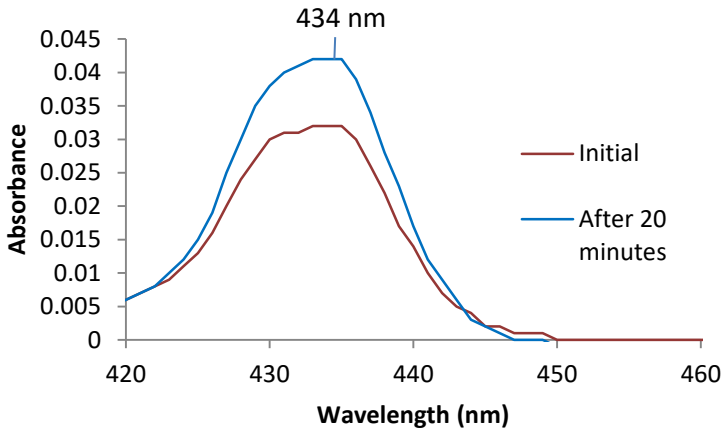

Figure 147: The spectrum of the porphyrin 2.40 immediately after addition to the 1.0 µM maquette solution and again 20 minutes later

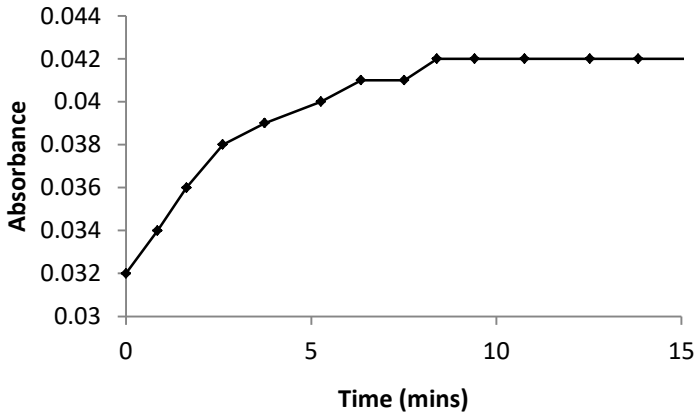

Figure 148: The absorption at 434 nm over time of porphyrin 2.40 (0.2 µM) in a 1.0 µM maquette solution shows that equilibrium was reached after 7 minutes

Zn butyl AABB diacid 2.41

A qualitative binding experiment was undertaken for porphyrin **2.41** to test for binding and for equilibration time. A portion of porphyrin was mixed into a 1.0 µM maquette solution and the spectrum recorded (porphyrin concentration 1.0 µM). The B peak was at 434 nm, indicating that the porphyrin was bound in the maquette and ligated to histidine. There were also two Q bands at 574 and 614 nm (Figure 149). The spectrum was stable over the 10 minutes for which it was observed, showing that this porphyrin reaches binding equilibrium with the maquette in less than 30 seconds.

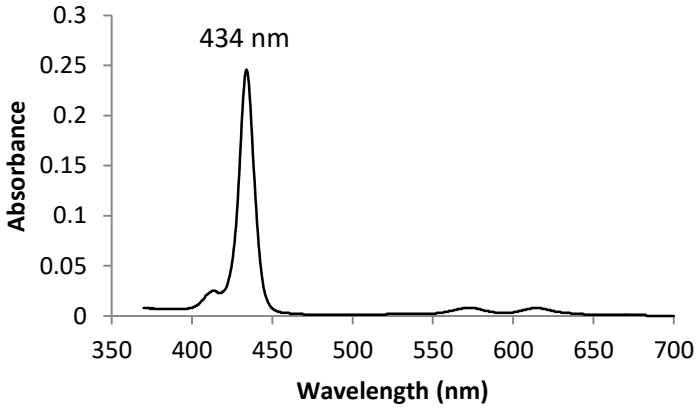

Figure 149: The spectrum of the porphyrin 2.41 in 1.0 µM maquette solution

A titration experiment was conducted to measure the K_d of the binding interaction. The absorbance at 434 nm was plotted against porphyrin concentration to obtain the curve shown in Figure 150. Similarly to the curve obtained for the Zn phenylporphyrin triacid, the post-saturation region displays a "dip" in the absorbance. This may be an indication that non-specific binding of excess porphyrin weakens histidine ligation of the porphyrins already bound and causes their spectrum to change. Indeed, the B peak of the bound porphyrin is observed to shift toward shorter wavelengths as well as decrease in intensity as more porphyrin is

added, as shown in Figure 151. Because of the dip in absorbance as further porphyrin was added, no K_d could be obtained for this binding interaction.

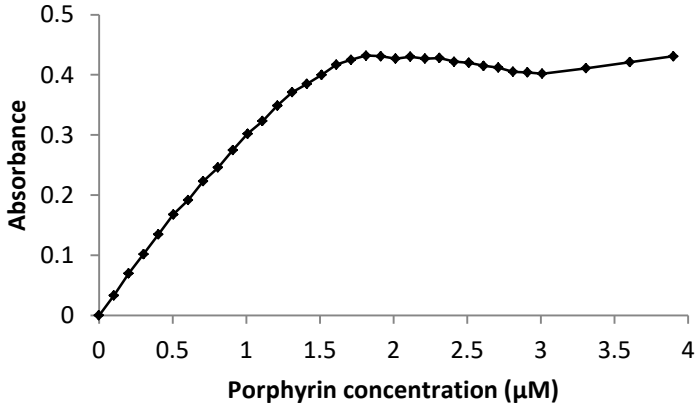

Figure 150: The absorbance at 434 nm plotted against porphyrin 2.41 concentration during the titration experiment

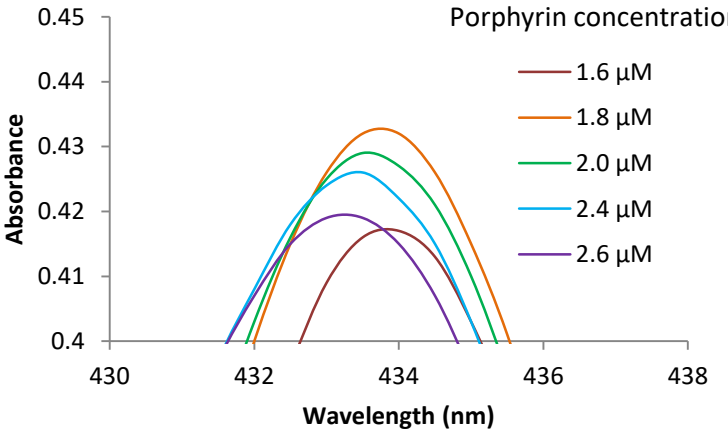

Figure 151: The top of the B peak of the bound porphyrin 2.41 during the titration at the maquette saturation point, showing the shift towards blue and decrease in intensity

Zn butylporphyrin triacid 2.42

A qualitative binding experiment was conducted for porphyrin **2.42** to test for maquette binding and to measure the equilibration time. The spectrum of the porphyrin immediately following addition to the 1.0 µM maquette solution is shown in Figure 152 (porphyrin concentration 0.2 µM). The B peak was at 433 nm, indicating that the porphyrin is bound to the maquette and ligated to histidine. The spectrum was stable over the 10 minutes for which it was monitored, indicating that this porphyrin reaches binding equilibrium before the spectrum was recorded approximately 30 seconds after mixing with the maquette.

The spectrum was also recorded in buffer solution, and in this case the B peak was at 423 nm and was quite sharp, indicating that the porphyrin is not in an aggregated state (Figure 152).

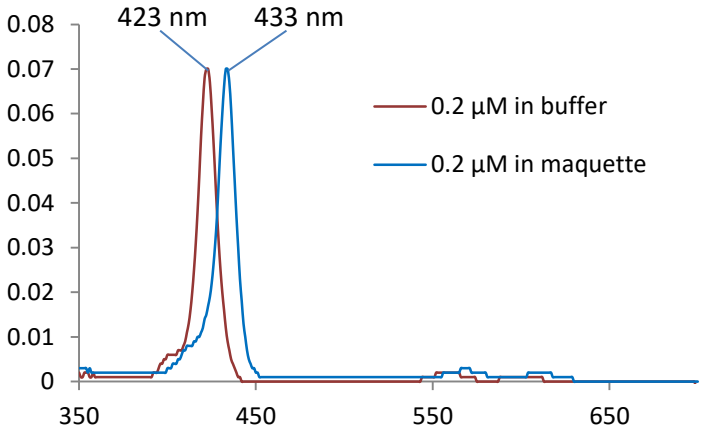

Figure 152: The spectrum of the porphyrin 2.42 in buffer and with 1.0 µM maquette

A titration experiment was conducted to measure the K_d of the binding interaction. The absorbance at 433 nm was plotted against porphyrin concentration to obtain the curve shown in Figure 153. As occurred for the Zn phenylporphyrin triacid **2.20** and the Zn butylporphyrin *AABB* diacid **2.41**, there is a "dip" after the maquette saturation point, which precluded K_d

determination. The spectral changes during the dip are shown in Figure 154, and involve a blue-shift and decrease in intensity as was observed for the *AABB* butylporphyrin diacid **2.41** (Figure 151).

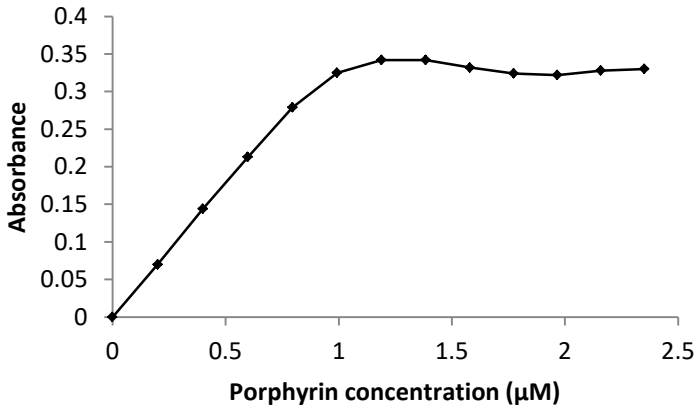

Figure 153: Absorbance at 433 nm plotted against porphyrin 2.42 concentration in a titration experiment

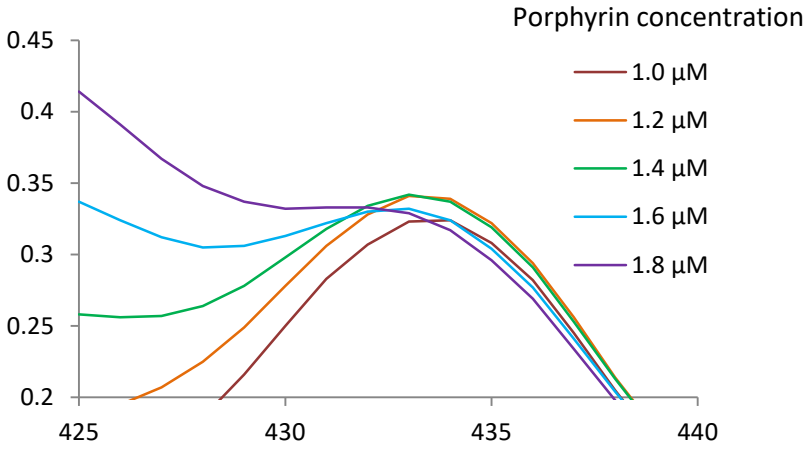

Figure 154: The top of the B peak of the bound porphyrin 2.42 during the titration showing the decrease in intensity and blue shift around the saturation point

Conclusion

The results of the binding experiments for the zinc butylporphyrins are summarised in Table 6. The fact that the monoacid **2.39** and the ABAB diacid **2.40** failed to bind to the maquette, while the analogous porphyins of the zinc phenylporphyrin benzoic acid series **2.17** and **2.18** did bind, indicates that butylporphyrins are inferior to phenylporphyrins rings in maquette binding. This is likely because butyl chains are less effective than benzene rings at supressing aggregation. The fact that the *AABB* diacid **2.41** and the triacid **2.42** do bind well further supports the conclusion for the the phenylporphyrin benzoic acids that the nature of the hydrophobic region is not especially important for binding to occur. However, the"dips" that were observed in the plots of the titration data for the *AABB* diacid **2.41** and for the triacid **2.42**, as had been observed previously for the triacid **2.20** of the zinc tetraphenylporphyrin series, confounded the determination of K_d values for the binding interactions. Again, this means that a more complex model and/or analysis method is required to interpret the result for these compounds.

Table 6: The results of the maquette binding experiment for the Zn butylporphyrin benzoic acid series

Porphyrin	Acid groups	Equilibration time	K_d
2.33	0	Doesn't bind	N/A
2.39	1	Doesn't bind	N/A
2.40	2	Doesn't bind	N/A
2.41	2	<30 sec.	Not calculable
2.42	3	<30 sec.	Not calculable

7.3.3 Zinc phenylporphyrin QASs 2.56 – 2.60

This series of quaternary ammonium salt (QAS) porphyrins (Figure 155) was produced in order to test the effect of using a different hydrophilic group on maquette binding. QASs are distinct from carboxylic acids in that they carry a positive charge rather than negative, their

ionic character is not pH dependent and they cannot participate in hydrogen bonding. Using these compounds was designed to probe whether carboxylic acid groups are necessary for maquette binding. If such contributions are significant, it was expected that by replacing these groups with QAS groups, that the binding affinity would be significantly reduced.

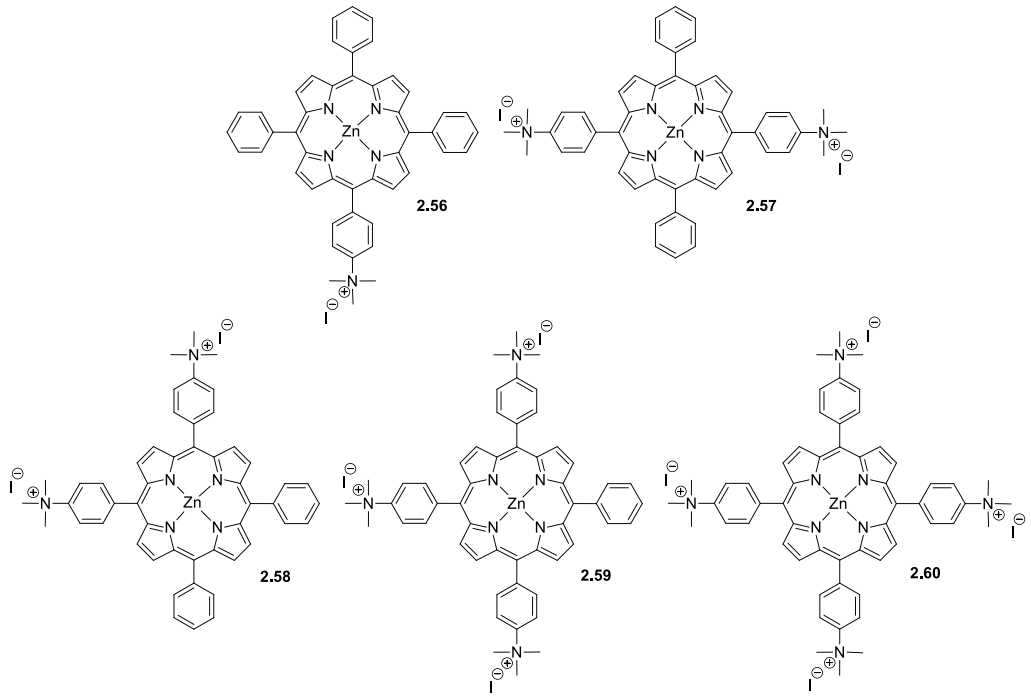

Figure 155: The zinc phenylporphyrin QAS series that was tested for maquette binding

Zn phenylporphyrin mono QAS 2.56

A qualitative binding experiment was conducted with porphyrin **2.56** to test for binding and equilibration time. A portion of the porphyrin solution was added to a 1.0 µM maquette solution to make a porphyrin concentration of 0.1 µM and the spectrum recorded immediately and then observed for the next 17 minutes. The initial and final spectra are shown in Figure 156.

The initial spectrum displays a peak at 433 nm with a very prominent shoulder at 417 nm. The peak at 433 nm is likely from the porphyrin in the maquette ligated to histidine, while the

peak at 417 nm is likely from the porphyrin in solution. After 17 minutes, the peak originally at 433 nm had become more intense, with the peak shifted slightly towards the blue to 431 nm. The fact that this peak has grown while the peak at 417 nm has disappeared indicates that the porphyrin has very likely left the solution and bound into the maquette over the course of the 17 minutes.

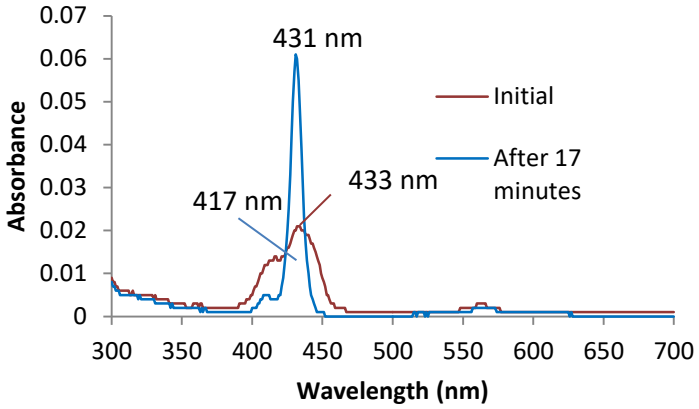

Figure 156: The spectrum of the porphyrin 2.56 immediately after addition to the 1.0 µM maquette solution and again 17 minutes later

The absorbance of the bound porphyrin B peak at 431 mm was plotted over time to create the curve shown in Figure 157. It shows that after 17 minutes the porphyrin had reached binding equilibrium. Because of the time required to reach equilibrium, a parallel equilibration experiment was performed rather than a titration. The absorbance of the bound porphyrin B peak at 431 nm was plotted against porphyrin concentration to obtain the curve shown in Figure 158.

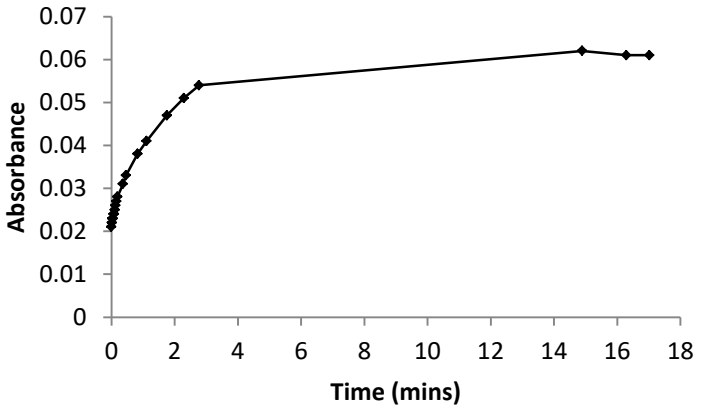

Figure 157: The absorbance of the bound porphyrin 2.56 peak at 433 nm over time as the mixture came to binding equilirium

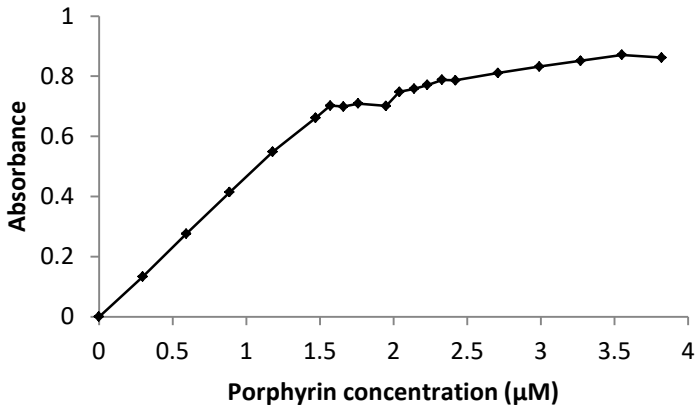

Figure 158: The absorbance at 431 nm vs porphyrin 2.56 concentration in a parallel equilibration experiment. The maquette concentration is 1.0 µM

As expected, the absorbance increased linearly at first as all of the porphyrin bound to the maquette. As the maquette became saturated, the curve changed gradient as the extra porphyrin added remained unbound. There appears to be a dip in absorbance post-saturation, but this may be due to measurement errors from measuring volumes on the µL scale. It may,

however, be the same phenomenon as was observed for the phenylporphyrin triacid **2.20**, the butylporphyrin *AABB* diacid **2.41** and triacid **2.42**.

Fitting Equation 1 to the data gives a K_d of 150 nM and an apparent porphyrin extinction coefficient of 570000 L mol^{-1} cm^{-1}. In this case the "dip" in the data was not large enough to interfere with the fitting. The binding ratio however appears to be 1.6:1 which is an unexpected result that cannot be easily explained. It may indicate that in fact this porphyrin binds to both binding sites in the maquette, with some of the maquette being inactive as previously discussed.

Zn phenylporphyrin ABAB di QAS 2.57

An equilibration experiment was carried out for porphyrin **2.57** to test for binding and to determine the equilibration time. The spectrum was recorded in a 1.0 μM maquette solution and in buffer and these are shown in Figure 159 (porphyrin concentration 0.5 μM). The spectrum in maquette solution displays a B peak at 432 nm, indicating that this porphyrin is bound inside the maquette and ligated to histidine. In the buffer solution, the B peak instead appears at 420 nm, as was expected for the unbound porphyrin in aqueous solution.

In the maquette solution the spectrum was stable, showing that the porphyrin reaches binding equilibrium in the ~30 seconds between the initial mixing and the recording of the spectrum.

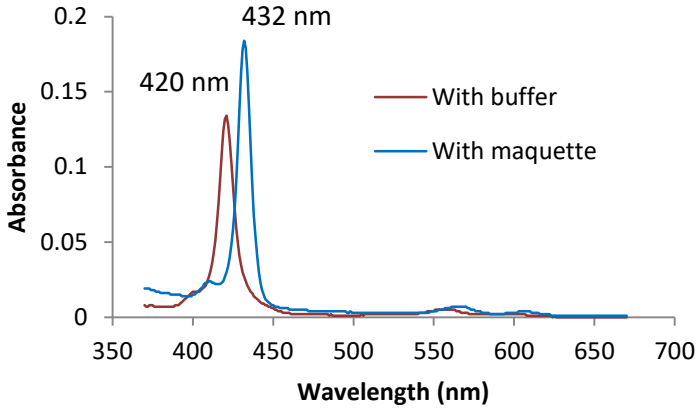

Figure 159: Spectra of the Zn phenylporphyrin *ABAB* di QAS 2.57 in buffer solution and with 1.0 µM maquette

A titration experiment was carried out in order to measure the K_d of the binding interaction. The absorbance of the bound porphyrin B peak at 432 nm was plotted against porphyrin concentration to obtain the curve shown in Figure 160. It displays the two linear regions linked by a curved region that was expected. Fitting Equation 1 to the data revealed a K_d of 6 nM, well below the threshold of 100 nM required and indicative of strong binding. The apparent porphyrin extinction coefficient was 590000 L mol^{-1} cm^{-1}, indicating no major errors had been made in measuring porphyrin quantities. The apparent binding ratio was 1.4:1, a similar result to that previously obtained that indicated that both binding sites bound porphyrins but that perhaps some of the maquette had become inactive. The result shows that this porphyrin binds quickly and strongly to the maquette.

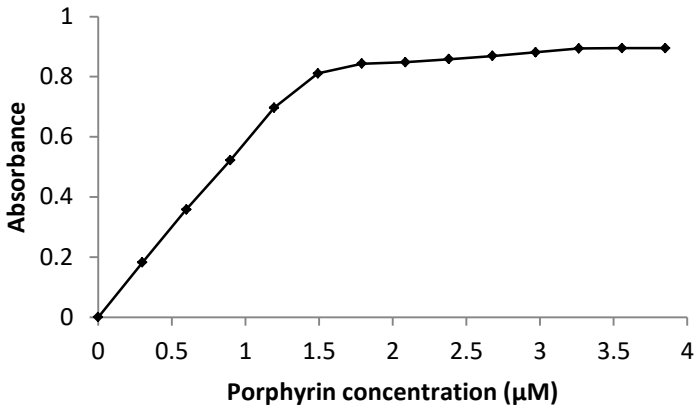

Figure 160: The curve generated from plotting the absorbance of the bound porphyrin B peak at 432 nm against porphyrin 2.57 concentration in the titration experiment

Zn phenylporphyrin AABB di QAS 2.58

An equilibration experiment was carried out with porphyrin **2.58** to test for binding and to determine the equilibration time. The spectrum of the porphyrin in the 1.0 µM maquette solution is shown in Figure 161 (porphyrin concentration 1.0 µM). The B peak is at 431 nm, indicating that the porphyrin is bound to the maquette and ligated to histidine. The spectrum was stable over the 10 minutes for which it was observed, indicating that it reached binding equilibrium in the ~30 seconds between the mixing with the maquette and the recording of the spectrum.

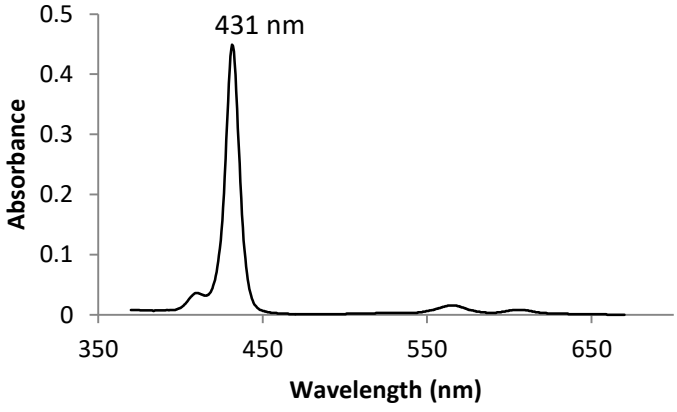

Figure 161: The spectrum of the Zn phenylporphyrin *AABB* di QAS 2.58 in the 1.0 µM maquette solution

A titration was carried out in order to measure the K_d of the binding interaction. The absorbance at the bound porphyrin B peak was plotted against the porphyrin concentration to produce the curve shown in Figure 162. It shows the expected two linear regions linked by a curved section. Fitting Equation 1 to the data produced a K_d of 20 nM, meaning that this porphyrin binds strongly. The apparent extinction coefficient of the porphyrin was 580000 L mol^{-1} cm^{-1}, indicating no major errors in measuring porphyrin quantities. The apparent binding ratio was 1.6:1, indicating that both binding sites of the maquette accepted porphyrin, but that some of the maquette may have become inactive.

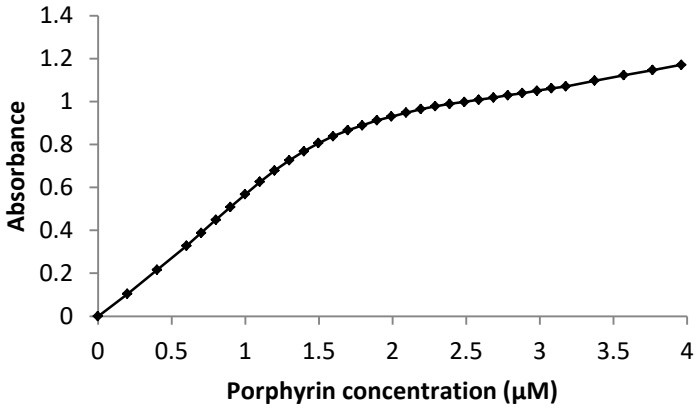

Figure 162: The absorbance at the bound porphyrin B peak at 431 nm *vs* porphyrin 2.58 concentration in the titration experiment

Zn phenylporphyrin tri QAS 2.59

An equilibration experiment was carried out with porphyrin **2.59** in order to test for binding and equilibration time. The spectrum of the porphyrin in a 1.0 μM solution of the maquette is shown in Figure 163 (porphyrin concentration 1.0 μM). The B peak appears at 432 nm, indicating that this porphyrin is bound in the maquette and ligated to histidine. The spectrum was stable, indicating that binding was completed in the ~30 seconds between the mixing of the porphyrin with the maquette solution and the recording of the spectrum.

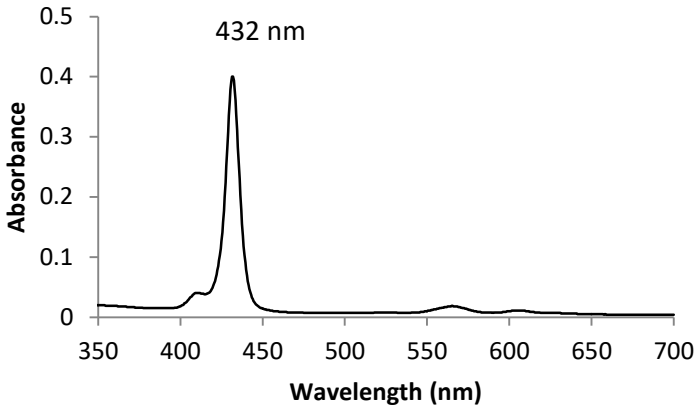

Figure 163: The spectrum of the Zn porphyrin tri QAS 2.59 in a 1.0 µM maquette solution

A titration was carried out in order to measure the K_d of the binding interaction. The absorbance at the bound porphyrin B peak at 432 nm was plotted against the porphyrin concentration to obtain the curve shown in Figure 164. It displays the expected two linear regions linked by a curved region. Fitting of Equation 1 to the data produced a K_d value of 23 nM, meaning that this porphyrin binds strongly. The apparent binding ratio was 2.0:1, and this is the first of the porphyrins to exhibit this binding ratio. However a significantly lower porphyrin extinction coefficient than for the other QAS porphyrins of the series (460000 L mol^{-1} cm^{-1}) was measured, and this may indicate that the porphyrin concentration was lower than expected, possibly due to the porphyrin containing some water when being weighed. Nevertheless, the low K_d result remains valid and shows a strong binding of the porphyrin to the maquette.

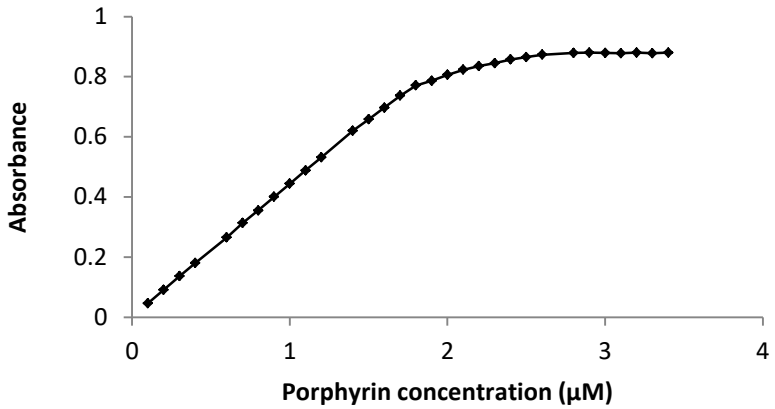

Figure 164: The absorbance at the bound porphyrin B peak at 432 nm plotted against porphyrin 2.59 concentration

Zn phenylporphyrin tetra QAS 2.60

An equilibration experiment was conducted with porphyrin **2.60** to test for binding and to determine equilibration time. The spectrum (Figure 165) in the buffer solution was as expected; the B peak was at 421 nm and was sharp, showing that this porphyrin did not possess a tendency to aggregate in aqueous solution. The four QAS groups provided enough polar groups to make this porphyrin highly water-soluble.

The spectra with the 1.0 μM maquette were somewhat surprising. It was expected that the porphyrin would not associate with the maquette at all and that the spectrum would be virtually identical to the spectrum in buffer, as had been the case with the tetracarboxylic acid. Actually, when the maquette was in a large excess, the B band of the tetra QAS porphyrin had a double peak: one at 421 nm and one at 431 nm. This indicated that a portion of the porphyrin was ligated to the the histidine of the maquette. When more porphyrin solution was added to the mixture, the peak at 421 nm grew at a much faster rate than the peak at 431 nm and eventually the peak at 431 nm was just a shoulder on the red side of the B band. The spectrum was observed over time and found to be stable. It seems that when the maquette is

in a large excess, some of this porphyrin will ligate to histidine, but that the binding is too weak to form a useful porphyrin-maquette complex.

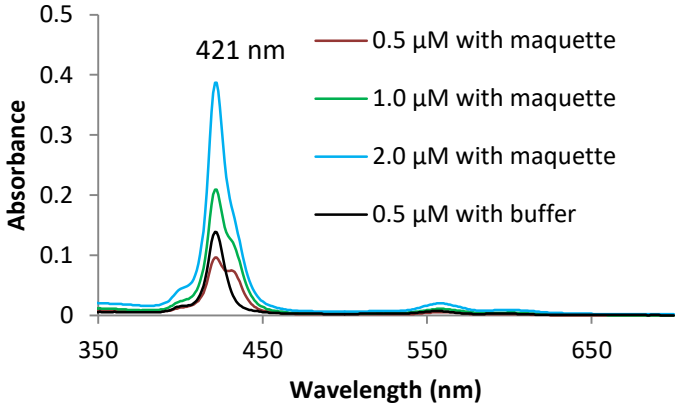

Figure 165: The spectra of the porphyrin 2.60 in 1.0 µM maquette solution at various concentrations, and in buffer solution

Conclusion

The results of the binding experiments for the zinc phenylporphyrin QASs are summarised in Table 7. This series of porphyrins bound similarly to the tetraphenylporphyrin carboxylic acid series, and significantly better than the butylporphyrin benzoic acid series. This shows that the maquette will bind both negatively and positively charged cofactors. The result that four of the five porphyrins in this series bound to the maquette further supports the conclusion that this maquette will accommodate a variety of different porphyrin cofactors as long as they have the right balance of hydrophobic and hydrophilic properties.

Table 7: The results of the maquette binding experiment for the Zn phenylporphyrin QAS series

Porphyrin	QAS groups	Equilibration time	K_d
2.56	1	17 mins	1.5×10^{-7} M
2.57	2	< 30 secs	6×10^{-9} M
2.58	2	< 30 secs	2×10^{-8} M
2.59	3	< 30 secs	2×10^{-8} M
2.60	4	Unclear	N/A

7.3.4 Ferrocene porphyrin triacid 2.63

An qualitative binding experiment was carried out with porphyrin **2.63** (porphyrin concentration 1.5 μM). In a buffer solution the porphyrin displayed its B peak (Figure 167) at 423 nm (Figure 166) but with a shoulder on the red side which may indicate the occurrance of some aggregation. In the 1.0 μM maquette solution the B peak appeared at 434 nm, showing that the porphyrin was ligated to histidine inside the maquette. Both spectra were stable over the 10 minutes for which they were observed.

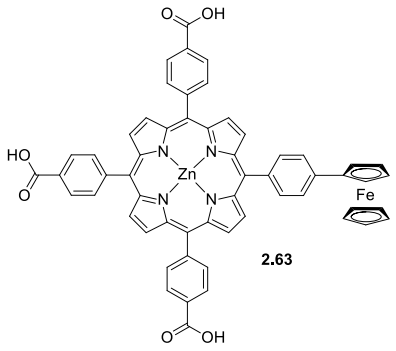

2.63

Figure 166: The zinc ferroceneporphyrin benzoic acid 2.63 that was tested for maquette binding

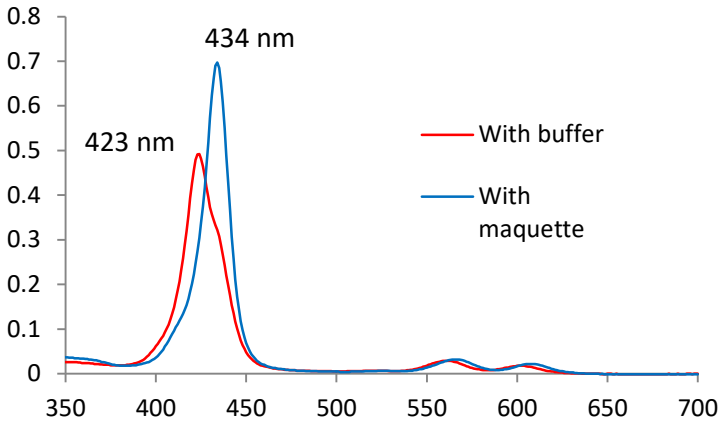

Figure 167: The spectra of the porphyrin 2.63 in buffer solution and in 1.0 µM maquette solution

A titration experiment was carried out in order to measure the K_d of the binding interaction. The absorbance of the bound porphyrin B peak at 434 nm was plotted against porphyrin concentration to obtain the curve shown in Figure 168. Fitting Equation 1 to the data produced a K_d of 315 nM, which does not the meet the arbitrarily-set threshold for good binding of 100 nM, but still may mean that the compound is useful if the maquette is present in excess.

The apparent porphyrin extinction coefficient was 410000 L mol^{-1} cm^{-1}, which was lower than expected and may indicate an error in the measurement of porphyrin mass or volume. The binding ratio was 1.3:1, and most likely indicates that this porphyrin binds to the maquette in the ratio 1:1.

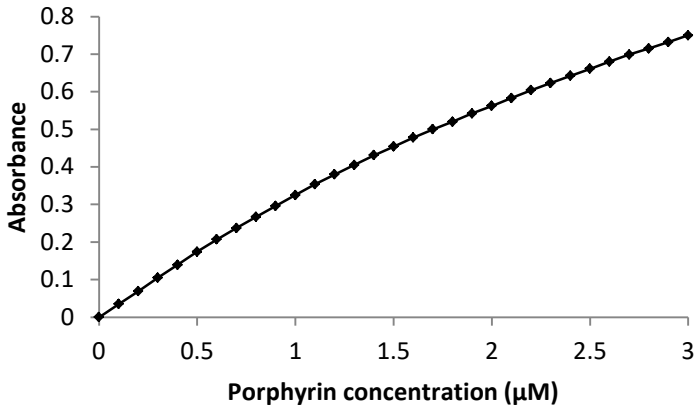

Figure 168: The absorbance of the bound porphyrin B peak at 434 nm plotted against porphyrin 2.63 concentration from the titration experiment

7.4 Binding of amphiphilic Fe porphyrins 2.23 – 2.25

Iron is the metal bound in heme, the natural porphyrin which functions most famously as an oxygen transporter but also as an electron shuttle as part of the cytochrome proteins in the vital process of electron transport in mitochondria. Porphyrin-bound iron is well ligated by axially opposed histidine residues which mean that it will bind strongly to proteins bearing such an arrangement. It also may act as an electron acceptor and when a porphyrin array contains an iron porphyrin and a zinc porphyrin, one would expect that charge separation would occur within the array.[151] The creation of artificial iron porphyrins capable of forming an ensemble with a maquette is therefore desirable, as they may be used to form a variety of functions. The synthesis of iron porphyrins was described in Chapter 2, and the binding of these porphyrins (Figure 169) to the maquette BT bis his is described below. Given the previous binding results with zinc porphyrins, only the best binding configurations, that is both diacids **2.23** and **2.25** and the triacid **2.25**, were investigated.

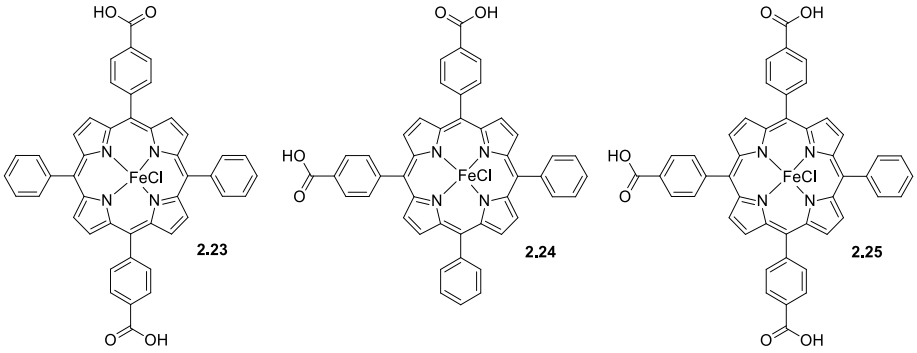

Figure 169: The iron phenylporphyrin benzoic acid series that was tested for maquette binding

FeCl phenylporphyrin ABAB diacid 2.23

Equilibration experiments were conducted with porphyrin **2.23** in buffer and maquette solutions. The porphyrin concentration was 0.1 µM in each case, and the maquette concentration was 1.0 µM. In the buffer solution the spectrum initially displayed a B band maximum at 405 nm (Figure 170). Over the course of 8 days, the intensity of the spectrum decreased and the absorbance maximum shifted to 410 nm. This decrease in intensity and the concurrent red shift may reflect the formation of J aggregates.[161] The decrease in intensity of porphyrin aggregate bands is well established.[162,163]

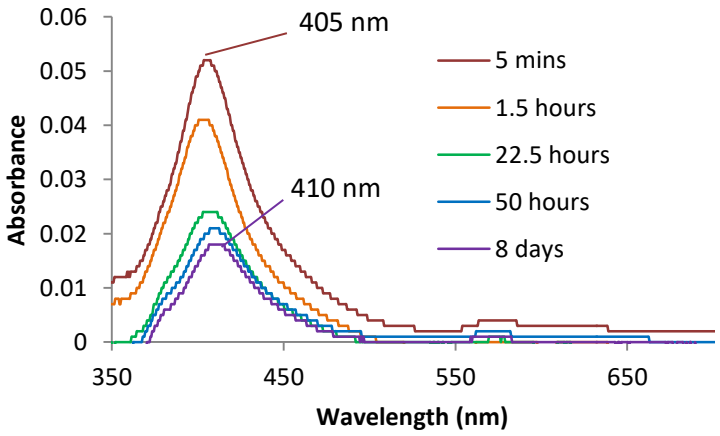

Figure 170: The spectra of the Fe phenylporphyrin *ABAB* diacid 2.23 (0.1 µM) in buffer solution over time

In contrast, the spectrum of the porphyrin with excess maquette (1.0 µM) initially displayed a B band maximum at 407 nm but over time the peak sharpened and increased in intensity, and the B peak maximum shifted to 419 nm (Figure 171). This large red shift and the increase in intensity indicates that this porphyrin is binding to the maquette and becoming ligated by the histidine pairs. The binding however is quite slow compared to that of the analogous zinc compound **2.18**.

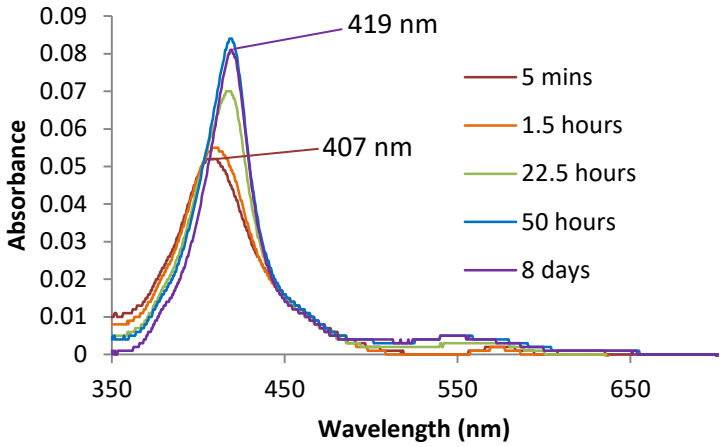

Figure 171: The spectra of the Fe phenylporphyrin *ABAB* diacid 2.23 (0.1 µM) with 1.0 µM maquette BT6 bis his over time

Fe phenylporphyrin AABB diacid 2.24

Equilibration experiments were conducted with porphyrin **2.24** in buffer and maquette solutions. The porphyrin concentration was 0.1 µM in each case, and the maquette concentration was 1.0 µM. The behaviour of porphyrin **2.24** was similar to the *ABAB* isomer **2.23** in that in buffer solution, the intensity of the absorption steadily decreased over the course of 8 days (Figure 172), and this was likely due to the porphyrin aggregation. Initially the absorbance maximum lay at 449 nm with a shoulder on the blue side of the B peak. Given the broad nature of this absorption and the position of the B band in DMSO at 411 nm (see experimental section), it is proposed that this broad B band in buffer results from the

immediate formation of both J aggregates (449 nm) and H aggregates.[161] After 8 days the peak at 449 nm had all but disappeared, leaving only a peak at 417 nm, indicative of H aggregates.[161]

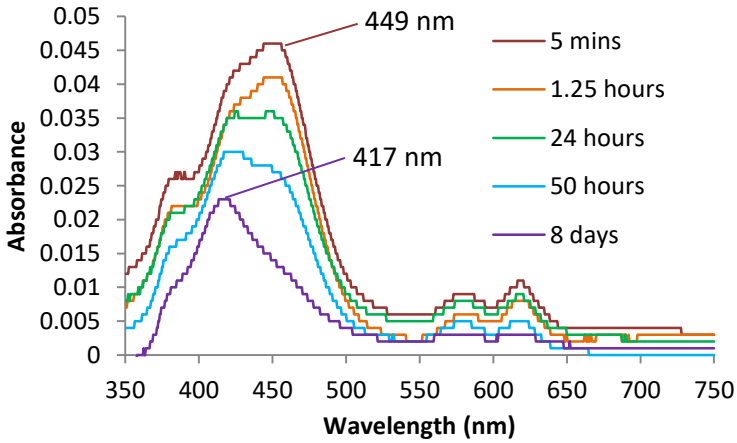

Figure 172: The spectra of the Fe phenylporphyrin *AABB* diacid 2.24 (0.1 µM) in buffer solution over time

In a solution containing excess maquette (Figure 173), the spectrum initially displayed an absorbance maximum at 421 nm with a shoulder on the red side, in a similar position to the initial maximum observed in the buffer solution at 449 nm. Over 8 days, the peak at 421 nm increased in intensity and the shoulder decreased. The loss of the 449 nm band is similar to the spectral behaviour in the buffer solution, the key difference being that the lower wavelength band increased in intensity rather than decreasing. Given the appearance of the B band for the maquette-bound porphyrin **2.23** at 419 nm, the growth of the peak at 421 nm for this porphyrin, **2.24** is evidence for its deaggregation and binding to the maquette. This result and that for the Fe *ABAB* porphyrin **2.23** are comparable to the analogous Zn porphyrin results albeit with a considerably slower binding that undoubtedly results from the more significant aggregation behaviour of the Fe porphyrins as well as the requirement for the second coordination.

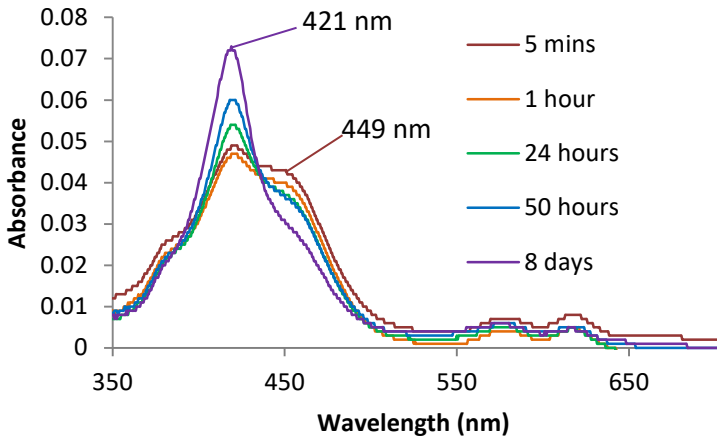

Figure 173: The spectra of the Fe phenylporphyrin *AABB* diacid 2.24 (0.1 µM) with 1.0 µM maquette BT bis his over time

FeCl phenylporphyrin triacid 2.25

An equilibration experiment was carried out with the porphyrin **2.25** in a solution of 1.0 µM maquette with spectra being recorded over a period of 239 minutes (Figure 174). The porphyrin concentration was 0.1 µM in each case, and the maquette concentration was 1.0 µM. Initially the absorbance maximum of the B peak lay at 408 nm, but over the course of the experiment the intensity of the absorbance increased substantially and the absorbance maximum shifted to 416 nm, a very similar behaviour to that observed for the *ABAB* diacid, only occurring much faster. This result indicated that this porphyrin does bind to the maquette, and at the fastest rate of the iron porphyrins tested, likely a result of its three hydrophilic groups making it less prone to aggregation in aqueous solution.

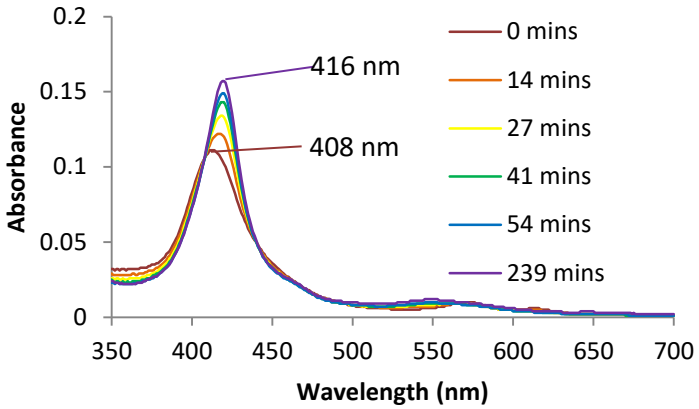

Figure 174: The spectrum of the Fe phenylporphyrin triacid 2.25 (0.1 µM) in 1.0 µM maquette solution over time

Conclusion

All of the iron porphyrins, **2.23** - **2.25** showed clear signs of binding to the maquette and becoming ligated to the histidine pairs. The binding was very slow, and titration experiments were not carried out because of this and no K_d values were obtained. Further study is required to determine conditions that would minimise aggregation and speed up the binding process, in order to allow the dtermination of the binding kinetics. This was beyond the scope of this thesis.

7.5 Binding of porphyrin dyads

The results of the maquette binding experiments with zinc porphyrins indicated that the maquette would accept a wide range of porphyrin geometries and hydrophilic/hydrophobic character. This encouraged the synthesis of amphiphilic porphyrin dyads (Chapters 4 and 5), and their binding to the maquette BT H7H112 was investigated, as detailed below.

ZnZn phenylene-linked porphyrin dyad triacid 4.17

Equilibration experiments were conducted for the dyad **4.17** (Figure 175) (1.0 μM) in both buffer and 1.0 μM maquette solutions (Figure 176 and Figure 177). In each solution, the spectra were similar in shape 5 minutes after initial mixing, but in buffer the B peak lay at 431 nm with a shoulder on the blue side, while the the spectrum in maquette solution had its B peak at 434 nm. After 7 days however, the spectrum in buffer still displayed the peak at 431 nm, but now the shoulder was more distinct and actually had a proper peak at 395 nm. The spectrum in the maquette solution after 24 hours still had the B peak at 434 nm, but the shoulder had diminished in intensity.

While this does not show the 10 nm red shift that is an obvious sign of histidine ligation, the spectra after 7 days in each case are quite different, indicating that the dyad does interact with the maquette in some way. The result provides insufficient information however to be sure that the dyad is entering the maquette and ligating to histidine.

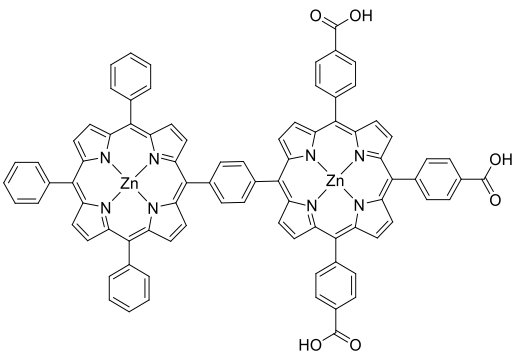

Figure 175: The ZnZn phenylene-linked triacid porphyrin dyad 4.17

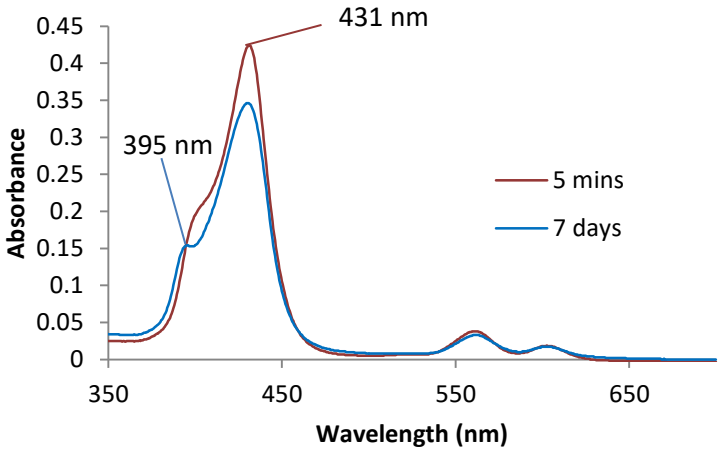

Figure 176: The spectrum of the ZnZn phenylene-linked dyad tricarboxylic acid 4.17 in buffer solution after 5 minutes and after 7 days

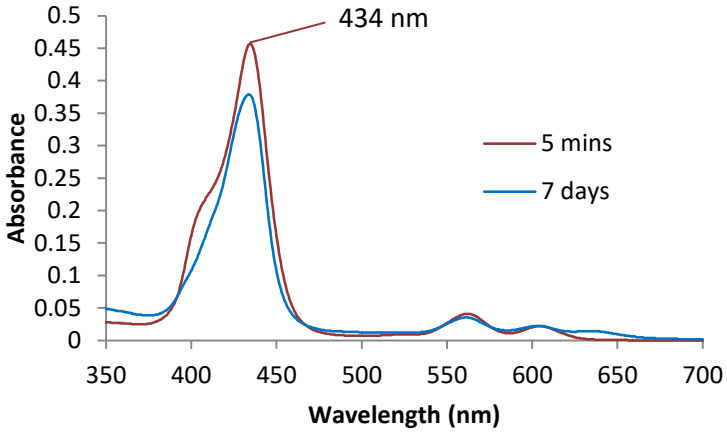

Figure 177: The spectrum of the ZnZn phenylene-linked dyad tricarboxylic acid 4.17 in 1.0 µM maquette solution after 5 minutes and after 7 days

ZnZn phenylene-linked porphyrin dyad tri QAS 4.18

Equilibration experiments were carried out with the tri QAS phenylene linked dyad **4.18** (Figure 178) (1.0 µM) in buffer and in 1.0 µM maquette solution. In both cases the absorbance maxima lay at 435 nm and the intensity of the spectrum decreased over time (Figure 179 and

Figure 180). The spectra in maquette and buffer were very similar, indicating that this dyad does not interact strongly with this maquette. The decrease in intensity is likely an indication of aggregation and precipitation from the solution.

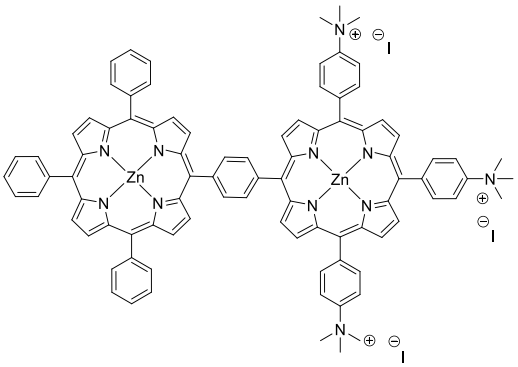

Figure 178: The ZnZn phenylene-linked tri QAS porphyrin dyad 4.18

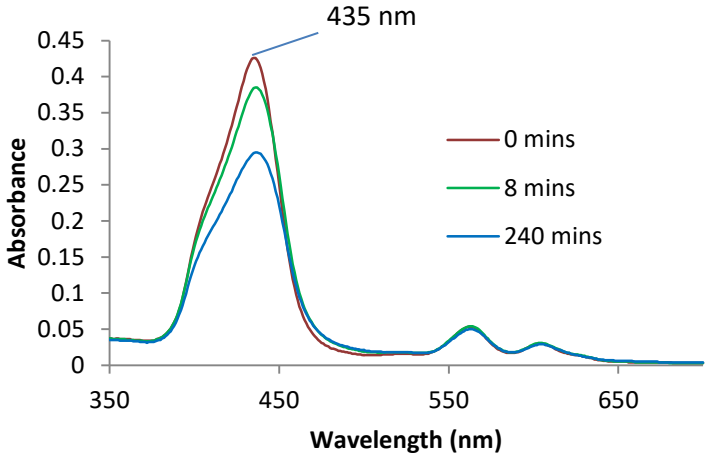

Figure 179: The spectrum of the ZnZn phenylene-linked dyad tri QAS 4.18 in buffer solution over time

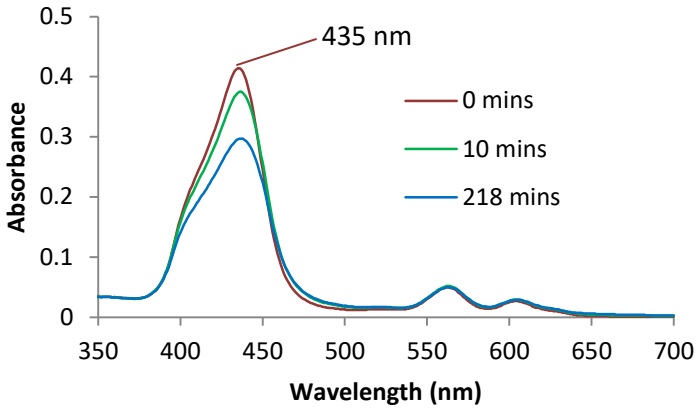

Figure 180: The spectrum of the ZnZn phenylene-linked dyad tri QAS 4.18 in 1.0 µM maquette solution over time

ZnZn vinyl-linked porphyin dyad tetraacid 5.13

To test for maquette binding, the vinyl linked dyad **5.13** (Figure 181) was mixed with buffer and 1.0 µM maquette solutions (dyad concentration 1.0 µM) and left for 24 hours before the spectra were recorded. The spectra are shown in Figure 182. The spectrum of the dyad in buffer solution displays an absorption maximum at 426 nm, while the porphyrin in the maquette solution displays its maximum at 432 nm. This shows that the dyad interacts with the maquette in some way, and the fact that the absorbance maximum is shifted by 8 nm in the presence of the maquette indicates possible ligation to histidine.

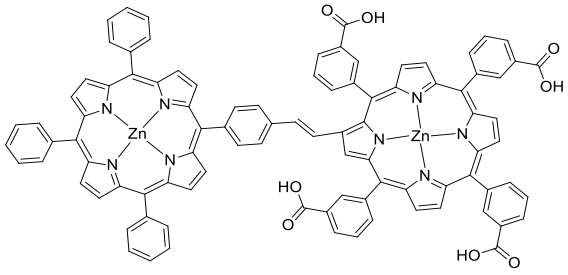

Figure 181: The vinyl-linked dyad 5.13

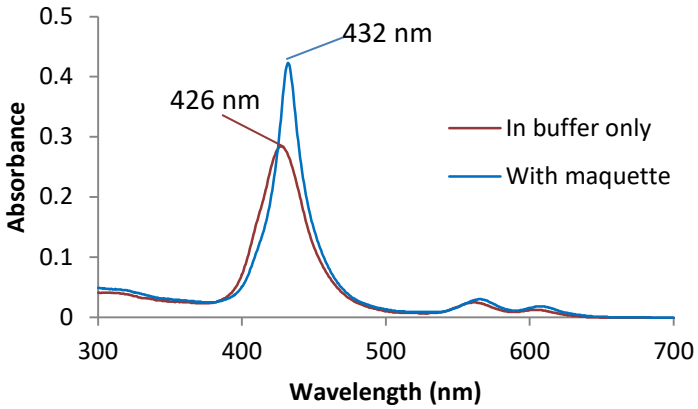

Figure 182: The spectra of the vinyl linked dyad 5.13 in buffer and 1.0 µM maquette solutions 24 hours after mixing

Conclusion

The results of for the ZnZn phenylene-linked porphyrin dyad triacid **4.17** and the ZnZn vinyl-linked porphyin dyad tetraacid **5.13** show clear evidence of an interaction between the dyad and the maquette. There is not enough information to ascertain the nature of the interaction, or if one of the porphyrins of the dyad is becoming ligated to histidine in the designed binding sites. Further work is required to investigate this further.

7.6 Chapter conclusion

In this chapter, a preliminary investigation into what range of hydrophilic and hydrophobic character was necessary in a porphyrin for binding to a maquette. The results demonstrate that extremes in hydrophobicity and hydrophilicity are not conducive to maquette-binding.

It was interesting that the *ABAB* oriented phenylporphyrin carboxylic acids and QAS bound well to the maquette, as it was expected that this arrangement of hydrophilic groups would not allow for the burying of the whole hydrophobic area in the maquette core. As expected, the *AABB* compounds bound quickly and strongly in each case. These compounds are evidently

hydrophilic enough not to aggreggate too strongly in aqueous solution, but still present a sufficiently large hydrophobic area to drive a strong binding association with the maquette. The porphyrins bearing three hydrophilic groups all bound quickly. This was not necessarily expected, as it was thought that perhaps these compounds would be so hydrophilic as to be quite stable in aqueous solution and for the driving force for maquette association to be minimal.

The fact that such a diverse range of porphyrins bound to the maquette shows that porphyrins do not have to be "tailor made" for the binding site, and provides confidence that amphiphilic porphyrins and porphyrin arrays produced in the future will also bind to the maquette.

The results for the binding of the porphyrin dyads were more complex to interpret, but the phenylene linked dyad tricarboxylic acid and the vinyl linked dyad showed clear signs of associating with the maquette. Further work is necessary to clarify this.

The variability in the binding ratios and the fact that they are non-integer values, may be due to partial protein degradation during shipping from our collaborators in the USA, resulting in a concentration of active protein that was lower than was measured *via* UV-vis absorption analysis.

Despite such issues, this work laid the foundation for further work by Chris Hobbs leading to a significant publication in Chemical Science[160] and has produced other promising results that will be utilised in future research.

Future work

The aim of this thesis was to undertake a survey of porphyrin functionality appropriate for maquette binding. The large porphyrin library produced in Chapter 2 was tested for maquette binding behaviour. Building on this work, the most promising of these were investigated in further detail by PhD student Chris Hobbs at UOW, collaborators Goutham Kodali and Christopher Moser of the Dutton group at UPenn, and by the group of Keith Gordon at the University of Otago. This work has now been published in Chemical Science.[160]

The investigation in this thesis has shown that a wide variety of compound types can be bound into maquettes, and has provided a library of synthetic porphyrins that are suitable for light harvesting for future energy transduction experiments. Experiments undertaken by Chris Hobbs at UOW using members of this porphyrin library have produced a porphyrin-maquette ensemble-based dye sensitised solar cell, and this work has been submitted for publication.

The technique of using HPLC analysis that was developed to quantify the isomeric purity of the *ABAB* and *AABB* isomers isolated from statistical mixtures is a valuable, generally applicable tool and a manuscript is currently in preparation for the publication of this work.

The challenge of the synthesis of amphiphilic porphyrin arrays containing more than two porphyrins is yet to be overcome. The work undertaken in these doctoral studies has shown that syntheses of such compounds (Chapters 4 and 5) share the common difficulty of purifying the porphyrin arrays from the by-products of the reactions. The metal tagging techniques developed during this research (Chapter 6) require further optimisation, but offer great promise in opening up possibilities for amphiphilic porphyrin array synthesis and a publication is expected to arise from this work.

Ultimately, the value of this work will be realised with the application of a multiporphyrin array maquette in a photosynthetic device. This thesis work has laid a sound foundation for such a development.

Experimental

Synthesis

All reagents and solvents were commercially available and used without additional purification, unless stated otherwise. Anhydrous solvents were used for all reactions, and those requiring an inert atmosphere were carried out under nitrogen.

TLC analysis was performed using Merck TLC silica gel 60 precoated aluminium silica TLC plates. Flash chromatography was performed using Merck silica gel 60 (0.040-0.063 mm).

Characterisation of products

NMR spectra were recorded on a Bruker Avance 400 spectrometer. The following abbreviations were used: s = singlet, d = doublet, t = triplet, sex. = sextet, m = multiplet. All coupling constants *J* were measured in hertz (Hz). Chemical shifts are reported in parts per million (ppm). Tetramethylsilane was used as the internal reference.

UV-vis absorption spectra were recorded on a Shimadzu UV-1800 spectrophotometer. Compounds were dissolved in chloroform, DMSO or DMF, depending on their solubility, and their spectra recorded.

Low resolution MALDI mass spectrometry was performed using an Shimadzu Axima Confidence spectrometer. Samples were dissolved in DCM or methanol and applied to the stainless steel sample plate. A saturated solution of α-cyano-4-hydroxycinnamic acid in DCM was then applied on top of the porphyrin sample to function as a matrix material. In most cases it was found that samples ionised equally well without the addition of the matrix.

High resolution mass spectrometry was performed using a Waters Xevo QToF-MS mass spectrometer, using an electrospray ionization source. Samples were infused at 5uL/min as methanolic solutions. The lockmass compound wass leucine encephalin.

Reversesd phase HPLC analysis was performed using an Agilent 1260 machine and a Grace RP18, 5 µm particle size, 250 mm length, 4.6 mm internal diameter column. The column temperature was held at 30 °C. The eluent flow rate was held at 1 mL/min. High purity acetonitrile and DI water were used to produce eluent mixtures.

Normal phase HPLC anaylsis was perfomed using a Shimadzu UFLC LC-20AT Prominence Liquid Chromatograph using a Grace silica, 5 µm particle size, 150 mm length, 4.6 mm internal diameter column. The column temperature was held at 30 °C. The eluent flow rate was held at 1 mL/min. High purity solvents were used to produce eluent mixtures.

Single porphyrins from statistical mixtures

Porphyrins were isolated from statistical mixtures prepared from the condensation of pyrrole with aldehydes bearing the required substituents. Only the tetraester porphyrin and tetranitro porphyrin were synthesised in dedicated reactions. Porphyrin carboxylic acids were prepared as the corresponding methyl esters and hydrolysed following chromatographic separation and zinc insertion. Porphyrin quaternary ammonium salts (QASs) were prepared as the corresponding dimethylamines, and methylated following chromatographic separation and zinc insertion with the exception of the tetra QAS, which was synthesised from the tetranitro porphyrin *via* the tetraamine.

Phenylporphyrin esters

This series of porphyrins was produced as a statistical mixture from a mixed-aldehyde condensation under the condtions of Adler.[31] 4-formylbenzoic acid methyl ester (2.30 g, 14 mmol), benzaldehyde (1.49 g, 14 mmol) and pyrrole (1.89 g, 28 mmol) were mixed in refluxing propanoic acid (100 mL). The mixture was stirred for 30 minutes at reflux. Air was bubbled through the mixture for 10 minutes with vigorous stirring before cooling to room temperature. The mixture was evaporated to dryness by rotary evaporation. The porphyrins were separated and purified by flash chromatography on silica using CH_2Cl_2 moving to 98:2 DCM:ethyl acetate following the elution of the diesters. Assessment of the purity of the porphyrins was performed by ^{1}H NMR but this was not applicable to the *ABAB* isomers because of complete spectral overlap with the *AABB* isomers. HPLC analysis using CH_2Cl_2 as the mobile phase was used to assess the isomeric purity, and a purity of greater than 95% was deemed to be acceptable. Yields were calculated based on conversion of pyrrole.

5,10,15,20-tetraphenylporphyrin 2.01[31]

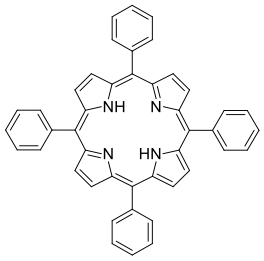

Chemical Formula: $C_{44}H_{30}N_4$
Exact Mass: 614.25
Molecular Weight: 614.74

0.078 g, 0.013 mmol, 2%.^{1}H NMR (400 MHz, $CDCl_3$): δ = -2.76 (s, 2H, NH), 7.71 – 7.80 (m, 12H, ArH), 8.19 - 8.24 (m, 8H, ArH), 8.84 (s, 8H, β pyr H). UV-vis ($CHCl_3$) λ_{max} (log ε) 418 (5.5), 512 (4.1), 550 (3.7), 590 (3.6), 645 (3.3). HRMS (ESI, MH^+): found: 615.2553, calcd. for $C_{44}H_{31}N_4$: 615.2549.

5,10,15-triphenyl-20-[4-(carboxy)phenyl]porphyrin methyl ester 2.02[164]

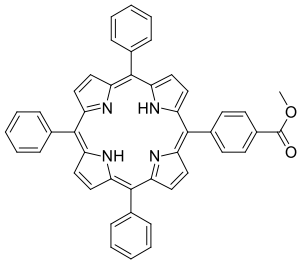

Chemical Formula: $C_{46}H_{32}N_4O_2$
Exact Mass: 672.25
Molecular Weight: 672.77

0.256 g, 0.381 mmol, 5%. ^{1}H NMR (400 MHz, $CDCl_3$): δ = -2.77 (s, 2H, NH), 4.12 (s, 3H, $OOCH_3$), 7.72 - 7.82 (m, 9H, ArH), 8.19 - 8.23 (m, 6H, ArH), 8.28 – 8.32 (m, 2H, ArH), 8.42 – 8.45 (m, 2H, ArH), 8.78 (d, *J* = 4.8 Hz, 2H, β pyr H), 8.85 (s, 4H, β pyr H), 8.86 (d, *J* = 4.9 Hz, 2H, β pyr H). UV-vis ($CHCl_3$) λ_{max} (log ε) 419 (5.5), 516 (4.1), 550 (3.7), 590 (3.5), 645 (3.4). HRMS (ESI, MH^+): found: 673.2623, calcd. for $C_{46}H_{33}N_4O_2$: 673.2604.

5,15-diphenyl-10,20-di[4-(carboxy)phenyl]porphyrin methyl ester 2.03[165]

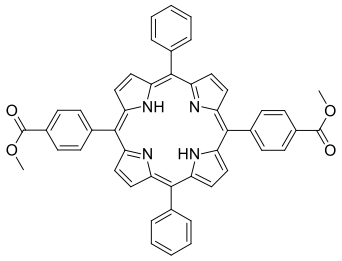

Chemical Formula: $C_{48}H_{34}N_4O_4$
Exact Mass: 730.26
Molecular Weight: 730.81

0.052 g, 0.071 mmol, 1%. ^{1}H NMR (400 MHz, $CDCl_3$): δ = -2.78 (s, 2H, NH), 4.11 (s, 6H, $OOCH_3$), 7.72 - 7.81 (m, 6H, ArH), 8.18 - 8.23 (m, 4H, ArH), 8.28 - 8.32 (m, 4H, ArH), 8.42 - 8.46 (m, 4H, ArH), 8.79 (d, *J* = 4.8 Hz, 4H, β pyr H), 8.86 (d, *J* = 4.8 Hz, 4H, β pyr H). UV-vis ($CHCl_3$) λ_{max} (log ε) 419 (5.4), 516 (4.1), 550 (3.7), 591 (3.5), 646 (3.3). HRMS (ESI, MH^+): found: 731.2665, calcd. for $C_{48}H_{35}N_4O_4$: 731.2658.

5,10-diphenyl-10,20-di[4-(carboxy)phenyl]porphyrin methyl ester 2.04[81]

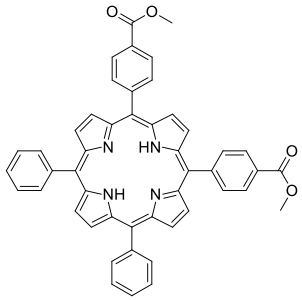

Chemical Formula: $C_{48}H_{34}N_4O_4$
Exact Mass: 730.26
Molecular Weight: 730.81

0.101 g, 0.138 mmol, 2%. ^{1}H NMR (400 MHz, $CDCl_3$): δ = -2.78 (s, 2H, NH), 4.11 (s, 6H, $OOCH_3$), 7.72 - 7.82 (m, 6H, ArH), 8.19 - 8.23 (m, 4H, ArH), 8.31 - 8.28 (m, 4H, ArH), 8.42 - 8.46 (m, 4H, ArH), 8.79 (d, *J* = 4.8 Hz, 2H, β pyr H), 8.80 (s, 2H, β pyr H), 8.85 (s, 2H, β pyr H), 8.87 (d, *J* = 4.8 Hz, 2H, β pyr H). UV-vis ($CHCl_3$) λmax (log ε) 420 (5.5), 516 (4.1), 550 (3.7), 590 (3.6), 646 (3.3). HRMS (ESI, (MH^+): found: 731.2673, calcd. for $C_{48}H_{35}N_4O_4$: 731.2658.

5-phenyl-10,15,20-tri[4-(carboxy)phenyl]porphyrin methyl ester 2.05[164]

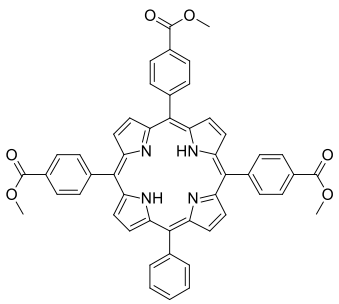

Chemical Formula: $C_{50}H_{36}N_4O_6$
Exact Mass: 788.26
Molecular Weight: 788.84

0.339 g, 0.430 mmol, 6%. ^{1}H NMR (400 MHz, $CDCl_3$): δ = -2.79 (s, 2H, NH), 4.11 (s, 9H, $OOCH_3$), 7.73 - 7.82 (m, 3H, ArH), 8.18 - 8.22 (m, 2H, ArH), 8.27 - 8.32 (m, 6H, ArH), 8.42 - 8.46 (m, 6H, ArH), 8.79 (d, *J* = 4.8 Hz, 2H, β pyr H), 8.81 (s, 4H, β pyr H), 8.87 (d, *J* = 4.8 Hz, 2H, β pyr H). UV-vis ($CHCl_3$) λmax (log ε) 420 (5.4), 516 (4.0), 550 (3.7), 590 (3.6), 646 (3.4). HRMS (ESI, MH^+): found: 789.2733, calcd. for $C_{50}H_{37}N_4O_6$: 789.2713.

Tetra[4-(carboxy)phenyl]porphyrin methyl ester 2.06[166]

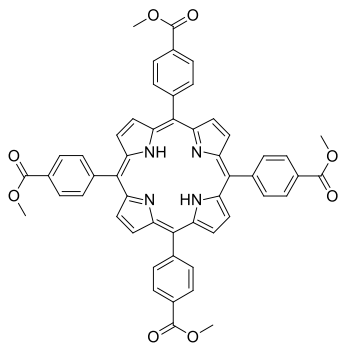

4-formylbenzoic acid methyl ester (2.189 g, 13.33 mmol) and pyrrole (0.895 g, 13.34 mmol) were added to refluxing propanoic acid (50 mL) and the mixture stirred at reflux for 30 mins. Air was bubbled through the mixture for 10 mins, which was then cooled to rt. The porphyrin crystallised and was collected by filtration and washed with 50 mL methanol. 0.494 g, 0.583 mmol, 18%. ^{1}H NMR (400 MHz, $CDCl_3$): δ = -2.80 (s, 2H, NH), 4.11 (s, 12H, $OOCH_3$), 8.27 - 8.31 (m, 8H, ArH), 8.81 (s, 8H, ArH), 8.44 - 8.47 (m, 8H, β pyr H). UV-vis ($CHCl_3$) λ_{max} (log ε) 420 (5.5), 516 (4.1), 550 (3.7), 590 (3.6), 647 (3.3). HRMS (ESI, MH^+): found: 847.2762, calcd. for $C_{52}H_{39}N_4O_8$: 847.2768.

Butylporphyrin esters

Pentanal (0.43 g, 5.0 mmol), 4-formylbenzoic acid methyl ester (0.82 g, 5.0 mmol) and pyrrole (0.67 g, 10 mmol) were dissolved in 1000 mL dichloromethane. Trifluoroacetic acid (1.7 mL, 22 mmol) was added to the stirred solution. Stirring continued 3h at 23 °C. DDQ (2.27 g, 10 mmol) was added and stirring continued for another hour. Triethylamine (3 mL, 22 mmol) added. Separated *via* chromatography on silica gel beginning with 80:20 DCM:hexane and moving to 95:5 DCM:methanol. Chromatography repeated and tetrabutyl porphyrin and mono ester porphyrin were isolated. The *syn* and *anti* diesters and the triester required a third round of chromatography before being isolated in pure form. The tetraester was not isolated. All of the porphyrins were then precipitated by addition of methanol and evaporation of the other solvents. Yields based on conversion of pyrrole.

5,10,15,20-tetrabutyl porphyrin 2.26[167]

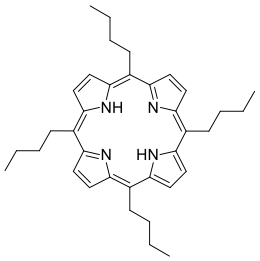

Chemical Formula: $C_{36}H_{46}N_4$
Exact Mass: 534.37
Molecular Weight: 534.78

0.004 g, 0.008 mmol, 0.3% ^{1}H NMR (400 MHz, $CDCl_3$): δ = -2.61(s, 2H, NH), 1.14 (t, *J* = 7.5 Hz, 12H, $CH_2C\mathbf{H_3}$), 1.82 (sex, *J* = 7.5 Hz, 8H, $C\mathbf{H_2}CH_3$), 2.47 – 2.55 (m, 8H, $C\mathbf{H_2}CH_2CH_3$), 4.94 (t, *J* = 7.9 Hz, 8H, $C\mathbf{H_2}CH_2CH_2CH_3$), 9.47 (s, 8H, β pyr H). UV-vis ($CHCl_3$) λ_{max} (log ε) 419 (5.4), 521 (3.9), 557 (3.7), 602 (3.3), 659 (3.5). HRMS (ESI, MH^+): found: 535.3805, calcd. for $C_{36}H_{47}N_4$: 535.3801.

5,10,15-tributyl-20-[4-(carboxy)phenyl]porphyrin methyl ester 2.27

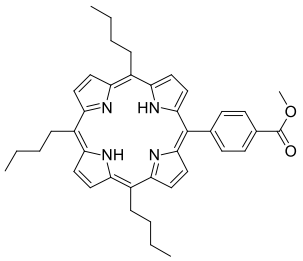

Chemical Formula: $C_{40}H_{44}N_4O_2$
Exact Mass: 612.35
Molecular Weight: 612.80

0.063 g, 0.103 mmol, 4% ^{1}H NMR (400 MHz, $CDCl_3$): δ = -2.64 (s, 2H, NH), 1.20 – 1.10 (m, 9H, $CH_2C\mathbf{H_3}$), 1.92 – 1.76 (m, 6H, $C\mathbf{H_2}CH_3$), 2.60 – 2.45 (m, 6H, $C\mathbf{H_2}CH_2CH_3$), 4.12 (s, 3H, $OOCH_3$), 4.96 (t, *J* = 7.9 Hz, 2H, $C\mathbf{H_2}CH_2CH_2CH_3$), 5.02 (t, *J* = 8.2 Hz, 2H, $C\mathbf{H_2}CH_2CH_2CH_3$), 8.23 – 8.27 (m, 2H, ArH), 8.40 – 8.44 (m, 2H, ArH), 8.73 (d, *J* = 5.0 Hz, 2H, β pyr H), 9.39 (d, *J* = 5.0 Hz, 2H, β pyr H), 9.51 (d, *J* = 5.0 Hz, 2H, β pyr H), 9.55 (d, *J* = 5.0 Hz, 2H, β pyr H). UV-vis ($CHCl_3$) λ_{max} (log ε) 419 (5.5), 520 (4.0), 555 (3.8), 598 (3.5), 655 (3.6). HRMS (ESI, (MH^+): found: 613.3543, calcd. for $C_{40}H_{45}N_4O_2$: 613.3543.

5,15-dibutyl-10,20-di[4-(carboxy)phenyl]porphyrin methyl ester 2.28

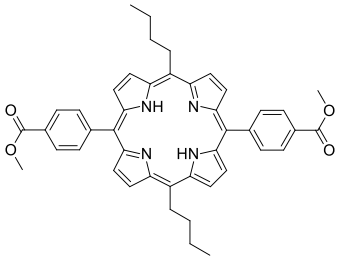

Chemical Formula: $C_{44}H_{42}N_4O_4$
Exact Mass: 690.32
Molecular Weight: 690.83

0.047 g, 0.068 mmol, 3% ^{1}H NMR (400 MHz, $CDCl_3$): δ = -2.69 (s, 2H, NH), 1.11 (t, *J* = 7.4 Hz, 6H, $CH_2C\mathbf{H_3}$), 1.80 (sex, *J* = 7.4 Hz, 4H, $C\mathbf{H_2}CH_3$), 2.55 – 2.45 (m, 4H, $C\mathbf{H_2}CH_2CH_3$), 4.13 (s, 6H, $OOCH_3$), 4.97 (t, *J* = 8.0 Hz, 4H $C\mathbf{H_2}CH_2CH_2CH_3$), 8.30 – 8.26 (m, 4H, ArH), 8.46 – 8.43 (m, 4H, ArH), 8.80 (d, *J* = 4.9 Hz, 4H, β pyr H), 9.44 (d, *J* = 4.9 Hz, 4H, β pyr H). UV-vis ($CHCl_3$) λ_{max} (log ε) 421 (5.8), 518 (4.5), 554 (4.2), 595 (3.9), 652 (4.0). HRMS (ESI, (MH^+): found: 691.3289, calcd. for $C_{44}H_{43}N_4O_4$: 691.3284.

5,10-dibutyl-10,20-di[4-(carboxy)phenyl]porphyrin methyl ester 2.29

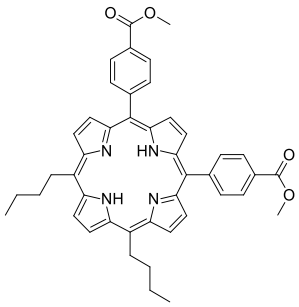

Chemical Formula: $C_{44}H_{42}N_4O_4$
Exact Mass: 690.32
Molecular Weight: 690.83

0.062 g, 0.090 mmol, 4% ^{1}H NMR (400 MHz, $CDCl_3$): δ = -2.69 (s, 2H, NH), 1.15 (t, *J* = 7.5 Hz, 6H, $CH_2C\mathbf{H_3}$), 1.84 (sex, 7.5 Hz, 4H, $C\mathbf{H_2}CH_3$), 2.50 – 2.60 (m, 4H, $C\mathbf{H_2}CH_2CH_3$), 4.11 (s, 6H, $OOCH_3$), 5.03 (t, *J* = 8.1 Hz, 4H, $C\mathbf{H_2}CH_2CH_2CH3$), 8.23 – 8.28 (m, 4H, ArH), 8.40 – 8.44 (m, 4H, ArH), 8.68 (s, 2H, β pyr H), 8.80 (d, *J* = 4.8 Hz, 2H, β pyr H), 9.47 (d, *J* = 4.8 Hz, 2H, β pyr H), 9.59 (s, 2H, β pyr H). UV-vis ($CHCl_3$) λ_{max} (log ε) 420 (5.4), 519 (3.9), 554 (3.6), 596 (3.4), 652 (3.4). HRMS (ESI, (MH^+)): found: 691.3286, calcd. for $C_{44}H_{43}N_4O_4$: 691.3284.

5-butyl-10,15,20-tri[4-(carboxy)phenyl]porphyrin methyl ester 2.30

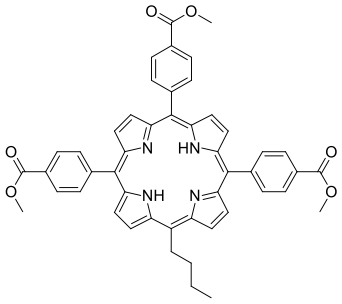

Chemical Formula: $C_{48}H_{40}N_4O_6$
Exact Mass: 768.29
Molecular Weight: 768.85

0.099 g, 0.129 mmol, 5% ^{1}H NMR (400 MHz, $CDCl_3$): δ = -2.74 (s, 2H, NH), 1.13 (t, *J* = 7.4 Hz, 3H, $CH_2C\mathbf{H_3}$), 1.83 (sex, *J* = 7.4 Hz, 2H, $C\mathbf{H_2}CH_3$), 2.49 – 2.59 (m, 2H, $C\mathbf{H_2}CH_2CH_3$), 4.10 (s, 3H, $OOCH_3$), 4.12 (s, 6H, $OOCH_3$), 5.04 (t, *J* = 7.9 Hz, 2H, $C\mathbf{H_2}CH_2CH_2CH_3$), 8.24 – 8.31 (m, 6H, ArH), 8.40 – 8.46 (m, 6H, ArH), 8.75 (s, 4H, β pyr H), 8.86 (d, *J* = 4.8 Hz, 2H, β pyr H), 9.52 (d, *J* = 4.8 Hz, 2H, β pyr H). UV-vis ($CHCl_3$) λ_{max} (log ε) 420 (5.5), 517 (4.2), 552 (3.9), 593 (3.6), 649 (3.6). HRMS (ESI, MH^+): found: 769.3024, calcd. for $C_{48}H_{41}N_4O_6$: 769.3026.

Aminoporphyrins

Benzaldehyde (0.796 g, 7.5 mmol), 4-(*N,N*-dimethylamino)benzaldehyde (1.124 g, 7.5 mmol) and pyrrole (1.006 g, 15 mmol) were dissolved in DCM (1500 mL). Trifluoroacetic acid (2.5 mL, 33 mmol) was added and the mixture stirred at 1h rt with light excluded. Chloranil (3.688 g, 15 mmol) was added and the mixture heated at reflux for 30 mins. Triethylamine (5 mL, 36 mmol) was added and the mixture evaporated to dryness. Separated *via*

chromatography on silica using DCM moving to 1:1:98 triethylamine:methanol:DCM following elution of the monoamine. Pure porphyrin fractions were concentrated and the products precipitated *via* the addition of methanol. Products were collected by filtration.

5,10,15-triphenyl-20-[N-dimethyl-4-aminophenyl]porphyrin 2.44[91]

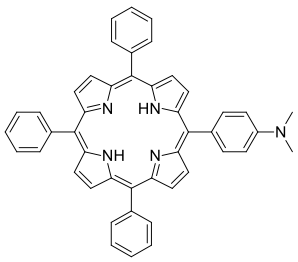

Chemical Formula: $C_{46}H_{35}N_5$
Exact Mass: 657.29
Molecular Weight: 657.80

0.076 g, 0.12 mmol, 3%. ^{1}H NMR (400 MHz, $CDCl_3$): δ = -2.71 (s, 2H, NH), 3.24 (s, 6H, NCH_3), 7.09 – 7.13 (m, 2H, ArH), 7.71 – 7.80 (m, 9H, ArH), 8.06 – 8.11 (m, 2H, ArH), 8.19 – 8.24 (m, 6H, ArH), 8.80 – 8.84 (m, 6H, , β pyr H), 8.95 (d, *J* = 4.8 Hz, 2H, β pyr H). UV-vis ($CHCl_3$) λ_{max} (log ε) 420 (5.3), 519 (4.1), 558 (3.9), 593 (3.6), 652 (3.6). HRMS (ESI, (MH^+): found: 658.2973, calcd. for $C_{46}H_{36}N_5$: 658.971.

5,15-diphenyl-10,20-di[N-dimethyl-4-aminophenyl]porphyrin 2.45

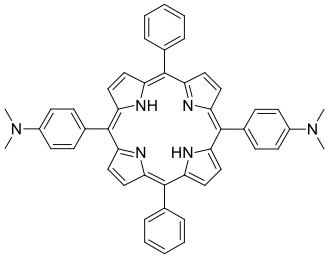

Chemical Formula: $C_{48}H_{40}N_6$
Exact Mass: 700.33
Molecular Weight: 700.87

0.027 g, 0.039 mmol, 1%. ^{1}H NMR (400 MHz, $CDCl_3$): δ = -2.66 (s, 2H, NH), 3.23 (s, 12H, NCH_3), 7.08 – 7.13 (m, 4H, ArH), 7.71 – 7.80 (m, 6H, ArH), 8.06 – 8.11 (m, 4H, ArH), 8.20 – 8.25 (m, 4H, ArH), 8.80 (d, *J* = 4.8 Hz, 4H, β pyr H), 8.93 (d, *J* = 4.8, 4H, β pyr H). UV-vis ($CHCl_3$) λ_{max} (log ε) 425 (5.1), 522 (4.0), 565 (4.0), 655 (3.7). HRMS (ESI, (MH^+): found: 701.3413, calcd. for $C_{48}H_{41}N_6$: 701.3393.

5,10-diphenyl-15,20-di[N-dimethyl-4-aminophenyl]porphyrin 2.46

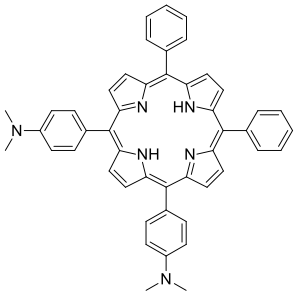

Chemical Formula: $C_{48}H_{40}N_6$
Exact Mass: 700.33
Molecular Weight: 700.87

0.004 g, 0.005 mmol, 0.2%. ^{1}H NMR (400 MHz, $CDCl_3$): δ = -2.65 (s, 2H, NH), 3.22 (s, 12H, NCH_3), 7.07 – 7.14 (m, 4H, ArH), 7.70 – 7.79 (m, 6H, ArH), 8.06 – 8.12 (m, 4H, ArH), 8.19 – 8.24 (m, 4H, ArH), 8.78 - 8.82 (m, 4H, β pyr H), 8.91 – 8.95 (m, 4H, β pyr H). UV-vis ($CHCl_3$) λ_{max} (log ε) 426 (5.1), 522 (3.9), 565 (3.9), 656 (3.6). HRMS (ESI, (MH^+): found: 701.3413, calcd. for $C_{48}H_{41}N_6$: 701.3393.

5-phenyl-10,15,20-tri[N-dimethyl-4-aminophenyl]porphyrin 2.47

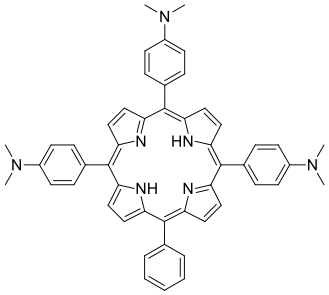

Chemical Formula: $C_{50}H_{45}N_7$
Exact Mass: 743.37
Molecular Weight: 743.94

0.022 g, 0.030 mmol, 0.8%. ^{1}H NMR (400 MHz, $CDCl_3$): δ = -2.62 (s, 2H, NH), 3.23 (s, 12H, NCH_3), 7.08 – 7.14 (m, 6H, ArH), 7.70 – 7.80 (m, 3H, ArH), 8.06 – 8.12 (m, 6H, ArH), 8.19 – 8.25 (m, 2H, ArH), 8.78 (d, *J* = 4.7 Hz, 2H, β pyr H), 8.89 – 8.93 (m, 6H, β pyr H). UV-vis ($CHCl_3$) λ_{max} (log ε) 434 (5.1), 526 (3.9), 570 (4.0), 660 (3.7). HRMS (ESI, (MH^+): found: 744.3818, calcd. for $C_{50}H_{46}N_7$: 744.3815.

5,10,15,20-tetra[4-nitrophenyl]porphyrin 2.49[94]

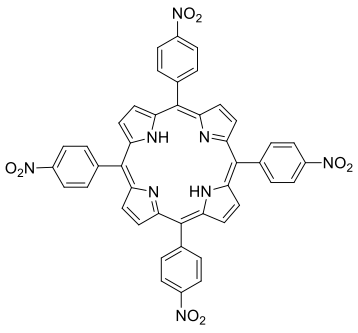

Chemical Formula: $C_{44}H_{26}N_8O_8$
Exact Mass: 794.19
Molecular Weight: 794.73

Synthesised according to a published procedure.[94] 4-Nitrobenzaldehyde (0.60 g, 4.0 mmol) was mixed with propionic acid (16 mL) and heated to reflux. Acetic anhydride (0.70 mL, 7.4 mmol) and pyrrole (0.27 g, 4.0 mmol) were added. The mixture was stirred at reflux for 45 mins and then allowed to cool to rt. A precipitate formed and this was collected by filtration. It was washed with pyridine (5 mL) and then with acetone (3 x 40 mL). 156 mg, 0.196 mmol, 20%. ^{1}H NMR (400 MHz, $CDCl_3$): δ = -2.81 (s, 2H, NH), 8.37 – 8.43 (m, 8H, ArH), 8.64 – 8.70 (m, 8H, ArH), 8.82 (s, 8H, β pyr H). UV-vis ($CHCl_3$) λ_{max} (log ε) 428 (5.1), 523 (3.7), 562 (3.9), 656 (3.6). HRMS (ESI, M^+): found: 795.1946, calcd. for $C_{44}H_{27}N_8O_8$: 795.1952

5,10,15,20-tetra[4-aminophenyl]porphyrin 2.50[94]

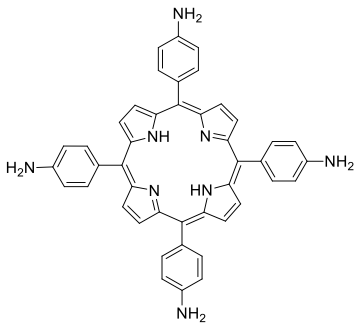

Chemical Formula: $C_{44}H_{34}N_8$
Exact Mass: 674.29
Molecular Weight: 674.79

5,10,15,20-Di[4-nitrophenyl]porphyrin (0.021 g, 0.026 mmol) was mixed with 32% HCl solution in water (5 mL). Heated to 70 °C with stirring and $SnCl_2$ (0.100 g, 0.527 mmol) was added. After 30 mins the mixture was filtered and the filtrate neutralised with solid $NaHCO_3$. Ammonia solution (28 %) in water was added. A precipitate formed and this was allowed to settle. The majority of the supernatant was decanted and the precipitate was collected by centrifugation and rinsed with ammonia solution before drying. 0.013 g, 0.020 mmol, 77%. ^{1}H NMR (400 MHz, $CDCl_3$): δ = -2.70 (s, 2H, NH), 7.04 – 7.08 (m, 8H, ArH), 7.96 – 8.01 (m, 8H, ArH), 8.89 (s, 8H, β pyr H). UV-vis (DMSO) λ_{max} (log ε) 439 (4.8), 581 (3.9), 668 (3.6). HRMS (ESI, M^+): found: 675.3002, clacd. for $C_{44}H_{35}N_8$: 675.2985.

Zinc metalated porphyrins

Typical zinc insertion conditions

To a solution of the *AABB* tetraphenyl porphyrin diester (18 mg, 0.025 mmol) in CH_2Cl_2 was added zinc acetate dihydrate (11 mg, 0.049 mmol) dissolved in 1 mL of methanol. The reaction was monitored by TLC using CH_2Cl_2 as mobile phase and was finished within two hours. The solution was concentrated by rotary evaporation and methanol added to induce precipitation of the zinc porphyrin which was then collected by filtration. Conversion to the zinc complex was quantitative except where noted otherwise.

Zn phenylporphyrin esters

Zn 5,10,15,20-tetraphenyl porphyrin 2.07[168]

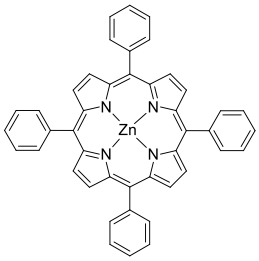

Chemical Formula: $C_{44}H_{28}N_4Zn$
Exact Mass: 676.16
Molecular Weight: 678.10

^{1}H NMR (400 MHz, $CDCl_3$): δ = 7.71 – 7.80 (m, 12H, ArH), 8.19 - 8.25 (m, 8H, ArH), 8.94 (s, 8H, β pyr H). UV-vis ($CHCl_3$) λ_{max} (log ε) 421 (5.5), 550 (4.1), 593 (3.5). HRMS (ESI, M^+): found: 676.1599, calcd. for $C_{44}H_{28}N_4O_4Zn$: 676.1605.

Zn 5,10,15-triphenyl-20-[4-(carboxy)phenyl]porphyrin methyl ester 2.08[169]

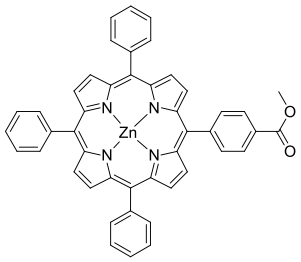

Chemical Formula: $C_{46}H_{30}N_4O_2Zn$
Exact Mass: 734.17
Molecular Weight: 736.14

^{1}H NMR (400 MHz, $CDCl_3$): δ = 4.12 (s, 3H, OCH_3), 7.71 - 7.81 (m, 9H, ArH), 8.19 – 8.24 (m, 6H, ArH), 8.29 – 8.34 (m, 2H, ArH), 8.41 - 8.45 (m, 2H, ArH), 8.89 (d, *J* = 4.7 Hz, 2H, β pyr H), 8.95 (s, 4H, β pyr H), 8.96 (d, *J* = 4.7 Hz, 2H, β pyr H). UV-vis ($CHCl_3$) λ_{max} (log ε) 423 (5.5), 551 (4.1), 593 (3.5). HRMS (ESI, M^+): found: 734.1654, calcd. for $C_{46}H_{30}N_4O_2Zn$: 734.1660.

Zn 5,15-diphenyl-10,20-di[4-(carboxy)phenyl]porphyrin methyl ester 2.09

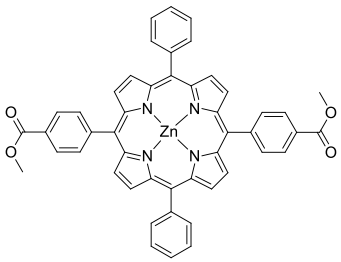

Chemical Formula: $C_{48}H_{32}N_4O_4Zn$
Exact Mass: 792.17
Molecular Weight: 794.17

^{1}H NMR (400 MHz, $CDCl_3$): δ = 4.14 (s, 6H, OCH_3), 7.75 - 7.84 (m, 6H, ArH), 8.21 – 8.26 (m, 4H, ArH), 8.31 – 8.35 (m, 4H, ArH), 8.44 – 8.48 (m, 4H, ArH), 8.92 (d, *J* = 6.5 Hz, 4H, β pyr H), 8.99 (d, *J* = 6.5 Hz, 4H, β pyr H). UV-vis ($CHCl_3$) λ_{max} (log ε) 424 (5.4), 551 (4.1), 594 (3.5). HRMS (ESI, M^+): found: 792.1718, calcd. for $C_{48}H_{32}N_4O_4Zn$: 792.1715.

Zn 5,10-diphenyl-15,20-di[4-(carboxy)phenyl]porphyrin methyl ester 2.10

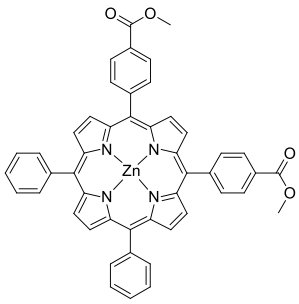

Chemical Formula: $C_{48}H_{32}N_4O_4Zn$
Exact Mass: 792.17
Molecular Weight: 794.17

^{1}H NMR (400 MHz, $CDCl_3$): δ = 4.11 (s, 6H, OCH_3), 7.72 - 7.81 (m, 6H, ArH), 8.19 - 8.24 (m, 4H, ArH), 8.28 – 8.32 (m, 4H, ArH), 8.42 – 8.45 (m, 4H, ArH), 8.89 (d, *J* = 4.8, 2H, β pyr H), 8.90 (s, 2H, β pyr H), 8.96 (s, 2H, β pyr H), 8.97 (d, *J* = 4.8, 2H, β pyr H). UV-vis ($CHCl_3$) λ_{max} (log ε) 424 (5.4), 552 (4.0), 594 (3.4). HRMS (ESI, M^+): found: 792.1716, calcd. for $C_{48}H_{32}N_4O_4Zn$: 792.1715.

Zn 5-phenyl-10,15,20-tri[4-(carboxy)phenyl]porphyrin methyl ester 2.11

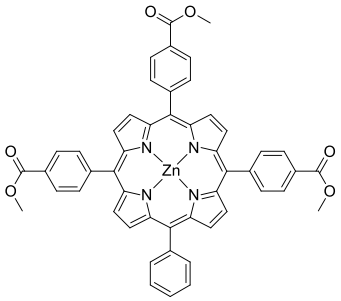

Chemical Formula: $C_{50}H_{34}N_4O_6Zn$
Exact Mass: 850.18
Molecular Weight: 852.21

^{1}H NMR (400 MHz, $CDCl_3$): δ = 4.11 (s, 9H, OCH_3), 7.72 - 7.81 (m, 3H, ArH), 8.18 – 8.23 (m, 2H, ArH), 8.28 – 8.33 (m, 6H, ArH), 8.41 – 8.46 (m, 6H, ArH), 8.90 (d, *J* = 4.8 Hz, 2H, β pyr H), 8.91 (s, 4H, β pyr H), 8.97 (d, *J* = 4.8 Hz, 2H, β pyr H). UV-vis ($CHCl_3$) λ_{max} (log ε) 425 (5.8), 553 (4.4), 595 (3.8). HRMS (ESI, M^+): found: 850.1767, calcd. for $C_{50}H_{34}N_4O_6Zn$: 850.1770.

Zn 5,10,15,20-tetra[4-(carboxy)phenyl]porphyrin methyl ester 2.12[170]

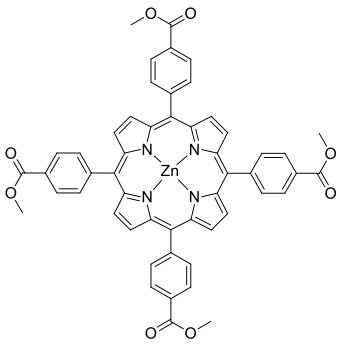

Chemical Formula: $C_{52}H_{36}N_4O_8Zn$
Exact Mass: 908.18
Molecular Weight: 910.24

^{1}H NMR (400 MHz, $CDCl_3$): δ = 4.11 (s, 12H, OCH_3), 8.28 - 8.32 (m, 8H, ArH), 8.43 - 8.47 (m, 8H, ArH), 8.92 (s, 8H, β pyr H). UV-vis ($CHCl_3$) λ_{max} (log ε) 426 (5.3), 554 (4.0), 595 (3.7). HRMS (ESI, M^+): found: 908.1846, calcd. for $C_{52}H_{36}N_4O_8Zn$: 908.1825.

Zn butylporphyrin esters

Zn 5,10,15,20-tetrabutyl porphyrin 2.33

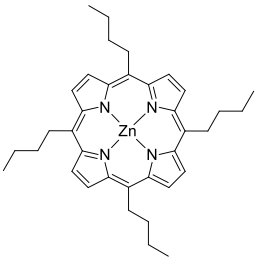

Chemical Formula: $C_{36}H_{44}N_4Zn$
Exact Mass: 596.29
Molecular Weight: 598.14

^{1}H NMR (400 MHz, $CDCl_3$): δ = 1.17 (t, *J* = 7.3 Hz, 12H, $CH_2\mathbf{CH_3}$), 1.87 (sex, *J* = 7.3 Hz, 8H, $C\mathbf{H_2}CH_3$), 2.51 - 2.61 (m, 8H, $C\mathbf{H_2}CH_2CH_3$), 4.99 (t, *J* = 8.2 Hz, 8H, $C\mathbf{H_2}CH_2CH_2CH_3$), 9.59 (s, 8H, β pyr H). UV-vis ($CHCl_3$) λ_{max} (log ε) 402 (4.6), 421(5.6), 556 (4.1), 595 (3.7). HRMS (ESI, M^+): found: 596.2875, calcd. for $C_{36}H_{44}N_4Zn$: 596.2857.

Zn 5,10,15-tributyl-20-[4-(carboxy)phenyl]porphyrin methyl ester 2.34

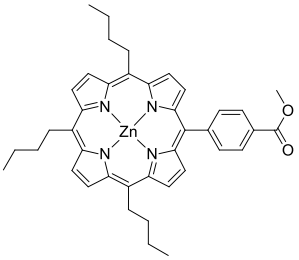

Chemical Formula: $C_{40}H_{42}N_4O_2Zn$
Exact Mass: 674.26
Molecular Weight: 676.17

^{1}H NMR (400 MHz, $CDCl_3$): δ = 1.15 (t, *J* = 7.4 Hz, 6H, $CH_2C\mathbf{H_3}$), 1.18 (t, *J* = 7.4 Hz, 3H, $CH_2C\mathbf{H_3}$), 1.79 - 1.94 (m, 6H, $C\mathbf{H_2}CH_3$), 2.49 - 2.61 (m, 6H, $C\mathbf{H_2}CH_2CH_3$), 4.13 (s, 3H, OCH_3), 4.93 - 5.01 (m, 6H, $C\mathbf{H_2}CH_2CH_2CH_3$), 8.24 - 8.28 (m, 2H, ArH), 8.41 - 8.45 (m, 2H, ArH), 8.83 (d, *J* = 4.6 Hz, 2H, β pyr H), 9.50 (d, *J* = 4.8 Hz, 2H, β pyr H), 9.57 (d, *J* = 5.0 Hz, 2H, β pyr H), 9.58 (d, *J* = 5.0 Hz, 2H, β pyr H). UV-vis ($CHCl_3$) λ_{max} (log ε) 422 (5.1), 555 (4.1), 598 (3.6). HRMS (ESI, M^+): found: 674.2607, calcd. for $C_{40}H_{42}N_4O_2Zn$: 674.2599.

Zn 5,15-dibutyl-10,20-di[4-(carboxy)phenyl]porphyrin methyl ester 2.35

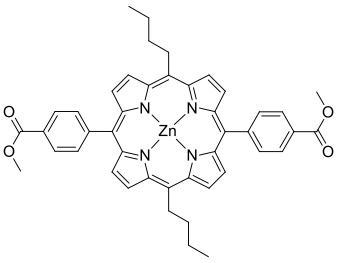

Chemical Formula: $C_{44}H_{40}N_4O_4Zn$
Exact Mass: 752.23
Molecular Weight: 754.19

^{1}H NMR (400 MHz, $CDCl_3$): δ = 1.14 (t, *J* = 7.5 Hz, 6H, $CH_2\mathbf{CH_3}$), 1.84 (sex, *J* = 7.5 Hz, 4H, $C\mathbf{H_2}CH_3$), 2.50 - 2.60 (m, 4H, $C\mathbf{H_2}CH_2CH_3$), 4.13 (s, 6H, OCH_3), 5.03 (t, *J* = 8.1 Hz, 4H, $C\mathbf{H_2}CH_2CH_2CH_3$), 8.27 – 8.29 (m, 2H, ArH), 8.29 – 8.31 (m, 2H, ArH), 8.42 – 8.45 (m, 2H, ArH), 8.45 – 8.47 (m, 2H, ArH), 8.91 (d, *J* = 4.8 Hz, 4H, β pyr H), 9.57 (d, *J* = 4.8 Hz, 4H, β pyr H). UV-vis ($CHCl_3$) λ_{max} (log ε) 424 (5.6), 555 (4.3), 597 (3.9). HRMS (ESI, M^+): found: 752.2341, calcd. for $C_{44}H_{40}N_4O_4Zn$: 752.2341.

Zn 5,10-dibutyl-15,20-di[4-(carboxy)phenyl]porphyrin methyl ester 2.36

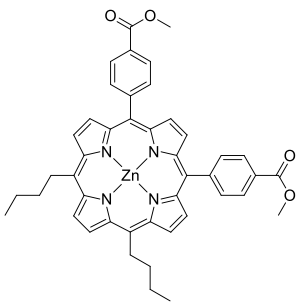

^{1}H NMR (400 MHz, $CDCl_3$): δ = 1.17 (t, *J* = 7.4 Hz, 6H, $CH_2C\mathbf{H_3}$), 1.87 (sex, *J* = 7.4 Hz, 4H, $C\mathbf{H_2}CH_3$), 2.51 - 2.61 (m, 4H, $C\mathbf{H_2}CH_2CH_3$), 4.11 (s, 6H, OCH_3), 5.02 (t, *J* = 8.2 Hz, 4H, $C\mathbf{H_2}CH_2CH_2CH_3$), 8.24 - 8.28 (m, 4H, ArH), 8.40 - 8.44 (m, 4H, ArH), 8.79 (s, 2H, , β pyr H), 8.89 (d, *J* = 4.6 Hz, 2H, β pyr H), 9.56 (d, *J* = 4.6 Hz, 2H, β pyr H), 9.63 (s, 2H, β pyr H). UV-vis ($CHCl_3$) λ_{max} (log ε) 424 (5.1), 554 (4.1), 598 (3.6). HRMS (ESI, M^+): found: 752.2345, calcd. for $C_{44}H_{40}N_4O_4Zn$: 752.2341.

Zn 5-butyl-10,15,20-tri[4-(carboxy)phenyl]porphyrin methyl ester 2.37

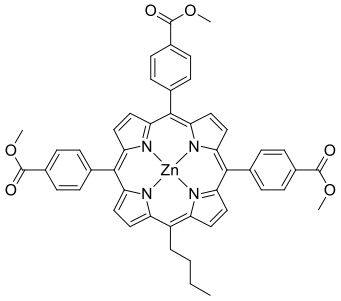

^{1}H NMR (400 MHz, $CDCl_3$): δ = 1.16 (t, *J* = 7.4 Hz, 3H, $CH_2C\mathbf{H_3}$), 1.87 (sex, *J* = 7.6 Hz, 2H, $C\mathbf{H_2}CH_3$), 2.54 - 2.64 (m, 2H, $C\mathbf{H_2}CH_2CH_3$), 4.10 (s, 3H), 4.12 (s, 6H, OCH_3), 5.09 (t, *J* = 7.7 Hz, 2H, $C\mathbf{H_2}CH_2CH_2CH_3$), 8.25 - 8.31 (m, 6H, ArH), 8.40 - 8.46 (m, 6H, ArH), 8.85 (d, *J* = 4.8 Hz, 2H, β pyr H), 8.86 (d, *J* = 4.8 Hz, 2H, β pyr H), 8.97 (d, *J* = 4.8 Hz, 2H, β pyr H), 9.64 (d, *J* = 4.8 Hz, 2H, β pyr H). UV-vis ($CHCl_3$) λ_{max} (log ε) 425 (5.7), 554 (4.3), 597 (3.8). HRMS (ESI, M^+): found: 830.2072, calcd. for $C_{48}H_{38}N_4O_6Zn$: 830.2083.

Zn phenylporphyrin amines

Zn 5,10,15-triphenyl-20-[N-dimethyl-4-aminophenyl]porphyrin 2.51

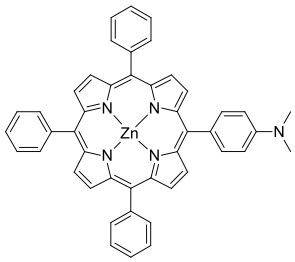

Chemical Formula: $C_{46}H_{33}N_5Zn$
Exact Mass: 719.20
Molecular Weight: 721.17

^{1}H NMR (400 MHz, $CDCl_3$): δ = 3.20 (s, 6H, NCH_3), 7.06 – 7.11 (m, 2H, ArH), 7.70 – 7.80 (m, 9H, ArH), 8.05 – 8.10 (m, 2H, ArH), 8.20 – 8.25 (m, 6H, ArH), 8.91 – 8.94 (m, 6H, β pyr H), 9.06 (d, *J* = 4.6 Hz, 2H, β pyr H). UV-vis ($CHCl_3$) λ_{max} (log ε) 425 (5.4), 553 (4.1), 596 (3.7). HRMS (ESI, M^+): found: 719.2039, calcd. for $C_{46}H_{33}N_5Zn$: 719.2027.

Zn 5,15-diphenyl-10,20-di[N-dimethyl-4-aminophenyl]porphyrin 2.52

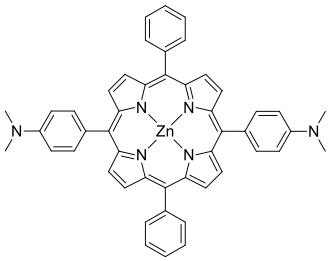

Chemical Formula: $C_{48}H_{38}N_6Zn$
Exact Mass: 762.24
Molecular Weight: 764.24

^{1}H NMR (400 MHz, $CDCl_3$): δ = 3.24 (s, 12H, NCH_3), 7.09 – 7.13 (m, 4H, ArH), 7.71 – 7.79 (m, 6H, ArH), 8.06 – 8.11 (m, 4H, ArH), 8.20 – 8.25 (m, 4H, ArH), 8.91 (d, *J* = 4.8 Hz, 4H, β pyr H), 9.04 (d, *J* = 4.8 Hz, 4H, β pyr H). UV-vis ($CHCl_3$) λ_{max} (log ε) 430 (5.0), 556 (3.8), 600 (3.6). HRMS (ESI, M^+): found: 762.2463, calcd. for $C_{48}H_{38}N_6Zn$: 762.2449.

Zn 5,10-diphenyl-15,20-di[N-dimethyl-4-aminophenyl]porphyrin 2.53

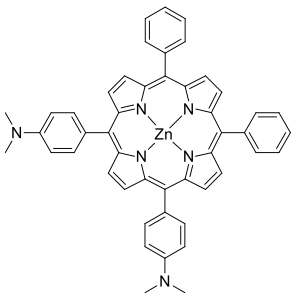

Chemical Formula: $C_{48}H_{38}N_6Zn$
Exact Mass: 762.24
Molecular Weight: 764.24

^{1}H NMR (400 MHz, $CDCl_3$): δ = 3.17 (s, 12H, NCH_3), 7.04 – 7.10 (m, 4H, ArH), 7.70 – 7.79 (m, 6H, ArH), 8.04 – 8.10 (m, 4H, ArH), 8.20 – 8.25 (m, 4H, ArH), 8.91 (d, *J* = 4.6 Hz, 2H, β pyr H), 8.91 (s, 2H, β pyr H), 9.04 (s, 2H, β pyr H), 9.04 (d, *J* = 4.6 Hz, 2H, β pyr H). UV-vis ($CHCl_3$) λ_{max} (log ε) 430 (5.3), 555 (4.1), 600 (3.8). HRMS (ESI, M^+): found: 762.2455, calcd. for $C_{48}H_{38}N_6Zn$: 762.2449.

Zn 5-phenyl-10,15,20-tri[N-dimethyl-4-aminophenyl]porphyrin 2.54

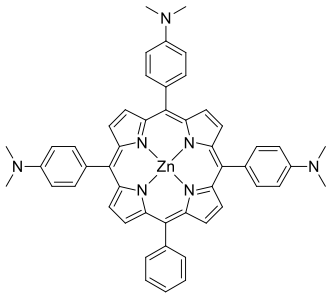

Chemical Formula: $C_{50}H_{43}N_7Zn$
Exact Mass: 805.29
Molecular Weight: 807.30

^{1}H NMR (400 MHz, $CDCl_3$): δ = 3.22 (s, 12H, NCH_3), 3.33 (s, 6H, NCH_3), 7.07 – 7.12 (m, 6H, ArH), 7.70 – 7.79 (m, 3H, ArH), 8.06 – 8.12 (m, 6H, ArH), 8.20 – 8.24 (m, 2H, ArH), 8.89 (d, *J* = 4.6 Hz, 2H, β pyr H), 9.06 (d, *J* = 4.6 Hz, 2H, β pyr H), 9.03 (s, 4H, β pyr H). UV-vis ($CHCl_3$) λ_{max} (log ε) 436 (5.2), 558 (4.0), 603 (3.9). HRMS (ESI, M^+): found: 805.2877, calcd. for $C_{50}H_{43}N_7Zn$: 805.2871.

Zn 5,10,15,20-tetra[4-aminophenyl]porphyrin 2.55[171]

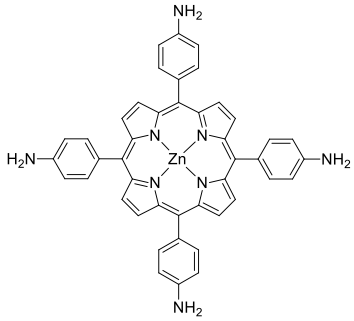

Chemical Formula: $C_{44}H_{32}N_8Zn$
Exact Mass: 736.20
Molecular Weight: 738.16

24% ^{1}H NMR (400 MHz, $CDCl_3$): δ = 7.80 – 7.94 (m, 4H), 8.05 – 8.20 (m, 4H), 8.84 – 9.04 (m, 8H). UV-vis ($CHCl_3$) λ_{max} (log ε) 412 (4.6), 439 (4.9), 578 (3.8), 668 (3.6). HRMS (ESI, M^+): found: 737.2136, calcd. For $C_{44}H_{33}N_8Zn$: 737.2120.

Iron-metalated phenylporphyrins

General iron insertion conditions: Porphyrin dissolved in DCM and heated to reflux. A solution of 10 equivalents of $FeCl_2.4H_2O$ dissolved in 1 mL of methanol and 10 equivalents of NaOAc dissolved in 1 mL of methanol was added. The mixture was stirred, and extra portions of $FeCl_2$ added until TLC analysis indicated completion. The mixture was washed three times with with HCl, dried with $MgSO_4$ and recovered by evaporation or addition of hexane.

FeCl 5,10,15-triphenyl-20-[4-(carboxy)phenyl]porphyrin methyl ester 2.13

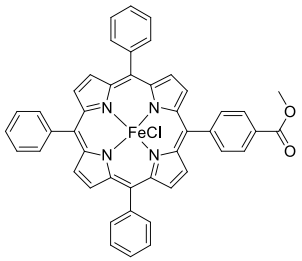

Chemical Formula: $C_{46}H_{30}ClFeN_4O_2$
Exact Mass: 761.14
Molecular Weight: 762.05

75% UV-vis (DMF) λ_{max} (log ε) 408 (4.7), 570 (3.6), 610 (3.3). HRMS (ESI, M^+): found 762.1449:, calcd. for $C_{46}H_{31}N_4O_2FeCl$: 762.1485.

FeCl 5,15-diphenyl-10,20-di[4-(carboxy)phenyl]porphyrin methyl ester 2.14

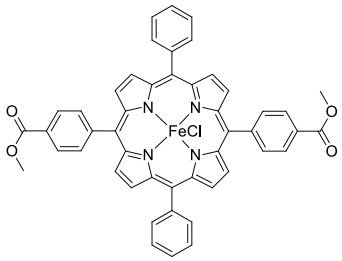

Chemical Formula: $C_{48}H_{32}ClFeN_4O_4$
Exact Mass: 819.15
Molecular Weight: 820.09

79% UV-vis (DMF) λ_{max} (log ε) 409 (4.7), 570 (3.6), 610 (3.3). HRMS (ESI, M^+): found: 784.1798, calcd. for $C_{48}H_{32}N_4O_4Fe$: 784.1773.

FeCl 5,10-diphenyl-15,20-di[4-(carboxy)phenyl]porphyrin methyl ester 2.15

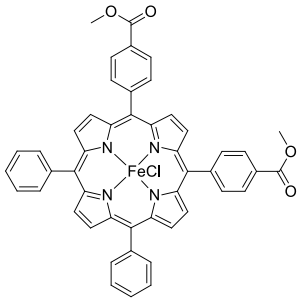

Chemical Formula: $C_{48}H_{32}ClFeN_4O_4$
Exact Mass: 819.15
Molecular Weight: 820.09

70% UV-vis (DMF) λ_{max} (log ε) 409 (4.7), 570 (3.6), 610 (3.3). HRMS (ESI, M^+): found: 784.1799, calcd. for $C_{48}H_{32}N_4O_2Fe$: 784.1733.

FeCl 5-phenyl-10,15,20-tri[4-(carboxy)phenyl]porphyrin methyl ester 2.16

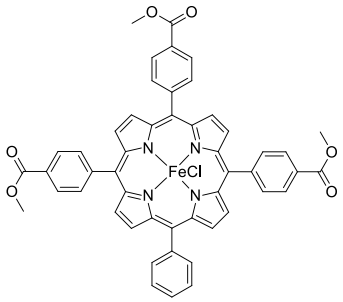

Chemical Formula: $C_{50}H_{34}ClFeN_4O_6$
Exact Mass: 877.15
Molecular Weight: 878.13

60% UV-vis (DMF) λ_{max} (log ε) 410 (4.8), 570 (3.6), 610 (3.3). HRMS (ESI, M^+): found: 842.1860, calcd. for $C_{50}H_{34}N_4O_6Fe$: 842.1828.

Porphyrin carboxylic acids

Typical ester hydrolysis conditions

Zn *ABAB* tetraphenylporphyrin diester (29 mg) was dissolved in a tetrahydrofuran (10 mL). A mixture of potassium hydroxide (116 mg, 2.08 mmol), water (0.9 mL) and methanol (9 mL) was added. The solution was heated at reflux for three hours and then allowed to cool to room temperature. 10 mL of water was added and the the organic solvents were evaporated by rotary evaporation. The solution was acidified with phosphoric acid solution, which induced precipitation of the porphyrin. Fe porphyrins were treated with 3% HCl instead. The porphyrin was compressed to a pellet by centrifugation at 2500 rpm for 10 mins. The supernatant liquid was then removed with a pipette, water added and centrifugation repeated. After four rounds of centrifugation the porphyrin was dried with a flow of nitrogen and then in a vacuum oven at 50 °C.

Zn phenylporphyrin carboxylic acids

Zn 5,10,15-triphenyl-20-[4-(carboxy)phenyl]porphyrin 2.17[172]

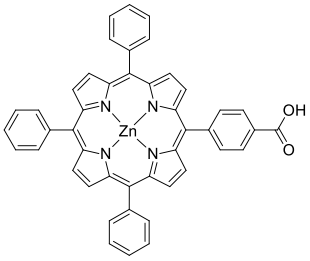

Chemical Formula: $C_{45}H_{28}N_4O_2Zn$
Exact Mass: 720.15
Molecular Weight: 722.11

87% ^{1}H NMR (400 MHz, D_6-DMSO): δ = 7.72 - 7.82 (m, 9H, ArH), 8.19 - 8.25 (m, 8H, ArH), 8.33 – 8.38 (m, 2H, ArH), 8.47 - 8.51 (m, 2H, ArH), 8.90 (d, *J* = 4.8 Hz, 2H, β pyr H), 8.96 (s, 4H, β pyr H), 8.98 (d, *J* = 4.8 Hz, 2H, β pyr H). UV-vis (DMSO) λ_{max} (log ε) 408 (4.6), 428 (5.6), 561 (4.3), 601 (4.0). HRMS (ESI, M^+): found: 720.1501, calcd. for $C_{45}H_{28}N_4O_2Zn$: 720.1504.

Zn 5,15-diphenyl-10,20-di[4-(carboxy)phenyl]porphyrin 2.18

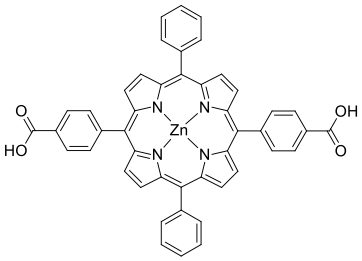

Chemical Formula: $C_{46}H_{28}N_4O_4Zn$
Exact Mass: 764.14
Molecular Weight: 766.12

90% ^{1}H NMR (400 MHz, D_6-DMSO): δ = 7.75 - 7.85 (m, 6H, ArH), 8.14 - 8.21 (m, 8H, ArH), 8.30 (d, *J* = 7.5 Hz, 4H, ArH), 8.77 (d, *J* = 4.6 Hz, 4H, β pyr H), 8.79 (d, *J* = 4.6 Hz, 4H, β pyr H). UV-vis (DMSO) λ_{max} (log ε) 408 (4.7), 429 (5.8), 561 (4.3), 601 (4.0). HRMS (ESI, M^+): found: 764.1425, calcd. for $C_{46}H_{28}N_4O_4Zn$: 764.1402.

Zn 5,10-diphenyl-15,20-di[4-(carboxy)phenyl]porphyrin 2.19

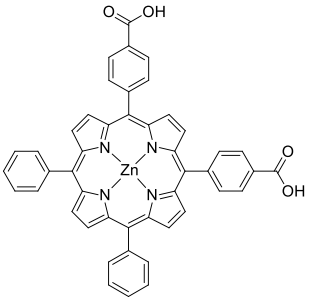

Chemical Formula: $C_{46}H_{28}N_4O_4Zn$
Exact Mass: 764.14
Molecular Weight: 766.12

78% ^{1}H NMR (400 MHz, D_6-DMSO): δ = 7.76 - 7.85 (m, 6H, ArH), 8.16 - 8.22 (m, 4H, ArH), 8.28 (d, *J* = 8.2 Hz, 4H, ArH), 8.35 (d, *J* = 8.1 Hz, 4H, ArH), 8.77 (d, *J* = 4.8 Hz, 4H, β pyr H), 8.79 (d, *J* = 4.8 Hz, 4H, β pyr H). UV-vis (DMSO) λ_{max} (log ε) 408 (4.6), 429 (5.7), 562 (4.3), 602 (4.1). HRMS (ESI, M^+): found: 764.1412, calcd. for $C_{46}H_{28}N_4O_4Zn$: 764.1402.

Zn 5-phenyl-10,15,20-tri[4-(carboxy)phenyl]porphyrin 2.20

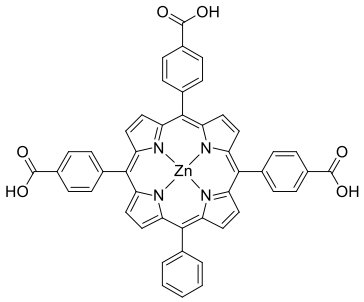

Chemical Formula: $C_{47}H_{28}N_4O_6Zn$
Exact Mass: 808.13
Molecular Weight: 810.13

73% ^{1}H NMR (400 MHz, D_6-DMSO): δ = 7.78 - 7.83 (m, 3H, ArH), 8.16 - 8.21 (m, 8H, ArH), 8.27 (d, *J* = 8.0 Hz, 6H, ArH), 8.35 (d, *J* = 8.0 Hz, 6H, ArH), 8.76 - 8.81 (m, 8H, β pyr H). UV-vis (DMSO) λ_{max} (log ε) 409 (4.5), 429 (5.6), 562 (4.2), 602 (4.0). HRMS (ESI, M^+): found: 808.1302, calcd. for $C_{47}H_{28}N_4O_6Zn$: 808.1300.

Zn 5,10,15,20-tetra[4-(carboxy)phenyl]porphyrin 2.21[173]

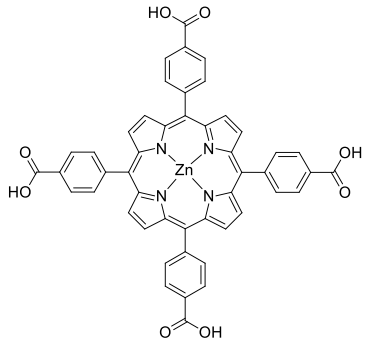

Chemical Formula: $C_{48}H_{28}N_4O_8Zn$
Exact Mass: 852.12
Molecular Weight: 854.14

79% ^{1}H NMR (400 MHz, D_6-DMSO): δ = 8.23 (d, *J* = 7.5 Hz, 8H, ArH), 8.32 (d, *J* = 7.5 Hz, 8H, ArH), 8.79 (s, 8H, β pyr H). UV-vis (DMSO) λ_{max} (log ε) 410 (4.5), 430 (5.5), 565 (4.7), 605 (4.6). HRMS (ESI, M^+): found: 853.1276, calcd. for $C_{48}H_{29}N_4O_8Zn$: 853.1277.

Zn butylporphyrin carboxylic acids

Zn 5,10,15-tributyl-20-[4-(carboxy)phenyl]porphyrin 2.39

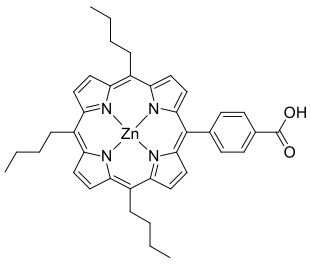

Chemical Formula: $C_{39}H_{40}N_4O_2Zn$
Exact Mass: 660.24
Molecular Weight: 662.14

92% ^{1}H NMR (400 MHz, D6-DMSO): δ = 1.09 (t, *J* = 7.6 Hz, 6H, $CH_2C\mathbf{H_3}$), 1.13 (t, *J* = 7.6 Hz, 3H, $CH_2C\mathbf{H_3}$), 1.74 – 1.88 (m, 6H, $C\mathbf{H_2}CH_3$), 2.38 – 2.50 (m, 6H, $C\mathbf{H_2}CH_2CH_3$), 4.94 – 5.07 (m, 6H, $C\mathbf{H_2}CH_2CH_2CH_3$), 8.09 – 8.16 (m, 2H, ArH), 8.24 – 8.34 (m, 2H, ArH), 8.71 (d, *J* = 4.6 Hz, 2H, β pyr H), 9.54 (d, *J* = 4.6 Hz, 2H, β pyr H),

9.63 (d, *J* = 4.8 Hz, 2H, β pyr H), 9.66 (d, *J* = 4.8 Hz, 2H, β pyr H). UV-vis (DMSO) λ_{max} (log ε) 408 (4.6), 428 (5.7), 567 (4.1), 608 (4.1). HRMS (ESI, M^+): found: 660.2427, calcd. for $C_{39}H_{40}N_4O_2Zn$: 660.2443.

Zn 5,15-dibutyl-10,20-di[4-(carboxy)phenyl]porphyrin 2.40

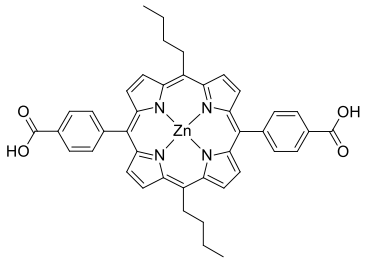

Chemical Formula: $C_{42}H_{36}N_4O_4Zn$
Exact Mass: 724.20
Molecular Weight: 726.14

87% ^{1}H NMR (400 MHz, D6-DMSO): δ = 1.08 (t, *J* = 7.6 Hz, 6H, $CH_2C\mathbf{H_3}$), 1.74 – 1.88 (m, 6H, $C\mathbf{H_2}CH_3$), 2.39 – 2.48 (m, 4H, $C\mathbf{H_2}CH_2CH_3$), 5.01 (t, *J* = 7.3 Hz, 4H, $C\mathbf{H_2}CH_2CH_2CH_3$), 8.22 (d, *J* = 8.0 Hz, 4H, ArH), 8.34 (d, *J* = 8.0 Hz, 4H, ArH), 8.76 (d, *J* = 4.6 Hz, 4H, β pyr H), 9.61 (d, *J* = 4.8 Hz, 4H, β pyr H). UV-vis (DMSO) λ_{max} (log ε) 410 (4.5), 430 (5.5), 564 (4.1), 608 (4.0). HRMS (ESI, M^+): found: 724.2014, calcd. for $C_{42}H_{36}N_4O_4Zn$: 724.2028.

Zn 5,10-dibutyl-15,20-di[4-(carboxy)phenyl]porphyrin 2.41

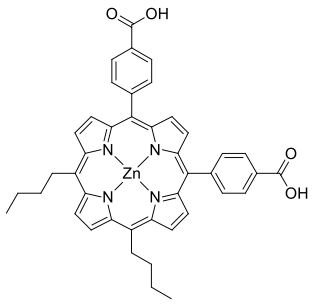

Chemical Formula: $C_{42}H_{36}N_4O_4Zn$
Exact Mass: 724.20
Molecular Weight: 726.14

91% ^{1}H NMR (400 MHz, D6-DMSO): δ = 1.12 (t, *J* = 7.1 Hz, 6H, $CH_2C\mathbf{H_3}$), 1.83 (sex, *J* = 7.1 Hz, 4H, $C\mathbf{H_2}CH_3$), 2.39 – 2.48 (m, 4H, $C\mathbf{H_2}CH_2CH_3$), 5.04 (t, *J* = 8.4 Hz, 4H, $C\mathbf{H_2}CH_2CH_2CH_3$), 7.98 (d, *J* = 6.7 Hz, 4H, ArH), 8.20 (d, *J* = 6.7 Hz, 4H, ArH), 8.68 (s, 2H, β pyr H), 8.77 (d, *J* = 4.8 Hz, 2H, β pyr H), 9.58 (d, *J* = 4.8 Hz, 2H, β pyr H), 9.69 (s, 2H, β pyr H). UV-vis (DMSO) λ_{max} (log ε) 408 (4.6), 429 (5.6), 565 (4.1), 606 (4.0). HRMS (ESI, M^+): found: 724.2020, calcd. for $C_{42}H_{36}N_4O_4Zn$: 724.2028.

Zn 5-butyl-10,15,20-tri[4-(carboxy)phenyl]porphyrin 2.42

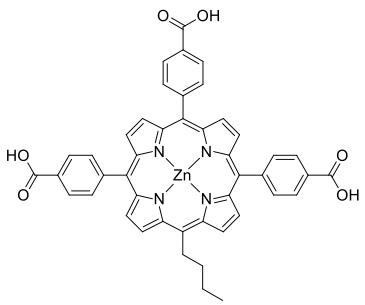

Chemical Formula: $C_{45}H_{32}N_4O_6Zn$
Exact Mass: 788.16
Molecular Weight: 790.14

80% ^{1}H NMR (400 MHz, D6-DMSO): δ = 1.10 (t, *J* = 7.0 Hz, 3H, $CH_2C\mathbf{H_3}$), 1.81 (sex, *J* = 7.0 Hz, 2H, $C\mathbf{H_2}CH_3$), 2.50 (m, 2H, $C\mathbf{H_2}CH_2CH_3$), 5.08 (t, *J* = 7.7 Hz, 2H, $C\mathbf{H_2}CH_2CH_2CH_3$), 8.20 – 8.28 (m, 6H, ArH), 8.30 – 8.38 (m, 6H, ArH), 8.71 – 8.75 (m, 4H, β pyr H), 8.82 (d, *J* = 4.2 Hz, 2H, β pyr H), 9.69 (d, *J* = 4.2 Hz, 2H, β

pyr H). UV-vis (DMSO) λ_{max} (log ε) 409 (4.6), 429 (5.7), 563 (4.2), 604 (4.0). HRMS (ESI, M^+): found: 788.1584, calcd. for $C_{45}H_{32}N_4O_6Zn$: 788.1613.

Fe phenylporphyrin carboxylic acids

FeCl 5,10,15-triphenyl-20-[4-(carboxy)phenyl]porphyrin 2.22[174]

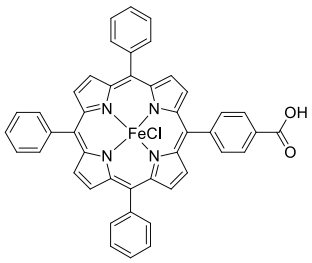

Chemical Formula: $C_{45}H_{28}ClFeN_4O_2$
Exact Mass: 747.13
Molecular Weight: 748.03

73% UV-vis (DMSO) λ_{max} (log ε) 415 (5.0), 495 (4.0), 528 (4.1), 686 (3.5). HRMS (ESI, M^+): found: 712.1572, calcd. for $C_{45}H_{28}N_4O_2Fe$: 712.1562.

FeCl 5,15-diphenyl-10,20-di[4-(carboxy)phenyl]porphyrin 2.23

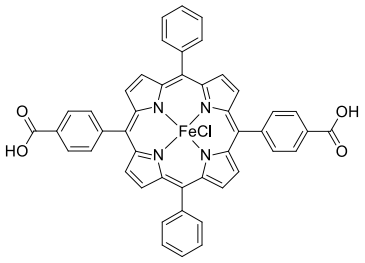

Chemical Formula: $C_{46}H_{28}ClFeN_4O_4$
Exact Mass: 791.11
Molecular Weight: 792.04

82% UV-vis (DMSO) λ_{max} (log ε) 411 (4.2), 567 (3.5), 612 (3.5). HRMS (ESI, M^+): found: 756.1465, calcd. for $C_{46}H_{28}N_4O_4Fe$: 756.1460.

FeCl 5,10-diphenyl-15,20-di[4-(carboxy)phenyl]porphyrin 2.24

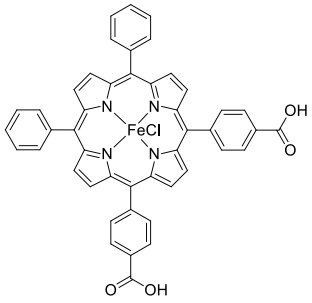

Chemical Formula: $C_{46}H_{28}ClFeN_4O_4$
Exact Mass: 791.11
Molecular Weight: 792.04

76% UV-vis (DMSO) λ_{max} (log ε) 411 (4.8), 570 (3.8), 613 (3.6). HRMS (ESI, M^+): found: 756.1449, calcd. for $C_{46}H_{28}N_4O_4Fe$: 756.1460.

FeCl 5-phenyl-10,15,20-tri[4-(carboxy)phenyl]porphyrin 2.25

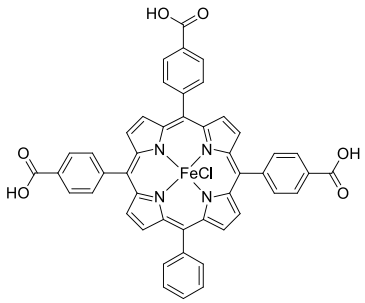

Chemical Formula: $C_{47}H_{28}ClFeN_4O_6$
Exact Mass: 835.10
Molecular Weight: 836.05

77% UV-vis (DMSO) λ_{max} (log ε) 416 (4.4), 528 (3.6), 568 (3.6), 611 (3.5), 674 (3.2). HRMS (ESI, M^+): found: 800.1368, calcd. for $C_{47}H_{28}N_4O_6Fe$: 800.1358.

Porphyrin Quaternary Ammonium Salts

Methylation conditions

Each porphyrin (approx 10 mg) was dissolved in a mixture of acetonitrile (1.0 mL) and iodomethane (0.5 mL). The mixture was heated in a microwave reactor at 50 °C (power 3W) for 3 hr and then evaporated to dryness to afford the methylated porphyrin product. Yields were quantitative.

Zn 5,10,15-triphenyl-20-[N,N,N-trimethyl-4-anilinium]porphyrin iodide 2.56

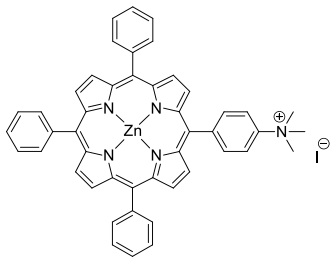

Chemical Formula: $C_{47}H_{36}IN_5Zn$
Exact Mass: 861.13
Molecular Weight: 863.11

^{1}H NMR (400 MHz, DMSO - d_6): δ = 3.92 (s, 9H, NCH_3), 7.77 – 7.87 (m, 9H, ArH), 8.15 – 8.20 (m, 6H, ArH), 8.35 – 8.46 (m, 4H, ArH), 8.74 (d, *J* = 4.6 Hz, 2H, β pyr H), 8.77 (d, *J* = 4.6 Hz, 2H, β pyr H), 8.79 (d, *J* = 4.6 Hz, 2H, β pyr H), 8.82 (d, *J* = 4.6 Hz, 2H, β pyr H). UV-vis (DMSO) λ_{max} (log ε) 408 (4.6), 428 (5.6), 561 (4.2), 601 (4.0). HRMS (ESI, ($M-I^-$)): found: 734.2276, calcd. for $C_{47}H_{36}N_5Zn$: 734.2262.

Zn 5,15-diphenyl-10,20-di[N,N,N-trimethyl-4-anilinium]porphyrin iodide 2.57

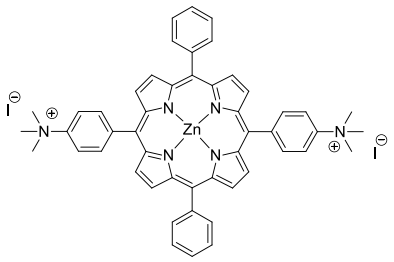

Chemical Formula: $C_{50}H_{44}I_2N_6Zn$
Exact Mass: 1046.10
Molecular Weight: 1048.11

^{1}H NMR (400 MHz, DMSO - d_6): δ = 3.92 (s, 18H, NCH_3), 7.80 – 7.88 (m, 6H, ArH), 8.15 – 8.20 (m, 4H, ArH), 8.35 – 8.45 (m, 8H, ArH), 8.76 (d, *J* = 4.6 Hz, 4H, , β pyr H), 8.82 (d, *J* = 4.6 Hz, 4H, , β pyr H). UV-vis (DMSO) λ_{max} (log ε) 409 (4.6), 430 (5.7), 562 (4.3), 604 (4.0). HRMS (ESI, 2 x ($M-2I^-$)): found: 792.2918, calcd. for $C_{50}H_{44}N_6Zn$: 792.2919.

Zn 5,10-diphenyl-15,20-di[N,N,N-trimethyl-4-anilinium]porphyrin iodide 2.58

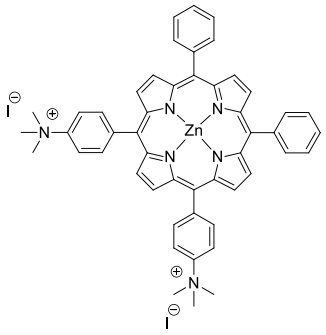

Chemical Formula: $C_{50}H_{44}I_2N_6Zn$
Exact Mass: 1046.10
Molecular Weight: 1048.11

^{1}H NMR (400 MHz, DMSO - d_6): δ = 3.92 (s, 18H, NCH_3), 7.78 – 7.86 (m, 6H, ArH), 8.15 – 8.19 (m, 6H, ArH), 8.36 – 8.45 (m, 8H, ArH), 8.74 (d, *J* = 4.6 Hz, 2H, β pyr H), 8.79 (d, *J* = 2.1 Hz, 4H, β pyr H), 8.83 (d, *J* = 4.6 Hz, 2H, β pyr H). UV-vis (DMSO) λ_{max} (log ε) 409 (4.7), 430 (5.8), 562 (4.4), 604 (4.1). HRMS (ESI, 2 x ($M-2I^-$)): found: 792.2914, calcd. for $C_{50}H_{44}N_6Zn$: 792.2919.

Zn 5-phenyl-10,15,20-tri[N,N,N-trimethyl-4-anilinium]porphyrin iodide 2.59

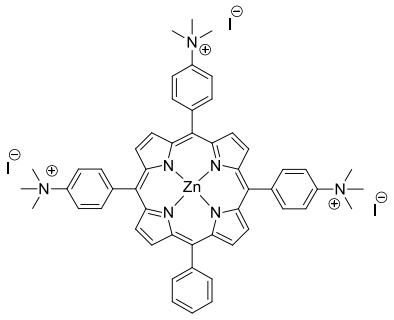

Chemical Formula: $C_{53}H_{52}I_3N_7Zn$
Exact Mass: 1231.07
Molecular Weight: 1233.12

^{1}H NMR (400 MHz, DMSO - d_6): δ = 3.93 (s, 27H, NCH_3), 7.81 – 7.91 (m, 3H, ArH), 8.19 – 8.24 (m, 2H, ArH), 8.39 – 8.46 (m, 6H, ArH), 8.47 – 8.53 (m, 6H, ArH), 8.80 (d, *J* = 4.9 Hz, 2H, β pyr H), 8.85 (d, *J* = 4.8 Hz, 2H, β pyr H), 8.87 (d, *J* = 4.8 Hz, 2H, β pyr H), 8.83 (d, *J* = 4.9 Hz, 2H, β pyr H). UV-vis (DMSO) λ_{max} (log ε) 410 (4.5), 431 (5.5), 564 (4.1), 605 (3.9). HRMS (ESI, 3 x ($M-3I^-$)): found: 850.3563, calcd. for $C_{53}H_{52}N_7Zn$: 850.3576.

Zn 5,10,15,20-tetra[N,N,N-trimethyl-4-anilinium]porphyrin iodide 2.60[96]

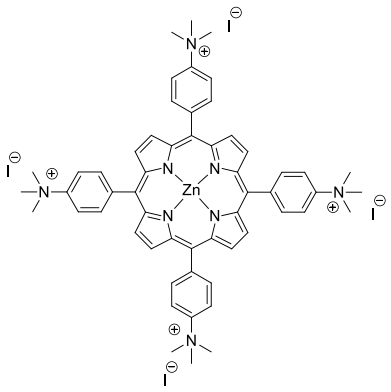

Chemical Formula: $C_{56}H_{60}I_4N_8Zn$
Exact Mass: 1416.04
Molecular Weight: 1418.13

^{1}H NMR (400 MHz, DMSO - d_6): δ = 3.93 (s, 36H, NCH_3), 8.39 (d, *J* = 8.7 Hz, 8H, ArH), 8.42 (d, *J* = 8.7 Hz, 8H, ArH), 8.79 (s, 8H, β pyr H). UV-vis (DMSO) λ_{max} (log ε) 411 (4.5), 432 (5.4), 565 (4.1), 606 (3.9). HRMS (ESI, 4 x ($M-4I^-$)): found: 908.4204, calcd. for $C_{56}H_{60}N_8Zn$: 908.4232.

Ferrocene porphyrins

5-(4-ferrocenephenyl)-10,15,20-tri[4-(carboxy)phenyl]porphyrin methyl ester 2.61

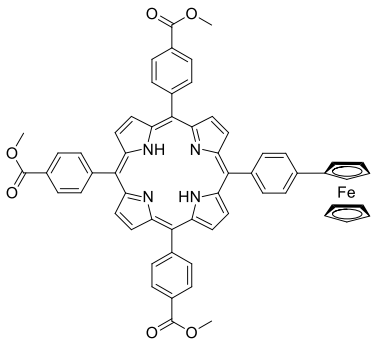

Chemical Formula: $C_{60}H_{44}FeN_4O_6$
Exact Mass: 972.26
Molecular Weight: 972.86

4-Formylbenzoic acid (methyl ester) (0.616 g, 3.75 mmol, 3 eq.), 4-ferrocenylbenzaldehyde (0.363 g, 1.25 mmol, 1 eq.) and pyrrole (0.335 g, 5 mmol, 4 eq.) were mixed in 500 mL of DCM. TFA (1.254 g, 11 mmol) was added, and the mixture stirred at rt 4.5 hrs. Chloranil (1.229 g, 5 mmol, 4 eq.) was added and the mixture heated at replux for 5 hours. The monoferrocenylporphyrin triester was isolated by flash chromatography using 2% EtOAc in DCM to eleute. Precipitation was induced by addition of methanol to afford the product, 45 mg, 3.7 %. ^{1}H NMR (400 MHz, $CDCl_3$): δ = -2.73 (s, 2H, NH), 4.14 (s, 9H, OCH_3), 5.27 (s, 5H, FcH), 4.51 (t, *J* = 1.83 Hz, 2H, FcH), 4.95 (t, *J* = 1.83 Hz, 2H, FcH), 7.89 (d, *J* = 8.24 Hz, ArH), 8.15 (d, *J* = 8.24 Hz, ArH), 8.30 – 8.35 (m, 6H, ArH), 8.40 – 8.50 (m, 6H, ArH), 8.83 (s, 4H, β-pyr. H), 8.84 (d, *J* = 4.76, 2H, β-pyr.) 8.99 (d, *J* = 4.76, 2H, β-pyr. H). UV-vis ($CHCl_3$) λ_{max} (log ε) 421 (5.6), 517 (4.3), 555 (4.0), 591 (3.8), 648 (3.7). HRMS (ESI, M^+): found:973.2723, calcd. for $C_{60}H_{45}FeN_4O_6$: 973.2688.

Zn 5-(4-ferrocenephenyl)-10,15,20-tri[4-(carboxy)phenyl]porphyrin methyl ester 2.62

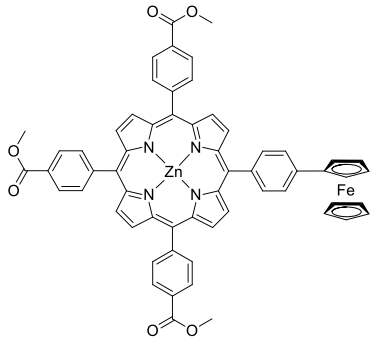

Zinc insertion was performed in the same manner as for the phenylporphyrin esters **2.01** – **2.06**. Yield was quantitative. ^{1}H NMR (400 MHz, $CDCl_3$): δ = 4.13 (s, 9H, OCH_3), 4.28 (s, 5H, FcH), 4.51 (t, *J* = 1.83 Hz, 2H, FcH), 4.95 (t, *J* = 1.83 Hz, 2H, FcH), 7.89 (d, 2H, *J* = 8.43 Hz, ArH), 8.16 (d, 2H, *J* = 8.43 Hz, ArH), 8.30 – 8.36 (m, 6H, ArH), 8.44 – 8.49 (m, 6H, ArH), 8.93 (s, 4H, β pyr H), 8.95 (d, *J* = 4.76 Hz, 2H, β pyr H), 9.09 (d, *J* = 4.76 Hz, 2H, β pyr H). UV-vis ($CHCl_3$) λ_{max} (log ε) 427 (5.6), 520 (4.3), 598 (4.0). HRMS (ESI, M^+): found: 1035.1847, calcd. for $C_{60}H_{45}FeN_4O_6Zn$: 1035.1823.

Zn 5-(4-ferrocenephenyl)-10,15,20-tri[4-(carboxy)phenyl]porphyrin 2.63

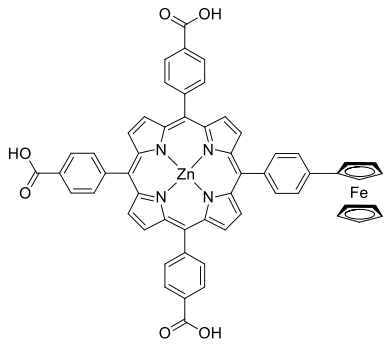

Hydrolysis was performed in the same manner as for the zinc phenlyporphyrin esters **2.07** – **2.12**. Yield was quantitative. ^{1}H NMR (400 MHz, DMSO - d_6): δ = 4.24 (s, 5H, FcH), 4.51 (t, *J* = 1.83 Hz, 2H, FcH), 5.08 (t, *J* = 1.83 Hz, 2H, FcH), 7.96 (d, *J* = 7.88 Hz, 2H, ArH), 8.11 (d, *J* = 7.88 Hz, 2H, ArH), 8.30 (d, *J* = 8.06 Hz, 6H, ArH), 8.33 – 8.40 (d, *J* = 8.06 Hz, 6H, ArH), 8.79 (s, 4H, β pyr H), 8.80 (d, *J* = 4.76 Hz, 2H, β pyr H), 8.90 (d, *J* = 4.76 Hz, 2H, β pyr H). UV-vis (DMSO) λ_{max} (log ε) 431 (5.2), 562 (3.8), 603 (3.6). HRMS (ESI, M^+): found: 993.1378, calcd. for $C_{57}H_{37}FeN_4O_6Zn$: 993.1354.

Pentafluorobenzene porphyrins

4-Formyl benzoic acid (methyl ester) (1.23 g, 7.5 mmol, 3 eq.), pentafluorobenzaldehyde (0.49 g, 2.5 mmol, 1 eq.) and pyrrole (0.671 g, 10 mmol, 4 eq.) were mixed in 1000 mL of DCM.

TFA (2.508 g, 22 mmol) was added, and the mixture stirred at rt for 5 hrs. DDQ (2.27 g, 10 mmol, 4 eq.) was added and the mixture heated at reflux for 5 hours. The *AABB* porphyrin diester and the porphyrin triester were isolated by flash chromatography using 2% EtOAc in DCM to elute. The pure fractions were concentration and the products precipitated by addition of methanol.

5,10-di(pentafluorophenyl)-10,20-di[4-(carboxy)phenyl]porphyrin methyl ester 2.66

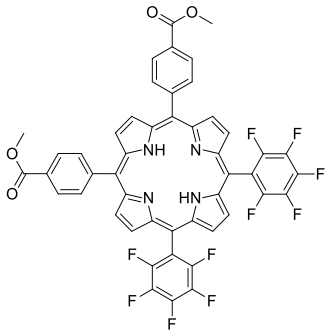

144 mg, 6%.^{1}H NMR (400 MHz, $CDCl_3$): δ = -2.80 (s, 2H, NH), 4.12 (s, 6H, OCH_3), 8.29 (d, *J* = 8.24 Hz, ArH), 8.46 (d, *J* = 8.24 Hz, ArH), 8.78 – 8.84 (m, 4H, β-pyr. H), 8.86 – 8.91 (m, 4H, β-pyr. H). UV-vis ($CHCl_3$) λ_{max} [nm] (log ε) 417 (5.2), 512 (3.9), 543 (3.4), 585 (3.4), 652 (2.9). HRMS (ESI, M^+): found: 911.1759, calcd. for $C_{48}H_{25}N_4O_4F_{10}$: 911.1716.

5-(pentafluorophenyl)-10,15,20-tri[4-(carboxy)phenyl]porphyrin methyl ester 2.67[175]

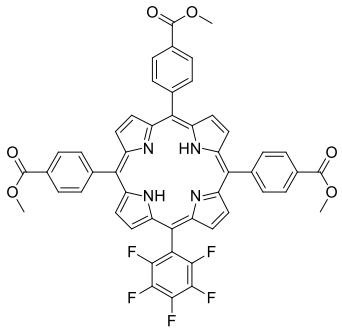

23 mg, 1%. ^{1}H NMR (400 MHz, $CDCl_3$): δ = -2.77 (s, 2H, NH), 4.14 (s, 3H, OCH_3), 4.14 (s, 6H, OCH_3), 8.29 – 8.35 (m, 6H, ArH), 8.44 – 8.52 (m, 6H, ArH), 8.80 – 8.87 (m, 6H, β-pyr. H), 8.90 – 8.93 (d, *J* = 5.13 Hz, 2H, β-pyr. H). UV-vis ($CHCl_3$) λ_{max} [nm] (log ε) 419 (5.3), 513 (3.9), 548 (3.4), 588 (3.4), 643 (2.9). HRMS (ESI, M^+): found: 879.2244, calcd. for $C_{50}H_{32}N_4O_6F_5$:879.2242.

Fe pentafluorophenylporphyrin esters

Fe insertion was performed in the same manner as for the phenylporphyrin esters (**2.13** – **2.16**).

FeCl 5,10-di(pentafluorophenyl)-10,20-di[4-(carboxy)phenyl]porphyrin methyl ester 2.68

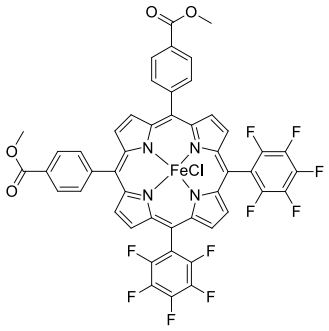

Chemical Formula: $C_{48}H_{22}ClF_{10}FeN_4O_4$
Exact Mass: 999.05
Molecular Weight: 999.99

65% UV-vis (DMF) λ_{max} (log ε) 407 (4.7), 568 (3.6), 610 (3.3). HRMS (ESI, M^+): found: 964.0820, calcd. for $C_{48}H_{22}N_4O_4F_{10}Fe$: 964.0831.

FeCl 5-(pentafluorophenyl)-10,15,20-tri[4-(carboxy)phenyl]porphyrin methyl ester 2.69

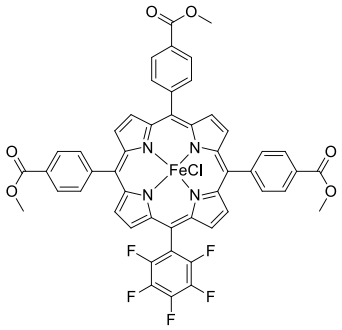

Chemical Formula: $C_{50}H_{29}ClF_5FeN_4O_6$
Exact Mass: 967.10
Molecular Weight: 968.08

70% UV-vis (DMF) λ_{max} (log ε) 407 (4.6), 568 (3.6), 610 (3.3). HRMS (ESI, M^+): found: 932.1341, calcd. for $C_{50}H_{29}N_4O_6F_5Fe$: 932.1357.

Porphyrin aldehydes

The tetraphenylporphyrin aldehydes were produced as a mixture in two stages before being separated chromatographically. Monoprotected phthalaldehyde **4.12** (2.20 g, 10 mmol, 1 eq.), benzaldehyde (1.06 g, 10 mmol, 1 eq.) and pyrrole (1.34 g, 20 mmol, 2 eq.) were mixed in DCM (2 L). TFA (5.02 g, 44 mmol) was added and the mixture stirred at rt for 3 hrs. Chloranil (4.92 g, 20 mmol) was added and the mixture heated at reflux for 15 mins. 10 mL triethylamine added and then the mixture evaporated to dryness. Porphyrins were separated from by-products *via* flash chromatography using 1% methanol in DCM. To remove the acetal protecting groups, porphyrins were dissolved in a mixture of DCM (50 mL) and TFA (50 mL) and water (20 mL) and stirred at rt for 6 hrs. The mixture was stirred with sat. $NaHCO_3$ until gas evolution ceased, before being extracted with DCM. Porphyrin aldehyde products were separated *via* flash chromatography using DCM to elute, moving to 1% EtOAc in DCM following the elution of the dialdehydes. Pure fractions were concentrated and the products precipitated *via* the addition of methanol. The products were collected by filtration.

5,10,15-triphenyl-20-(4-formylphenyl)porphyrin 4.06[122]

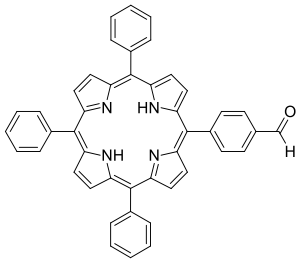

Chemical Formula: $C_{45}H_{30}N_4O$
Exact Mass: 642.24
Molecular Weight: 642.75

49 mg, 1.5%. ^{1}H NMR (400 MHz, $CDCl_3$): δ = -2.76 (s, 2H, NH), 7.72 – 7.82 (m, 9H, ArH), 8.19 – 8.24 (m, 6H, ArH), 8.28 (d, *J* = 8.37 Hz, 2H, ArH), 8.41 (d, *J* = 8.37 Hz, 2H, ArH), 8.77 (d, *J* = 4.78 Hz, 2H, β-pyr. H), 8.85 (s, 4H, β-pyr. H), 8.87 (d, *J* = 4.78 Hz, 2H, β-pyr. H), 10.37 (s, 1H, CHO). UV-vis ($CHCl_3$) λ_{max} (log ε) 420 (4.4),517(3.0), 552(2.6), 590(2.5), 650(2.4). HRMS (ESI, M^+): found: 643.2510, calcd. for $C_{45}H_{31}N_4O$: 643.2498.

5,15-diphenyl-10,20-di(4-formylphenyl)porphyrin 4.07

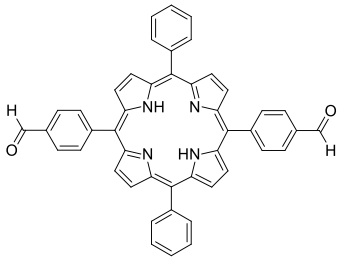

Chemical Formula: $C_{46}H_{30}N_4O_2$
Exact Mass: 670.24
Molecular Weight: 670.76

18 mg, 0.5%. ^{1}H NMR (400 MHz, $CDCl_3$): δ = -2.77 (s, 2H, NH), 7.72 – 7.84 (m, 6H, ArH), 8.18 – 8.25 (m, 4H, ArH), 8.29 (d, *J* = 8.21 Hz, 4H, ArH), 8.40 (d, *J* = 8.21 Hz, 4H, ArH), 8.79 (d, *J* = 4.69 Hz, 4H, β-pyr. H), 8.88 (d, *J* = 4.69 Hz, 4H, β-pyr. H), 10.39 (s, 2H, CHO). UV-vis ($CHCl_3$) λ_{max} (log ε) 421(4.4), 517(3.0), 552(2.7), 591(2.5), 648(2.4). HRMS (ESI, M^+): found: 671.2457, calcd. for $C_{46}H_{31}N_4O_2$: 671.2447.

5,10-diphenyl-15,20-di(4-formylphenyl)porphyrin 4.08

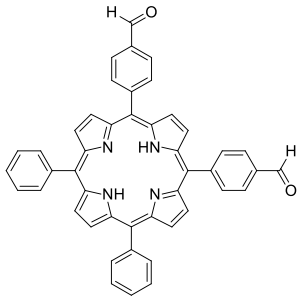

Chemical Formula: $C_{46}H_{30}N_4O_2$
Exact Mass: 670.24
Molecular Weight: 670.76

37 mg, 1.1%. ^{1}H NMR (400 MHz, $CDCl_3$): δ = -2.76 (s, 2H, NH), 7.72 – 7.82 (m, 6H, ArH), 8.18 – 8.24 (m, 4H, ArH), 8.28 (d, *J* = 8.40 Hz, 4H, ArH), 8.40 (d, *J* = 8.40 Hz, 4H, ArH), 8.78 (d, *J* = 4.88 Hz, 2H, β-pyr. H), 8.80 (s, 2H, β-pyr. H), 8.86 (s, 2H, β-pyr. H), 8.88 (d, *J* = 4.88 Hz, 2H, β-pyr. H), 10.39 (s, 2H, CHO). UV-vis ($CHCl_3$) λ_{max} (log ε) 422(4.5), 517(3.0), 552(2.7), 594(2.5), 648(2.4). HRMS (ESI, M^+): found: 671.2446, calcd. for $C_{46}H_{31}N_4O_2$: 671.2447.

5-phenyl-10,15,20-tri(4-formylphenyl)porphyrin 4.09

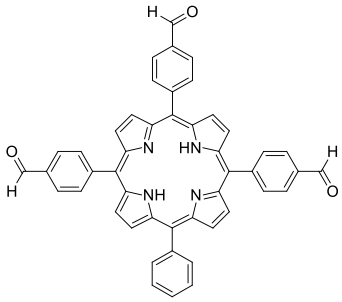

Chemical Formula: $C_{47}H_{30}N_4O_3$
Exact Mass: 698.23
Molecular Weight: 698.77

97 mg, 2.8%. ^{1}H NMR (400 MHz, $CDCl_3$): δ = -2.76 (s, 2H, NH), 7.73 – 7.84 (m, 3H, ArH), 8.18 – 8.24 (m, 2H, ArH), 8.29 (d, *J* = 8.01 Hz, 6H, ArH), 8.40 (d, *J* = 8.01 Hz, 6H, ArH), 8.79 (d, *J* = 4.88 Hz, 2H, β-pyr. H), 8.81 (s, 4H, β-pyr. H), 8.89 (d, *J* = 4.88 Hz, 2H, β-pyr. H). UV-vis ($CHCl_3$) λ_{max} (log ε) 422(4.5), 517(3.2), 553(2.9), 590(2.7), 647(2.6). HRMS (ESI, M^+): found: 699.2387, calcd. for $C_{47}H_{31}N_4O_3$: 699.2396.

5-phenyl-15-(4-formylphenyl)porphyrin 2,2-dimethyl- 1,3-propanediol acetal 5.03

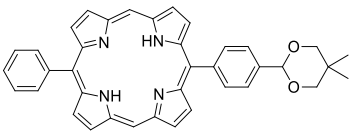

Chemical Formula: $C_{38}H_{32}N_4O_2$
Exact Mass: 576.25
Molecular Weight: 576.69

Mono protected phthalaldehyde **4.12** (0.112 g, 0.5 mmol, 1 eq.), benzaldehyde (0.056 g, 0.5 mmol, 1eq.) and dipyrromethane (0.146 g, 1.0 mmol, 2 eq.) were dissolved in DCM (100 mL). TFA (0.110 g, 1.0 mmol) was added, and the mixture stirred at rt for 8 hrs. DDQ (0.023 g, 1.0 mmol) was added and the mixture stirred at rt for 18 hours. The mixture was neutralised by stirring with with sat. $NaHCO_3$ (100 mL). Extracted with DCM and concentrated *via* rotary evaporation. The products were separated *via* flash chromatography using DCM to elute. Pure fractions were concentrated *via* rotary evaportation and crystallised *via* addition of methanol. 26 mg, 9%. ^{1}H NMR (400 MHz, $CDCl_3$): δ = -2.78 (s, 2H, NH), 0.92 (s, 3H, CH_3), 1.47 (s, 3H, CH_3), 3.86 (d, *J* = 10.76 Hz, 2H, CH_2), 3.97 (d, *J* = 10.76 Hz, 2H, CH_2), 5.76 (s, 1H, CH), 7.78 - 7.83 (m, 3H, ArH), 7.97 (d, *J* = 7.82 Hz, 2H, ArH), 8.25 – 8.32 (m, 4H, ArH), 9.07 (d, *J* = 4.69 Hz, 2H, β-pyr. H), 9.08 (d, *J* = 4.69 Hz, 2H, β-pyr. H), 9.38 (d, *J* = 4.69 Hz, 2H, β-pyr. H), 9.39 (d, *J* = 4.69 Hz, 2H, β-pyr. H), 10.31 (s, 2H, *meso* H). UV-vis ($CHCl_3$) λ_{max} (log ε) 408(4.4), 503(3.1), 537(2.8), 575(2.5), 630(2.1). HRMS (ESI, M^+): found: 577.2600, calcd. for $C_{38}H_{33}N_4O_2$: 577.2604.

5-phenyl-15-(4-formylphenyl)porphyrin 5.04

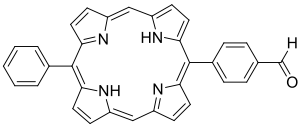

Chemical Formula: $C_{33}H_{22}N_4O$
Exact Mass: 490.18
Molecular Weight: 490.55

The protected compound **5.03** (25 mg, 0.043 mmol) was dissolved in a mixture of DCM (5 mL), TFA (5 mL) and water (1.7 mL) and stirred at rt for 1 hr. Sat. $NaHCO_3$ (30 mL) was added and stirred until gas evolution ceased. The organic layer was collected, dried with $MgSO_4$, filtered and evaportated to afford the product. 20 mg, 95%. ^{1}H NMR (400 MHz, $CDCl_3$): δ = -3.10 (s, 2H, NH), 7.77 – 7.86 (m, 3H, ArH), 8.25 – 8.31 (m, 2H, ArH), 8.34 (d, *J* = 8.40 Hz, 2H, ArH), 8.47 (d, *J* = 8.40 Hz, 2H, ArH), 9.02 (d, *J* = 4.69 Hz, 2H, β-pyr. H), 9.10 (d, *J* = 4.69 Hz, 2H, β-pyr. H), 9.41 (d, *J* = 4.69 Hz, 2H, β-pyr. H), 9.43 (d, *J* = 4.69 Hz, 2H, β-pyr. H), 10.35 (s, 2H, *meso* H), 10.43 (s,

2H, CHO). UV-vis ($CHCl_3$) λ_{max} (log ε) 411(4.4), 503(3.1), 541(2.8), 576(2.6), 631(2.2). HRMS (ESI, M^+): found: 491.1882, calcd. for $C_{33}H_{23}N_4O$: 491.1872.

Phenylene-linked dyads

2H2H phenylene-linked dyad triester 4.11

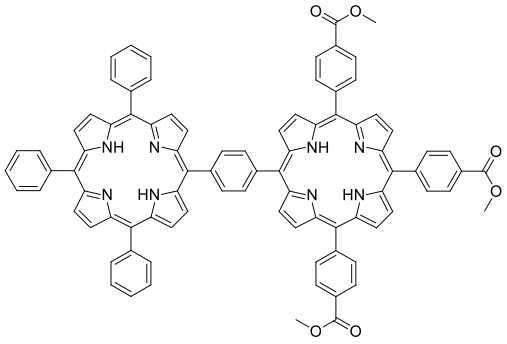

Tetraphenylporphyrin monoaldehyde **4.06** (160 mg, 0.249 mmol, 1 eq.), 4-formylbenzoic acid, methyl ester (572 mg, 3.48 mmol, 14 eq.) and pyrrole (251 mg, 3.74 mmol, 15 eq.) were mixed in DCM (373 mL). TFA (937 mg, 8.218 mmol) was added and the mixture stirred at rt 17 hrs. Chloranil (918 mg, 3.74 mmol) was added and the mixture heated at reflux for 1 hr. Triethylamine (2 mL) was added and the mixture evaporated to dryness. The dyad product was isolated *via* flash chromatography using 2% EtOAc in DCM. 93 mg, 28%. ^{1}H NMR (400 MHz, $CDCl_3$): δ = -2.70 (s, 2H, NH), -2.68 (s, 2H, NH), 4.06 (s, 3H, OCH_3), 4.07 (s, 6H, OCH_3), 7.67 – 7.79 (m, 9H, ArH), 8.16 – 8.20 (m, 2H, ArH), 8.21 – 8.25 (m, 4H, ArH), 8.27 (d, *J* = 8.24 Hz, 2H, ArH), 8.29 – 8.34 (d, *J* = 8.24 Hz, 4H, ArH), 8.40 (d, *J* = 8.24 Hz, 2H, ArH), 8.43 (d, *J* = 8.24 Hz, 4H, ArH), 8.55 (d, *J* = 8.24 Hz, 2H, ArH), 8.58 (d, *J* = 8.24 Hz, 2H, ArH), 8.78 (d, *J* = 4.58 Hz, 2H, β-pyr. H), 8.80 (d, *J* = 4.58 Hz, 2H, β-pyr. H), 8.82 (d, *J* = 4.58 Hz, 2H, β-pyr. H), 8.84(d, *J* = 4.58 Hz, 2H, β-pyr. H), 8.93 (d, *J* = 4.58 Hz, 2H, β-pyr. H), 8.97 (d, *J* = 4.58 Hz, 2H, β-pyr. H), 9.23 (d, *J* = 4.58 Hz, 2H, β-pyr. H), 9.27 (d, *J* = 4.58 Hz, 2H, β-pyr. H). UV-vis ($CHCl_3$) λ_{max} (log ε) 419(5.7), 428(5.8), 517(4.6), 552(4.4), 591(4.4), 648(4.3). HRMS (ESI, M^+): found: 1325.4734, calcd. for $C_{88}H_{61}N_8O_6$: 1325.4714.

ZnZn phenylene-linked dyad triester 4.15

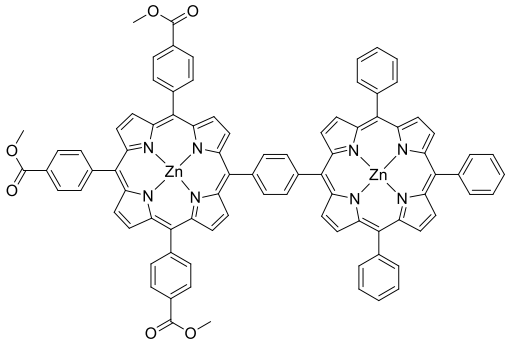

2H2H phenylene-linked dyad triester **4.11** (11 mg, 0.008 mmol) was dissolved in DCM (50 mL). Zinc acetate dihydrate (6.5 mg, 0.030 mmol) was dissolved in methanol (1 mL) and added to the dyad solution. Stirred at rt 21 hrs. The mixture was concentrated *via* rotary evaportation and precipitation of the product was induced *via* addition of methanol and collected by filtration. 9.4 mg, 81%. ^{1}H NMR (400 MHz, $CDCl_3$): δ = 4.13 (s, 3H, OCH_3), 4.15 (s, 6H, OCH_3), 7.74 – 7.84 (m, 6H, ArH), 8.23 – 8.28 (m, 2H, ArH), 8.29 – 8.33 (m, 4H, ArH), 8.34 (d, *J* = 8.24 Hz, 2H, ArH), 8.39 (d, *J* = 8.24 Hz, 4H, ArH), 8.47 (d, *J* = 8.24 Hz, 2H, ArH), 8.50 (d, *J* = 8.24 Hz, 4H, ArH), 8.61 (d, *J* = 8.43 Hz, 2H, ArH), 8.64 (d, *J* = 8.43 Hz, 2H, ArH), 8.96 (d, *J* = 4.76 Hz, 2H, β-pyr. H), 8.98 (d, *J* = 4.76 Hz, 2H, β-pyr. H), 9.00 (d, *J* = 4.76 Hz, 2H, β-pyr. H), 9.02 (d, *J* = 4.76 Hz, 2H, β-pyr. H), 9.11 (d, *J* = 4.76 Hz, 2H, β-pyr. H), 9.16 (d, *J* = 4.76 Hz, 2H, β-pyr. H), 9.42 (d, *J* = 4.76 Hz, 2H, β-pyr. H), 9.46 (d, *J* = 4.76 Hz, 2H, β-pyr. H). UV-vis ($CHCl_3$) λ_{max} (log ε) 424(5.7), 434(5.8), 557(4.6), 598(4.4). HRMS (ESI, M^+): found: 1449.2985, calcd. for $C_{88}H_{57}N_8O_6Zn_2$: 1449.2984.

ZnZn phenylene-linked dyad triacid 4.17

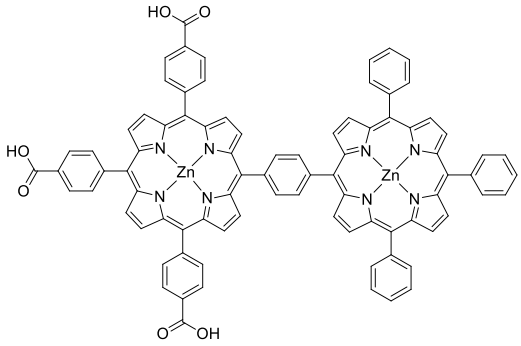

ZnZn phenylene-linked dyad triester **4.15** (6.3 mg, 0.0043 mmol) was dissolved in a mixture of tetrahydrofuran (10 mL), water (0.9 mL), methanol (9 mL) and potassium hydroxide (116 mg, 2.08 mmol). The mixture was stirred at reflux for 3 hrs. Water (5 mL) was added and the organic solvents evaporated *via* rotary evaporation. The solution was acidified with phosphoric acid solution, which induced precipitation of the porphyrin, and this was collected by three repetitions of centrifugation, with 95% of supernatant being removed and replaced with water

each time. 5.7 mg, 94%. ^{1}H NMR (400 MHz, $CDCl_3$): δ = 7.79 – 7.91 (m, 9H, ArH), 8.20 – 8.25 (m, 2H, ArH), 8.25 – 8.30 (m, 4H, ArH), 8.30 – 8.45 (m, 12H, ArH), 8.61 (s, 4H, ArH), 8.80 – 8.87 (m, 8H, β-pyr. H), 8.97 (d, *J* = 4.78 Hz, 2H, β-pyr. H), 8.99 (d, *J* = 4.78 Hz, 2H, β-pyr. H), 9.33 (d, *J* = 4.61 Hz, 2H, β-pyr. H), 9.35 (d, *J* = 4.61 Hz, 2H, β-pyr. H). UV-vis (DMSO) λ_{max} (log ε) 427(5.7), 438(5.8), 563(4.6), 604(4.4). HRMS (ESI, M^+): found: 1407.2667, calcd. for $C_{89}H_{51}N_8O_3Zn_2$: 1407.2667.

2H2H phenylene-linked dyad tri(dimethylamine) 4.13

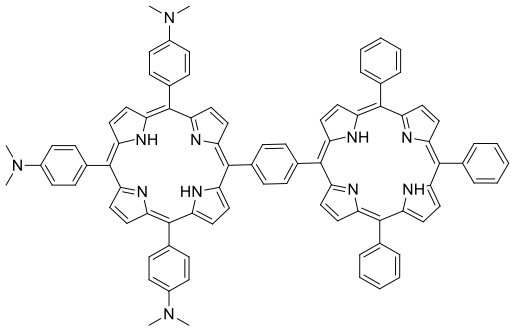

Tetraphenylporphyrin monoaldehyde **4.06** (100 mg, 0.156 mmol, 1 eq.), 4-*N,N*-dimethyaminobenzaldehyde (325 mg, 2.178 mmol, 14 eq.), and pyrrole (157 mg, 2.334 mmol, 15 eq.) were mixed in DCM (233 mL). TFA (585 mmol, 5.134 mmol) was added and the mixture stirred at rt for 2 hrs. Chloranil (574 mg, 2.334 mmol) was added and the mixture heated at reflux for 1 hr. Triethylamine (1 mL) was added and evaporated to dryness. The dyad was isolated *via* flash chromatography using 0.5% methanol, 0.1% triethylamine in DCM. 13.5 mg, 7%. ^{1}H NMR (400 MHz, $CDCl_3$): δ = -2.60 (s, 2H, NH), -2.45 (s, 2H, NH), 3.26 (s, 6H, NCH_3), 3.28 (s, 12H, NCH_3), 7.11 – 7.20 (m, 6H, ArH), 7.73 – 7.86 (m, 9H, ArH), 8.14 (d, *J* = 8.43 Hz, 2H, ArH), 8.17 (d, *J* = 8.43 Hz, 4H, ArH), 8.24 – 8.28 (m, 2H, ArH), 8.28 – 8.33 (m, 4H, ArH), 8.61 (d, *J* = 8.43 Hz, 2H, ArH), 8.64 (d, *J* = 8.43 Hz, 2H, ArH), 8.89 (d, *J* = 8.58 Hz, 2H, β-pyr. H), 8.91 (d, *J* = 8.58 Hz, 2H, β-pyr. H), 8.94 – 8.99 (m, 4H, d, β-pyr. H), 9.04 (d, *J* = 4.95 Hz, 2H, β-pyr. H), 9.11 (d, *J* = 4.76 Hz, 2H, β-pyr. H), 9.24 (d, *J* = 4.76 Hz, 2H, β-pyr. H), 9.32 (d, *J* = 4.76 Hz, 2H, β-pyr. H). UV-vis ($CHCl_3$) λ_{max} (log ε) 419(4.6), 433(4.5), 519(3.6), 571(3.5), 653(3.2). HRMS (ESI, M^+): found: 1280.5859, calcd. for $C_{88}H_{70}N_{11}$: 1280.5816.

ZnZn phenylene-linked dyad tri(dimethylamine) 4.16

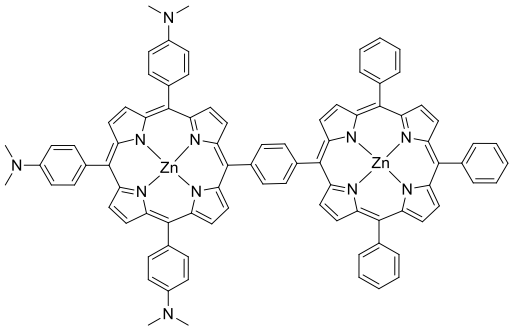

2H2H Phenylene-linked dyad tri(dimethylamine) **4.13** (10 mg, 0.0078 mmol) was dissolved in DCM (10 mL). Zinc acetate dihydrate (7 mg, 0.032 mmol) was dissolved in methanol (1 mL) and added to the dyad solution and the mixture stirred at rt for 17 hrs. The mixture was then concentrated *via* rotary evaporation and precipitation of the product was induced *via* the addition of methanol and collected by filtration. 10.5 mg, 96%. ^{1}H NMR (400 MHz, $CDCl_3$): δ = 3.13 (s, 12H, NCH_3), 3.14 (s, 12H, NCH_3), 7.04 – 7.09 (m, 6H, ArH), 7.75 – 7.84 (m, 9H, ArH), 8.11 (d, *J* = 8.43 Hz, 2H, ArH), 8.14 (d, *J* = 8.43 Hz, 4H, ArH), 8.25 – 8.29 (m, 2H, ArH), 8.30 – 8.34 (m, 4H, ArH), 8.59 – 8.65 (m, 4H, ArH), 9.00 (d, *J* = 4.58 Hz, 2H, β-pyr. H), 9.02 (d, *J* = 4.58 Hz, 2H, β-pyr. H), 9.06 (d, *J* = 4.58 Hz, 2H, β-pyr. H), 9.16 (d, *J* = 4.58 Hz, 2H, β-pyr. H), 9.22 (d, *J* = 4.58 Hz, 2H, β-pyr. H), 9.37 (d, *J* = 4.58 Hz, 2H, β-pyr. H), 9.46 (d, *J* = 4.58 Hz, 2H, β-pyr. H). UV-vis ($CHCl_3$) λ_{max} (log ε) 422(4.6), 439(4.5), 558(3.5), 605(3.3). HRMS (ESI, M^+): found: 1404.4072, calcd. for $C_{88}H_{66}N_{11}Zn_2$: 1404.4086.

ZnZn phenylene-linked dyad tri QAS 4.18

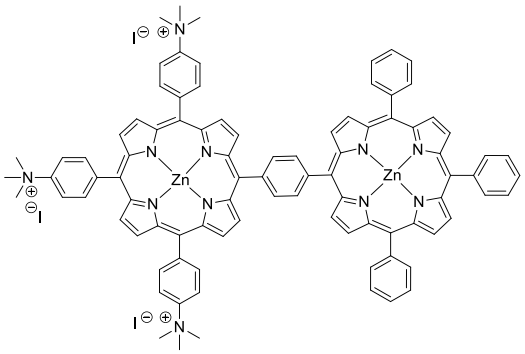

Chemical Formula: $C_{91}H_{74}I_3N_{11}Zn_2$
Exact Mass: 1829.18
Molecular Weight: 1833.11

ZnZn Phenylene-linked dyad tri(dimethylamine) **4.16** (4.5 mg, 0.0032 mmol) was dissolved in a mixture of acetonitrile (1 mL) and methyl iodide (0.5 mL). The mixture was heated with microwave irradiation at 50 °C for 3 hrs. Volatiles were evaporated to afford the product. 5.2 mg, 0.0028 mmol, 89%. ^{1}H NMR (400 MHz, $CDCl_3$): δ = 3.95 (s, 9H, NCH_3), 3.97 (s, 18H, NCH_3), 7.79 – 7.92 (m, 9H, ArH), 8.18 – 8.25 (m, 2H, ArH), 8.25 – 8.31 (m, 4H, ArH), 8.39 – 8.49 (m, 8H, ArH), 8.52 (d, *J* = 8.79 Hz, 4H, ArH), 8.59 (d, *J* = 8.43 Hz, 2H, ArH), 8.63 (d, *J* = 8.43 Hz, 2H, ArH), 8.81 – 8.86 (m, 6H, β-pyr. H), 8.87 (d, *J* = 4.58 Hz, 2H, β-pyr. H), 8.94 (d, *J* = 4.58 Hz, 2H, β-pyr. H), 8.97 (d, *J* = 4.58 Hz, 2H, β-pyr. H), 9.31 (d, *J* = 4.58 Hz, 2H, β-pyr. H), 9.37 (d, *J* = 4.58 Hz, 2H, β-pyr. H). UV-vis (DMSO) λ_{max} (log ε) 427(5.4), 437(5.5), 562(4.3), 603(4.1). HRMS (ESI, 3 x (M-3I$^-$)): found: 1448.4705, calcd. for $C_{91}H_{74}N_{11}Zn_2$: 1448.4712

Vinyl-linked dyads via Wittig reaction

2H2H Wittig dyad tetraester 5.08

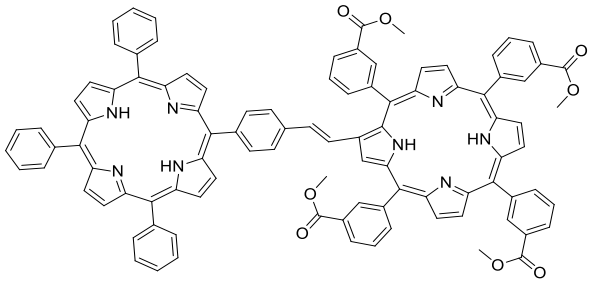

Chemical Formula: $C_{98}H_{68}N_8O_8$
Exact Mass: 1484.52
Molecular Weight: 1485.64

Tetraphenylporphyrin monoaldehyde **4.06** (9.5 mg, 0.015 mmol) and tetraphenylporphyrin tetraester phosphonium salt **5.01** (22 mg, 0.018 mmol) were dissolved in chloroform (7 mL). DBU (62 mg, 0.20 mmol) was added and the mixture stirred at rt 1 hr. The mixture was washed twice with 0.1 M HCl and the organic layer dried over $MgSO_4$. Isomerisation: the product was dissolved in a mixture of DCM

(3 mL), TFA (3 mL) and water (1 mL) and stirred at rt for 1 hr. The mixture was neutralised with sat. $NaHCO_3$ and extracted with DCM (3 x 20 mL). The products were purified *via* flash chromatography with DCM used as eluent. 10.6 mg, 0.0071 mmol, 48%. ^{1}H NMR (400 MHz, $CDCl_3$): δ = -2.70 (s, 2H, NH), -2.55 (s, 2H, NH), 3.90 (s, 3H, OCH_3), 4.00 (s, 3H, OCH_3), 4.01 (s, 3H, OCH_3), 4.04 (s, 3H, OCH_3), 7.18 (d, *J* = 15.18 Hz, 1H, vinyl H), 7.55 (d, *J* = 15.18 Hz, 1H, vinyl H), 7.60 (d, *J* = 8.03 Hz, 2H, ArH), 7.73 – 7.82 (m, 9H, ArH), 7.84 – 7.91 (m, 2H, ArH), 7.91 – 8.02 (m, 2H, ArH), 8.19 (d, *J* = 8.20 Hz, 2H, ArH), 8.22 – 8.28 (m, 6H, ArH), 8.39 – 8.45 (m, 2H, ArH), 8.50 (d, *J* = 8.03 Hz, 4H, ArH), 8.55 – 8.61 (m, 2H, ArH), 8.73 – 8.83 (m, 6H, m, 4H, β-pyr. H and ArH), 8.86 (s, 4H, β-pyr. H), 8.90 – 8.93 (m, 4H, β-pyr. H), 8.95 – 9.01 (m, 4H, β-pyr. H), 9.03 (s, 1H, β-pyr. H). UV-vis ($CHCl_3$) λ_{max} (log ε) 423 (5.8), 511 (4.1), 571 (4.3), 624 (4.2), 652 (3.9). HRMS (ESI, M^+): found: 1485.5236, calcd. for $C_{98}H_{69}N_8O_8$: 1485.5238.

ZnZn Wittig dyad tetraester 5.12

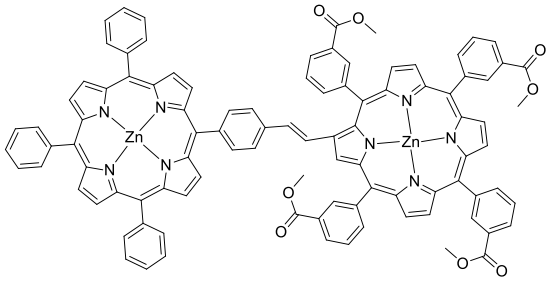

2H2H Wittig dyad tetraester **5.08** (7.0 mg, 0.0048 mmol) was dissolved in DCM (10 mL). Zinc acetate dihydrate (19 mg, 0.087 mmol) was dissolved in methanol (1 mL) and added to the dyad solution. Stirred at rt 3 hrs, concentrated on rotovap and the product precipitated *via* addition of methanol. 6.0 mg, 0.0037, 78%. ^{1}H NMR (400 MHz, $CDCl_3$): δ = 3.90 (s, 3H, OCH_3), 3.99 (s, 3H, OCH_3), 4.00 (s, 3H, OCH_3), 4.03 (s, 3H, OCH_3), 7.21 (d, *J* = 15.89 Hz, 1H vinyl H), 7.49 – 7.55 (m, 3H, vinyl H and ArH), 7.60 (d, *J* = 8.20 Hz, ArH), 7.73 – 7.82 (m, 9H, ArH), 7.83 – 7.91 (m, 2H, ArH), 7.91 – 8.01 (m, 2H, ArH), 8.20 (d, *J* = 8.20 Hz, 2H, ArH), 8.22 – 8.30 (m, 6H, ArH), 8.40 – 8.46 (m, 2H, ArH), 8.47 – 8.54 (m, 4H, ArH), 8.54 – 8.59 (m, 2H, ArH), 8.84 – 8.94 (m, 8H, ArH and β-pyr. H), 8.97 (s, 4H, β-pyr. H), 9.03 (d, *J* = 4.61 Hz, 2H, β-pyr. H), 9.09 (d, *J* = 4.61 Hz, 2H, β-pyr. H), 9.13 (s, 1H, β-pyr. H). UV-vis ($CHCl_3$) λ_{max} (log ε) 426(5.8), 560(4.4), 599(4.3). HRMS (ESI, M^+): found: 1609.3503, calcd. for $C_{98}H_{65}N_8O_8Zn_2$: 1609.3508.

ZnZn Wittig dyad tetraacid 5.13

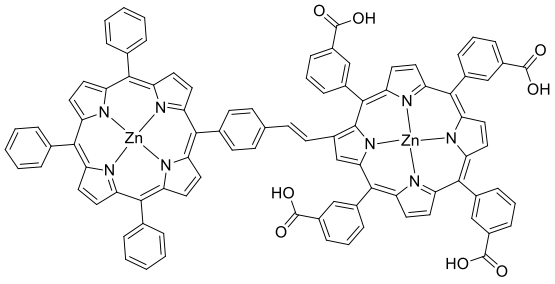

Chemical Formula: $C_{94}H_{56}N_8O_8Zn_2$
Exact Mass: 1552.28
Molecular Weight: 1556.26

ZnZn Wittig dyad tetraester **5.12** (2.3 mg, 1.42 µmol) was dissolved in a mixture of of tetrahydrofuran (5 mL), water (0.5 mL), methanol (5 mL) and potassium hydroxide (58 mg, 1.03 mmol). The mixture was stirred and heated at 50 °C for 5 hrs. The solution was acidified with phosphoric acid solution which induced precipitation of the porphyrin, and this was collected by three repetitions of centrifugation, with 95% of supernatant being removed and replaced each time. 1.0 mg, 0.64 µmol, 45%. ^{1}H NMR (400 MHz, DMSO - d_6): δ = 7.3 (d, *J* = 16.75 Hz, 1H, vinyl H), 7.58 (d, *J* = 16.75 Hz, 1H, vinyl H), 7.66 (d, *J* = 8.20 Hz, 2H, ArH), 7.75 – 7.86 (m, 9H, ArH), 8.00 – 8.14 (m, 2H, ArH), 8.14 – 8.29 (m, 12H, ArH), 8.30 – 8.36 (m, 2H, ArH), 8.37 – 8.46 (m, 2H, ArH), 8.49 – 8.54 (m, 4H, ArH), 8.57 – 8.86 (m, 12H, vinyl H and β-pyr. H), 8.89 – 8.97 (m, 4H, β-pyr. H), 9.14 (s, 1H, β-pyr. H). UV-vis (DMSO) λ_{max} (log ε) 429(5.9), 561(4.5), 603(4.3). HRMS (ESI, M^+): found: 1553.2895, calcd. for $C_{94}H_{57}N_8O_8Zn_2$: 1553.2882.

Vinyl linked dyad via Knoevenagel reaction and precursors

5-(4-cyanomethylphenyl)-10,15,20-tri(4-ethylphenyl)porphyrin 5.19

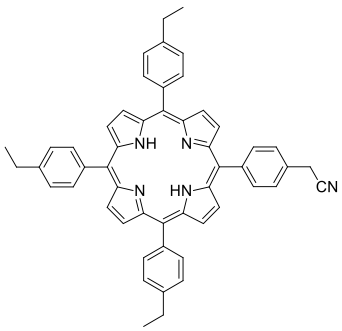

Chemical Formula: $C_{52}H_{43}N_5$
Exact Mass: 737.35
Molecular Weight: 737.93

This compound was synthesised in two steps *via* the benzyl bromide intermediate **5.18** (not isolated), which was converted to the nitrile *via* nucleophilic substitution with cyanide. 4-formylbenzyl bromide (0.995 g, 5.0 mmol, 1 eq.), 4-ethylbenzaldehyde (0.671, 5.0 mmol, 1 eq.) and pyrrole (0.672 mg, 10.0 mmol) were dissolved in DCM (1.00 L). TFA (2.5 g, 22 mmol) was added and the mixture stirred at rt for 3 hrs. DDQ (2.29 g, 10 mmol) was added and

the mixture stirred for 1 hr. Triethylamine (4 mL) was added and the mixture was concentrated *via* rotary evaporation. Methanol (500 mL) was added, which induced precipitation of the porphyrin products. 1.199 g isolated. Cyanide substitution: 20 mg of the porphyrin mixture was dissolved in 10 mL dioxane. NaCN (44 mg, 0.89 mmol) and water (2 mL) were added and the mixture heated at reflux for 48 hrs. The solution was washed with 3 x 100 mL water and extracted with DCM. The monocyanoporphyrin product was isolated *via* flash chromatography with DCM as eluent. 3.5 mg, 88% over both steps. ^{1}H NMR (400 MHz, $CDCl_3$): δ = -2.78 (s, 2H, NH), 1.53 (t, *J* = 7.51 Hz, 9H, CH_3), 3.01 (q, *J* = 7.51 Hz, 6H, C**H$_2$**CH_3), 4.10 (s, 2H, CH_2CN), 7.58 (d, *J* = 7.88 Hz, 6H, ArH), 7.71 (d, *J* = 8.06 Hz, 2H, ArH), 8.12 (d, *J* = 7.88 Hz, 6H, ArH), 8.23 (d, *J* = 8.06 Hz, 2H, ArH), 8.76 (d, *J* = 4.76 Hz, 2H, β-pyr. H), 8.86 (s, 4H, β-pyr. H), 8.88 (d, *J* = 4.76 Hz, β-pyr. H). UV-vis ($CHCl_3$) λ_{max} (log ε) 420 (4.4),517(3.0), 552(2.5), 590(2.4), 650(2.3). HRMS (ESI, M^+): found: 738.3608, calcd. for $C_{52}H_{44}N_5$: 738.3597.

5-(4-bromomethylphenyl)-10,15,20-tri(4-ethylphenyl)porphyrin 5.17

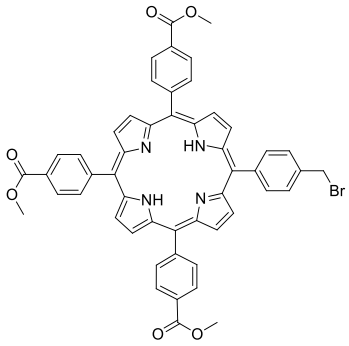

Chemical Formula: $C_{51}H_{37}BrN_4O_6$
Exact Mass: 880.19
Molecular Weight: 881.77

4-Formylbenzyl bromide **5.21** (0.498 mg, 2.5 mmol, 1 eq.), 4-formylbenzoic acid, methyl ester (0.410 mg, 2.5 mmol, 1 eq.) and pyrrole (0.355 mg, 5.0 mmol, 2 eq.) were mixed in DCM (500 mL). TFA (1.58 g, 11 mmol) was added and the mixture stirred at rt for 3 hrs. Chloranil (1.23 g, 5.0 mmol) was added and the mixture heated at reflux for 1 hr. Neutralised with sat. $NaHCO_3$ (20 mL) and extracted with DCM then evaporated to dryness. The product was purified *via* flash chromatography using 3% EtOAc in DCM. Precipitation was induced *via* addition of methanol. 127 mg, 0.144 mmol, 12%. ^{1}H NMR (400 MHz, $CDCl_3$): δ = -2.80 (s, 2H, NH), 4.11 (s, 9H, OCH_3), 4.85 (s, 2H, CH_2Br), 7.80 (d, *J* = 8.10 Hz, 2H, ArH), 8.19 (d, *J* = 8.10 Hz, 2H, ArH), 8.29 (d, *J* = 8.30 Hz, 6H, ArH), 8.45 (d, *J* = 8.30 Hz, 6H, ArH), 8.80 (d, *J* = 4.77 Hz, 2H, β-

pyr. H), 8.81 (s, 4H, β-pyr. H), 8.86 (d, *J* = 4.77 Hz, 2H, β-pyr. H). UV-vis ($CHCl_3$) λ_{max} (log ε) 420 (5.4), 516 (4.0), 552 (3.7), 591 (3.5), 646 (3.4). HRMS (ESI, M^+): found: 881.1990, calcd. for $C_{51}H_{38}N_4O_6Br$: 881.1975.

5-(4-cyanomethylphenyl)-10,15,20-tri(4-carboxyphenyl)porphyrin methyl ester 5.16

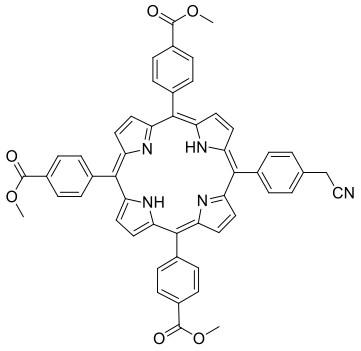

Chemical Formula: $C_{52}H_{37}N_5O_6$
Exact Mass: 827.27
Molecular Weight: 827.88

Monobromoporphyrin triester **5.17** (51 mg, 0.061 mmol) was dissolved in DMF (5 mL). NaCN (25 mg, 0.51 mmol) was added and stirred at 50 °C for 30 mins. DCM (30 mL) was added and the mixture washed with sat. NaCl (3 x 20 mL). The organic layer was collected, dried with $MgSO_4$, filtered and evaporated. The monocyanoporphyrin product was isolated *via* flash chromatography using 10% EtOAc in DCM. The product was precipitated *via* addition of methanol. 27 mg, 0.0326 mmol, 53%. ^{1}H NMR (400 MHz, $CDCl_3$): δ = -2.80 (s, 2H, NH), 4.11 (s, 9H, OCH_3), 4.12 (s, 2H, CH_2CN), 7.74 (d, *J* = 8.24, 2H, ArH), 8.23 (d, *J* = 8.24, 2H, ArH), 8.29 (d, *J* = 8.24, 6H, ArH), 8.45 (d, *J* = 8.24, 6H, ArH), 8.79 – 8.84 (m, 8H, β-pyr. H). UV-vis ($CHCl_3$) λ_{max} (log ε) 421(4.1), 516(2.7), 552(2.4), 591(2.3), 648(2.1). HRMS (ESI, M^+): found: 828.2834, calcd. for $C_{52}H_{38}N_5O_6$: 828.2822.

Knoevenagel dyad 5.23

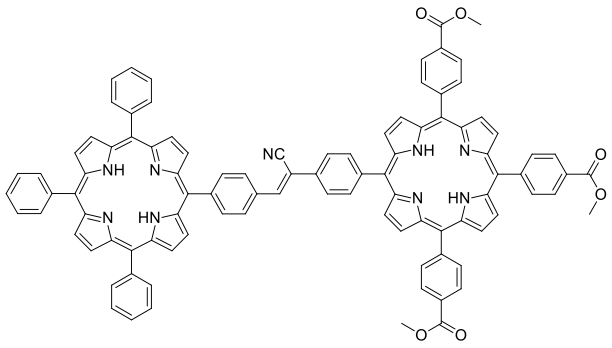

Chemical Formula: $C_{97}H_{65}N_9O_6$
Exact Mass: 1451.51
Molecular Weight: 1452.61

Monocyanoporphyrin triester **5.16** (3.0 mg, 0.00362 mmol) and tetraphenylporphyrin monoaldehyde (3.5 mg, 0.00544 mmol) were dissolved in DCM (5 mL). DBU (100 mg, 0.657 mmol) was added and the mixture stirred at rt for 30 mins. The mixture was submitted to flash chromatography with 8% EtOAc in DCM to afford the product. 1mg, 6.9 µmol, 19%. ^{1}H NMR (400 MHz, $CDCl_3$): δ = -2.74 (s, 2H, NH), -2.71

(s, 2H, NH), 4.12 (s, 3H, OCH_3), 4.13 (s, 6H, OCH_3), 7.81 (s, 1H, vinyl H), 7.72 – 7.83 (m, 9H, ArH), 8.20 – 8.29 (m, 8H, ArH), 8.29 – 8.37 (m, 6H, ArH), 8.37 – 8.51 (m, 12H, ArH), 8.82 – 8.99 (m, 16H, β-pyr. H). UV-vis ($CHCl_3$) λ_{max} (log ε) 421(4.6), 516(2.7), 552(2.6), 591(2.6), 647(2.6). HRMS (ESI, M^+): found: 1452.5176, calcd. for $C_{97}H_{66}N_9O_6$: 1452.5136.

Metalated porphyrins for faciliated separation

Ag 5,10,15-triphenyl-20-(4-formylphenyl)porphyrin 6.01

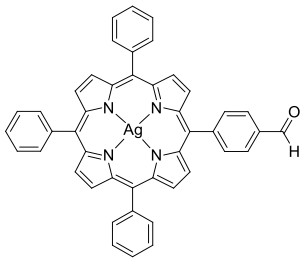

Chemical Formula: $C_{45}H_{28}AgN_4O$
Exact Mass: 747.13
Molecular Weight: 748.60

Tetraphenylporphyrin monoaldehyde (13.6 mg, 0.0221 mmol) was dissolved in DCM (10 mL). $AgOOCF_3$ (20 mg, 0.088 mmol) and NaOAc (18 mg, 0.22 mmol) were each dissolved in methanol (1 mL) and added to the porphyrin solution. The mixture was heated at reflux for 1 hr. The mixture was passed through a pad of silica and the product isolated by evaporating the solvents. 11 mg, 0.0147 mmol, 66%. UV-vis ($CHCl_3$) λ_{max} (log ε) 427(4.4), 508(2.6), 542(3.1), 576(2.6), 611(2.5). HRMS (ESI, M^+): found: 748.1380, calcd. for $C_{45}H_{29}N_4OAg$: 748.1392.

MnCl 5,10-diphenyl-15,20-di(4-formylphenyl)porphyrin 6.11

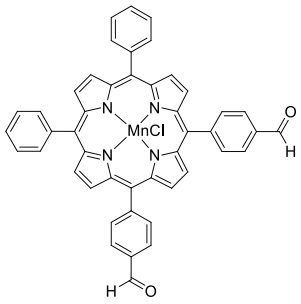

Chemical Formula: $C_{46}H_{28}ClMnN_4O_2$
Exact Mass: 758.13
Molecular Weight: 759.13

AABB tetraphenylporphyrin dialdehyde (100 mg, 0.149 mmol) was dissolved in DMF (100 mL) and the mixture heated to 100 °C. $MnCl_2$ (316 mg, 2.51 mmol) was added and stirring continued for 3 hrs. More $MnCl_2$ (300 mg, 2.38 mmol) was added and stirring continued for 20 more hours. Evaporated to dryness and then redissolved in DCM (100 mL) and washed with water (3 x 100 mL). The organic layer contained the porphyrin and was dried with $MgSO_4$, filtered and evaporated. 110 mg, 0.145 mmol, 97%. UV-vis (DMF) λ_{max} (log ε) 372(3.7), 395(3.7), 451(3.9), 468(4.0),

539(2.8), 578(3.0), 618(3.0). HRMS (ESI, M^+): found: 723.1595, calcd. for $C_{46}H_{28}N_4O_2Mn$: 723.1593.

AABB phenylene linked porphyrin triad hexaester 4.20

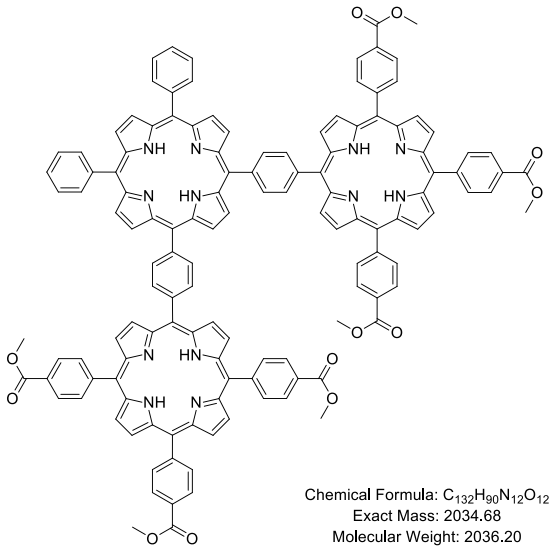

This compounds was formed in two steps using a manganese-tagged porphyrin dialdehyde to form the triad, with manganese being subsequently removed. MnCl *AABB* tetraphenylporphyrin dialdehyde (31 mg, 41 µmol, 1 eq.), 4-formylbenzoic acid, methyl ester (161 mg, 980 µmol, 24 eq.) and pyrrole (68 mg, 1021 µmol, 25 eq.) were mixed in DCM (102 mL). TFA (256 mg, 2246 µmol) was added and the mixture stirred at rt 8 hrs. DDQ (232 mg, 1021 µmol) was added and the mixture stirred 30 mins. Triethylamine (1 mL) was added and the mixture evaporated to dryness. The residue was submitted to flash chromatography, initially with 1% methanol in DCM as eluent. Elution was continued until the eluent became colourless. The eluent was then changed to 3% methanol in DCM. Dark coloured material then eluted, and analysis with MALDI MS detected an ion at m/z 2090, and this was attributed to the Mn-tagged triad. The chromatography procedure was repeated on the triad-containing fraction in order to remove all traces of the tetraphenylporphyrin tetraester by-product. The triad-containing mixture was then dissolved in THF (30 mL) and $NaBH_4$ was added. The mixture was stirred 30 mins before 32% aq. HCl (0.5 mL) was added. The mixture was stirred 30 mins before triethylamine (1 mL) was added. The mixture was evaporated to dryness and the demetalated triad isolated by flash chromatography with 3% EtOAc in DCM used to elute. 6.4 mg, 3.1 µmol, 8%. ^{1}H NMR (400 MHz, $CDCl_3$): δ = -2.52 (s, 2H, NH), -2.68 (s, 4H, NH), 4.06 (s, 6H, OCH_3), 4.08 (s, 12H, OCH_3), 7.68 - 7.82 (m, 6H, ArH), 8.24 – 8.30 (m, 8H, ArH), 8.33 (d, *J* = 8.43 Hz, 8H, ArH), 8.41 ppm (d, *J* = 8.24 Hz, 4H, ArH), 8.44 (d, *J* =

8.24 Hz, 8H, ArH), 8.61 (d, *J* = 8.06 Hz, 4H, ArH), 8.67 (d, *J* = 8.06 Hz, 4H, ArH), 8.80 (d, *J* = 7.33 Hz, 4H, ArH), 8.81 (d, *J* = 7.33 Hz, 4H, ArH), 8.89 (s, 2H, β-pyr. H), 8.95 (d, *J* = 4.76 Hz, 4H, β-pyr. H), 9.02 (d, *J* = 4.76 Hz, 2H, β-pyr. H), 9.28 (d, *J* = 4.76 Hz, 2H, β-pyr. H), 9.30 (br. s, 4H, β-pyr. H), 9.44 (s, 2H, β-pyr. H). UV-vis ($CHCl_3$) λ_{max} (log ε) 427 (5.8), 518 (4.6), 554 (4.4), 591 (4.2), 648 (4.0). HRMS (ESI, M^+): found: 2035.6862, calcd. for $C_{132}H_{91}N_{12}O_{12}$: 2035.6879.

Maquette binding experiments

The buffer solution used in the experiments contained 20 mM CHES, 150 mM KCl and was adjusted to pH 9 by the addition of 5M KOH solution dropwise. A stock solution of both BTH7H112 and BT bis-his maquettes with a concentration of 1.0 μM in the above buffer solution was produced and used for all experiments. The concentration of this maquette solution was determined by measuring its absorbance at 280 nm. The extinction coefficient at this wavelength was calculated based on analysis of its amino acid sequence, and was attributable only to the four tryptophan residues.[157] A value of 22000 M^{-1} cm^{-1} was obtained.

A typical titration experiment was performed as follows: A sample of the porphyrin material to be tested for binding was put in an eppendorf tube and its mass recorded. This was dissolved in 1000 μL DMSO. A portion of this solution was mixed with 1000 μL DMSO in a second eppendorf tube to produce a concentration of 300 μM. A 3000 μL sample of maquette solution was put into a cuvette. A 1 μL portion of porphyrin solution was added to the maquette solution and mixed thoroughly before the UV-vis absorption spectrum was recorded. Each such addition would raise the concentration of porphyrin in the maquette by approximately 0.1 μM, and the presise concentration of porphyrin was determined assuming that the volumes of water and DMSO were simply additive. This process was repeated until approximately four equivalents of porphyrin had been added. The absorbance at the

wavelength of the maximum absorbance of the maquette-bound porphyrin was plotted against porphyrin concentration.

The K_d value, and other variables in Equation 1, were determined by fitting the equation to the data using the software Fityk.[158] Although the concentration of maquette binding site had been experimentally determined previously, if the equation could not be fit to the data it became necessary to allow this value also to be varied during the fitting process, and thus was obtained an apparent maquette binding site concentration.

References

(1) Blankenship, R. E. *Molecular Mechanisms of Photosynthesis*; 2014.

(2) Wei, X.; Su, X.; Cao, P.; Liu, X.; Chang, W.; Li, M.; Zhang, X.; Liu, Z. *Nature* **2016**, *534*, 69.

(3) Officer, D. L.; Wagner, P.; Wagner, K.; Dutton, P. L.; Gordon, K. *Grant Proposal: Artificial Photosynthesis: Developing a Simple, Functional, Light Harvesting Porphyrin-Protein Ensemble.*

(4) Neveu, C. Photosystem II structural visualisation generated from Loll *et al.* data https://upload.wikimedia.org/wikipedia/commons/thumb/7/7e/PhotosystemII.PNG/1024px-PhotosystemII.PNG (accessed Oct 10, 2016).

(5) Loll, B.; Kern, J.; Saenger, W.; Zouni, A.; Biesiadka, J. *Nature* **2005**, *438*, 1040.

(6) About: Photosynthetic Antenna Research Centre https://parc.wustl.edu/about (accessed Oct 10, 2016).

(7) Lambreva, M. D.; Russo, D.; Polticelli, F.; Scognamiglio, V.; Antonacci, A.; Zobnina, V.; Campi, G.; Rea, G. *Curr. Protein Pept. Sci.* **2014**, *15*, 285.

(8) Shibamoto, T.; Kato, Y.; Sugiura, M.; Watanabe, T. *Biochemistry* **2009**, *48*, 10682.

(9) Retegan, M.; Cox, N.; Lubitz, W.; Neese, F.; Pantazis, D. A. *Phys. Chem. Chem. Phys.* **2014**, *16* (24), 11901.

(10) Voloshin, R. A.; Rodionova, M. V.; Zharmukhamedov, S. K.; Hou, H. J. M.; Shen, J.-R.; Allakhverdiev, S. I. In *Applied Photosynthesis - New Progress*; Najafpour, M. M., Ed.

(11) Askerka, M.; Wang, J.; Brudvig, G. W.; Batista, V. S. *Biochemistry* **2014**, *53* (44), 6860.

(12) Zouni, A.; Witt, H. T.; Kern, J.; Fromme, P.; Krauss, N.; Saenger, W.; Orth, P. *Nature* **2001**, *409*, 739.

(13) Bertini, I.; Cavallaro, G.; Rosato, A. *Chem. Rev.* **2006**, *106* (1), 90.

(14) Fasan, R. *ACS Catal.* **2012**, *2* (4), 647.

(15) Atassi, M. Z.; Childress, C. *Protein J.* **2005**, *24* (1), 37.

(16) Cytochrome c https://en.wikipedia.org/wiki/Cytochrome_c (accessed Oct 10, 2016).

(17) Bushnell, G. W.; Louie, G. V.; Brayer, G. D. *J. Mol. Biol.* **1990**, *214* (2), 585.

(18) Huang, S. S.; Gibney, B. R.; Stayrook, S. E.; Leslie Dutton, P.; Lewis, M. *J. Mol. Biol.* **2003**, *326* (4), 1219.

(19) Rabanal, F.; Degrado, W. F.; Dutton, P. L. *J. Am. Chem. Soc.* **1996**, *118* (2), 473.

(20) Skalicky, J. J.; Gibney, B. R.; Rabanal, F.; Bieber Urbauer, R. J.; Dutton, P. L.; Wand, A. J. *J. Am. Chem. Soc.* **1999**, *121* (21), 4941.

(21) Sharp, R. E.; Moser, C. C.; Rabanal, F.; Dutton, P. L. *Proc. Natl. Acad. Sci. U. S. A.* **1998**, *95* (18), 10465.

(22) Rabanal, F.; Gibney, B. R.; DeGrado, W. F.; Moser, C. C.; Leslie Dutton, P. *Inorgnica Chim. Acta* **1996**, *243*, 213.

(23) Watkins, D. W.; Armstrong, C. T.; Beesley, J. L.; Marsh, J. E.; Jenkins, J. M. X.; Sessions, R. B.; Mann, S.; Anderson, J. L. R. *BBA - Bioenerg.* **2016**, *1857* (5), 493.

(24) Zhuang, J.; Amoroso, J. H.; Kinloch, R.; Dawson, J. H.; Baldwin, M. J.; Gibney, B. R. *Inorg. Chem.* **2004**, *43* (26), 6828.

(25) Koder, R. L.; Dutton, P. L. *Dalton Trans.* **2006**, *25*, 3045.

(26) Anderson, J. L. R.; Armstrong, C. T.; Kodali, G.; Lichtenstein, B. R.; Watkins, D. W.; Mancini, J. A.; Boyle, A. L.; Farid, T. A.; Crump, M. P.; Moser, C. C.; Dutton, P. L. *Chem. Sci.* **2014**, *5* (2), 507.

(27) Lichtenstein, B. R.; Bialas, C.; Cerda, J. F.; Fry, B. A.; Dutton, P. L.; Moser, C. C. *Angew. Chem. Int. Ed. Engl.* **2015**, *54*, 13626.

(28) Sanders, J. K. M.; Bampos, N.; Clyde-Watson, Z. E.; Darling, S. L.; Hawley, J. C.; Kim, H.-J.; Mak, C. C.; Webb, S. J. In *The Porphyrin Handbook*; Kadish, K. M., Smith, K. M., Guilard, R., Eds.; 2000.

(29) Shifman, J. M.; Gibney, B. R.; Sharp, R. E.; Dutton, P. L. *Biochemistry* **2000**, *39*, 14813.

(30) Tetraphenylporphyrin, [TPP] http://omlc.org/spectra/PhotochemCAD/html/099.html (accessed Nov 3, 2016).

(31) Adler, A. I.; Finarelli, J. *J. Org. Chem.* **1967**, *32*, 476.

(32) Lindsey, J. S.; Hsu, H. C.; Schreiman, I. C. *Tetrahedron Lett.* **1986**, *27* (41), 4969.

(33) Lindsey, J. S. In *The Porphyrin Handbook*; Kadish, K. M., Smith, K. M., Guilard, R., Eds.; 2000.

(34) Drain, C. M.; Gong, X.; Ruta, V.; Soll, C. E.; Chicoineau, P. F. *J. Comb. Chem.* **1999**, *1* (4), 286.

(35) Manaka, J. S.; Lawrence, D. S. *Tetrahedron Lett.* **1989**, *30* (50), 6989.

(36) Lee, C.; Lindsey, J. S. *Tetrahedron* **1994**, *50* (39), 11427.

(37) Sobral, A. J. F. N.; Rebanda, N. G. C. L.; Da Silva, M.; Lampreia, S. H.; Ramos Silva, M.; Matos Beja, A.; Paixão, J. A.; Rocha Gonsalves, A. M. D. A. *Tetrahedron Lett.* **2003**, *44* (20), 3971.

(38) Geier III, G. R.; Littler, B. J.; Lindsey, J. S. *J. Chem. Soc. Perkin Trans. 2* **2001**, 701.

(39) Okujima, T.; Kikkawa, T.; Nakano, H.; Kubota, H.; Fukugami, N.; Ono, N.; Yamada, H.; Uno, H. *Chem. - A Eur. J.* **2012**, *18* (40), 12854.

(40) Wang, Q.; Campbell, W. M.; Bonfantani, E. E.; Jolley, K. W.; Officer, D. L.; Walsh, P. J.; Gordon, K.; Humphry-Baker, R.; Nazeeruddin, M. K.; Grätzel, M. *J. Phys. Chem. B* **2005**, *109* (32), 15397.

(41) Zahran, Z. N.; Naruta, Y. *Chem. Commun.* **2015**, *51* (95), 16900.

(42) Nielsen, I. M. B.; Leung, K. *J. Phys. Chem. A* **2010**, *114* (37), 10166.

(43) Weng, Z.; Jiang, J.; Wu, Y.; Wu, Z.; Guo, X.; Materna, K. L.; Liu, W.; Batista, V. S.; Brudvig, G. W.; Wang, H. *J. Am. Chem. Soc.* **2016**, *138* (26), 8076.

(44) Shimazaki, Y.; Nagano, T.; Takesue, H.; Ye, B.-H.; Tani, F.; Naruta, Y. *Angew. Chem. Int. Ed.* **2004**, *43* (1), 98.

(45) Zhang, Y.; Liu, S.; Wang, L.; Liu, W.; Sun, R.; Ye, J. *Mater. Lett.* **2015**, *144*, 5.

(46) Fleischer, E. B.; Krishnamurthy, M. *J. Am. Chem. Soc.* **1972**, *94* (4), 1382.

(47) Tabata, M.; Nishimoto, J. In *The Porphyrin Handbook*; Kadish, K. M., Smith, K. M., Guilard, R., Eds.; 2000.

(48) Beyene, B. B.; Mane, S. B.; Hung, C. *Chem. Commun.* **2015**, *51*, 15067.

(49) Gomes, M. C.; Silva, S.; Faustino, M. A. .; Neves, M. G. P. M. S.; Almeida, A.; Cavaleiro, J. A. S.; Tomé, J. P. C.; Cunha, Â. *Photochem. Photobiol.* **2013**, *12*, 262.

(50) Abd, M.; Aleem, E.; Ali, A.; Elhady, O. M. *Tetrahedron Lett.* **2016**, *57* (3), 435.

(51) Gianferrara, T.; Bergamo, A.; Bratsos, I.; Milani, B.; Spagnul, C.; Sava, G.; Alessio, E. *J. Med. Chem.* **2010**, *53* (12), 4678.

(52) Jee, J.; Eigler, S.; Jux, N.; Zahl, A.; Eldik, R. Van. *Inorg. Chem. 2007* **2007**, *46* (8), 3336.

(53) Villari, V.; Mineo, P.; Micali, N. *Nanotechnology* **2007**, *18* (37), 375503.

(54) Zhang, H.; Zhang, B.; Zhu, M.; Grayson, S. M.; Schmehl, R.; Jayawickramarajah, J. *Chem. Commun.* **2014**, *50*, 4853.

(55) Pisarek, S.; Maximova, K.; Gryko, D. *Tetrahedron* **2014**, *70* (38), 6685.

(56) Choi, K.; Lee, D.; Jang, W. *Bull. Korean Chem. Soc.* **2010**, *31* (3).

(57) Kuciauskas, D.; Liddell, P. a.; Lin, S.; Johnson, T. E.; Weghorn, S. J.; Lindsey, J. S.; Moore, A. L.; Moore, T. A.; Gust, D. *J. Am. Chem. Soc.* **1999**, *121* (37), 8604.

(58) Burrell, A. K.; Officer, D. L.; Plieger, P. G.; Reid, D. C. W. *Chem. Rev.* **2001**, *101* (9), 2751.

(59) Morisue, M.; Hoshino, Y.; Shimizu, M.; Uemura, S. *Chem. Eur. J.* **2016**, *22* (37), 13019.

(60) Furutsu, D.; Satake, A.; Kobuke, Y. *Inorg. Chem.* **2005**, *44* (13), 4460.

(61) Norsten, T.; Branda, N. *Chem. Commun.* **1998**, 1257.

(62) Dubowchik, G. M.; Hamilton, A. D. *Chem. Commun.* **1987**, 293.

(63) Yu, L.; Lindsey, J. S. *Tetrahedron* **2001**, *57*, 9285.

(64) Locos, O.; Bašić, B.; McMurtrie, J. C.; Jensen, P.; Arnold, D. P. *Chem. Eur. J.* **2012**, *18*, 5574.

(65) Tsuda, A.; Osuka, A. *Science.* **2001**, *293* (5527), 79.

(66) Wennerström, O.; Ericsson, H.; Raston, I.; Svensson, S.; Pimlott, W. *Tetrahedron Lett.* **1989**, *30* (9), 1129.

(67) Meier, H.; Kobuke, Y.; Kugimiya, S.; Chemistry, S. *Tetrahedron* **1989**, 923.

(68) Naruta, Y.; Sasayama, M.; Sasaki, T. *Angew. Chem. Int. Ed. Engl.* **1994**, *33* (18), 1839.

(69) Officer, D. L.; Burrell, A. K.; Reid, D. C. W. *Chem. Commun.* **1996**, *14*, 1657.

(70) Clark, W.; Still, W. C.; Kahn, M.; Mitra, A. *J. Org. Chem.* **1978**, *43* (14), 2923.

(71) Hambright, P. In *Porphyrin Handbook*; Kadish, K. M., Smith, K. M., Guilard, R., Eds.; 2000.

(72) Harris, D. *Quantitative Chemical Analysis*, 8th ed.; New York, 2010.

(73) Housecroft, C. E. .; Constable, E. C. *Chemistry : an introduction to organic, inorganic and physical chemistry*, 4th ed.; Harlow : Pearson, 2010.

(74) Ringuet, M.; Pottier, R. H.; Kennedy, J. C. International Patent: Porphyrin Derivatives. WO92/06097, 1992.

(75) Borocci, S.; Marotti, F.; Mancini, G.; Monti, D.; Pastorini, A. *Langmuir* **2001**, *17* (23), 7198.

(76) Guo, X.; Shen, D. H.; Li, Y. Y.; Tian, M.; Liu, Q.; Guo, C. C.; Liu, Z. G. *J. Mol. Catal. A Chem.* **2011**, *351*, 174.

(77) Choi, K.-H.; Wang, K.-K.; Shin, E. P.; Oh, S.-L.; Jung, J.-S.; Kim, H.-K.; Kim, Y.-R. *J. Phys. Chem. C* **2011**, *115*, 3212.

(78) Bandi, V.; Gobeze, H. B.; Karr, P. A.; D'Souza, F. *J. Phys. Chem. C* **2014**, *118* (33), 18969.

(79) Bakar, M. B.; Oelgemöller, M.; Senge, M. O. *Tetrahedron* **2009**, *65* (34), 7064.

(80) Notaras, E. G. A.; Fazekas, M.; Doyle, J. J.; Blau, W. J.; Senge, M. O. *Chem. Commun.* **2007**, *21*, 2166.

(81) Senge, M. O.; Ryppa, C.; Fazekas, M.; Zawadzka, M.; Dahms, K. *Chem. - A Eur. J.* **2011**, *17* (48), 13562.

(82) Feng, D. W.; Chung, W.-C. C.; Wei, Z. W.; Gu, Z.-Y. Y.; Jiang, H.-L. L.; Chen, Y.-P. P.; Darensbourg, D. J.; Zhou, H.-C. C. *J. Am. Chem. Soc.* **2013**, *135* (45), 17105.

(83) Nur, H.; Hamid, H.; Endud, S.; Hamdan, H.; Ramli, Z. *Mater. Chem. Phys.* **2006**, *96* (2–3), 337.

(84) Burns, D. H.; Lai, J.-J.; Smith, K. M. *J. Chem. Soc. Perkin Trans. I* **1988**, *1988* (12), 3119.

(85) Juillard, S.; Bondon, A.; Simonneaux, G. *Eur. J. Inorg. Chem.* **2007**, *26*, 4138.

(86) Song, B.; Park, B.; Han, C. *Bull. Korean Chem. Soc.* **2002**, *23* (1), 119.

(87) Oulmi, D.; Maillard, P.; Guerquin-Kern, J.-L.; Huel, C.; Momenteau, M. *J. Org. Chem.* **1995**, *60* (6), 1554.

(88) Balakumar, A.; Lysenko, A. B.; Carcel, C.; Malinovskii, V. L.; Gryko, D. T.; Schweikart, K. H.; Loewe, R. S.; Yasseri, A. A.; Liu, Z.; Bocian, D. F.; Lindsey, J. S. *J. Org. Chem.* **2004**, *69* (5), 1435.

(89) Singh, K.; Behal, S.; Hundal, M. S. *Tetrahedron* **2005**, *61* (27), 6614.

(90) Fleischer, E. B.; Shachter, A. M. *Inorg. Chem.* **1991**, *30* (19), 3763.

(91) Ojadi, E. C. A.; Linschitz, H.; Gouterman, M.; Walter, R. I.; Lindsey, J. S.; Wagner, R. W.; Droupadi, P. R.; Wang, W. *J. Phys. Chem.* **1993**, *97*, 13192.

(92) Sadegh, F.; Bagheri, O.; Moghadam, M.; Mirkhani, V.; Tangestaninejad, S.; Mohammadpoor-Baltork, I. *J. Organomet. Chem.* **2014**, *759*, 46.

(93) Taylor, P.; Li, X.; Qiu, J.; Zhang, L.; Mu, J. *J. Dispers. Sci. Technol.* **2007**, *28*, 1081.

(94) Guo, Z.; Mao, J.; Ouyang, Q.; Zhu, Y.; He, L.; Lv, X.; Liang, L.; Ren, D.; Chen, Y.; Zheng, J. *J. Dispers. Sci. Technol.* **2009**, *31* (1), 57.

(95) Liu, J.; Shi, S.; Ji, L.; Mei, W. *Transit. Met. Chem.* **2005**, *30*, 684.

(96) Kalyanasundaram, K. *J. Chem. Soc. Faraday Trans. 2* **1983**, *79* (9), 1365.

(97) Grigg, B. R.; Sweeney, A.; Johnson, A. W.; Fischer, H.; Orth, H.; Grigg, R.; Sweeney, A.; Jackson, H. *J. Am. Chem. Soc. Perkin 1* **1972**, 1789.

(98) Imahori, H.; Mori, Y.; Matano, Y. *J. Photochem. Photobiol. C Photochem. Rev.* **2003**, *4* (1), 51.

(99) Boyd, P. D. W.; Burrell, A. K.; Campbell, W. M.; Cocks, P. A.; Gordon, K. C.; Jameson, G. B.; Officer, D. L.; Zhao, Z. *Chem. Commun.* **1999**, 637.

(100) Guldi, D. M.; Imahori, H.; Tamaki, K.; Kashiwagi, Y.; Yamada, H.; Sakata, Y.; Fukuzumi, S. *J. Phys. Chem. A* **2004**, *108* (4), 541.

(101) Poddutoori, P.; Co, D. T.; Samuel, A. P. S.; Kim, C. H.; Vagnini, M. T.; Wasielewski, M. R. *Energy Environ. Sci.* **2011**, *4* (7), 2441.

(102) Zhou, Y.; Ngo, K. T.; Zhang, B.; Feng, Y.; Rochford, J. *Organometallics* **2014**, *33*, 7078.

(103) Sorai, M.; Kaneko, Y.; Hashiguchi, T. *J. Phys. Chem. Solids* **2014**, *75* (5), 656.

(104) Chang, C. P.; Weng, C. M.; Hong, F. E. *Inorganica Chim. Acta* **2010**, *363* (2), 412.

(105) Moore, K. T.; Fletcher, J. T.; Therien, M. J. *J. Am. Chem. Soc.* **1999**, *121* (22), 5196.

(106) Dommaschk, M.; Gutzeit, F.; Boretius, S.; Haag, R.; Herges, R. *Chem. Commun.* **2014**, *50* (83), 12476.

(107) Krishnan, R.; Parthiban, A. *J. Fluor. Chem.* **2014**, *162*, 17.

(108) Osteryoung, J. G.; Osteryoung, R. A. *Anal. Chem.* **1985**, *57* (1), 101A.

(109) Tabbì, G.; Di Mauro, G.; Purrello, R.; Bonomo, R. P. *Dalton Trans.* **2011**, *40* (16), 4223.

(110) Bhugun, I.; Lexa, D.; Savéant, J. *J. Am. Chem. Soc.* **1996**, *118* (7), 1769.

(111) Miao, J.; Zhu, L. *Chem. - An Asian J.* **2010**, *5* (7), 1634.

(112) Acharya, R.; Paudel, L.; Joseph, J.; McCarthy, C. E.; Dudipala, V. R.; Modarelli, J. M.; Modarelli, D. A. *J. Org. Chem.* **2012**, *77* (14), 6043.

(113) Li, J.; Cai, Z.; Xu, S.; Liao, C. *J. Liq. Chromatogr. Relat. Technol.* **2011**, *34* (March 2013), 1578.

(114) Kashiyama, Y.; Ogawa, N. O.; Shiro, M.; Tada, R.; Kitazato, H.; Ohkouchi, N. *Biogeosciences* **2008**, *5* (3), 797.

(115) Fateen, E.; Abd-elfattah, A.; Gouda, A. *Egypt. J. Med. Hum. Genet.* **2011**, *12* (1), 49.

(116) Benton, C. M.; Kee, C.; Ritchie, H. J.; Moniz, C.; Jones, D. J. L.; Lim, C. K.; Ritchie, H. J.; Moniz, C.; Jones, D. J. L.; Kee, C.; Ritchie, H. J.; Moniz, C.; Jones, D. J. L. *Biomed. Chromatogr.* **2012**, *26* (3), 331.

(117) General HPLC Column Care www.nestgrp.com/pdf/colcare.pdf (accessed Oct 10, 2016).

(118) Kirschbaum, K. M.; Grellner, W.; Rochholz, G.; Musshoff, F.; Madea, B. *J. Anal. Toxicol.* **2011**, *35*, 124.

(119) Ariffin, M. M.; Anderson, R. A. *J. Chromatogr. B Anal. Technol. Biomed. Life Sci.* **2006**, *842*, 91.

(120) Schad, G. J.; Euerby, M. R.; Skellern, G. G.; Tettey, J. N. A. *Anal. Bioanal. Chem* **2012**, *404*, 239.

(121) Méndez, A.; Bosch, E.; Rosés, M.; Neue, U. D. *J. Chromatogr. A* **2003**, *986* (1), 33.

(122) Liu, G.; Khlobystov, A. N.; Charalambidis, G.; Coutsolelos, A. G.; Briggs, G. A. D.; Porfyrakis, K. *J. Am. Chem. Soc.* **2012**, *134* (4), 1938.

(123) Zhang, X.; Hou, L.; Cnossen, A.; Coleman, A. C.; Ivashenko, O.; Rudolf, P.; Van Wees, B. J.; Browne, W. R.; Feringa, B. L. *Chem. - A Eur. J.* **2011**, *17* (32), 8957.

(124) Bhat, A. R.; Athar, F.; Van Zyl, R. L.; Chen, C.-T.; Azam, A. *Chem. Biodivers.* **2008**, *5* (5), 764.

(125) Bailey, W. F.; Luderer, M. R.; Jordan, K. P. *J. Org. Chem.* **2006**, *71*, 2825.

(126) Hong, S.; Rohman, M. R.; Jia, J.; Kim, Y.; Moon, D.; Kim, Y.; Ko, Y. H.; Lee, E.; Kim, K. *Angew. Chemie - Int. Ed.* **2015**, *54* (45), 13241.

(127) Piet, J. J.; Taylor, P. N.; Wegewijs, B. R.; Anderson, H. L.; Osuka, A.; Warman, J. M. *J. Phys. Chem. B* **2001**, *105*, 97.

(128) Bonfantini, E. E.; Officer, D. L.; North, P. *Tetrahedron Lett.* **1993**, *34* (52), 8531.

(129) Campbell, W. M.; Jolley, K. W.; Wagner, P.; Wagner, K.; Walsh, P. J.; Gordon, K. C.; Schmidt-mende, L.; Nazeeruddin, M. K.; Wang, Q.; Grätzel, M.; Officer, D. L. *J. Phys. Chem. C* **2007**, *111* (32), 11760.

(130) Mozer, A. J.; Griffith, M. J.; Tsekouras, G.; Wagner, P.; Wallace, G. G.; Mori, S.; Sunahara, K.; Miyashita, M.; Earles, J. C.; Gordon, K. C.; Du, L.; Katoh, R.; Furube, A.; Officer, D. L. *J. Am. Chem. Soc.* **2009**, *131* (43), 15621.

(131) Campbell, W. M. PhD Thesis: Porphyrins for Surface Modification, 2001.

(132) Jyothish, K.; Wang, Q.; Zhang, W. *Adv. Synth. Catal.* **2012**, *354* (11–12), 2073.

(133) Reid, D. C. PhD Thesis: A Building Block Approach to Porphyrin Arrays, 1998.

(134) Smith, M. B. .; March, J. *March's Advanced Organic Chemistry*, 6th ed.; Wiley, 2007.

(135) Guillot, R.; Loupy, A.; Meddour, A.; Pellet, M.; Petit, A. *Tetrahedron* **2005**, *61* (42), 10129.

(136) Jiang, B.; Yang, S.; Niver, R.; Jones, W. E. *Synth. Met.* **1998**, *94*, 205.

(137) Wen, L.; Li, M.; Schlenoff, J. B. *J. Am. Chem. Soc.* **1997**, *119*, 7726.

(138) Lindsey, J. S.; Schreiman, I. C.; Hsu, H. C.; Kearney, P. C.; Marguerettaz, A. M. *J. Org. Chem.* **1987**, *52* (5), 827.

(139) Jackson, T.; Woo, L. W. L.; Trusselle, M. N.; Chander, S. K.; Purohit, A.; Reed, M. J.; Potter, B. V. L. *Org. Biomol. Chem.* **2007**, 2940.

(140) Pan, X.; Huang, R.; Zhang, J.; Ding, L.; Li, W.; Zhang, Q.; Liu, F. *Tetrahedron Lett.* **2012**, *53* (40), 5364.

(141) Chen, Z. X.; Xu, G. Y.; Yang, G. C.; Wang, W. *React. Funct. Polym.* **2004**, *61* (1), 139.

(142) Aakeröy, C. B.; Smith, M. M.; Desper, J. *Cryst. Eng. Comm.* **2012**, *14*, 71.

(143) Pieck, J. C.; Kuch, D.; Grolle, F.; Linne, U.; Haas, C.; Carell, T. *J. Am. Chem. Soc.* **2006**, *128* (5), 1404.

(144) Sundaresan, A. K.; Ramamurthy, V. *Org. Lett.* **2007**, *9* (18), 3575.

(145) Lomenzo, S. A.; Rhoden, J. B.; Izenwasser, S.; Wade, D.; Kopajtic, T.; Katz, J. L.; Trudell, M. L. *J. Med. Chem.* **2005**, *48* (5), 1336.

(146) Lee, J.; Jin, M. K.; Kang, S. U.; Su, Y. K.; Lee, J.; Shin, M.; Hwang, J.; Cho, S.; Choi, Y. S.; Choi, H. K.; Kim, S. E.; Suh, Y. G.; Lee, Y. S.; Kim, Y. H.; Ha, H. J.; Toth, A.; Pearce, L. V.; Tran, R.; Szabo, T.; Welter, J. D.; Lundberg, D. J.; Wang, Y.; Lazar, J.; Pavlyukovets, V. A.; Morgan, M. A.; Blumberg, P. M. *Bioorganic Med. Chem. Lett.* **2005**, *15* (18), 4143.

(147) Liu, G.; Zhou, W.; Zhang, J.; Zhao, P. *J. Polym. Sci. Part A Polym. Chem.* **2012**, *50* (11), 2219.

(148) Zhu, L.; Ang, C. Y.; Li, X.; Nguyen, K. T.; Tan, S. Y.; Ågren, H.; Zhao, Y. *Adv. Mater.* **2012**, *24* (29), 4020.

(149) Taha, N.; Sasson, Y.; Chidambaram, M. *Appl. Catal. A Gen.* **2008**, *350* (2), 217.

(150) Kulchat, S.; Meguellati, K.; Lehn, J. *Helv. Chim. Acta* **2014**, *97*, 1219.

(151) Hodgkiss, J. M.; Krivokapić, A.; Nocera, D. G. *J. Phys. Chem. B* **2007**, *111* (28), 8258.

(152) Collman, J. P.; Bencosme, C. S.; Durand, R. R.; Kreh, R. P.; Anson, F. C. *J. Am. Chem. Soc.* **1983**, *105* (10), 2699.

(153) Buchler, J. W.; Dreher, C.; Kunzel, F. M. *Struct. Bond.* **1995**, *84*, 1.

(154) Oar, M. A.; Dichtel, W. R.; Serin, J. M.; Fre, J. M. J.; Rogers, J. E.; Slagle, J. E.; Fleitz, P. A.; Tan, L.; Base, W. A. F. *Chem. Mater.* **2006**, *18*, 3682.

(155) Chen, A.; Wang, H.; Li, X. *Chem. Commun. (Camb).* **2005**, *1* (14), 1863.

(156) Takeda, J.; Ohta, S. .; Hirobe, M. . *J. Am. Chem. Soc.* **1987**, *109* (25), 256.

(157) Pace, C. N.; Vajdos, F.; Fee, L.; Grimsley, G.; Gray, T. *Protein Sci.* **1995**, *4* (11), 2411.

(158) Wojdyr, M. *J. Appl. Cryst.* **2010**, *43*, 1126.

(159) Zeng, X. L.; Tang, K.; Zhou, N.; Zhou, M.; Hou, H. J. M.; Scheer, H.; Zhao, K. H.; Noy, D. *J. Am. Chem. Soc.* **2013**, *135* (36), 13479.

(160) Kodali, G.; Mancini, J. A.; Solomon, L. A.; Episova, T. V.; Roach, N.; Hobbs, C. J.; Wagner, P.; Mass, O. A.; Aravindu, K.; Barnsley, J. E.; Gordon, K. C.; Officer, D. L.; Dutton, P. L.; Moser, C. C. *Chem. Sci.* **2016**.

(161) Maiti, N. C.; Mazumdar, S.; Periasamy, N. *J. Phys. Chem. B* **1998**, *102* (97), 1528.

(162) Zimmermann, J.; Siggel, U.; Fuhrhop, J.-H.; Röder, B. *J. Phys. Chem. B* **2003**, *107*, 6019.

(163) Micali, N.; Monsu' Scolaro, L.; Romeo, A.; Mallamace, F. *Phys. Rev. E* **1998**, *57* (5), 5766.

(164) Zhao, X.; Yuan, L.; Zhang, Z. Q.; Wang, Y. S.; Yu, Q.; Li, J. *Inorg. Chem.* **2016**, *55* (11), 5287.

(165) Đorđević, L.; Marangoni, T.; De Leo, F.; Papagiannouli, I.; Aloukos, P.; Couris, S.; Pavoni, C. E.; Monti, F.; Armaroli, N.; Prato, E. M.; Bonifazi, D. *Phys. Chem. Chem. Phys.* **2016**, *18* (18), 11858.

(166) Huang, G.; Yang, L.; Ma, X.; Jiang, J.; Yu, S.; Jiang, H. *Chem. - A Eur. J.* **2016**, *22*, 3470.

(167) Plamont, R.; Kikkawa, Y.; Takahashi, M.; Kanesato, M.; Giorgi, M.; Chan Kam Shun, A.; Roussel, C.; Balaban, T. S. *Chem. - A Eur. J.* **2013**, *19* (34), 11293.

(168) Robotham, B.; Lastman, K. A.; Langford, S. J.; Ghiggino, K. P. *J. Photochem. Photobiol. A Chem.* **2013**, *251*, 167.

(169) Kang, M. S.; Oh, J. B.; Roh, S. G.; Kim, M.; Lee, J. K.; Jin, S.; Kim, H. K. *Bull. Korean Chem. Soc.* **2007**, *28* (1), 33.

(170) Sakuma, T.; Sakai, H.; Araki, Y. *Phys. Chem. Chem. Phys.* **2016**, *18*, 5453.

(171) Meng, W.; Breiner, B.; Rissanen, K.; Thoburn, J. D.; Clegg, J. K.; Nitschke, J. R. *Angew. Chemie - Int. Ed.* **2011**, *50* (15), 3479.

(172) Chambrier, I.; Banerjee, C.; Remiro-buenaman, S.; Chao, Y.; Cammidge, A. N.; Bochmann, M. *Inorg. Chem.* **2015**, *54* (15), 7368.

(173) Rochford, J.; Chu, D.; Hagfeldt, A.; Galoppini, E. *J. Am. Chem. Soc.* **2007**, *129* (15), 4655.

(174) Warren, J. J.; Menzeleev, A. R.; Kretchmer, J. S.; Miller, T. F.; Gray, H. B.; Mayer, J. M. *J. Phys. Chem. Lett.* **2013**, *4* (3), 519.

(175) Sun, S.; Pan, M.; Hu, X.; Shao, W.; Li, J.; Zhang, F. *Catal. Letters* **2016**, *146* (6), 1087.